

**Investigation into the role of Glycogen
Synthase Kinase 3 (GSK-3) in
Dictyostelium discoideum and the role
of GSK-3 binding partners in
Dictyostelium discoideum and
mammalian cells**

Josephine E. Forde

School of Biosciences

Cardiff University

PhD Thesis

Submitted: November 2009

UMI Number: U585360

All rights reserved

INFORMATION TO ALL USERS

The quality of this reproduction is dependent upon the quality of the copy submitted.

In the unlikely event that the author did not send a complete manuscript and there are missing pages, these will be noted. Also, if material had to be removed, a note will indicate the deletion.



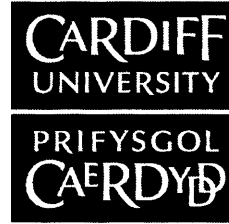
UMI U585360

Published by ProQuest LLC 2013. Copyright in the Dissertation held by the Author.
Microform Edition © ProQuest LLC.

All rights reserved. This work is protected against
unauthorized copying under Title 17, United States Code.



ProQuest LLC
789 East Eisenhower Parkway
P.O. Box 1346
Ann Arbor, MI 48106-1346



DECLARATION

This work has not previously been accepted in substance for any degree and is not concurrently submitted in candidature for any degree.

Signed *J Ford* (candidate) Date ... *14/05/2010*

STATEMENT 1

This thesis is being submitted in partial fulfillment of the requirements for the degree of *PhD* (insert MCh, MD, MPhil, PhD etc, as appropriate)

Signed *J Ford* (candidate) Date ... *14/05/2010*

STATEMENT 2

This thesis is the result of my own independent work/investigation, except where otherwise stated. Other sources are acknowledged by explicit references.

Signed *J Ford* (candidate) Date ... *14/05/2010*

STATEMENT 3

I hereby give consent for my thesis, if accepted, to be available for photocopying and for inter-library loan, and for the title and summary to be made available to outside organisations.

Signed *J Ford* (candidate) Date ... *14/05/2010*

STATEMENT 4: PREVIOUSLY APPROVED BAR ON ACCESS

I hereby give consent for my thesis, if accepted, to be available for photocopying and for inter-library loans **after expiry of a bar on access previously approved by the Graduate Development Committee.**

Signed (candidate) Date

Acknowledgements

I could not have completed PhD project alone. I am indebted to my supervisors Professor Trevor Dale and Professor Adrian Harwood whose differing supervision styles complemented each other so well. Their guidance and enthusiasm, as well as their experimental knowledge, have been invaluable to me.

I would like to thank all members, past and present, of the Dale and Harwood labs for their help and advice throughout the course of my project. In particular I would like to thank Ms Elizabeth Fraser and Dr Christine Humphreys for advice and for useful discussions, Miss Kirsty Richardson for her assistance with the FACS analysis, Dr Jonathan Ryves for his assistance with kinase assays and Dr Regina Teo for useful discussions on all things 'Dicty' related.

I would also like to thank Dr Peter Watson for his advice, infectious enthusiasm and assistance in all things microscopy based.

My parents, Pauline and Eamonn Forde have been a constant source of moral support throughout this project and Gareth, for being so understanding and putting up with the constant "I'll just be another hour...".

Abstract. The serine/threonine kinase glycogen synthase kinase-3 (GSK-3) was initially identified as a key regulator of insulin-dependent glycogen synthesis. GSK-3 was subsequently shown to function in a wide range of cellular processes including differentiation, growth, motility and apoptosis. A number of mechanisms have been shown to allow differential regulation of GSK-3; these include modulation by upstream signals, control of substrate specificity and GSK-3 localisation. The aim of this project was to better characterise the role of GSK-3 in the social amoeba *Dictyostelium discoideum* and to investigate the possibility that GSK-3 activity is directed through interactions with specific GSK-3 binding proteins.

In this study I generated both mammalian and *Dictyostelium* cell lines expressing GSK-3 homologues tagged with GFP. I demonstrated that the addition of this tag did not obviously alter cellular localization or the ability of GSK-3 to interact with known protein binding partners. I also confirmed that these fusion proteins retained kinase activity and that the levels of GSK-3 β over-expression used in this study were not detrimental to cell viability.

I further characterized the role of GSK-3 in the social amoebae *Dictyostelium*, using both knockout and over-expression cell lines to demonstrate that this protein fulfils multiple roles during early development. Dark-field time-lapse microscopy techniques were employed to identify a role for GSK-3 in co-ordinating chemotaxis and cellular polarization. During the course of this project I also identified a requirement for GskA in cytokinesis when cells were grown in shaking culture.

Finally, both the mammalian and *Dictyostelium* cell lines generated in this study were used for affinity chromatography experiments and a number of potential GSK-3 binding partners were identified.

Table of contents

CHAPTER 1	7
INTRODUCTION	7
1.1 Introduction	8
1.2 GSK-3 genes	9
1.3 GSK-3 substrates	13
1.4 Inhibitory phosphorylation of GSK-3	16
1.5 Activating phosphorylation of GSK-3	17
1.6 Regulation of glycogen synthesis	19
1.7 Regulation of the canonical Wnt pathway	20
1.8 Regulation of Hedgehog signal transduction	24
1.9 Regulation of the cytoskeleton by GSK-3	27
1.10 Regulation of apoptosis and cell viability	29
1.11 Regulation of transcription factors	29
1.12 The role of GSK-3 in <i>Dictyostelium</i>	30
1.13 <i>Dictyostelium</i> chemotaxis	33
1.14 <i>Dictyostelium</i> Cytokinesis	34
1.15 Aims of this study	38
CHAPTER 2	39
MATERIALS AND METHODS	39
2.1 Cloning	40
2.1.1 <i>Dictyostelium</i> Vectors	40
2.1.2 Mammalian Vectors	41
2.2 PCR	43
2.3 Cell culture	44
2.3.1 <i>Dictyostelium</i> cell culture	44
2.3.2 Mammalian cell culture	44

2.4 Transformations	45
2.4.1 Dictyostelium transformations	45
2.4.2 <i>Mammalian</i> transformation	46
2.5 Screening of clones	48
2.5.1 Screening of <i>Dictyostelium</i> clones	48
2.5.2 Screening of T-REx 293 GSK3 β -GFP and GFP cell lines	48
2.6 Immunofluorescence	49
2.6.1 Dictyostelium immunofluorescence	49
2.6.2 Mammalian immunofluorescence	49
2.7 Western blot	50
2.7.1 Dictyostelium western blots	50
2.7.2 Mammalian western blots	50
2.8 FACS sorting of Dictyostelium cells	51
2.9 Mammalian LacZ Assay	52
2.10 Mammalian Wst-1 Assay	52
2.11 Kinase Assay	53
2.11.1 Dictyostelium kinase assay	53
2.11.2 Mammalian kinase assay	54
2.12 Dictyostelium Cell Sizing	54
2.13 Dictyostelium Multinucleate Assay	54
2.14 Dictyostelium Cell Proliferation Assay	55
2.15 Dictyostelium Development assay	55
2.16 Dictyostelium cAMP pulse assay	56
2.17 Affinity purifications	56
2.17.1 Dictyostelium affinity purifications	56
2.17.2 Mammalian affinity purifications	57
2.18 SILAC	59
2.19 Mass Spectrometry Analysis	60
2.19.1 In-gel digestion	60
2.19.2 LC-MS/MS	60
2.20 SILAC coupled Mass Spectrometry Analysis	61
2.20.1 Gel electrophoresis and in-gel digestion	61
2.20.2 LC-MS/MS	61
2.20.3 Quantification and Bioinformatic Analysis	62

CHAPTER 3	64
CHARACTERIZATION OF GSK3B-GFP AND GSKA-GFP CELL LINES	64
3.1 Generation of Dictyostelium GskA-GFP cell lines	65
3.2 Generation of T-REx GSK3 β -GFP cell lines	70
3.3 Localization of GskA-GFP and GSK3 β -GFP	75
3.4 Assessment of kinase activity	78
3.5 Conclusions	82
CHAPTER 4	83
THE ROLE OF GSK-3 IN <i>DICTYOSTELIUM DISCOIDEUM</i>	83
4.1 GskA performs a role during early development	84
4.2 <i>gskA</i> null cells do not stream or polarize	89
4.3 GskA performs a role during cytokinesis	92
4.4 Ax2/ <i>gsk</i> - cells are smaller than their Ax2 counterparts	96
4.5 Conclusions	98
CHAPTER 5	101
IDENTIFICATION OF GSK-3 BINDING PARTNERS	101
5.2 Isolation of potential GSK-3 interaction proteins	105
5.2.1 Initial affinity purifications	105
5.2.2 Utilization of chemical cross-linking	107
5.3 Analysis of proteins that co-purified with GskA	108
5.4 SILAC-linked Mass Spectrometry	112
5.3 Analysis of SILAC results	115
5.3.1 STRING analysis	117
5.4 Validation of interactions	120
5.5 Conclusions	122

CHAPTER 6	125
DISCUSSION	125
6.1 The role of GskA in Dictyostelium	127
6.1.1 Potential mechanisms linked to direct action of GskA	128
6.1.2. Potential mechanisms linked to changes in gene expression	129
6.2 The role of key residues of GskA	131
6.2.1 Separation of the functions performed by GskA during development	131
6.2.2. Regulatory roles of Y214 and R96	132
6.3 Identification of potential GSK-3 interaction partners	133
6.3.1 Identification of ribosomal proteins as GSK-3 binding partners	134
6.3.2 Potential GskA interaction partners	134
6.3.3 Potential GSK3 β interaction partners	136
6.4 Conclusions	140
APPENDIX	141
GO term analysis	146
BIBLIOGRAPHY	155

Chapter 1

Introduction

1.1 Introduction

The aim of this project was to better characterise the role of the serine/threonine kinase Glycogen Synthase Kinase 3 (GSK-3) in the social amoeba *Dictyostelium discoideum*, and to investigate the possibility that GSK-3 activity is directed through interactions with specific protein binding proteins.

GSK-3 is a highly conserved kinase that functions in multiple signalling pathways including Wnt and Hedgehog signal transduction, protein synthesis, glycogen metabolism, mitosis and apoptosis. These many roles of GSK-3 cannot be separated either temporally or spatially and GSK-3 is itself subject to stringent regulation via several mechanisms:

- Splice variants of *GSK-3* exhibit differential activity towards specific substrates
- GSK-3 isoforms perform tissue specific roles
- Direct phosphorylation of an N-terminal serine residue of GSK-3 (S9 of GSK-3 β) is associated with inhibition of kinase activity
- Direct phosphorylation of a tyrosine residue located within the catalytic domain of GSK-3 (Y216 of GSK-3 β) is associated with an increase in kinase activity
- Differential localization of GSK-3 affects the ability of the kinase to target specific substrates
- Interactions between GSK-3 and scaffolding proteins direct or inhibit the activity of GSK-3 towards specific substrates

In this study I examined the role of GSK-3 in *Dictyostelium*, and investigated whether this protein was subject to these same mechanisms of regulation. I also investigated whether the activity of either mammalian GSK-3 β or *Dictyostelium* GskA was directed through previously uncharacterized protein binding interactions.

1.2 GSK-3 genes

GSK-3 was originally identified in mammals [6, 7], and homologues have been found in all eukaryotes. These homologues share a significant degree of sequence homology; species as distant as humans and *Dictyostelium* share over 80% similarity within their kinase domains [12] (Figure 1.1). Protein function is also well conserved between GSK-3 proteins from distantly related species: mammalian *GSK-3 β* under the control of the GAPDH promoter was able to rescue a temperature sensitivity defect in *Saccharomyces cerevisiae* cells in which all four GSK-3 homologues have been deleted [13].

Two GSK-3 isoforms encoded by distinct genes have been identified in mammals: GSK-3 α (51 KDa) and GSK-3 β (47 KDa). Both proteins are widely expressed, with particularly high levels in the brain [16]. The α and β isoforms share over 98% identity within their kinase domains but differ in their N-termini [22]. Despite a high degree of similarity and functional overlap, these isoforms are not redundant *in vivo*; *GSK-3 β* -null mice reportedly die during embryogenesis (between E13.5 and E14.5) as a result of liver degeneration caused by widespread hepatocyte apoptosis [23]. This phenotype is similar to that observed in *Rel-A*- [26] and *I κ B kinase-2*- [27] null mice and was thought to be indicative of a role for GSK-3 β in the NF κ B signalling pathway. Recently, however, *GSK-3 β* -null mice were crossed to a different genetic background, and while the authors reported that these mice died perinatally, they did not exhibit liver degeneration, instead these mice exhibited defects in mid-line development [28]. In contrast, *GSK-3 α* -null mice were found to be viable but displayed altered glucose and insulin sensitivity [29].

GSK-3 β can be differentially spliced; Mukai *et al.* [30] identified a variant containing a 13-amino acid insert within the kinase domain (GSK-3 β 2) (Figures 1.1 and 1.2) that was preferentially expressed in the brain and had decreased activity towards the microtubule-binding proteins Tau and MAP1B [30, 31]. The mechanism by which this insertion alters the biochemical properties of the protein remains unclear. Very few kinases exhibit differential splicing within their catalytic domain. Exceptions to this rule include JNK [32] and MEK5 [37]; splice variants of these proteins contain additional amino acids between subdomains IX and X of their catalytic domains [39]. Alternatively spliced JNK [32] exhibits altered activity towards known substrates, while an insert within the same

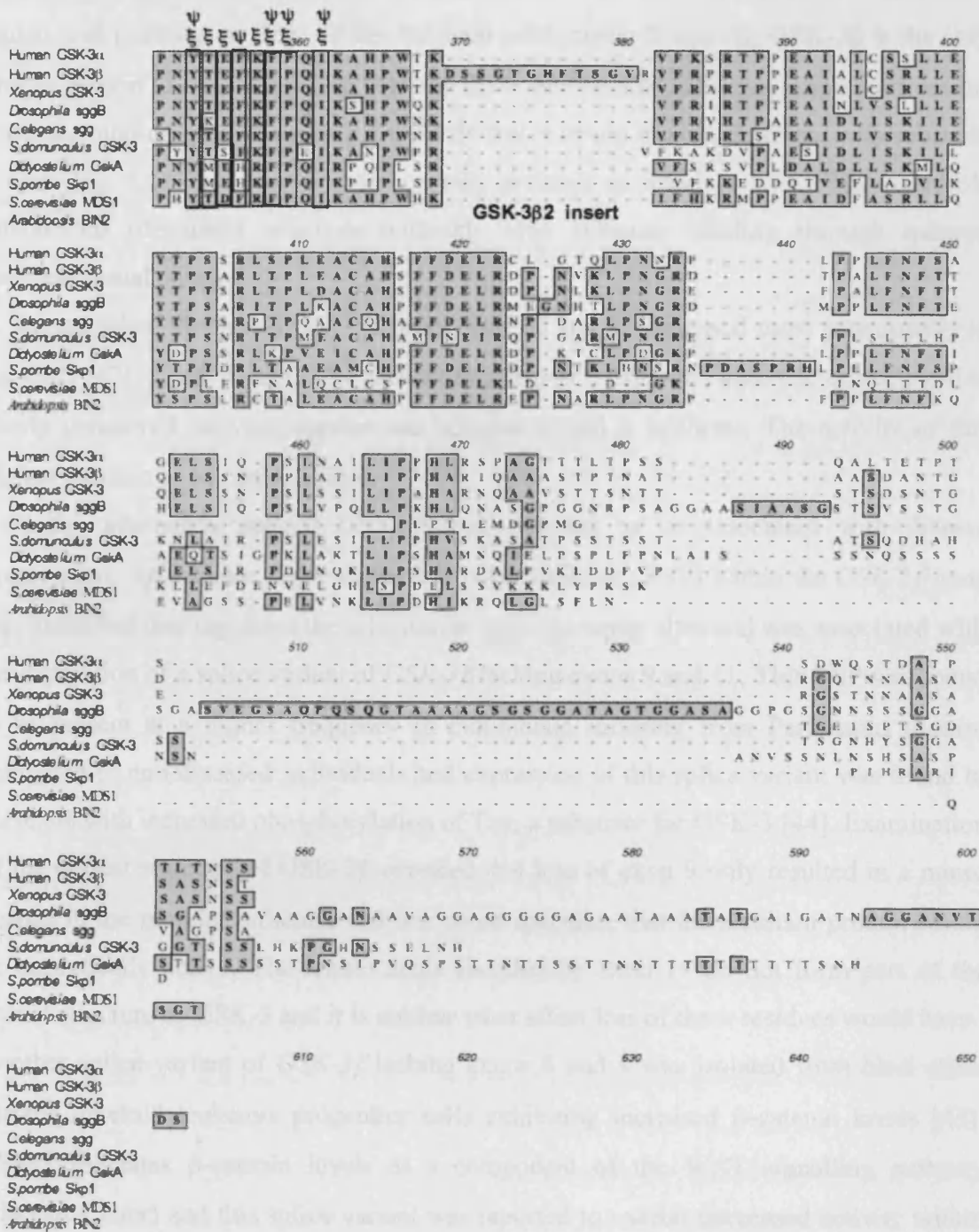


Figure 1.1 Alignment of GSK-3 proteins

All sequences were obtained from the NCBI website. Key residues involved in primed substrate recognition (R96, R180 and K205), autoinhibition (S9) and increased activity (Y216) are highlighted. Residues that contact Axin (ξ) or FRAT (ψ) are also highlighted. Mutation of K85 renders the kinase inactive.

region of MEK5 alters the intracellular localisation of the kinase [37]. The site of the 13-amino acid insertion in GSK-3 β lies between subdomains X and XI; GSK-3 β is the only known protein to exhibit splicing between these subdomains. This site is remote from the substrate-binding groove, making it unlikely that it would directly interfere with substrate access (Fig. 1.2). Instead, the insertion may promote or interfere with GSK-3-scaffold interactions (discussed later) or indirectly alter substrate binding through induced conformational changes.

A second splice variant of GSK-3 β lacks exon 10 and is expressed most prominently in the CNS [42]. Exon 10 of GSK-3 β encodes a region outside the catalytic domain and is poorly conserved between species and between α and β isoforms. The activity of this variant remains to be characterised.

Recently, alternately spliced GSK-3 β was reported to be associated with disease progression. An intronic single nucleotide polymorphism (SNP) within the GSK-3 β gene was identified that regulated the selection of splice acceptor sites and was associated with the expression of a splice variant of GSK-3 β lacking exons 9 and 11. This SNP was found to be present at a higher frequency in individuals suffering from Parkinsons disease compared to non-diseased individuals and expression of this splice variant was found to correlate with increased phosphorylation of Tau, a substrate for GSK-3 [44]. Examination of the crystal structure of GSK-3 β revealed that loss of exon 9 only resulted in a minor change in the proteins structure and one could speculate that the resultant protein would be catalytically active. The amino acids encoded by exon 11 do not form part of the crystal structure of GSK-3 and it is unclear what affect loss of these residues would have.

Another splice variant of GSK-3 β lacking exons 8 and 9 was isolated from blast crisis chronic myeloid leukemia progenitor cells exhibiting increased β -catenin levels [45]. GSK-3 regulates β -catenin levels as a component of the WNT signalling pathway (discussed later) and this splice variant was reported to exhibit decreased activity within this pathway [45]. The validity of these findings requires further investigation. However, examination of the crystal structure of GSK-3 β revealed that loss of the amino acids encoded by exons 8 and 9 would result in a substantial modification in protein structure. It may be that this splice variant exhibits an inability to phosphorylate and regulate β -catenin levels because the protein is non-functional.

1.3 GSK-3 substrates

GSK-3 demonstrates a preference for pre-phosphorylated (primed) substrates, recognizing the consensus sequence S/T-X-X-X-Phospho-S/T, where the first S/T residue is the target for GSK-3 phosphorylation, 'X' represents any amino acid and the S/T C-terminal to the GSK-3 target residue has undergone priming phosphorylation [48]. The relative activity of GSK-3 towards individual substrates differs considerably. However, the requirement for priming of substrates is observed across a range of substrates. Priming decreases the K_m of the substrate: for example, prior phosphorylation of the GSK-3 substrate β -catenin by casein kinase 1 at S45 decreased the K_m 30-fold [49].

The crystal structure of GSK-3 β has been elucidated [41, 50, 51] and provided insight into the mechanism by which phospho-primed substrates are recognised. The residues R96, R180 and K205 were found to be located within close proximity of each other on the surface of the protein and create a region of positive charge (Figure 1.2). This region was proposed to interact with the primed phospho-S/T residue and to align the substrate within the substrate-binding groove such that the kinase activation loop and catalytic residues are optimally orientated [50]. Consistent with this proposal, mutation of substrate-priming sites dramatically reduced GSK-3 phosphorylation [54, 55], while a corresponding mutation in GSK-3 β that substituted the positive charge of R96 for an alanine residue dramatically reduced the ability of the protein to phosphorylate its primed targets [55, 56]. The importance of priming phosphorylation for GSK-3 function is supported by the observation that the key residues (R96, R180 and K205) are found in all GSK-3 homologues examined (Figure 1.1).

Specific substrates are primed for GSK-3 phosphorylation by different priming kinases, whose activity can be regulated in a pathway-specific manner. Consequently, the affinity of GSK-3 towards specific substrates can be controlled by the availability and activity of the priming kinase for a given substrate. For example, the collapsin response mediator

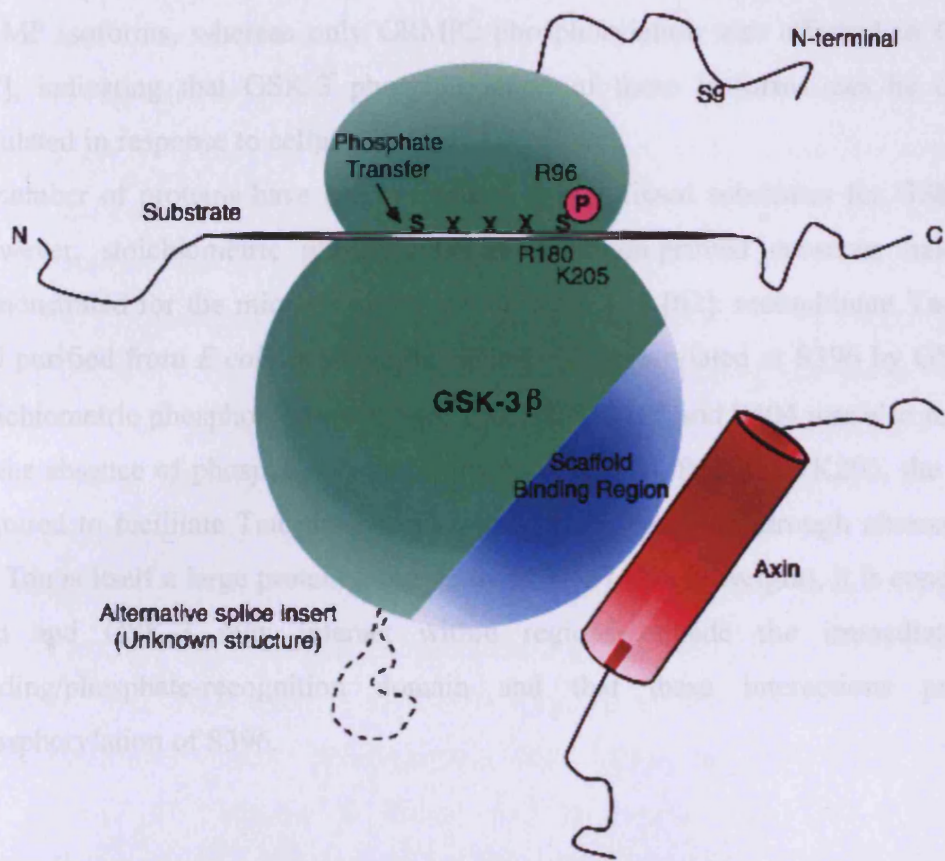


Figure 1.2. Schematic representation of GSK-3 β

Residues involved in primed substrate recognition (R96, R180 and K205) and autoinhibition (S9) are highlighted. The scaffold-binding region (SBR) is marked in blue; this region interacts with scaffolding proteins including Axin (shown in red) and FRAT.

proteins CRMP2 and CRMP4 were both identified as substrates for GSK-3. CRMP2 was found to be primed by Cdk5 alone, whereas either Cdk5 or DYRK2 were able to prime CRMP4 [57]. Inhibition of both Cdk5 and DYRK2 prevented phosphorylation of both CRMP isoforms, whereas only CRMP2 phosphorylation was affected in *Cdk5*^{-/-} cells [57], indicating that GSK-3 phosphorylation of these isoforms can be differentially regulated in response to cellular cues.

A number of proteins have been presented as un-primed substrates for GSK-3 [58-60]. However, stoichiometric phosphorylation of an un-primed substrate has only been demonstrated for the microtubule-binding protein Tau [62]: recombinant Tau, expressed and purified from *E.coli*, is stoichiometrically phosphorylated at S396 by GSK-3 β . Sub-stoichiometric phosphorylation at S46, T50, S202, T205 and S404 was also reported [62]. In the absence of phospho-substrate contacts with R96, R180 and K205, the interactions required to facilitate Tau phosphorylation must be provided through alternative means. As Tau is itself a large protein (ranging from 50–67 kDa in weight), it is conceivable that Tau and GSK-3 may interact within regions outside the immediate substrate binding/phosphate-recognition domain and that these interactions promote the phosphorylation of S396.

1.4 Inhibitory phosphorylation of GSK-3

The kinase activity of GSK-3 was found to be inhibited through phosphorylation of a serine residue located at the N-terminus of the protein (S21 and S9 of GSK-3 α and GSK-3 β , respectively) [63, 64]. Dajani *et al.* [50] demonstrated that a phospho-peptide based on the N-terminus of GSK-3 β could act as a competitive inhibitor towards primed GSK-3 substrates. This led to the suggestion that the phosphorylated N-terminus of GSK-3 auto-inhibits its activity by looping back into its own active site. The proposal being that the phospho-serine interacted with the region of positive charge generated by R96, R180 and K205 (residues refer to GSK-3 β), mimicking the primed residue of a GSK-3 substrate (Figure 1.2). Consistent with this mechanism of inhibition, substitution of R96 for an alanine residue abolished the ability of the phosphorylated N-terminal peptide to inhibit GSK-3 β activity [56].

A number of kinases have been reported to phosphorylate S21/9 of GSK-3 α and GSK-3 β in the context of specific signalling pathways: PKB targeted GSK-3 in response to insulin signalling [65], PKA targeted GSK-3 in response to increases in cAMP levels [66], p90^{RSK}/MAPKAP kinase-1 phosphorylated GSK-3 following activation by EGF or PDGF [64, 67] and p70 ribosomal S6 kinase (p70^{S6K}) phosphorylated GSK-3 in response to stimulation by insulin and other growth factors [63]. Phospho-S21/9 autoinhibition was also suggested to be involved in the regulation of GSK-3 activity during Wnt signalling [68, 69] and in the control of microtubule stability [70, 71] (see later for detailed discussions of these functions). It was therefore surprising that homozygous knock-in mice in which both S21 and S9 of GSK-3 α and GSK-3 β were replaced with alanine residues were viable and healthy [72]. Glycogen metabolism was partially disrupted in these mice (discussed below). However, McManus *et al.* [72] reported no other obvious phenotypes and specifically demonstrated that Wnt signalling was not affected. Analogous studies in *Drosophila* showed that the equivalent S9A pseudosubstrate mutation did not interfere with insulin/PI3K-dependent growth regulation, although a S9E mutation showed signs of mild Wnt pathway deregulation [73]. It is therefore tempting to speculate that, despite the literature to the contrary and with the exception of glycogen metabolism, S21/9 phosphorylation does not represent a primary mechanism by

which GSK-3 activity is regulated. Instead, serine phosphorylation of GSK-3 may represent a means of subtly altering GSK-3 activity within specific signalling pathways. The observation that S9 of GSK-3 β is only conserved in metazoans (excluding *Caenorhabditis elegans*) further supports the idea that this is a recent adaptation and perhaps a less essential mechanism of GSK-3 regulation.

1.5 Activating phosphorylation of GSK-3

GSK-3 is a member of the CMGC family of protein kinases. This group consists of cyclin-dependent kinases (CDKs), mitogen-activated protein kinases (MAPKs), glycogen synthase kinases (GSKs) and CDK-like kinases (CLKs) [39, 74]. The kinase activity of several CMGC family members, including MAPK2 (also known as ERK2), is dependent upon the phosphorylation of tyrosine (Y185 in MAPK2) and threonine (T183 in MAPK2) residues located within the activation loop of the protein [75]. Phosphorylation of MAPK2 by MEK was reportedly required to bring the activation loop into an active conformation for substrate binding and resulted in a 100- to 500-fold increase in activity [75]. Hughes *et al.* [76] investigated the possibility that GSK-3 β activity was regulated in a similar fashion; Y216 was identified as being phosphorylated *in vivo*, and phosphorylation of this residue was later shown to be associated with a 5-fold increase in K_{cat} [50, 76]. In place of the phospho-T183 located in the activation loop of MAPK2, GSK-3 β has a valine residue (V214). However, structural comparisons suggest that the primed phosphate of GSK-3 β 's substrate would occupy a 3-dimensional location equivalent to the phosphate of MAPK2's T183 suggesting that the primed substrate of GSK-3 may functionally substitute for the activating changes induced by MEK phosphorylation of T183 in MAPK2. The conformational change associated with Y216 phosphorylation in GSK-3 β is minimal, and the un-phosphorylated protein is active [50]. The underlying mechanisms responsible for regulating tyrosine phosphorylation of GSK-3 remain controversial. Recombinant GSK-3 β expressed and purified from *E. coli* was found to be phosphorylated on Y216 and underwent further phosphorylation upon incubation with Mg^{2+} ATP [62, 76, 77]. However, this phosphorylation was not shown to be stoichiometric. Lochhead *et al.* [78] recently proposed that GSK-3 autophosphorylation represents a transient capacity, specific to a partially folded state, for

GSK-3 to target its own tyrosine residues. However, it remains unclear whether GSK-3 autophosphorylation is an intramolecular rather than intermolecular event.

Mammalian GSK-3 was also reportedly phosphorylated by distinct tyrosine kinases *in trans*. For example, in neuronal cells, the tyrosine kinase Pyk2 phosphorylated GSK-3 β following stimulation with lysophosphatidic acid (LPA) [79] although the physiological phosphatase(s) that dephosphorylate tyrosine residues within GSK-3 remain to be identified.

In *Dictyostelium*, a role for GSK-3 tyrosine phosphorylation has been defined in the regulation of cell differentiation and patterning during development (discussed in detail later). In the absence of an abundant food source, *Dictyostelium* aggregate, using cAMP as a chemoattractant. The 7-transmembrane receptor cAR3 [80] responded to increased cAMP levels by activating the tyrosine kinase ZAK-1. ZAK-1, in turn, phosphorylates GskA (GSK-3) on Y214 (analogous to Y216 of GSK-3 β) as well as Y220 [81, 82]. Mutation of either Y214 or Y220 of GskA reduced kinase activity [81]. The Y220 residue that was phosphorylated by ZAK-1 is conserved in mammalian GSK-3 β (Y222) but was not found to be phosphorylated in preparations from insect cells that were catalytically active and contained phospho-Y216 [50].

1.6 Regulation of glycogen synthesis

GSK-3 was originally identified for its role as a negative regulator of glycogen synthesis [6] (for a review see [83]). In the absence of insulin, the metabolic enzyme glycogen synthase (GS) was found to be phosphorylated by casein kinase II (CK2) at S657 [84]. This primed GS for sequential phosphorylation at S653, S649, S645 and S641 by GSK-3 and inhibited GS activity [7, 48]. Increases in blood glucose lead to the release of insulin, which in turn initiates a signalling cascade involving the insulin receptor (IR), the insulin receptor substrate (IRS) and the activation of both phosphoinositide 3 kinase (PI3K) and protein kinase B (PKB) [85]. Active PKB was found to inhibit GSK-3 by phosphorylating S21 and S9 of the GSK-3 α and GSK-3 β isoforms, respectively [65]. Inhibition of GSK-3 leads to the accumulation of active GS and the subsequent assembly of UDP-glucose into glycogen.

Recently, evidence has emerged that GSK-3 α and GSK-3 β perform tissue specific roles in the regulation of this pathway. Both GSK-3 α and GSK-3 β were expressed and phosphorylated by PKB in response to insulin signalling in both hepatic and skeletal muscle tissue [29, 86]. However, GSK-3 α was found to principally regulate GS activity within hepatic cells [29] while GSK3 β was primarily responsible for the regulation of GS activity within skeletal muscle [72, 86].

This is the first clear example of where both GSK-3 α and GSK-3 β are capable of performing a common role in a pathway but their activities are differentially directed in a tissue specific manner. The idea that GSK-3 isoforms perform functionally divergent, tissue specific roles would argue that additional levels of regulation must be employed to compartmentalize these proteins such as differential expression, intracellular localization or scaffolding into different multi-protein complexes.

1.7 Regulation of the canonical Wnt pathway

The Wnt signal transduction pathway has been shown to direct many differentiation events during embryonic development and to regulate stem cell fate in adult organisms (for reviews see [87-89]). In the ‘canonical’ Wnt signalling pathway, Wnt ligands were found to stabilise levels of the transcriptional activator β -catenin (Figure 1.3). Stable β -catenin was shown to complex with TCF/LEF transcription factors and initiate transcription of Wnt target genes. GSK-3 has been shown to phosphorylate several intracellular components of the Wnt signal transduction pathway, the most well characterized of these being β -catenin. In the absence of Wnt ligands, β -catenin was shown to be phosphorylated at S45 by casein kinase 1 α (CK1 α) [55, 90], which primed it for sequential GSK-3 phosphorylation at T41, S37 and S33 [91, 92]. Phosphorylated β -catenin was recognised by the F-box protein β TrCP, a component of the E3 ubiquitin ligase complex, and targeted it for degradation via polyubiquitination and proteasomal degradation [93].

β -catenin alone was found to be a poor substrate for GSK-3 *in vitro*. Efficient phosphorylation of β -catenin required the formation of a multi-protein complex (also known as the ‘destruction complex’) that minimally comprised the scaffolding protein Axin, adenomatous polyposis coli (APC), CK1 α and either GSK-3 isoform [94-96]. Axin directly bound and mediated interactions between CK1 α , GSK-3 and their substrate β -catenin [94-97]. Axin was found to bind GSK-3 at a site distant from the substrate-binding domain in a region defined as the ‘scaffold-binding region’ (SBR) [98] (Figure 1.2). In the presence of Axin, GSK-3-directed phosphorylation of β -catenin increased 600 000-fold relative to the un-scaffolded reaction [49, 96]. Axin itself is a substrate for GSK-3, and phosphorylation decreased its proteolysis and increases β -catenin binding [94, 96, 99], although the GSK-3 target residues within Axin have not been directly identified. The tumour suppressor protein APC was found to bind both Axin and β -catenin and is also a substrate of GSK-3; APC is phosphorylated on a series of 20-amino acid repeats in a CK1- and GSK-3-dependent manner [100-102]. APC phosphorylation increases its affinity for β -catenin by 300- to 500-fold [103]. Xing *et al.* [104] proposed that APC phosphorylation regulates the dynamics of β -catenin binding

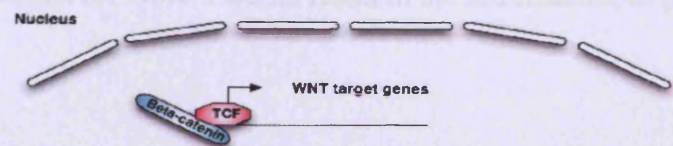
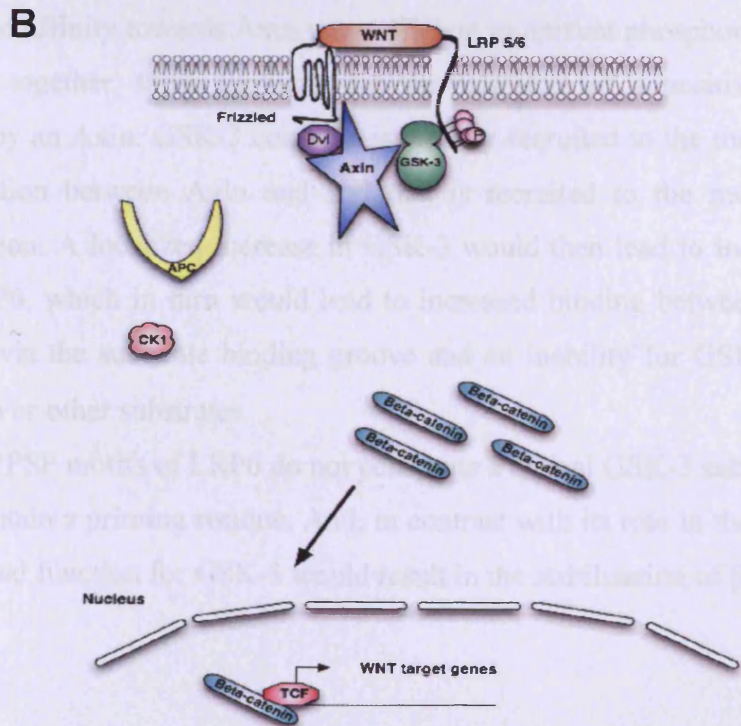
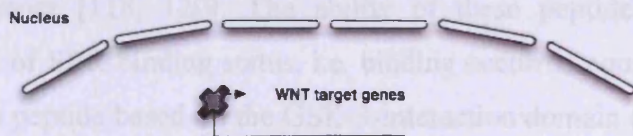
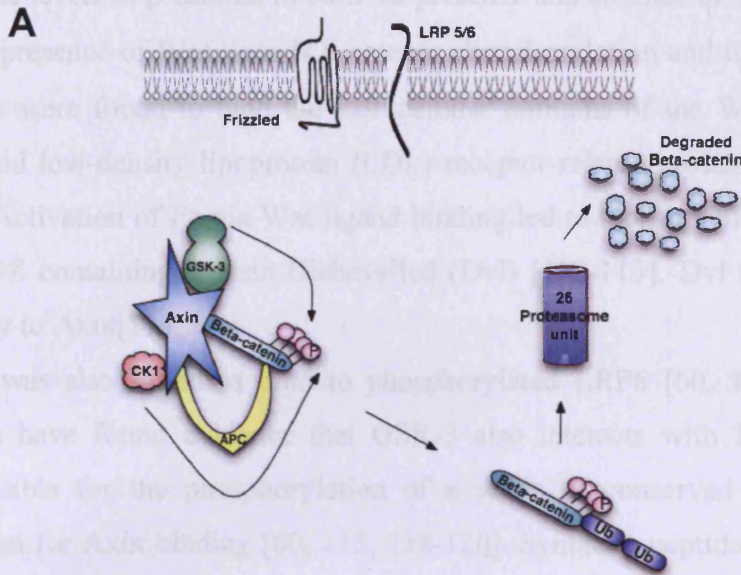


Figure 1.3. Schematic representation of WNT signal transduction

A. In the absence of a WNT ligand the destruction complex, consisting minimally of Axin, GSK-3, APC and CK1 α , mediates the phosphorylation of β -catenin. Phospho- β -catenin is then ubiquitinated and undergoes proteolysis.

B. In the presence of a WNT ligand the destruction complex fails to target β -catenin for degradation. This may involve the translocation of Axin and GSK-3 to the plasma membrane. β -catenin translocates to the nucleus where it binds to TCF and acts as a transcriptional activator of WNT target genes.

and release during a cycle of β -catenin degradation. Similarly, Ha *et al.* [105] proposed that the levels of phospho and non-phospho APC function as a rheostat to control the absolute levels of β -catenin in both the presence and absence of Wnt ligands.

In the presence of Wnt ligands β -catenin phosphorylation and turnover is inhibited. Wnt ligands were found to bind the extracellular domains of the Wnt co-receptors Frizzled (Fz) and low-density lipoprotein (LDL) receptor-related protein (LRP) 6 (LRP6) [106-109]. Activation of Fz via Wnt ligand binding led to recruitment and phosphorylation of the PDZ containing protein Dishevelled (Dvl) [110-113]. Dvl has been shown to bind directly to Axin[114].

Axin was also found to bind to phosphorylated LRP6 [60, 115-117]. Several recent studies have found evidence that GSK-3 also interacts with LRP6 and is the kinase responsible for the phosphorylation of a series of conserved PPPSP motifs that are essential for Axin binding [60, 115, 118-120]. Synthetic peptides based on these PPPSP motifs were found to bind GSK-3 and acted as competitive inhibitors in a phospho-specific manner [118, 120]. The ability of these peptides to bind to GSK-3 was independent of SBR binding status, i.e. binding occurred equally well in the presence or absence of a peptide based on the GSK-3-interaction domain (GID) of Axin. Conversely, Zeng *et al* [115] found GSK-3 was only able to phosphorylate LRP6 when bound to Axin; mutation of the SBR region of GSK-3 (L396Q), such that the protein exhibited reduced affinity towards Axin was sufficient to prevent phosphorylation of LRP6 *in vivo*. Taken together, these findings may be indicative of a positive feedback mechanism whereby an Axin: GSK-3 complex is initially recruited to the membrane, perhaps via an interaction between Axin and Dvl that is recruited to the membrane following Wnt activation. A localized increase in GSK-3 would then lead to increased phosphorylation of LRP6, which in turn would lead to increased binding between GSK-3 and phospho-LRP6 via the substrate binding groove and an inability for GSK-3 to phosphorylate β -catenin or other substrates.

The PPPSP motifs of LRP6 do not constitute a typical GSK-3 substrate site, since they do not contain a priming residue. And, in contrast with its role in the turnover complex, this proposed function for GSK-3 would result in the stabilisation of β -catenin.

In *Xenopus* embryos, Wnt signalling was proposed to promote the dissociation of GSK-3 from Axin through the action of FRAT, also known as GBP (GSK-3-binding protein). FRAT/GBP contains a GSK-3 interaction domain (GID) and was found to compete with Axin for binding to the SBR of GSK-3 [121]. Depletion of FRAT/GBP prevented β -catenin/TCF-dependent transcription and the formation of the *Xenopus* primary embryonic axis, while ectopic expression of FRAT/GBP induced axis duplication and the accumulation of β -catenin [122]. However, FRAT homologues have not been found in *Drosophila* or *C. elegans*, suggesting that the protein is not a central component of a primitive Wnt pathway. Furthermore, Van Amerongen *et al.* [123] showed that the three murine FRAT homologues are dispensable for Wnt signal transduction during development.

In addition to directing the efficient phosphorylation of β -catenin, it has recently been proposed that the Axin: GSK-3 complex may perform a more general role in the regulation of cellular signalling. Kim *et al.* [124] identified 42 proteins that were candidates for GSK-3-regulated phosphorylation, proteasomal degradation or both. This study identified transcription factors, RNA associated proteins, metabolic proteins, proteins that formed part of the cytoskeleton or membrane and signalling molecules that were all targets for GSK-3 directed phosphorylation and/or degradation. Interestingly, phosphorylation of 12 of these proteins could be inhibited through the addition of a peptide based on the GID of Axin. Indicating that phosphorylation of these substrates may require the formation of a multi-protein complex. Furthermore, levels of these 12 proteins were stabilized by the addition of Wnt ligands, indicating that a branch or branches of the Wnt signal transduction pathway were responsible for regulating the absolute levels of these proteins in the cell.

1.8 Regulation of Hedgehog signal transduction

The Hedgehog (Hh) and Wnt signalling pathways frequently cooperate to direct cellular proliferation, differentiation and pattern formation during embryonic development. GSK-3 plays a role in regulating proteolysis in both the Wnt and Hh pathways, and it has been suggested that this role may reflect the evolution of two pathways from a common, ancestral signal transduction module (reviewed in [125-127]).

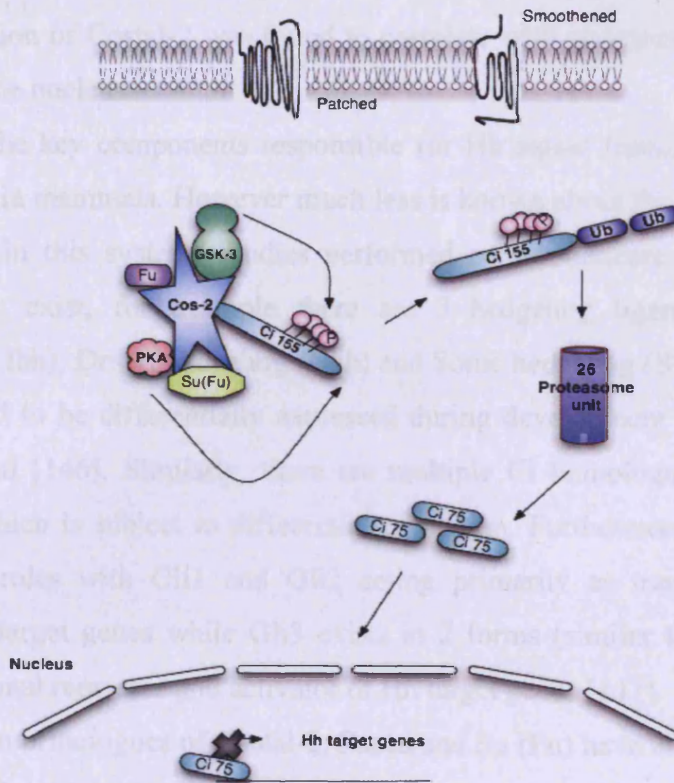
The Hedgehog signal transduction pathway was initially identified and characterized in *Drosophila* where there is a single Hedgehog ligand (Hh) (Figure 1.4). Hh ligands were shown to stabilize and stimulate the activity of full-length cubitus interruptus (Ci), a protein shown to act as a transcriptional activator of Hh target genes [128, 129].

In the absence of Hh ligands, Ci was found to be phosphorylated at S856 and S892 by PKA and subsequently at S852, S884 and S888 by GSK-3 [130, 131]. Phospho-Ci was further phosphorylated by members of the CK1 family, leading to its recognition by β TrCP and proteosomal processing [131, 132]. In contrast with Wnt signalling, in which β -catenin is fully degraded, full-length Ci (Ci155) was found to be only partially processed, generating a truncated protein (Ci75) that acts as a transcriptional repressor of Hh target genes [129].

As discussed previously, efficient β -catenin phosphorylation requires the formation of the multi-protein destruction complex. Similarly, efficient phosphorylation of Ci155 was found to be dependent on the formation of a multi-protein complex known as the 'hedgehog-signaling complex' (HSC). This multi-protein complex consists minimally of the kinesin-like protein Costal-2, and the serine/threonine kinase Fused (Fu), Suppressor of fused (Su (Fu)), PKA, GSK-3 and CK1 [21, 133-135]. In addition to facilitating efficient phosphorylation of Ci155, this complex was found to localize to microtubules in an ATP dependent manner and prevented the nuclear translocation of Ci155 [21, 133-136].

In the absence of Hh ligands the transmembrane Hh receptor protein Patched (Ptc) was found to inhibit the activity of a second Hh receptor protein, Smoothened (Smo) [137]. At present, the mechanisms involved in this inhibition remain poorly understood. However it is likely that alterations in phosphorylation state, protein stability and subcellular localization are involved [138-140].

A



B

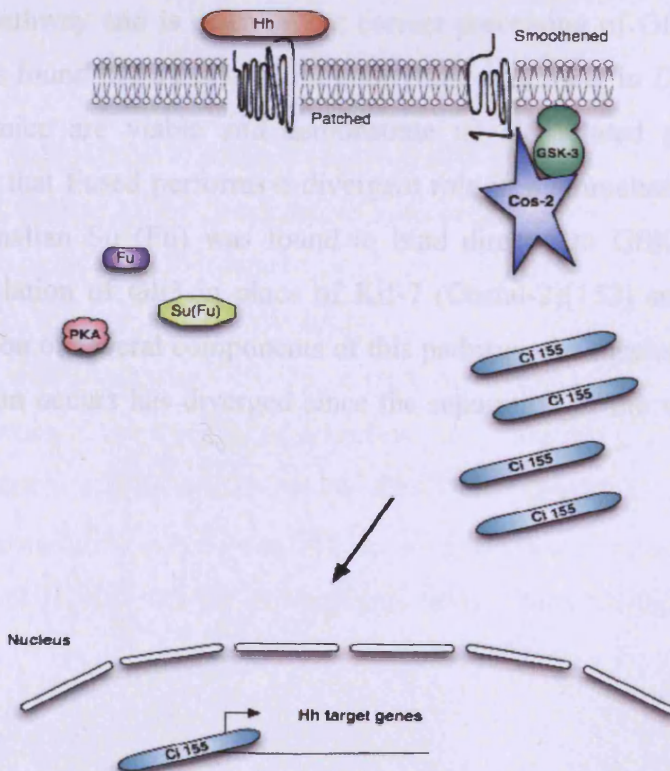


Figure 1.4. Schematic representation of Hh signal transduction

A. In the absence of a Hedgehog (Hh) ligand the 'Hh signalling complex', consisting minimally of Costal-2, GSK-3, Fused, Suppressor of Fused, and PKA mediates the phosphorylation of full length Cubitus interruptus (Ci155). Phospho-Ci is the ubiquitinated and undergoes partial proteolysis to form Ci(75). Ci(75) translocates to the nucleus where it acts as a transcriptional repressor of Hh target genes.

B. In the presence of a Hh ligand the Ci(155) is no longer phosphorylated or processed. This may involve the recruitment of Costal-2 and GSK-3 to the plasma membrane by Smoothed. Ci155 translocates to the nucleus where it acts as a transcriptional activator of Hh target genes.

In response to an Hh ligand, repression of Smo was shown to be alleviated [140-142]. Smo was found to bind directly to Costal-2, sequestering it to the membrane [143-145]. Translocation of Costal-2 was found to correlate with accumulation and translocation of Ci155 to the nucleus.

Many of the key components responsible for Hh signal transduction in *Drosophila* are conserved in mammals. However much less is known about the mechanisms of Hh signal signalling in this system. Studies performed so far indicate that additional levels of complexity exist, for example there are 3 hedgehog ligands in mammals; Indian hedgehog (Ihh), Desert hedgehog (Dhh) and Sonic hedgehog (Shh). Each of these ligands were found to be differentially expressed during development with Shh being the most wide-spread [146]. Similarly, there are multiple Ci homologues; Gli1, Gli2 and Gli3, each of which is subject to differential regulation. Furthermore, these proteins perform divergent roles with Gli1 and Gli2 acting primarily as transcriptional activators of hedgehog target genes while Gli3 exists in 2 forms (similar to Ci) and acts as both a transcriptional repressor and activator of Hh target genes [147].

Mammalian orthologues of Costal-2, Fused and Su (Fu) have all been identified. Kif-7, a member of the kinesin family has been proposed to be the mammalian orthologue of Costal-2. Recent mouse knockout studies have confirmed that Kif-7 is a component of the Shh pathway and is essential for correct processing of Gli3 in mammals [148, 149]. Fused was found to be essential for embryonic patterning in *Drosophila* [150]. However *Fu* null mice are viable and demonstrate no Hh related phenotypes [151] perhaps indicating that Fused performs a divergent role in mammalian Hh signalling. Similarly, the mammalian Su (Fu) was found to bind directly to GSK-3 and facilitate efficient phosphorylation of Gli3 in place of Kif-7 (Costal-2) [152] suggesting, that despite the conservation of several components of this pathway, the mechanisms by which Hh signal transduction occurs has diverged since the separation of the vertebrate and invertebrate lineages.

1.9 Regulation of the cytoskeleton by GSK-3

Neurons are highly polarized cells consisting of a single axon and multiple dendrites that are structurally and functionally distinct [153]. Initially, a nerve cell body will generate lamellipodia at the cell surface, followed by the extension of multiple immature neurites. During this process, one neurite will undergo a transition and initiate a period of rapid growth to form an axon. The remaining immature neurites develop more slowly and become dendrites [154]. Multiple signalling pathways cooperate to bring about these changes in cell structure, and GSK-3 performs roles in several of these pathways.

The extension of immature neurites requires the assembly of a stable microtubule infrastructure. Microtubules consist of α - and β -tubulin dimers and cycle between phases of growth and shrinkage (reviewed in [155]). Polymerization and stability of microtubules is regulated by a number of microtubule-associated proteins (MAPs). GSK-3 has been shown to phosphorylate several MAPs, including CLASP2[156], APC [157], Tau [158] and MAP2C [159]. Each of these MAPs influences stability through direct interactions with microtubules, but the mechanisms remain unclear. GSK-3-phosphorylated forms of APC, Tau and MAP2C all exhibit decreased affinity towards microtubules and fail to stabilize them [157-159]. Components of the Wnt signalling pathway may regulate the ability of GSK-3 to phosphorylate these targets; Dishevelled (Dvl) and Axin were both shown to localize to microtubules and influence their stability by inhibiting GSK-3 activity [160], although the mechanism is not known. Unlike the canonical Wnt pathway, this system does not influence gene transcription, indicating that these proteins function in a microtubule-specific pathway [160].

The establishment of the presumptive axon seemingly requires the inhibition of GSK-3 activity; Jiang et al. [161] demonstrated that S9-phosphorylated GSK-3 β localized most strongly to the tip of the presumptive axon. Furthermore, treatment with GSK-3 inhibitors, shRNA against GSK-3 β or peptides containing a GID led to the formation of multiple axons at the expense of dendrites [161]. Recently, Gärtner et al. [162] reported that the neurons of S21A GSK-3 α /S9A GSK-3 β double knock-in mice develop normally. The neurons of these mice were still sensitive to GSK-3 inhibitors, indicating that while regulation of GSK-3 activity is important, serine phosphorylation alone is not sufficient

to determine the identity of the presumptive axon. It was interesting that peptides containing a GID caused the formation of multiple axons, suggesting that scaffolding proteins may interact with and direct GSK-3 activity within these cells.

Neurite retraction also correlated with GSK-3 activity; the inhibitory guidance molecule Semaphorin-3A (Sema3A) was shown to influence the availability of phospho-S9 GSK-3 β located at the leading edge of the axon and caused neurite retraction [163]. The GSK-3 substrates CRMP2 and CRMP4 were both identified as downstream targets of Sema3A signalling, and phosphorylation of these proteins reduced their ability to stabilise growth cones via the actin cytoskeleton [164, 165].

Careful regulation of microtubule dynamics is also required during mitosis to orient and assemble a spindle apparatus that accurately segregates chromosomes. Wakefield et al. [70] reported that GSK-3 β localises specifically to mitotic microtubules and to the centrosome. Furthermore, inhibition of GSK-3 caused defects in astral microtubule length, chromosome alignment and an increase in the frequency of micronuclei [70, 166, 167], suggesting that GSK-3 activity is required during mitosis. Loss-of-function studies in a number of systems have shown that cell division can proceed in the absence of GSK-3 but report that the process is more prone to error and delay. In *S. cerevisiae*, deletion of the *GSK-3* homologue *MCK1* increased the rate of mitotic chromosome loss [168], while in *C. elegans*, RNAi depletion of *GSK-3* interfered with mitotic spindle orientation in 4 cell-stage embryos [169]. In *Drosophila* embryos, loss of *GSK-3* (*sgg*) interfered with interactions between spindle tubules and cortical actin [170]. Depletion of other canonical components of the Wnt signalling pathway induced related phenomena. For example, loss of *APC* in *Xenopus* extracts or expression of truncated APC in colorectal tumour cells was associated with defects in mitotic spindle assembly [171, 172]. Similarly, loss of β -catenin or expression of *AXIN2* was found to be associated with increases in mitotic errors [91, 173]. These findings, in conjunction with the characterisation of the roles of Dvl and Axin during neurite extension, may be indicative of a central role for components of the Wnt pathway in the regulation of microtubule dynamics.

1.10 Regulation of apoptosis and cell viability

GSK-3 was shown to induce apoptosis in response to a range of stimuli including DNA damage [52], hypoxia [174], removal of NGF [175] or BDNF [176], exposure to staurosporine and heat shock [177]. GSK-3 elicits a response to these stimuli through the regulation of transcription factors (discussed below) including p53 [52] and heat shock factor-1 [178]. Furthermore, as part of a pro-apoptotic signalling cascade, GSK-3 phosphorylates and inhibits the translation initiation factor eIF2B, providing a link between the global regulation of protein synthesis and cell survival [179, 180]. Conversely, complete loss of GSK-3 β also resulted in apoptosis due to a failure to activate the TNF α /NF κ B survival signalling pathway [23]. These observations make it difficult to predict the outcome of GSK-3 inhibition in particular systems due to the range of potentially conflicting roles that may be played.

1.11 Regulation of transcription factors

A plethora of putative GSK-3 substrates have been identified, a large proportion of these are transcription factors that include c-Jun [181, 182], c-Myc [183], CREB [184], NFATc [185, 186], HSF-1 [178, 187] and STATa [188]. GSK-3 negatively regulates the activity of these transcription factors via a number of different mechanisms. For example, N-terminal phosphorylation of NFATc or STATa by GSK-3 induced nuclear export [185, 188], while phosphorylation of c-Myc at S62 by GSK-3 targeted the protein for ubiquitin-mediated proteolysis [183]. In contrast, c-Jun, CREB, HSF-1 and NFATc exhibited reduced binding affinity towards their target DNA sequences following GSK-3-directed phosphorylation [186, 187, 189, 190].

The ability of GSK-3 to target transcription factors clearly requires multiple levels of regulation to ensure differential targeting of substrates. Specifically, localisation of GSK-3 is fundamental in regulating its activity towards transcription factors in the same way that localization of GSK-3 to mitotic spindles is key to regulating its role in spindle dynamics. Removal of growth factors or treatment with staurosporine causes nuclear accumulation of GSK-3 that presumably alters the access of GSK-3 to nuclear targets. Conversely, both FRAT- and Axin-bound GSK-3 were shown to be exported from the

nucleus via a CRM-1-dependent mechanism [191, 192]. Mutations to the SBR of GSK-3 enhanced nuclear accumulation, suggesting that scaffolding proteins including Axin and FRAT are at least in part responsible for GSK-3 nuclear export.

1.12 The role of GSK-3 in *Dictyostelium*

Dictyostelium amoebae exist as individual cells in the presence of an abundant food source. Upon starvation, up to 100,000 amoebae will aggregate to form a multicellular structure (Figure 1.5). The aggregation of single cells is coordinated by the pulsatile release of cyclic AMP (cAMP). cAMP acts as a chemo attractant and as a regulator of developmental gene expression via signal transduction through a family of cAMP receptors, cAR1 and cAR3 which have a high affinity for cAMP, and low-affinity cAMP receptors cAR2 and cAR4.

Under these conditions cells form a mound surrounded by an extracellular matrix and begin to differentiate into pre-spore and pre-stalk cells [193]. These cells re-distribute themselves within the mound as it becomes a finger-like structure and frequently topple over to form migratory slugs. Upon finding favourable conditions a slug will undergo terminal differentiation to form a fruiting body consisting of a ball of spores supported on a stalk.

The *Dictyostelium* genome encodes a single GSK-3 homologue, GskA. Expression of GskA is not essential for cell survival; *gskA* null cells are viable [194]. However, these cells do exhibit developmental abnormalities; slugs migrate shorter distances and fruiting bodies develop with an enlarged basal disc and small spore head [194].

The pre-stalk marker *ecmB* was found to be ectopically expressed in *gskA* null cells [194]. Expression of *ecmB* and subsequent stalk cell differentiation is inhibited by cAMP while spore cell differentiation requires cAMP. Since loss of GskA results in aberrant *ecmB* expression and expansion of the proportion of stalk cells it would suggest that GskA normally acts as part of a pathway to repress stalk cell differentiation during development [194, 195].

In addition to inappropriate *ecmB* expression, Strmecki et al [196] reported that 193 genes exhibited altered expression in the *gskA* null cell line. A list of these genes with details of the fold change in expression was provided in a personal communication with

Gareth Bloomfield (Appendix Table A.1). Analysis of the gene ontology (GO) terms for these genes revealed that a significant number of proteins that were under-represented in the *gskA* nulls were associated with catabolic and proteolytic processes (Appendix Table A.2). A significant number of genes that were reportedly over-represented are associated with processing of ATP, and biosynthetic and metabolic pathways linked to ribonucleotides (Appendix Table A.3).

The dual-specificity kinase, Zak1, was found to act downstream of cAR3 and directly phosphorylate Tyr214 of GskA (analogous to Tyr 216 of mammalian GSK-3 β) [80, 82]. As described previously, phosphorylation of Tyr214 is associated with an increase in kinase activity. It has been suggested that the combinatorial actions of ZAK1 and an unidentified tyrosine phosphatase may act to differentially regulate GskA activity during development and as such direct differential expression of cell type markers[81].

Despite the identification of a role for GskA during development and the characterization of the downstream consequences of its loss, only a single GskA substrate has been identified; the transcription factor STATa. Phosphorylation of STATa by GskA is associated with increased nuclear export [188]. A comprehensive list of STATa target genes is not yet available so it is unclear whether the effects on gene expression seen in the *gskA* null cell line can be solely attributed to mis-regulation of STATa activity. However, given the large number of GSK-3 substrates identified in other systems this is unlikely.

There is emerging evidence that GskA activity may be directed towards specific substrates by interacting with binding proteins; specific point mutations (V267G and E268R) introduced into the scaffold-binding region of mammalian GSK-3 β were found to completely abrogate an interaction with Axin, while the ability of GSK-3 β to associate with FRAT was only minimally affected. To date, no Axin homologue has been identified in *Dictyostelium*. However, Fraser et al [98] reported that expression of mutated GskA V267G/E268R in wild type *Dictyostelium* (Ax2) cells resulted in an altered morphology: cells failed to polarize correctly, exhibited a rounder leading edge and very slow contraction of the cell rear. Indeed, the trailing edge of the cell was often dragged along as a bulge. Additional bulges and constrictions were also observed along

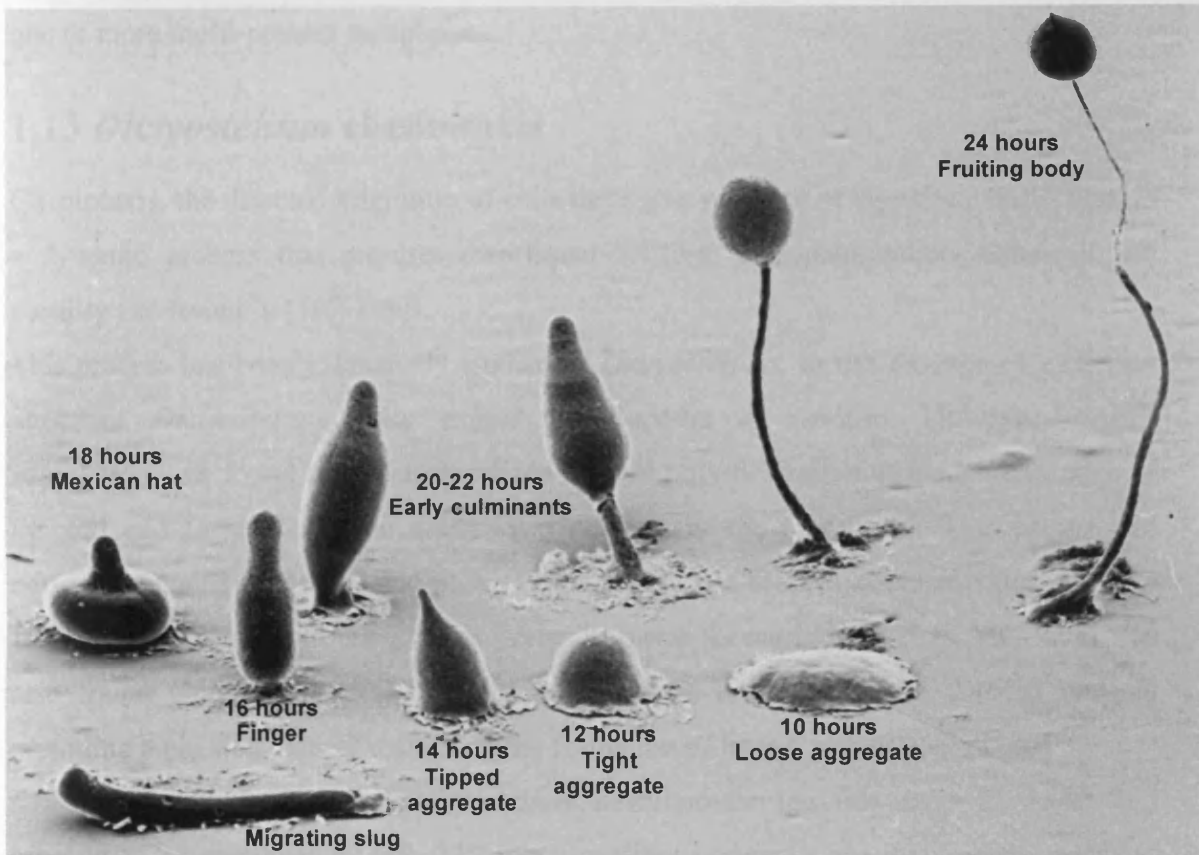


Figure 1.5 The *Dictyostelium* developmental cycle

In response to starvation, cells aggregate together using cAMP as a chemo-attractant, forming a loose aggregate after approximately 10 hours. These aggregates become tighter over the next few hours and form a finger-like structure. These finger-like structures frequently topple over to form pseudoplasmodium or 'slugs', which migrate towards a source of light. Upon finding favourable conditions a slug will re-enter development and over the next 8 hours undergo terminal differentiation to form a mature fruiting body.

This image is used with permission of copyright holders

(Copyright, M.J. Grimson & R.L. Blanton, Biological Sciences Electron Microscopy Laboratory, Texas Tech University)

the body of the cell. The dominant effect of expressing this mutated protein could lead one to propose that GskAs role(s) in *Dictyostelium* is directed through the formation of one or more multi-protein complexes.

1.13 *Dictyostelium* chemotaxis

Chemotaxis, the directed migration of cells through a gradient of signalling molecules, is a dynamic process that requires directional sensing, cell polarization, adhesion and motility (reviewed in [197-199]).

This process has been extensively studied in *Dictyostelium*. In the absence of a chemo-attractant *Dictyostelium* cells extend pseudopodia at random. However, cAMP stimulation was found to lead to localized F-actin polymerization at the leading edge of the cell and formation of an actomyosin network at the rear [200]. This actomyosin network contains myosin II and provides the contractile force that helps release the cell from the substratum, allowing the posterior to move forward [201, 202]. Myosin II was also found along the lateral sides of cells, where it increases the cortical tension, providing a physical barrier restricting the formation of lateral pseudopodia [200].

Efficient chemotaxis during *Dictyostelium* development requires cells to detect and respond to extracellular cAMP. Multiple signalling pathways are involved in directing chemotaxis, including the PI3K/ PI(3,4,5)P₃ signalling pathway. The cAMP receptors and heterotrimeric G-proteins responsible for binding cAMP and transmitting the signal to downstream effectors were found to be uniformly distributed over the cell surface [203, 204]. Binding of cAMP to its receptor led to the localized activation of Ras, which in turn activated phosphatidylinositol-3-kinase (PI3K) [205]. Following Ras activation, PI3K was recruited to the membrane where it is responsible for the phosphorylation of PI(4,5)P₂ to form PI(3,4,5)P₃ [206-208]. Concurrently, PTEN, the phosphatase responsible for de-phosphorylating PI(3,4,5)P₃ to form PI(4,5)P₂, dissociated from the plasma membrane at the leading edge and was restricted to the lateral sides and rear of the cell [207, 208]. These events led to the localized synthesis and accumulation of PI(3,4,5)P₃ at the leading edge of the cell and subsequent F-actin polymerization.

PI(3,4,5)P₃ was found to recruit pleckstrin homology (PH) domain-containing proteins, such as cytosolic regulator of adenylate cyclase (CRAC), PhdA and PkbA to the plasma membrane. Indeed, the localized accumulation of PI(3,4,5)P₃ has frequently be visualized by through expression of this PH domain fused to GFP [209-214].

Although the precise mechanisms by which PI(3,4,5)P₃ accumulation promotes F-actin polymerization remain unclear it is likely that this ability to locally concentrate PH-domain containing-proteins is pivotal; loss of PhdA or PkbA led to a reduction in actin polymerization and cellular polarization respectively[215, 216].

Cellular polarization defined by the asymmetric accumulation of PI(3,4,5)P₃ at the leading edge of the cell and PTEN at the rear became further pronounced over time through the ability of PI3K to associate with, and become concentrated at sites enriched in cortical F-actin. Cellular polarization also involved the rearrangement of microtubules to enable motor proteins such as dynein and kinesin to perform directed membrane trafficking, and reorientation of the microtubule-organizing centre (MTOC) towards the direction of migration.

Lithium, a GSK-3 inhibitor, has been shown to affect chemotaxis, and it has been proposed that this affect may be mediated through inhibition of GSK-3[217]. However, until recently this suggestion has not been explored further (See Chapter 4 for details).

1.14 Dictyostelium Cytokinesis

Cytokinesis involves a highly co-ordinated series of events that leads to the formation of two daughter cells [218-220] (Figure 1.6). Initially, a mitotic spindle forms and chromosomes become aligned along the equator of the cell. During anaphase, as the chromosomes separate and move towards opposite poles of the cell, the contractile ring, consisting of actin filaments interspersed with myosin II, accumulates equatorially at the cell cortex. Myosin II-dependent constriction of the contractile ring causes furrowing of the cell membrane and as telophase progresses the cleavage furrow constricts so that only a cytoplasmic bridge links the two daughter cells. Finally, the two cells are separated following scission of this cytoplasmic bridge. This method of cytokinesis is termed 'cytokinesis A'.

In *Dictyostelium*, cells that lacked the gene encoding myosin II heavy chain (*mhcA*) or had the *mhcA* gene silenced by over-expression of antisense RNA failed completely to undergo cytokinesis when grown in shaking culture [221, 222]. These cells increased in size and accumulated nuclei until they eventually lysed. However, these cells were viable when grown on a solid surface [221, 222]. Neujahr et al [223, 224] report that when grown on a solid surface these cells were capable of forming a cleavage furrow and divided via a process termed ‘cell-cycle coupled, adhesion dependent cytokinesis’ or ‘cytokinesis B’. This method of cytokinesis was found to be an extremely robust process, despite taking approximately twice as long as cytokinesis A [225].

Nagasaki et al [226] reported that when these large, multinucleate *mhcA* null cells were allowed to adhere to a solid surface these cells rapidly underwent a series of divisions to become mono-nucleate. This method of cytokinesis was not linked to progression of the cell cycle, and involved the cells forming multiple leading edges that tore the cell into multiple fragments. This process was later termed ‘traction-mediated cytofission’ or ‘cytokinesis C’ [226, 227].

More recently, a fourth method of cytokinesis has been described, ‘cytokinesis D’, which requires the assistance of a neighbouring cell. This neighbouring cell performs the role of ‘midwife’ by chemotaxing towards the equator of the mitotic cell and passing over the intracellular bridge between daughter cells aiding severage [226, 228]. This method of completing cytokinesis is clearly different to typical scission and appears to occur at low frequency in *Dictyostelium* unless the pathways controlling Cytokinesis A and Cytokinesis B are both disrupted. Nagasaki et al [228] demonstrated that nearly half the cytokinesis events that occurred in *mhcA* null cells involved the attraction of a neighbouring cell to the cleavage region. Furthermore, Nagasaki et al [228] demonstrated that cells that lacked gene encoding the beta subunit of the trimeric G protein (G_{β}) and were incapable of chemotaxis, did not show such midwifery. The authors also demonstrated that in wild-type cells, PI(3,4,5)P₃ became enriched in the anterior region of midwifing cells, consistent with the view that this midwifery was directed by chemotaxis towards a source of cAMP.

The underlying signalling pathways responsible for mediating the different forms of cytokinesis remain largely unclear, however there is emerging evidence PI3K signalling

performs a role in more than one method of cytokinesis. Janetopoulos et al [229] found that cells lacking both PI3K and PTEN activity (*pi3k*¹⁻²⁻, *pten* null cells) failed to divide when grown in shaking culture. The authors demonstrated that in wild-type cells, Ras, PI3K and associated PI(3,4,5)P₃ accumulation was uniformly suppressed at the onset of cytokinesis as cells rounded up [229, 230]. Concurrently, PTEN was found to be evenly distributed at the cellular cortex. As cells progressed through mitosis, PTEN localisation became limited to the developing furrow, which coincided with myosin II accumulation. Simultaneously, activated Ras and PI(3,4,5)P₃ could be seen to gradually accumulate to the polar ruffles during spindle assembly, cell elongation, and cytokinesis [229, 230]. When the daughter cells separated from one another, cortically localized PI(3,4,5)P₃ increased dramatically, resulting in high levels of random pseudopod extension [230]. Cells lacking G_β (*gβ*⁻) still exhibited Ras activation, and associated PI3K / PI(3,4,5)P₃ signalling, during cytokinesis, suggesting that a G_β-independent Ras/PI3K signalling pathway may perform a fundamental role in regulating cytokinesis A.

1.15 Aims of this study

The aim of this study was to gain a better understanding of the mechanisms of cytokinesis in Dictyostelium.

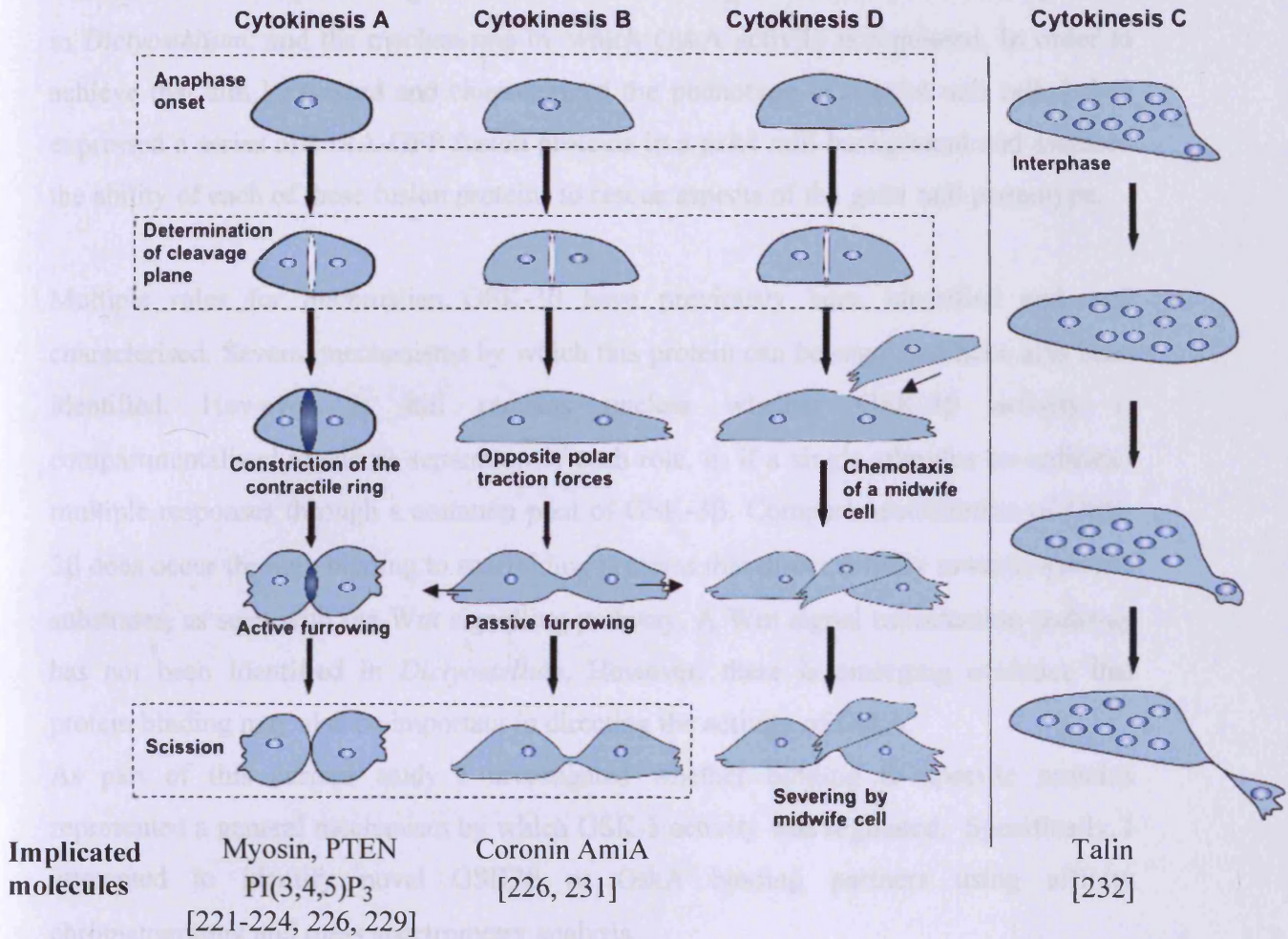


Figure 1.6. Mechanisms of cytokinesis in Dictyostelium

Dictyostelium undergo cytokinesis via one of four proposed models. Cytokinesis A is a myosin-dependent, adhesion independent method while Cytokinesis B represents a myosin-independent, adhesion-dependent method. Cytokinesis C occurs when cells that have become multi-nucleate in shaking culture are returned to a solid surface. This form of cytokinesis occurs independent of position in the cell cycle (shown here at a lower 'magnification'). Cytokinesis D requires the services of a midwife cell to complete cytokinesis.

Proteins implicated in each of these models are highlighted.

Based on a diagram in Uyeda, T.Q. and A. Nagasaki, Variations on a theme: the many modes of cytokinesis. Curr Opin Cell Biol, 2004. 16(1): p. 55-60.

1.15 Aims of this study

The aim of this study was to gain a better understanding of the role performed by GskA in *Dictyostelium*, and the mechanisms by which GskA activity is regulated. In order to achieve that aim I assessed and characterized the phenotype of a *gskA* null cell. I then expressed a series of GskA-GFP fusion proteins in a *gskA* null background and assessed the ability of each of these fusion proteins to rescue aspects of the *gskA* null phenotype.

Multiple roles for mammalian GSK-3 β have previously been identified and well characterised. Several mechanisms by which this protein can be regulated have also been identified. However, it still remains unclear whether GSK-3 β activity is compartmentalized to ensure separation of each role, or if a single stimulus co-ordinates multiple responses through a common pool of GSK-3 β . Compartmentalization of GSK-3 β does occur through binding to scaffolding proteins that direct activity towards specific substrates, as seen with the Wnt signalling pathway. A Wnt signal transduction pathway has not been identified in *Dictyostelium*. However, there is emerging evidence that protein binding may also be important in directing the activity of GskA.

As part of this current study I investigated whether binding to specific proteins represented a general mechanism by which GSK-3 activity was regulated. Specifically, I attempted to identify novel GSK3 β or GskA binding partners using affinity chromatography and mass spectrometry analysis.

Chapter 2

Materials and Methods

2.1 Cloning

Throughout this project, all plasmids constructed were primarily screened by restriction digest. All enzymes were supplied by New England Biolabs and used in the appropriate buffer. For screening of plasmid clones, approximately 0.5 µg of DNA from each was digested with enzyme and analysed by agarose gel electrophoresis. Clones to be used for protein expression were then subsequently sequenced. Ligations were carried out at room temperature for approximately 1-2 hours using T4 DNA ligase (New England Biolabs). Generally a 3:1 molar ratio of vector : insert was used.

2.1.1 Dictyostelium Vectors

pDXA GFP2

The pDXA GFP2 (Accession No. AF269235) vector contains coding sequence for the GFPmut2 variant of green fluorescent protein flanked by multiple cloning sites allowing incorporation of additional coding sequence to produce either N or C-terminal fusion proteins. GFPmut2 expression is under the control of the constitutive actin promoter *act15* [233]. This vector provides G418 resistance and contains Ddp2; a cis-acting extrachromosomal replication element. To enable extrachromosomal replication pDXA GFP2 must be co-transfected with the pREP vector, in the absence of pREP this vector will be maintained via chromosomal integration [234].

pDXA GskA-GFP2

H. Williams previously cloned the coding region of *GskA* into pDXA GFP2 via Kpn1 and Nsi1 restriction sites, such that a GskA-GFP2 fusion protein was expressed under the control of *act15*.

pDXA GskA-GFP2 Y214G / pDXA GskA-GFP2 R96E / pDXA GskA-GFP2 K85R

H. Williams previously introduced separate point mutations into the coding region of the pDXA GskA-GFP2 vector using the Stratagene QuikChange Site-Directed Mutagenesis Kit as per the manufacturers direction. Mutations were introduced to alter K85, R96 or Y214 of GskA to arginine (K85), glutamic acid (R96) and glycine (Y214) residues.

2.1.2 Mammalian Vectors

pSK(-) GSK-3 β

The coding region of human GSK-3 β was previously cloned into the vector pSK(-) via EcoR1/HincII restriction sites, such that a C-terminally tagged 6xHis-GSK-3 β fusion protein was encoded. This plasmid was a kind gift from the Woodgett lab.

pEGFP-N3

The pEGFP-N3 vector (Accession No. U57609) is commercially available from BDBioscience. This vector contains coding sequence for the EGFPmut1 variant of green fluorescent protein, which contains the double-amino-acid substitution of Phe-64 to Leu and Ser-65 to Thr [235]. The coding sequence of the EGFP gene also contains more than 190 silent base changes that correspond to human codon-usage preferences [236]. A multiple cloning sites located upstream of the EGFPmut1 coding region allows incorporation of additional coding sequence to produce C-terminal fusion proteins. EGFPmut1 expression is under the control of the constitutive CMV promoter. This vector confers G418 resistance.

pEGFP-N3-GSK-3 β

The coding region of GSK-3 β (lacking the STOP codon) was cloned into the pEGFP-N3 vector via NdeI and KpnI restriction sites, GSK-3 β -EGFPmut1 fusion protein was expressed under the control of the CMV promoter.

pCR-Blunt II-TOPO GSK-3 β

A PCR product encoding the coding region of GSK-3 β , flanked 5' by NdeI and AflIII restriction sites and 3' by a KpnI restriction site, was introduced into the pCR-Blunt II-TOPO vector as per manufacturers instructions. This plasmid was used as an intermediate between PCR product and the pEGFP-N3-GSK-3 β vector.

pcDNA5/FRT/TO

The pcDNA5/FRT/TO vector is commercially available from Invitrogen and is designed for use with the Flp-In T-REx System. The pcDNA5/FRT/TO vector encodes a hybrid human cytomegalovirus (CMV) / Tetracycline Operator 2 (TetO₂) promoter. Briefly, this promoter consists of a CMV immediate early enhance/promoter into which 2 copies of the TetO₂ sequence have been inserted in tandem. These TetO₂ sequences are 19 nucleotides long each, and act to confer regulation by tetracycline to the promoter [237-241]. Down-stream of the CMV/TetO₂ promoter is a multiple cloning site that allows incorporation of a gene of interest. The pcDNA5/FRT/TO vector also contains a single Flp recombinase target (FRT) site for Flp recombinase-mediated integration of the vector into the Flp-In T-REx HEK 293 host cell line when co-transfected with the pOG44 vector. This vector confers hygromycin resistance.

pcDNA5/FRT/TO GSK-3 β -GFP

The coding region of GSK-3 β -EGFPmut1 was cloned into the pcDNA5/FRT/TO vector via AflIII and NotI restriction sites, such that a GSK-3 β -EGFPmut1 fusion protein was expressed under the control of the CMV/TetO₂ hybrid promoter.

pcDNA5/FRT/TO EGFPmut1

The coding region of EGFPmut1 was cloned into the pcDNA5/FRT/TO vector via KpnI and NotI restriction sites, such that the EGFPmut1 protein was expressed under the control of the CMV/TetO₂ hybrid promoter.

pOG44

The pOG44 vector is a Flp recombinase expression vector, commercially available from Invitrogen and is designed to be used with the Flp-In T-REx System. When cotransfected with the pcDNA5/FRT/TO vector into the Flp-In 293 host cell line, the Flp recombinase expressed from pOG44 mediates integration of the pcDNA5/FRT/TO vector into the genome via Flp recombination target sites. The pOG44 vector encodes a CMV promoter, followed by a synthetic intron (to enhance expression of *FLP* gene) and *FLP* gene in series. This vector confers ampicillin resistance.

pcDNA 3.1 FLAG-Ax1

E. Fraser previously constructed a vector encoding a quadruple FLAG tagged portion of Axin (corresponding to amino acids 367-701) under the control of a CMV promoter. This plasmid contains a pcDNA3.1+ backbone (Invitrogen).

pcDNA 3.1 FLAG-Ax1 L521P

E. Fraser previously introduced point mutations into the coding region of the pcDNA 3.1 FLAG-Ax1 vector using the Stratagene QuikChange Site-Directed Mutagenesis Kit as per the manufacturers direction. A mutation was introduced to alter L521 of Axin to a proline residue.

pcDNA 3.1 FLAG-FRAT

E. Fraser previously constructed a vector encoding a quadruple FLAG tagged FRAT under the control of a CMV promoter. This plasmid contains a pcDNA3.1+ backbone (Invitrogen).

pcDNA 3.1 FLAG-FRAT K208A/E209Q

E. Fraser previously introduced point mutations into the coding region of the pcDNA 3.1 FLAG-FRAT vector using the Stratagene QuikChange Site-Directed Mutagenesis Kit as per the manufacturers direction. Mutations were introduced to alter K208 and E209 to alanine and glutamine residues respectively.

2.2 PCR

cDNA encoding GSK3 β was amplified by PCR using the Pfu proofreading polymerase (Promega) as per the manufacturers instructions. The following primers were used: GCAGGCCATATGCTTAAGTGATCATGTCA / ACAATTATCGATGGTGGAGTTG GAAGC. The PCR product was then gel-purified and cloned into pCR-Blunt II-TOPO (Invitrogen) before validation.

2.3 Cell culture

2.3.1 Dictyostelium cell culture

Dictyostelium cells were grown axenically in HL-5 medium (14 g/L proteose peptone, 7 g/L yeast extract, 13.5 g/L glucose, 0.5 g/L Na₂HPO₄, 0.5 g/L KH₂PO₄, pH 6.4.) (Formedium) for normal culture and antibiotic selections. All transformed cell lines were grown in the presence of 40 µg ml⁻¹ Geneticin (G418). The *gskA* null strain [194] was grown in the presence of 10 µg ml⁻¹ Blasticidin. Cells were also allowed to develop on SM agar plates (10 g/L proteose peptone, 1 g/L yeast extract, 10 g/L glucose, 1.9 g/L KH₂PO₄, 1.3 g/L K₂HPO₄·3H₂O, 0.49 g/L MgSO₄, 17 g/L agar) on a lawn of *Klebsiella aerogenes* by standard methods.

For long-term storage of cell lines, cells were resuspended in freezing media at 10⁷ cells ml⁻¹ then frozen at -80°C in 500 µl aliquots in cryovials. Cells were restored from long-term storage by rapidly defrosting and re-suspending them in axenic media before transferring to 9cm plate with 1% heat killed *E. coli*.

Except where otherwise stated, the Ax2 strain was used as wild-type and the (Ax2)/*gskA* null strain was used as the parent of all mutants. Cells were both starved and washed in KK2 buffer (16.5 mM KH₂PO₄, 3.8 mM K₂HPO₄ pH 6.2). When required, cells were pelleted by centrifugation at 700 x g for 2 minutes.

2.3.2 Mammalian cell culture

The Flp-InTM T-RExTM 293 cell line is commercially available from Invitrogen and is derived from human embryonic kidney (HEK) -293 cells [242]. This parental cell line was obtained from the American Type culture collection (item number CRL-1573). The Flp-In T-REx 293 cell line has previously been transfected such that two cassettes have integrated randomly into the genome (Figure 2.1). The first of these cassettes encodes a *LacZ*-Zeocin fusion gene expressed from an SV40 promoter. The *LacZ*-Zeocin fusion gene incorporates an FRT site directly downstream of the ATG start codon. This cassette confers Zeocin resistance to the cells that, following transfection (and integration through the aforementioned FRT site) of the pcDNA5/FRT/TO vector is lost.

The second cassette encodes the Tetracycline repressor (*TetR*) gene under control of a CMV promoter, followed by a Blasticidin resistance gene under control of an SV40 promoter. In the absence of tetracycline, the tetracycline repressor protein binds to and prevents expression from the CMV/TetO₂ hybrid promoter located on the pcDNA5/FRT/TO vector.

Flp-In T-REx 293 cells were grown in D-MEM supplemented with 10% heat inactivated Fetal Calf Serum (Gibco), 1% Pen/Strep, 0.5% L-Glutamine 50mg/ml (GIBCO).

Prior to transfection, media was supplemented with 100µg/ml zeocin and 12µg/ml blasticidin. Following transfection, media was supplemented with 300µg/ml hygromycin and 12mg/ml blasticidin.

For long-term storage of cell lines, cells were resuspended in freezing media at 10⁷ cells ml⁻¹ then frozen at -80°C in 1ml aliquots in cryovials. Cells were restored from long-term storage by rapidly defrosting and re-suspending them in warm tissue culture media before transferring to T80 tissue culture flask (Nunc).

In all cases, except where otherwise stated, the Flp-In T-REx 293 cells was used as wild-type and is the parent of all mutants. When required, cells were pelleted by centrifugation at 750 x g for 5 minutes.

2.4 Transformations

2.4.1 Dictyostelium transformations

Cells were transformed by electroporation as previously described [243-245]. Briefly, 10⁷ cells, growing in log-phase were washed once in ice-cold electroporation buffer (50mM sucrose in KK2) before being resuspended to a final volume of 800µl in an electroporation cuvette. 20µg of plasmid DNA was then added and incubated on ice for 10 minutes. Cells were electroporated at 1kV before a further 10 minute incubation on ice. The cells were then transferred into a 10cm petri dish and 8µl of salt solution (0.1M MgCl₂, 0.1M CaCl₂) added. After a further 20 minutes the cells were then finally resuspended in 10 ml of non-selective axenic media containing Streptomycin sulphate and 1% heat killed *E. coli*.

After 24 hours, cells were transferred into 6 x 96 well plates in the presence of 40 µg/ml G418. After approximately 2 weeks, multiple clones were selected and transferred into individual wells of a 24 well plate for screening.

2.4.2 Mammalian transformation

Cells were transfected using TransFectin™ lipid reagent (BioRad) as per the manufacturers instructions. Briefly, cells were seeded onto 6-well plates the day before transfection, such that they were approximately 80% confluent on the day of transfection. On the day of transfection, the cell media was aspirated and replaced with 2 ml media containing no antibiotics. Cells were allowed to settle for a minimum of two hours.

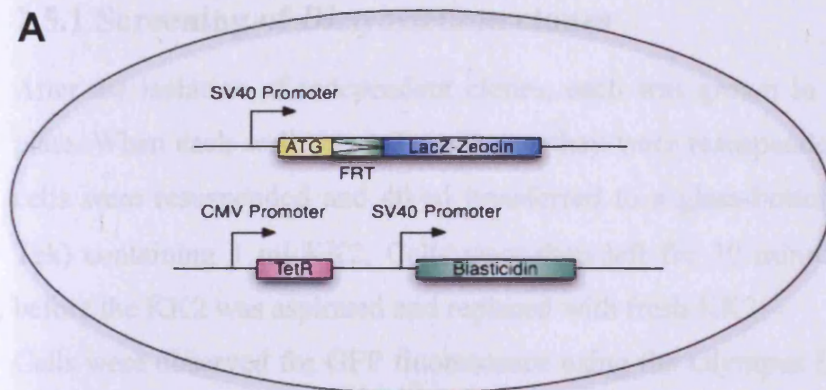
500µl of DNA-TransFectin complexes (2.2µg plasmid DNA; 10:1 ratio of pOG44 plasmid to plasmid of interest, 8µl TransFectin reagent, all in 500µl Optimem) was added and cells were left for a further 4 hours. After 4 hours the media was aspirated off and replaced with antibiotic free media.

After 24 hours, cells were washed with PBS and treated with trypsin. Cells were resuspended in 3ml of media and transferred to 9cm plates containing 7ml of antibiotic free media. Cells were incubated over night to allow them to recover from trypsin treatment and attach to the plate. After 24 hours, media was aspirated and replaced with media containing 300µg/ml hygromycin and 12µg/ml blasticidin.

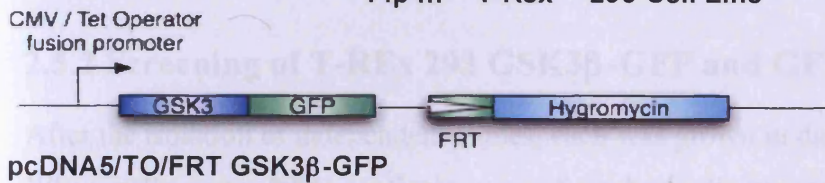
After approximately 2 weeks, multiple clones were seen and transferred into individual wells of a 24 well plate for screening.

2.5 Screening of Clones

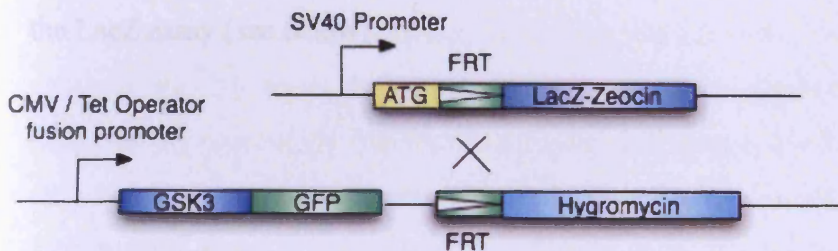
A



Flp-In™ T-Rex™-293 Cell Line



B



C

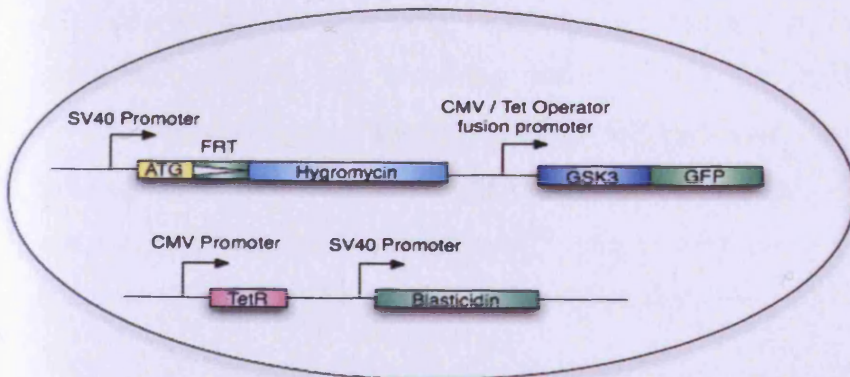


Figure 2.1. Schematic representation of Flp-In T-Rex system

A. The Flp-In T-Rex 293 cell line are derived from HEK293 cells and contain 2 cassettes integrated into their genome. The first encodes a LacZ-Zeocin fusion protein downstream of an FRT site. The second encodes the Tetracycline repressor (TetR) protein under the control of a CMV promoter.

The plasmid pcDNA5/TO/FRT GSK3β-GFP encodes GSK3β-GFP under the control of a CMV/Tet operator fusion promoter.

B. Following transfection into the Flp-In T-Rex 293 cells, the PCDNA/TO/FRT Gsk3β-GFP plasmid undergoes site directed integration into the genome via a Flp recombinase reaction.

C. The resultant T-Rex GSK3β-GFP cell line contains a stably integrated cassette encoding the GSK3β-GFP fusion. In the absence of Tetracycline or tetracycline derivative the protein product of the TetR gene sits on the Tet Operator promoter sequence preventing gene expression. In the presence of Tetracycline the Tet repressor protein undergoes a conformational change such that it can no longer bind to the Tet Operator sequence and gene expression of the GSK3β-GFP fusion can occur.

2.5 Screening of clones

2.5.1 Screening of *Dictyostelium* clones

After the isolation of independent clones, each was grown in 1ml culture in a 24 well plate. When each well became confluent, they were resuspended in KK2. After 2 hours, cells were resuspended and 40 μ l transferred to a glass-bottomed chamber slide (Lab-Tek) containing 1 ml KK2. Cells were then left for 30 minutes to attach and recover before the KK2 was aspirated and replaced with fresh KK2.

Cells were observed for GFP fluorescence using the Olympus IX71 inverted microscope with a 20x objective, fluorescent cells were selected for further analysis.

2.5.2 Screening of T-REx 293 GSK3 β -GFP and GFP cell lines

After the isolation of independent clones, each was grown in duplicate in a 24 well plate. When cells were 80% confluent one of each duplicate was treated with 0.5mg/ml doxycyclin for 4 hours. Following incubation, media was aspirated from wells cells and cells were harvested in 4xNuPage buffer and assessed by western blot.

Cells were further assessed to ensure integration had occurred into the correct site using the LacZ assay (see below).

2.6 Immunofluorescence

2.6.1 Dictyostelium immunofluorescence

For immunofluorescence imaging, cells were seeded onto 16mm glass coverslips, and allowed to adhere for 30 minutes. Coverslips were then washed twice in KK2 and fixed in 3% paraformaldehyde (in water) for 20 minutes. Cross-linking was quenched in 30mM glycine. Coverslips were then washed three times with PBS and cells were permeabilised in 0.1% TritonX (in PBS) for 5 minutes. Slides were washed in PBS and incubated in 3%BSA (in PBS) for 1 hour. Samples were then stained with M2-mouse α -Sgg primary antibody (1:1,000 dilution Upstate) for one hour, washed three times, and then a Alexa Fluor 647-conjugated α -mouse IgG secondary antibody (1:1,000, Sigma) for a further hour. Coverslips were washed three times (PBS) and incubated with 1 μ g/ml 4',6-Diamidino-2-phenylindole dihydrochloride (DAPI) in water. Coverslips were then washed in water and mounted on slides using Mowiol. Images were taken using the Olympus IX71 inverted microscope with an oil immersion 60x objective.

2.6.2 Mammalian immunofluorescence

For immunofluorescence imaging, cells were seeded onto 16mm glass coverslips, and cultured for 24 hours before being induced for a further 24 hours with 2ng/ml doxycycline. Coverslips were washed twice in PBS and fixed in 3% paraformaldehyde (in PBS) for 20 minutes. Cross-linking was quenched in 30mM glycine. Coverslips were then washed three times with PBS and cells were permeabilised in 0.1% TritonX (in PBS) for 5 minutes. Slides were washed in PBS and incubated in 3%BSA (in PBS) for 1 hour. Samples were then stained with rabbit α -GSK3 β primary antibody (1:1,000 dilution BD Biosciences) for one hour, washed three times, and then a Alexa Fluor 647-conjugated α -rabbit IgG secondary antibody (1:1,000, Sigma) for a further hour. Coverslips were washed three times (PBS) and incubated with 1 μ g/ml 4',6-Diamidino-2-phenylindole dihydrochloride (DAPI) in water. Coverslips were then washed in water and mounted on slides using Mowiol. Images were taken using the Olympus IX71 inverted microscope with an oil immersion 60x objective.

2.7 Western blot

2.7.1 Dictyostelium western blots

For western blotting, 10^7 cells were lysed in 500 μ l lysis buffer (100mM NaCl, 50mM Tris, 0.5% NP-40, 10% glycerol) supplemented with a Roche complete inhibitor tablet. 500 μ l of NuPage buffer (50 mM Tris-HCL pH 6.8, 100 mM dithiothreitol, 2% SDS, 0.1% bromophenol blue, 10% glycerol) was added and samples were boiled for 5 minutes to denature proteins before running on a 4-12% Bis-Tris gel (Invitrogen). The protein from 1.5×10^5 cells was loaded per lane. Western blotting was then carried out using standard methods. A table giving details of the antibodies used in this study can be found below. In all cases Pierce ECL reagent was used as HRP substrate.

2.7.2 Mammalian western blots

Unless otherwise stated, cells from a one well of a 6-well dish were lysed 500 μ l of NuPage buffer (50 mM Tris-HCL pH 6.8, 100 mM dithiothreitol, 2% SDS, 0.1% bromophenol blue, 10% glycerol) and samples were boiled for 5 minutes to denature proteins. Samples were then passed through a fine-gauge needle several times before running on a 4-12% Bis-Tris gel (Invitrogen). 10 μ l was loaded per lane. Western blotting was then carried out using standard methods. A table giving details of the antibodies used in this study can be found below. In all cases Pierce ECL reagent was used as HRP substrate.

Antibody	Species raised in	Dilution used at	Supplier
Anti-CSRP2	Chicken	1:1000	Sigma
Anti-CSNK2A2	Goat	1:1000	Sigma
Anti-Sgg (Used to detect GskA)	Mouse	1:1000	UpState
Anti-GAP-DH	Mouse	1:1000	Sigma
Anti-GFP	Mouse	1:10000	Roche
Anti-alpha tubulin	Mouse	1:1000	Sigma
Anti-LimE	Mouse	1:10	c/o Prof. Annette Müller-Taubenberger
Anti-HNRNP	Mouse	1:1000	Sigma
Anti-GSK-3 β	Rabbit	1:1000	BD Biosciences
Anti-FttB	Rabbit	1:10000	c/o Prof. Annette Müller-Taubenberger
Anti-MLCKA	Rabbit	1:2000	c/o Prof. John Spudich
Anti-TaIB	Rabbit	1:2000	c/o Prof. Kei Inouye
Anti-SUPT16h	Rabbit	1:1000	Sigma
Anti-Sod1	Rabbit	1:1000	Sigma
Anti-mouse	Horse	1:10000	VectaLabs
Anti-rabbit	Goat	1:10000	VectaLabs
Anti-goat	Horse	1:10000	VectaLabs

Table 2.1 List of antibodies used in this study

2.8 FACS sorting of Dictyostelium cells

FACS sorting of Dictyostelium cells was performed with the help of Kirsty Richardson using the FACS Aria cell sorter from BD Biosciences. Following transformation, cells designated for FACS analysis were not transferred to 96-well plates but were left to grow in a 9cm dish. After approximately 2 weeks, when multiple colonies were visible, the selective axenic media was aspirated and replaced with low fluorescent media (11g/L Glucose, 0.68g/L KH₂PO₄, 5g/L Casein Peptone, 6.8mg/L NH₄Cl, 37.1mg/L MGCl₂, 1.1mg/L CaCl₂, 8.11mg/L FeCl₃, 4.48mg/L Na₂-EDTA, 2.30mg/L ZnSO₄, 1.11mg/L H₃BO₃, 0.51mg/L MnCl₂.4H₂O, 0.17mg/L CoCl₂, 0.15mg/L CuSO₅.5H₂O 0.1mg/L

(NH₄)₆MO₇O₂₄.4H₂O) (Formedium). 24 hours later cells were harvested and washed twice in ice cold KK2 before being resuspended to a final volume of 10⁷ cells/ml and held on ice. Immediately prior to sorting, cells were passed through a sterile 40µm cell strainer (BD Biosciences) to prevent cell clumping. Cells were loaded into the FACS Aria cell sorter and separated based on GFP fluorescence. Following sorting, cells were centrifuged at 700 g, and resuspended in non-selective axenic media containing Streptomycin sulphate and 1% heat killed *E. coli*. Cells were transferred to well of a 6-well dish and allowed to recover.

After 24 hours, cells were transferred into 6x96 well plates in the presence of 40 µg/ml G418. After approximately 2 weeks, multiple clones were selected and transferred into individual wells of a 24 well plate for screening.

2.9 Mammalian LacZ Assay

LacZ assays were performed using the Beta-Glo system (Promega). Cells were cultured to ~80% confluency before being seeded into 96 well plates at a density of 3X10⁵ cells/ml. 48 hours later, cells were lysed by the addition of 30µl Glo-lysis buffer (Promega) and shaken at room temperature for 30 minutes. 30µl of Beta-Glo reagent was added to the cell lysate, which was shaken for a further thirty minutes at room temperature before luminescence levels were assessed using the FluoStar Optima.

2.10 Mammalian Wst-1 Assay

Wst-1 assays were performed using the 'Cell Proliferation Reagent WST-1' (Roche). Cells were cultured to ~80% confluency before being seeded into 96 well plates at a density of 3X10⁵ cells/ml, reference wells containing media but no cells were included on each plate. 24 hours later, cells were induced with 0ng/ml, 5ng/ml, 10ng/ml, 20ng/ml, 40ng/ml, 60ng/ml, 80ng/ml or 100ng/ml doxycycline. Cells were incubated for 24 or 48 hours. 10ml of Wst-1 reagent was added to each well and plates were incubated for a further hour. Absorbance readings at 450nm and 590nm were taken using the FluoStar Optima.

2.11 Kinase Assay

Dr William Ryves synthesized both the pre-phosphorylated and un-phosphorylated forms of the GSM peptide substrate used in this study. The GSM peptide has the following sequence – RRRPASVPPSPSLSRHSSSHQRR where S indicates a phospho-serine introduced during synthesis.

2.11.1 Dictyostelium kinase assay

Cells were seeded onto SM agar with *Klebsiella aerogenes* at a density of 10^6 cells/ml and cultured for 48 hours. Cells were then harvested and washed in KK2 to remove any bacteria before being pelleted, frozen on dry ice and lysed (lysis buffer: 150mM NaCl, 50mM Tris, 0.5% NP-40, 10% glycerol supplemented with a Roche complete inhibitor tablet). Samples were held on ice for 20 minutes before being centrifuged at 4000rpm and being passed through a $0.2\mu\text{M}$ filter.

Samples were normalized based on their GFP fluorescence. Briefly, 50ul of neat lysate and lysate diluted 1:2 and 1:4 were added in triplicate to a black-walled 96 well plate with a series of GFP standards (Roche). Fluorescence levels were assessed using the FluoStar Optima.

Lysates containing 35 μg GFP were added to 20 μl GFP-Trap coupled to agarose beads (Chromotek) and incubated for 1 hour at 4°C. Beads were washed 3 times with kinase buffer (150mM NaCl, 50mM Tris, 10% glycerol) and re-suspended in 400 μl of kinase buffer. 10 μl of each bead suspension was added in triplicate to a black-walled 96 well plate. (20 μl of the bead suspension was removed to a separate tube, centrifuged to remove buffer and re-suspended in 20 μl NuPage buffer, boiled for 5 minutes and 10 μl was run on a 4-12% Bis-Tris gel for western blot to confirm equal loading.)

40 μl of a master mix containing 50 μM ATP, 12.5 μM MgCl_2 and 425 μM GSM substrate was added to each well and samples were incubated at room temperature for 32 minutes. Where activity was measured over a series of time points samples were incubated for 2, 4, 8, 16, 32 or 64 minutes. 50 μl of Kinase-Glo reagent (Promega) was added directly to the 96-well plate and was incubated at room temperature for a further 30 minutes. Luminescence levels were assessed using the FluoStar Optima.

2.11.2 Mammalian kinase assay

Cells were cultured to ~50% confluency in 4 xT180 flasks before being induced with 2ng/ml doxycycline for 24 hours. Cells were harvested, washed in PBS and 5×10^7 cells were pelleted, frozen on dry ice and lysed (lysis buffer: 150mM NaCl, 50mM Tris, 0.5% NP-40, 10% glycerol supplemented with a Roche complete inhibitor tablet). Samples were held on ice for 20 minutes before being centrifuged at 4000rpm and being passed through a 0.2 μ M filter.

Lysates were added to 20 μ l of GFP-Trap coupled to agarose beads (Chromotek) and incubated for 1 hour at 4°C. Beads were washed 3 times with kinase buffer (150mM NaCl, 50mM Tris, 10% glycerol) and re-suspended in 400 μ l of kinase buffer. 10 μ l of each bead suspension was added in triplicate to a black-walled 96 well plate. 40 μ l of a master mix containing 50 μ M ATP, 12.5 μ M MgCl₂ and 425 μ M GSM substrate was added to each well and samples were incubated at room temperature for 2, 4, 8, 16, 32 or 64 minutes. 50 μ l of Kinase-Glo reagent (Promega) was added directly to the 96-well plate and was incubated at room temperature for a further 30 minutes.

2.12 Dictyostelium Cell Sizing

Cells were grown to 80% confluency before being washed in KK2 and resuspended at a density of 10^6 cells/ml. 30 μ l of each cell sample was transferred to a glass-bottomed chamber slide (Lab-Tek) containing 1 ml axenic media and allowed to adhere for 30 minutes. 5 Timelapse images were taken 5 seconds apart using the Olympus IX71 inverted microscope with a 20x objective.

2.13 Dictyostelium Multinucleate Assay

Cells were cultured to 80% confluency before being washed in KK2 and re-suspended in fresh axenic media at a density of 10^5 cells/ml. Cells were grown in shaking culture for 48 hour before being seeded onto 16mm glass coverslips, and allowed to adhere for 10 minutes. Coverslips were then washed in KK2 and fixed in methanol at -20°C for 4 minutes. Coverslips were then washed in KK2, and incubated with 1 μ g/ml 4',6-Diamidino-2-phenylindole dihydrochloride (DAPI) in water for 5 minutes. Coverslips

were washed in water and mounted on slides using Mowiol. Images were taken using the Olympus IX71 inverted microscope with a 20x objective. To ensure that data were not biased, 25 images (creating a 5 by 5 grid) were taken at a time where only the initial field of view is defined.

2.14 Dictyostelium Cell Proliferation Assay

To assess proliferation rates in shaking culture cells were cultured to 80% confluency before being washed in KK2 and resuspended in fresh axenic media at a density of 10^5 cells/ml. Cells were grown in shaking culture and samples were periodically removed and counted in triplicate on a haemocytometer (3 separate samples of 10 μ l each, counted once).

To assess proliferation rates on SM agar, cells were cultured to 80% confluency before being washed in KK2 and re-suspended at 10^5 cells/ml. 1 μ l of cells was spotted onto an SM agar plate spread with *Klebsiella aerogenes*. Each plate was prepared with 3 separate repeats for each cell line and a total of 6 plates prepared, creating 18 repeats for each cell line.

2.15 Dictyostelium Development assay

Cells were cultured to 80% confluency before being washed in KK2 and resuspended in fresh KK2 at a density of 10^6 cells/ml. 12-well plates were prepared containing 200 μ l non-nutrient KK2 agar in each well. 1ml of cells was seeded into each well and allowed to adhere for 30 minutes before excess liquid was aspirated off. Timelapse images of cells were taken every 5 minutes, under dark-field conditions using Olympus IX71 inverted microscope with a 4x objective. The availability of an automatic stage made it possible to take multiple fields of view and as such 9 images, creating a 3 by 3 grid, were taken for each sample. Images were processed using ImageJ to create a 'montage movie' consisting of all 9 fields of view.

2.16 Dictyostelium cAMP pulse assay

Cells were cultured to 80% confluency before being washed in KK2 and re-suspended in fresh KK2 at a density of 10^6 cells/ml. 6-well plates were prepared containing 1ml of non-nutirent KK2 agar in each well. 5ml of cells was seeded into each well and allowed to adhere for 30 minutes before excess liquid was aspirated off. Timelapse images of cells were taken every 30 seconds, under dark-field conditions using an Olympus IX71 inverted microscope with a 4x objective. The availability of an automatic stage made it possible to take multiple fields of view and as such 9 images, creating a 3 by 3 grid, were taken for each sample. Images were processed using ImageJ to create a 'montage movie' consisting of all 9 fields of view.

2.17 Affinity purifications

2.17.1 Dicytostelium affinity purifications

Non-crosslinked samples

Cells were seeded onto SM agar with *Klebsiella aerogenes* at a density of 10^6 cells/ml and cultured for 48hours. Cells were harvested and washed in KK2 to remove any bacteria before being resuspended in fresh KK2 at a density of 10^8 cells/ml and cultured in shaken suspension for 4 hours. After 4 hours, 50ml of each cell suspension was pelleted and frozen on dry ice before being lysed in 10ml lysis buffer (150mM NaCl, 50mM Tris, 10% glycerol supplemented with a Roche complete inhibitor tablet). Samples were incubated on ice for 20 minutes, centrifuged at 16,000rpm and passed through a $0.2\mu\text{M}$ filter. 100 μl of protein-G sepharose beads (GE Healthcare) covalently bound to anti-GFP antibody (Roche)(at a concentration of 2mg/ml) were added to each supernatant, these were incubated at 4°C for 1 hour. Beads were pelleted at 500g and washed 3 times with wash buffer (150mM NaCl, 50mM Tris, 10% glycerol supplemented with a Roche complete inhibitor tablet) before being resuspended in 50 μl glycine (0.1M, pH2.5). Samples were incubated for 5 minutes at room temperature before being centrifuged at 500g. The supernatant was removed to a separate tube containing 7.5 μl Tris-HCl (1.5M, pH9.0). The elution process was repeated and 50 μl of NuPage buffer was added to each sample, which were then boiled. Samples were dried in a vacuum

before being reconstituted with 20µl water and loaded onto a 4-12% Bis-Tris gel. This gel was then stained with a colloidal coomassie stain (Invitrogen).

Cross-linked samples

Cells were prepared as before. However, following the step where cells were shaken in KK2 for 4 hours, 50ml of each cell suspension was pelleted, re-suspended in 50ml 1% Paraformaldehyde (in water) and incubated for 20 minutes. Cross-linking was quenched by the addition of glycine (to a final concentration of 1.25mM) and a further incubation of 5 minutes. Samples were then pelleted and washed twice in KK2 before being lysed in 10ml lysis buffer (150mM NaCl, 50mM Tris, 0.1% NP-40 and 10% glycerol supplemented with a Roche complete inhibitor tablet). Samples were incubated on ice for 20 minutes, centrifuged at 16,000rpm and passed through a 0.2µM filter. 50µl of a GFP-Trap coupled to agarose beads (Chromotek) were added to each supernatant, these were incubated at 4°C for 1 hour. Beads were pelleted at 500g and washed 3 times with wash buffer (150mM NaCl, 50mM Tris, 10% glycerol supplemented with a Roche complete inhibitor tablet) before being resuspended in 50µl NuPage buffer. Samples were boiled at 95° for 5 minutes (this reversed the cross-linking) and loaded onto a 4-12% Bis-Tris gel which was subsequently stained with a colloidal coomassie stain (Invitrogen).

Bands of interest were excised within a lamina flow-hood and shipped to the FingerPrints Proteomics Facility at Dundee University for analysis (see below for details).

2.17.2 Mammalian affinity purifications

Pull-downs to confirm interaction with known binding partners

T-REx GSK3β-GFP and T-REx GFP cells were cultured to 60% confluency in 9cm dishes in media containing no antibiotics before being transfected using TransFectin lipid reagent (BioRad) as per the manufacturers instructions. Plasmids encoding FLAG-Axin1 (367-701), FLAG-Axin (367-701) L392P, Flag-FRAT and Flag-FRAT K208A/E209Q were each separately transfected into both cell lines; 3ml of DNA-TransFectin complexes (10µg plasmid DNA and 50µl TransFectin reagent each in 1.5ml OptiMem) was added and cells were left for 4 hours. After 4 hours the media was aspirated off and replaced with antibiotic free media.

24 hours later cells were induced with 2ng/ml doxycycline and incubated for a further 24 hours. Cells were then washed off the plate in 10ml PBS and were washed a further twice in PBS before being pelleted and lysed in 5ml of lysis buffer: 150mM NaCl, 50mM Tris, 0.5% NP-40, 10% glycerol supplemented with a Roche complete inhibitor tablet. Samples were incubated on ice for 20 minutes, centrifuged at 4000rpm and passed through a 0.2 μ M filter. 20 μ l of GFP-binder beads (Chromotek) were added to each supernatant and were incubated at 4^oC for 1 hour. Beads were centrifuged at 500g and washed twice in wash buffer 1 (150mM NaCl, 50mM Tris, 10% glycerol supplemented with a Roche complete inhibitor tablet), twice in wash buffer 2 (as wash buffer 1 but 300mM NaCl) and twice in wash buffer 3 (as wash buffer 1 but 600mM NaCl). Beads were re-suspended in 50 μ l NuPage buffer and boiled for 5 minutes to release and denature bound proteins. At each stage 100 μ l samples were taken and added to an equal amount of NuPage buffer to be loaded for western blot analysis.

Non-crosslinked samples

T-REx GSK3 β -GFP and T-REx GFP cells were cultured to 70% confluency before being induced with 10ng/ml doxycycline for 4 hours. Cells were harvested and lysed in 10ml lysis buffer (150mM NaCl, 50mM Tris, 10% glycerol supplemented with a Roche complete inhibitor tablet). Samples were incubated on ice for 20 minutes, centrifuged at 16,000rpm and passed through a 0.2 μ M filter. 100 μ l of protein-G sepharose beads (GE Healthcare) covalently bound to anti-GFP antibody (Roche)(at a concentration of 2mg/ml) were added to each supernatant, these were incubated at 4^oC for 1 hour. Beads were pelleted at 500g and washed 3 times with wash buffer (150mM NaCl, 50mM Tris, 10% glycerol supplemented with a Roche complete inhibitor tablet) before being resuspended in 50 μ l glycine (0.1M, pH2.5). Samples were incubated for 5 minutes at room temperature before being centrifuged at 500g. The supernatant was removed to a separate tube containing 7.5 μ l Tris-HCl (1.5M, pH9.0). The elution process was repeated and 50 μ l of NuPage buffer was added to each sample, which were then boiled. Samples were dried in a vacuum before being reconstituted with 20 μ l water and loaded onto a 4-12% Bis-Tris gel. This gel was then stained with a silver stain (GE Healthcare).

Cross-linked samples

T-REx GSK3 β -GFP and T-REx GFP cells were cultured to 70% confluency before being induced with 2ng/ml doxycycline for 24 hours. Cells were harvested and re-suspended at a density of 10^7 cells/ml in 1% Paraformaldehyde (in PBS) and incubated for 20 minutes. Cross-linking was quenched by the addition of glycine (to a final concentration of 1.25mM) and a further incubation of 5 minutes. Samples were then pelleted and washed twice in PBS before being lysed in 10ml lysis buffer (150mM NaCl, 50mM Tris, 0.1% NP-40 and 10% glycerol supplemented with a Roche complete inhibitor tablet). Samples were incubated on ice for 20 minutes, centrifuged at 16,000rpm and passed through a 0.2 μ M filter. 50 μ l of GFP-binder beads (Chromotek) were added to each supernatant, these were incubated at 4°C for 1 hour. Beads were pelleted at 500g and washed 3 times with wash buffer (150mM NaCl, 50mM Tris, 10% glycerol supplemented with a Roche complete inhibitor tablet) before being resuspended in 50 μ l NuPage buffer. Samples were then boiled and loaded onto a 4-12% Bis-Tris gel which was subsequently stained with a colloidal coomassie stain (Invitrogen).

2.18 SILAC

Cells were grown in custom-made DMEM (minus arginine and lysine; Pierce) supplemented with 10% dialyzed fetal calf serum (Pierce) and 1% penicillin/streptomycin, 12mg/ml blasticidin (both Invitrogen) and 300 μ g/ml hygromycin (Roche). L -arginine (84 μ g/ml) and L- lysine (146 μ g/ml lysine) were added to the 'light' media, while L -arginine 13 C and L -lysine 13 C were added to the 'heavy' media at the same concentrations (all Pierce). T-REx GSK3 β -GFP cells were cultured in 'heavy' media while T-REx GFP cells were cultured in 'light' media. Both cell lines were cultured for 8 cell doublings to ensure complete incorporation of isotopic amino acids [246, 247].

T-REx GSK3 β -GFP and T-REx GFP cells were cultured to 50-60% confluency before being induced with 2ng/ml and 0.4ng/ml doxycycline respectively for 24 hours. Cells were harvested and washed twice in PBS before being resuspended in 10ml lysis buffer (50mM NaCl, 10mM Tris, 0.5% NP-40 supplemented with a Roche complete inhibitor tablet) and incubated for 20 minutes on ice. Samples were spun at 4000rpm for 15

minutes before being passed through a 0.2 μ M filter. Total protein levels were measured using the BCA protein quantification kit (Pierce). Samples containing 27mg total protein were combined with 100 μ l GFP binder beads (Chromotek) and incubated at 4°C for 1 hour. Beads were spun briefly at 300g, washed once in PBS and re-suspended in 30ml NuPage buffer. Beads were boiled for 3 minutes, NuPage buffer removed and shipped on ice to Dundee Cell Products for analysis.

2.19 Mass Spectrometry Analysis

(Performed by FingerPrints Proteomics Facility)

2.19.1 In-gel digestion

Each gel slice was subjected to in-gel digestion with trypsin. The resulting tryptic peptides were extracted by 1% formic acid, acetonitrile, lyophilized in a speedvac, (Helena Biosciences) and resuspended in 1% formic acid.

2.19.2 LC-MS/MS

Trypsin digested peptides were separated using an Ultimate U3000 (Dionex Corporation) nanoflow Liquid Chromatography (LC)-system consisting of a solvent degasser, micro and nanoflow pumps, flow control module, UV detector and a thermostated autosampler. 10 μ l of sample (a total of 2 μ g) was loaded with a constant flow of 20 μ l/min onto a PepMap C18 trap column (0.3 mm id x 5 mm, Dionex Corporation). After trap enrichment peptides were eluted off onto a PepMap C18 nano column (75 μ m x 15 cm, Dionex Corporation) with a linear gradient of 5-35% solvent B (90% acetonitrile with 0.1% formic acid) over 65 minutes with a constant flow of 300 nl/min. The HPLC system was coupled to a Linear Trap Quadrupole (LTQ) Orbitrap XL (Thermo Fisher Scientific Inc) via a nano Electro-spray (ES) ion source (Proxeon Biosystems). The spray voltage was set to 1.2 kV and the temperature of the heated capillary was set to 200°C. Full scan MS survey spectra (m/z 335-1800) in profile mode were acquired in the Orbitrap with a resolution of 60,000 after accumulation of 500,000 ions. The five most intense peptide ions from the preview scan in the Orbitrap were fragmented by collision induced dissociation (normalised collision energy 35%, activation Q 0.250 and activation time 30

ms) in the LTQ after the accumulation of 10,000 ions. Maximal filling times were 1,000 ms for the full scans and 150 ms for the MS/MS scans. Precursor ion charge state screening was enabled and all unassigned charge states as well as singly charged species were rejected. The dynamic exclusion list was restricted to a maximum of 500 entries with a maximum retention period of 90 seconds and a relative mass window of 10 ppm. The lock mass option was enabled for survey scans to improve mass accuracy [248]. Data were acquired using the Xcalibur software. Results were returned as two Mascot searches, the entire NCBI nr and of the NCBI nr database selected for taxonomy 'Dictyostelium discoideum'.

2.20 SILAC coupled Mass Spectrometry Analysis

(Performed by Dundee Cell Products Ltd)

2.20.1 Gel electrophoresis and in-gel digestion

Each sample was reduced in SDS PAGE loading buffer containing 10mM DTT and alkylated in 50 mM iodoacetamide prior to being boiled and then separated by one-dimensional SDS-PAGE (4–12% Bis-Tris Novex mini-gel, Invitrogen) and visualized by colloidal Coomassie staining (Novex, Invitrogen). The entire protein gel lane was excised and cut into 10 gel slices each. Every gel slice was subjected to in-gel digestion with trypsin [249]. The resulting tryptic peptides were extracted by 1% formic acid, acetonitrile, lyophilized in a speedvac, (Helena Biosciences) and resuspended in 1% formic acid.

2.20.2 LC-MS/MS

Trypsin digested peptides were separated using an Ultimate U3000 (Dionex Corporation) nanoflow Liquid chromatography (LC)-system consisting of a solvent degasser, micro and nanoflow pumps, flow control module, UV detector and a thermostated autosampler. 10 µl of sample (a total of 2 µg) was loaded with a constant flow of 20µl/min onto a PepMap C18 trap column (0.3 mm id x 5 mm, Dionex Corporation). After trap enrichment peptides were eluted off onto a PepMap C18 nano column (75 µm x 15 cm, Dionex Corporation) with a linear gradient of 5-35% solvent B (90% acetonitrile with

0.1% formic acid) over 65 minutes with a constant flow of 300 nl/min. The HPLC system was coupled to a Linear trap quadrupole (LTQ) Orbitrap XL (Thermo Fisher Scientific Inc) via a nano electro spray (ES) ion source (Proxeon Biosystems). The spray voltage was set to 1.2 kV and the temperature of the heated capillary was set to 200°C. Full scan MS survey spectra (m/z 335-1800) in profile mode were acquired in the Orbitrap with a resolution of 60,000 after accumulation of 500,000 ions. The five most intense peptide ions from the preview scan in the Orbitrap were fragmented by collision induced dissociation (normalised collision energy 35%, activation Q 0.250 and activation time 30 ms) in the LTQ after the accumulation of 10,000 ions. Maximal filling times were 1,000 ms for the full scans and 150 ms for the MS/MS scans. Precursor ion charge state screening was enabled and all unassigned charge states as well as singly charged species were rejected. The dynamic exclusion list was restricted to a maximum of 500 entries with a maximum retention period of 90 seconds and a relative mass window of 10 ppm. The lock mass option was enabled for survey scans to improve mass accuracy [248]. Data were acquired using the Xcalibur software.

2.20.3 Quantification and Bioinformatic Analysis

Quantification was performed with MaxQuant version 1.0.7.4 [250], and was based on two-dimensional centroid of the isotope clusters within each SILAC pair. To minimize the effect of outliers, protein ratios were calculated as the median of all SILAC pair ratios that belonged to peptides contained in the protein. The percentage variability of the quantitation was defined as the standard deviation of the natural logarithm of all ratios used for obtaining the protein ratio multiplied by a constant factor 100.

The generation of peak list, SILAC- and extracted ion current-based quantitation, calculated posterior error probability, and false discovery rate based on search engine results, peptide to protein group assembly, and data filtration and presentation was carried out using MaxQuant. The derived peak list was searched with the Mascot search engine (version 2.1.04; Matrix Science, London, UK) against a concatenated database combining 80,412 proteins from International Protein Index (IPI) human protein database version 3.6 (forward database), and the reversed sequences of all proteins (reverse database). Alternatively, database searches were done using Mascot (Matrix Science) as the

database search engine and the results saved as a peptide summary before quantification using MSQuant (<http://msquant.sourceforge.net/>). Parameters allowed included up to three missed cleavages and three labeled amino acids (arginine and lysine). Initial mass deviation of precursor ion and fragment ions were up to 7 ppm and 0.5 Da, respectively. The minimum required peptide length was set to 6 amino acids. To pass statistical evaluation, posterior error probability (PEP) for peptide identification (MS/MS spectra) should be below or equal to 0.1. The required false positive rate (FPR) was set to 5% at the peptide level. False positive rates or PEP for peptides were calculated by recording the Mascot score and peptide sequence length-dependent histograms of forward and reverse hits separately and then using Bayes' theorem in deriving the probability of a false identification for a given top scoring peptide. At the protein level, the false discovery rate (FDR) was calculated as the product of the PEP of a protein's peptides where only peptides with distinct sequences were taken into account. If a group of identified peptide sequences belong to multiple proteins and these proteins cannot be distinguished, with no unique peptide reported, these proteins are reported as a protein group in MaxQuant. Proteins were quantified if at least one MaxQuant-quantifiable SILAC pair was present. Identification was set to a false discovery rate of 1% with a minimum of two quantifiable peptides. The set value for FPR/PEP at the peptide level ensures that the worst identified peptide has a probability of 0.05 of being false; and proteins are sorted by the product of the false positive rates of their peptides where only peptides with distinct sequences are recognized. During the search, proteins are successively included starting with the best-identified ones until a false discovery rate of 1% is reached; an estimation based on the fraction of reverse protein hits.

Enzyme specificity was set to trypsin allowing for cleavage of N-terminal to proline and between aspartic acid and proline. Carbamidomethylation of cysteine was searched as a fixed modification, whereas *N*-acetyl protein, and oxidation of methionine were searched as variable modifications.

Chapter 3

Characterization of GSK3 β -GFP and GskA-GFP cell lines

The primary objectives of this project were to characterize the role of GskA in *Dictyostelium* and to establish whether protein binding, or scaffolding of GSK-3 represented a common mechanism by which GSK-3 activity could be compartmentalized and directed towards specific substrates.

In this chapter I describe the generation and characterization of both *Dictyostelium* and T-REx HEK 293 cell lines expressing GskA-GFP and GSK3- β -GFP fusion proteins that will be used to facilitate those aims. I also describe the generation of a series of *Dictyostelium* cell lines expressing GskA-GFP fusion proteins harbouring point mutations that were used to further characterize the mechanisms by which GskA activity is regulated. I demonstrate that cell viability is not affected by the levels of GSK-3 over-expression used in this study, that cellular localization was not altered by the addition of a GFP tag and that these GFP-fusion proteins were catalytically active.

3.1 Generation of *Dictyostelium* GskA-GFP cell lines

As described in Chapter 1, GskA is not essential for *Dictyostelium* cell viability, and *gskA* null cell lines have previously been generated in two different cell backgrounds [194, 195]. In this study, *gskA* null cells generated in an Ax2 background were used.

The plasmid pDXA GskA-GFP2, encoding a GskA-GFP fusion protein and conferring G-418 resistance was electroporated into the *gskA* null cell line. This plasmid cannot replicate and exist extra-chromosomally unless it is co-transfected with the plasmid pREP. In the absence of the pREP plasmid, the pDXA GskA-GFP2 plasmid can only be maintained through chromosomal integration [234]. This approach was used to ensure stable expression from a single or low number of plasmid copies. Protein expression was initially screened through observation of GFP fluorescence and subsequently by western transfer, using as controls Ax2 and *gskA* null strains (Figure 3.1A). Clones expressing GskA-GFP at endogenous, or close to endogenous levels were selected for further analysis.

Point mutation of specific residues of GSK-3 has previously been used as a method to characterize the role GSK3 β in mammalian cells; mutation of Lys85 rendered the protein catalytically inactive [251], mutation of Arg96 prevented GSK3 β from interacting

efficiently with its primed substrates [54, 55] and mutation of Tyr216 reduced the catalytic activity of the protein [73]. (Figure 1.1 and Figure 1.2) As part of this study analogous mutations were generated in *Dictyostelium* GskA in order to dissect the functional role of GskA; Plasmids that encoded GskA-GFP fusion proteins that contained a point mutation at Lys85 (K85R), Arg96 (R96E) or Tyr214 (Y214G) were each electroporated into the *gskA* null cell line. Again, clones were initially screened for GFP fluorescence and subsequently by western transfer (Figure 3.1B-E). The epitope recognised by the antibody used to detect GskA in this study extended over the Y214 residue, and as such an additional western transfer was performed using an anti-GFP antibody in order to accurately determine expression levels in the GskA-GFP Y214G cell lines. The *gskA*-GskA-GFP clone-2 cell line was used as an additional control.

The GskA-GFP R96E cell lines generated in this study all demonstrated greatly elevated levels of the GskA fusion protein compared to both wild type and other mutated GskA-GFP fusions despite the plasmid being constructed from the same 'parent' plasmid (Figure 3.1B). Sequencing of the GskA-GFP R96E plasmid did not reveal any indication as to why expression was higher.

In an attempt to recover clones expressing GskA-GFP R96E at lower levels cell were sorted using fluorescence activated cell sorting (FACS); heterogeneous populations of cells transformed with either pDXA GskA-GFP2 R96E or pDXA GFP2 (a plasmid expressing GFP only) were cultured in low fluorescent media overnight before being sorted into four arbitrary categories based on their levels of fluorescence (Figure 3.2). These cells were then plated into 96-well plates at low density, such that one would expect to recover individual colonies from one well in every ten. Very few GskA-GFP2 R96E expressing colonies were recovered using this method and those that were recovered expressed high levels of the fusion protein. Cells transformed with the pDXA GFP2 plasmid did yield the expected frequency of colonies and these colonies exhibited the expected levels of fluorescence (and inferred protein expression) based on their sorting, indicating that the FACS itself was not responsible for the low number of GskA-GFP2 R96E expressing colonies recovered.

Those colonies expressing GskA-GFP2 R96E that were recovered following FACS continued to express high levels of the protein. As such these cells were not used for

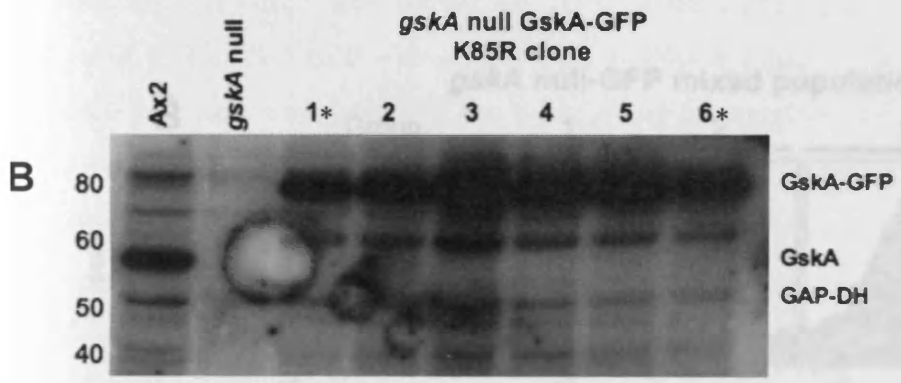
further experiments as it was possible that the extended culturing and the stresses of the FACS may have introduced new mutations. Instead, colonies from the original transformations were used for further experiments.

The plasmid pDXA GFP2 was electroporated into both Ax2 and *gskA* null cell lines to be used as controls for later experiments. Individual clones were selected for GFP fluorescence and where possible clones that expressed GFP at similar levels to the *gskA*-GskA-GFP clone 2 were selected for further experiments (data not shown).



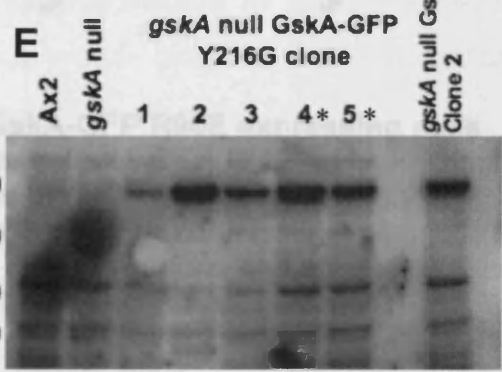
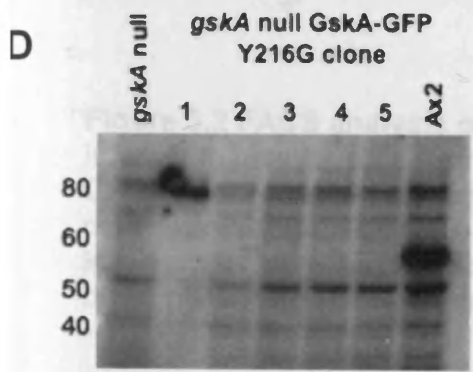
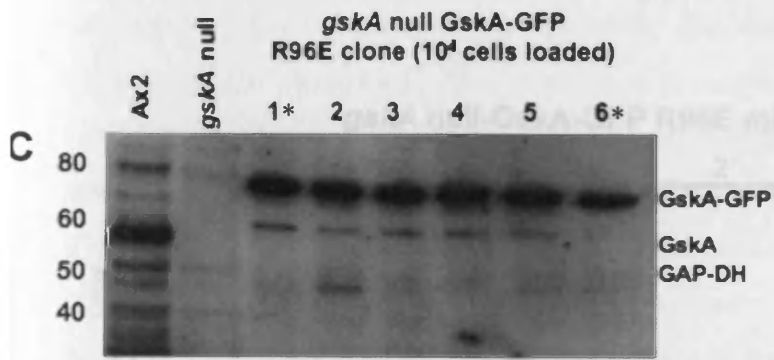
Figure 3.1 Western blot analysis of GskA-GFP constructs in an *gskA* null background.

The equivalent of 10^5 cells were loaded for each sample with the exception of GskA-GFP R96E mutant clones where 10^4 cells were loaded. A-D were immunoblotted with anti-Sgg (*Drosophila* GSK-3 homologue) and anti-GAP-DH antibodies.



E was immunoblotted with anti-GFP and anti-GAP-DH antibodies.

Clones used in later experiments are marked with an (*)



3.2 Generation of T-REX GSK3 β -GFP cell lines

In order to express a GskA-GFP fusion protein in mammalian cells the plasmid

200

100

50

0

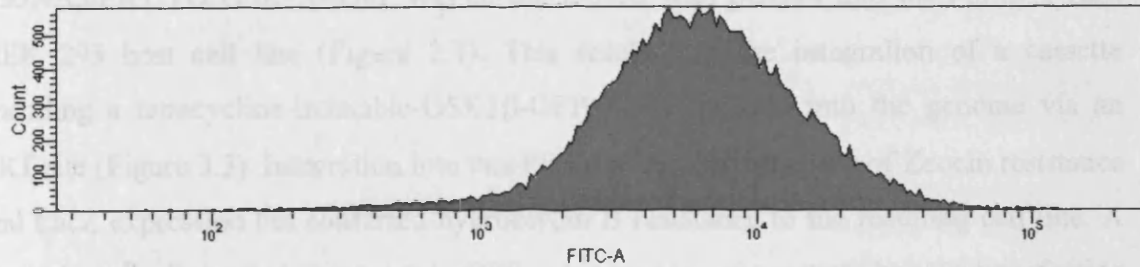
Count

10² 10³ 10⁴ 10⁵

FITC-A

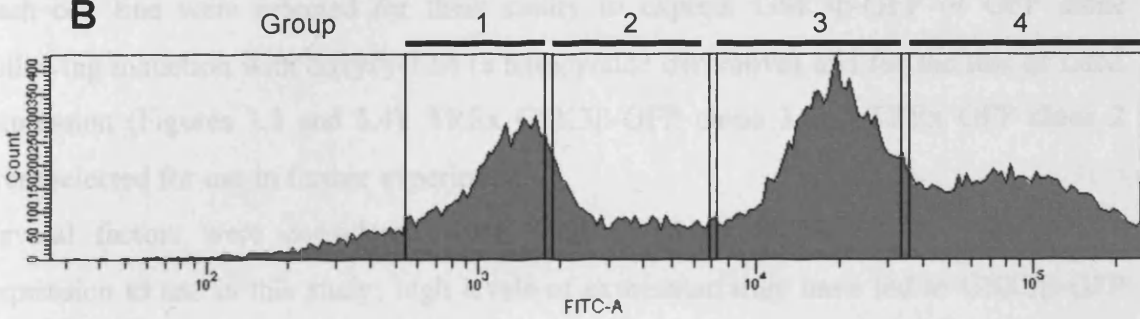
A

gskA null-GskA-GFP clone 2



B

gskA null-GFP mixed population



C

gskA null-GskA-GFP R96E mixed population

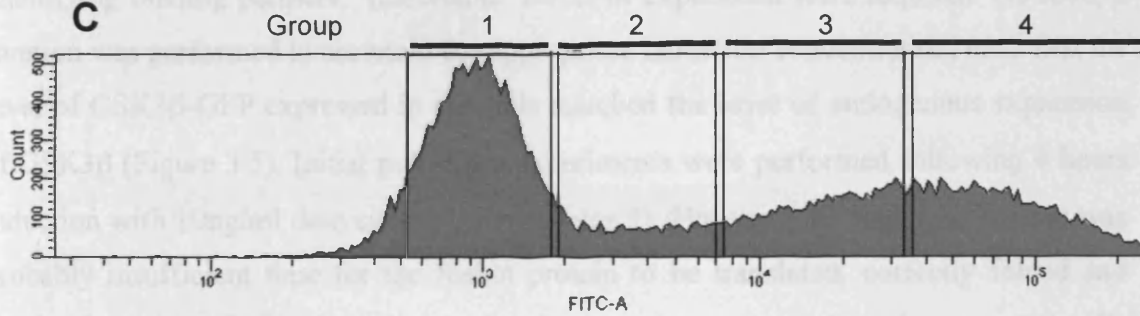


Figure 3.2 FACS analysis of GskA-GFP R96E expressing cells

In order to recover cells expressing GskA-GFP R96E at levels similar to *gskA* null-GskA-GFP clone 2, mixed populations of cells were subjected to FACS. Mixed populations of cells expressing GskA-GFP R96E or GFP alone both exhibited a range of fluorescence levels. Cells were sorted into 4 arbitrary groups and allowed to recover overnight before being plated into 96-well plates to recover individual clones.

3.2 Generation of T-REx GSK3 β -GFP cell lines

In order to express a Gsk3 β -GFP fusion protein in mammalian cells the plasmid pcDNA5/FRT/TO GSK-3 β -GFP was co-transfected with pOG44 into the Flp-In T-REx HEK 293 host cell line (Figure 2.1). This resulted in the integration of a cassette encoding a tetracycline-inducible-GSK3 β -GFP fusion protein into the genome via an FRT site (Figure 3.3). Integration into this FRT site resulted in a loss of Zeocin resistance and LacZ expression but conferred hygromycin B resistance to the resulting cell line. A control cell line that expressed GFP alone was generated by co-transfecting pcDNA5/FRT/TO GFP with pOG44 into the Flp-In T-REx HEK 293 host cell. Clones of each cell line were selected for their ability to express GSK3 β -GFP or GFP alone following induction with doxycycline (a tetracycline derivative) and for the loss of LacZ expression (Figures 3.3 and 3.4). TREx GSK3 β -GFP clone 3 and TREx GFP clone 2 were selected for use in further experiments.

Several factors were considered when thinking about the levels of GSK3 β -GFP expression to use in this study; high levels of expression may have led to GSK3 β -GFP forming non-specific interactions within the cell and the identification of GSK3 β 's inclusion in non-physiologically relevant protein complexes. However for the purposes of identifying binding partners, 'reasonable' levels of expression were required. As such, a titration was performed to ascertain the appropriate induction concentration, such that the level of GSK3 β -GFP expressed in the cells matched the level of endogenous expression of GSK3 β (Figure 3.5). Initial pull-down experiments were performed following 4 hours induction with 10ng/ml doxycycline (see Chapter 5). However, in hindsight 4 hours was probably insufficient time for the fusion protein to be translated, correctly folded and incorporated into GSK3 β -containing protein complexes. Later experiments used cells induced for 24 hours with 2ng/ml doxycyclin (Figure 3.5).

Wst-1 assays were used to assess cell viability; Wst-1 is a tetrazolium salt that is cleaved by mitochondrial dehydrogenases into formazan [252]. This reaction results in a colour change from light to dark red. The amount of formazan produced directly correlates with the number of metabolically active cells in a population. Therefore, by treating cells with Wst-1 and measuring the amount of formazan produced it was possible to make

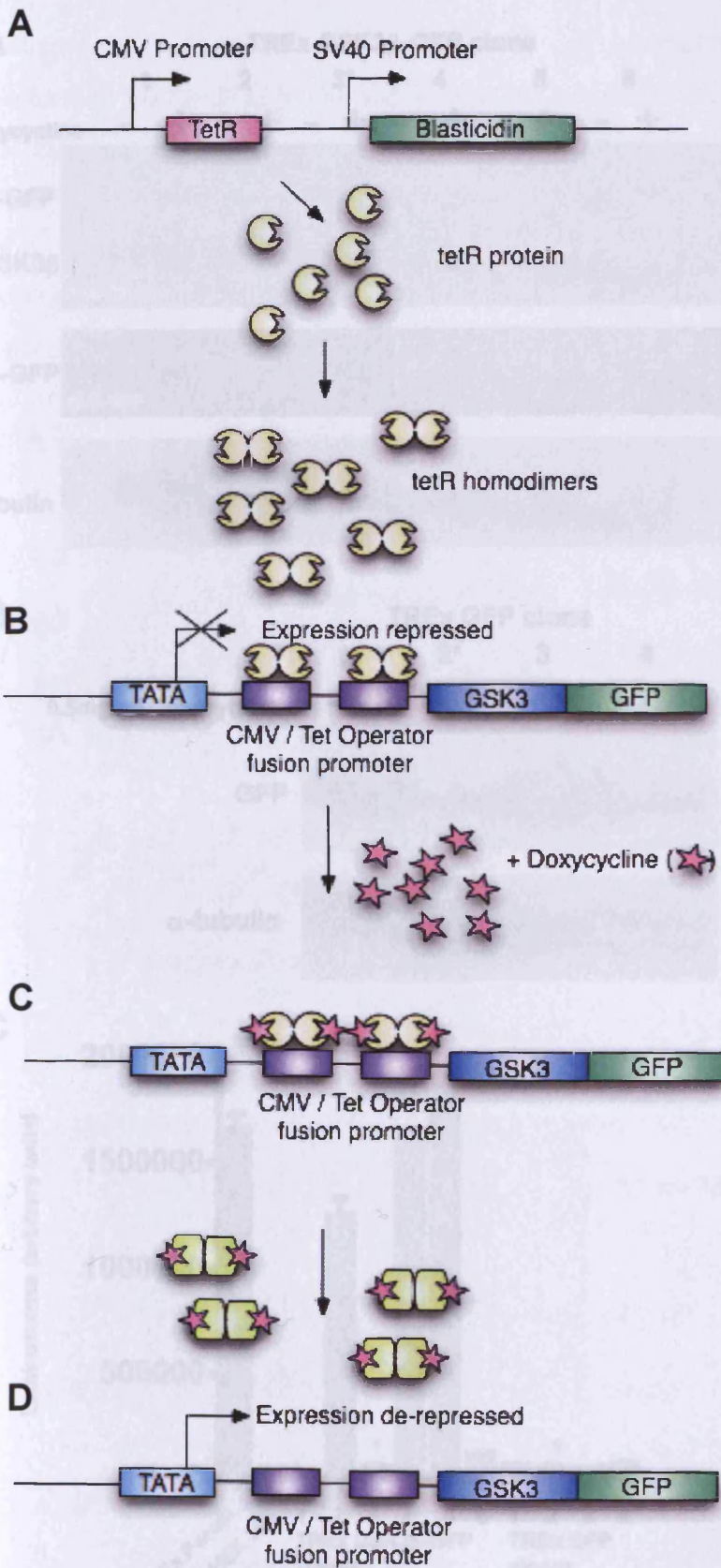


Figure 3.3 Mechanism of Tetracycline/Doxycycline induction

A. Tet repressor (TetR) protein is expressed in T-REx HEK 293 cells

B. TetR homodimers bind to the Tet operator sequences, repressing transcription of the GSK-3 β -GFP fusion gene.

C. When added, doxycycline binds to the tetR homodimers.

D. Binding of Doxycycline to tetR homodimers causes a conformational change in tetR leading to its release from the Tet operator sequences and induction of transcription from the GSK-3 β -GFP fusion gene.

(This schematic is based on the diagram included in Invitrogen manual for the T-REx system)

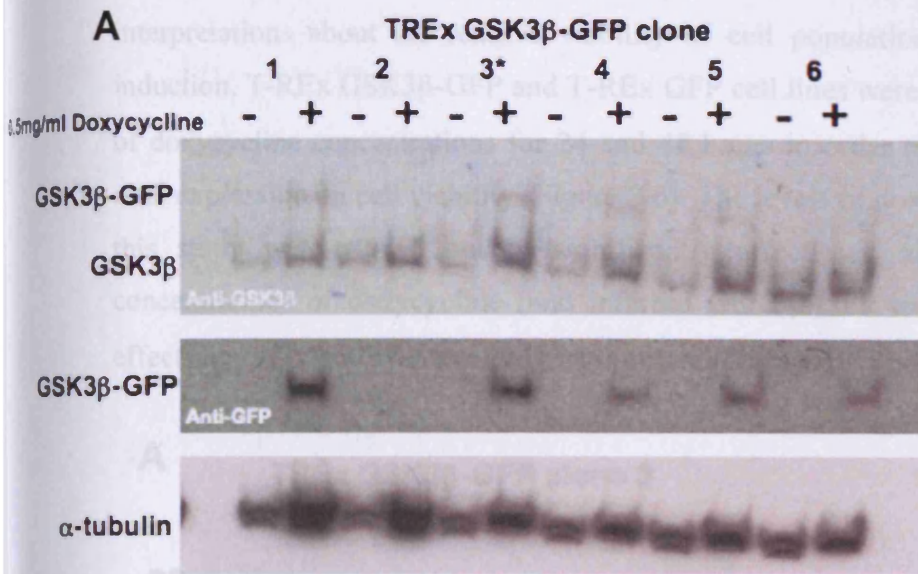
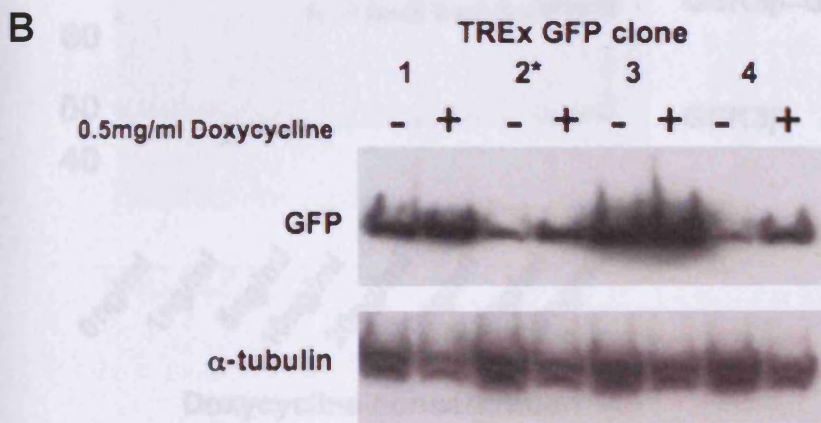


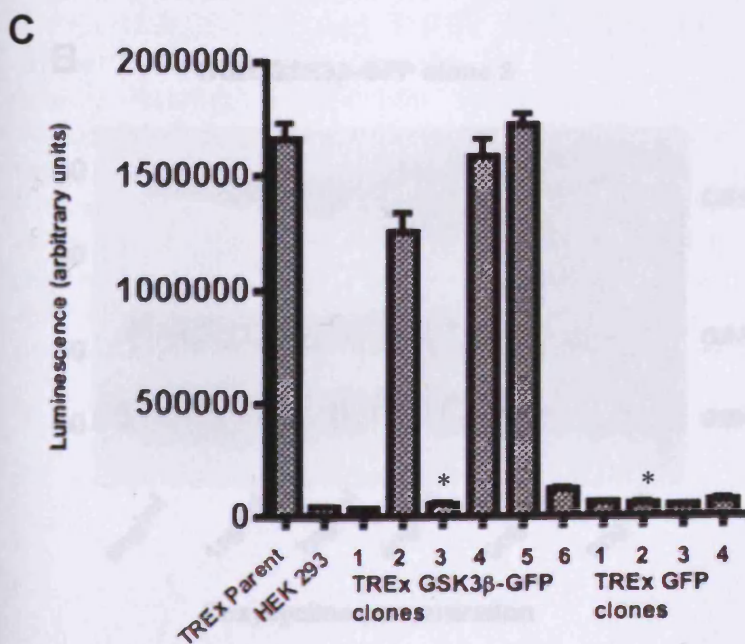
Figure 3.4. Western blot analysis of T-REx GSK3 β -GFP and T-REx GFP clones

A. T-REx GSK3 β -GFP clones +/- treatment with doxycycline 4 hours prior to lysis. Samples were immunoblotted with anti-GSK3 β , anti-GFP and anti- α -tubulin antibodies.

B. T-REx GFP clones +/- treatment with doxycycline 4 hours prior to lysis. Samples were immunoblotted with anti-GFP and anti- α -tubulin antibodies.



C β -galactosidase activity within T-REx GSK3 β -GFP and T-REx GFP clones was measured using the beta-glo assay system that utilized β -galactosidase for an enzymatic reaction that culminated in the generation of light. β -galactosidase activity was directly proportional to the amount of light produced. The data presented are means +/- standard deviation ($n = 8$).



TREx GSK3 β -GFP clone 3 and TREx GFP clone 2 were selected for use in further experiments

interpretations about the relative viability of cell populations following Doxycycline induction. T-REx GSK3 β -GFP and T-REx GFP cell lines were both induced with a range of doxycycline concentrations for 24 and 48 hours in order to fully assess the effect of over expression on cell viability (Figure 3.6). The levels of doxycycline induction used in this study were shown not to significantly affect cell viability. However, higher concentrations of doxycycline (and inferred GSK3 β -GFP expression) did have minor effects on cell viability compared to control cell lines expressing GFP alone.

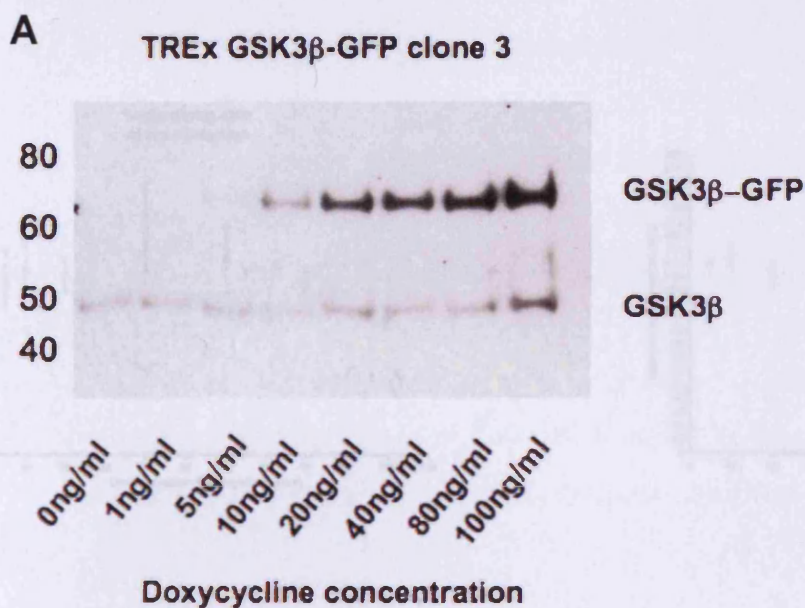
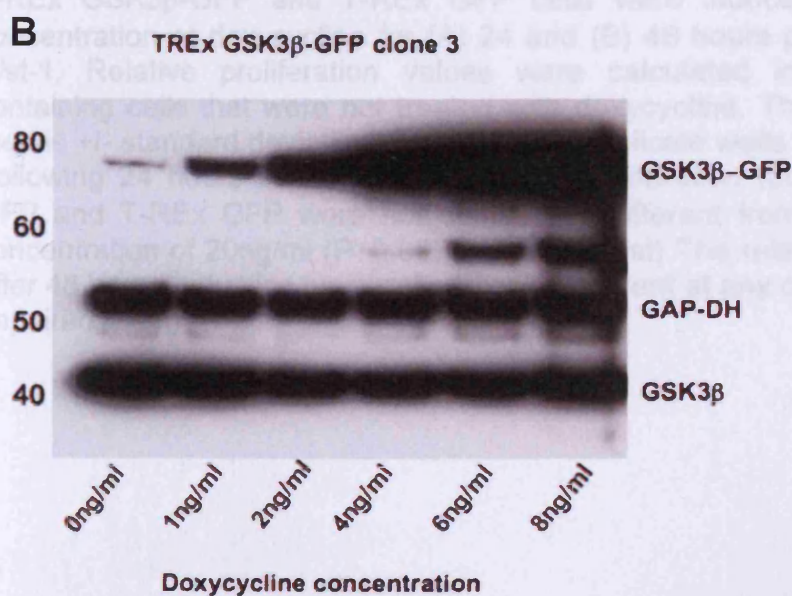


Figure 3.5. Western blot analysis of Doxycycline titration in T-REx GSK3 β -GFP

A. T-REx GSK3 β -GFP cells were treated with the indicated concentration of Doxycycline for 4 hours and immunoblotted with Anti-GSK3 β .



B. T-REx GSK3 β -GFP cells were treated with the indicated concentration of Doxycycline for 24 hours and immunoblotted with Anti-GSK3 β .

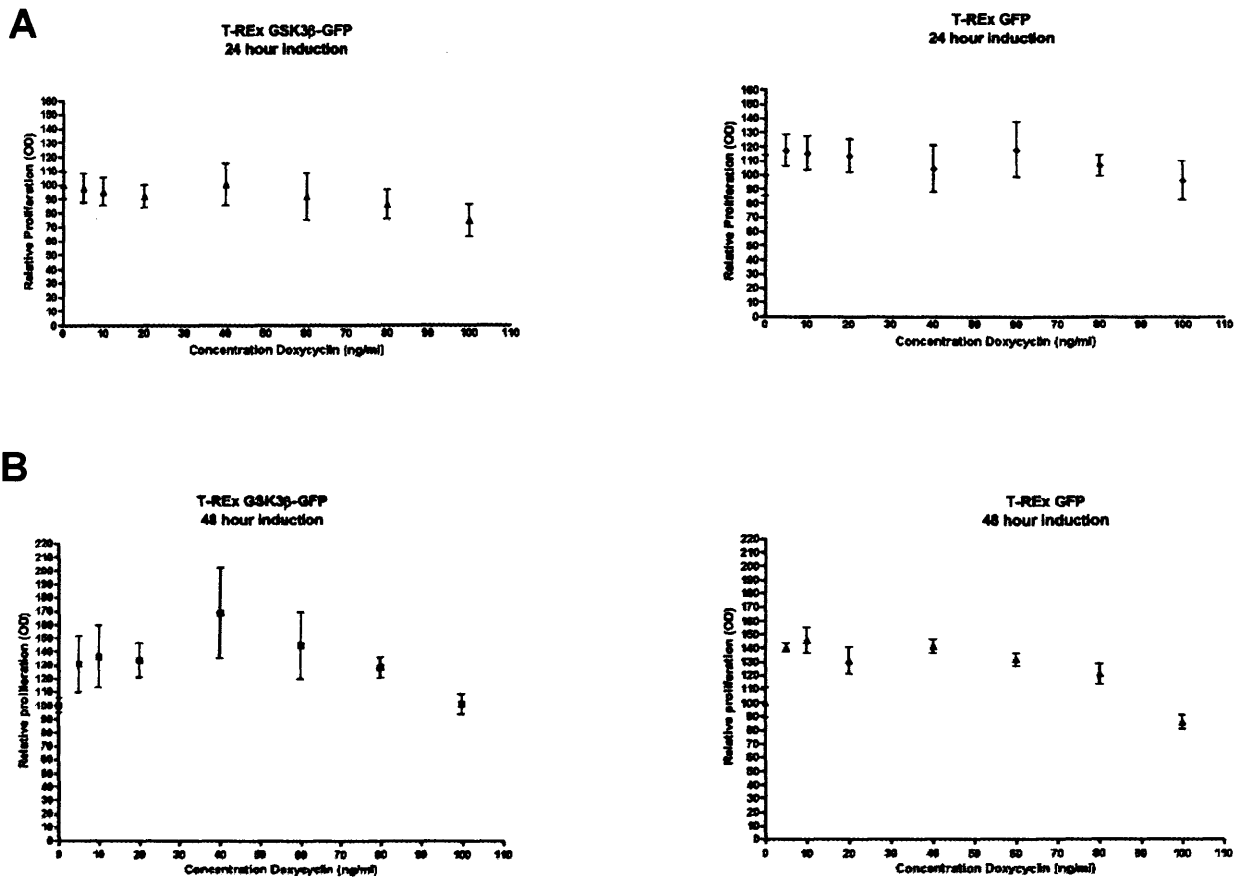


Figure 3.6 Wst-1 Assays

T-REx GSK3 β -GFP and T-REx GFP cells were induced with the indicated concentration of doxycycline for (A) 24 and (B) 48 hours prior to treatment with Wst-1. Relative proliferation values were calculated in reference to wells containing cells that were not treated with doxycycline. The data presented are means \pm standard deviation of the mean of triplicate wells ($n = 3$)

Following 24 hours induction, the relative proliferation rates of T-REx GSK3 β -GFP and T-REx GFP were not statistically different from each other up to a concentration of 20ng/ml ($P > 0.05$, unpaired t -test) The relative proliferation rates after 48 hours induction were not statically different at any concentration ($P > 0.05$, unpaired t -test).

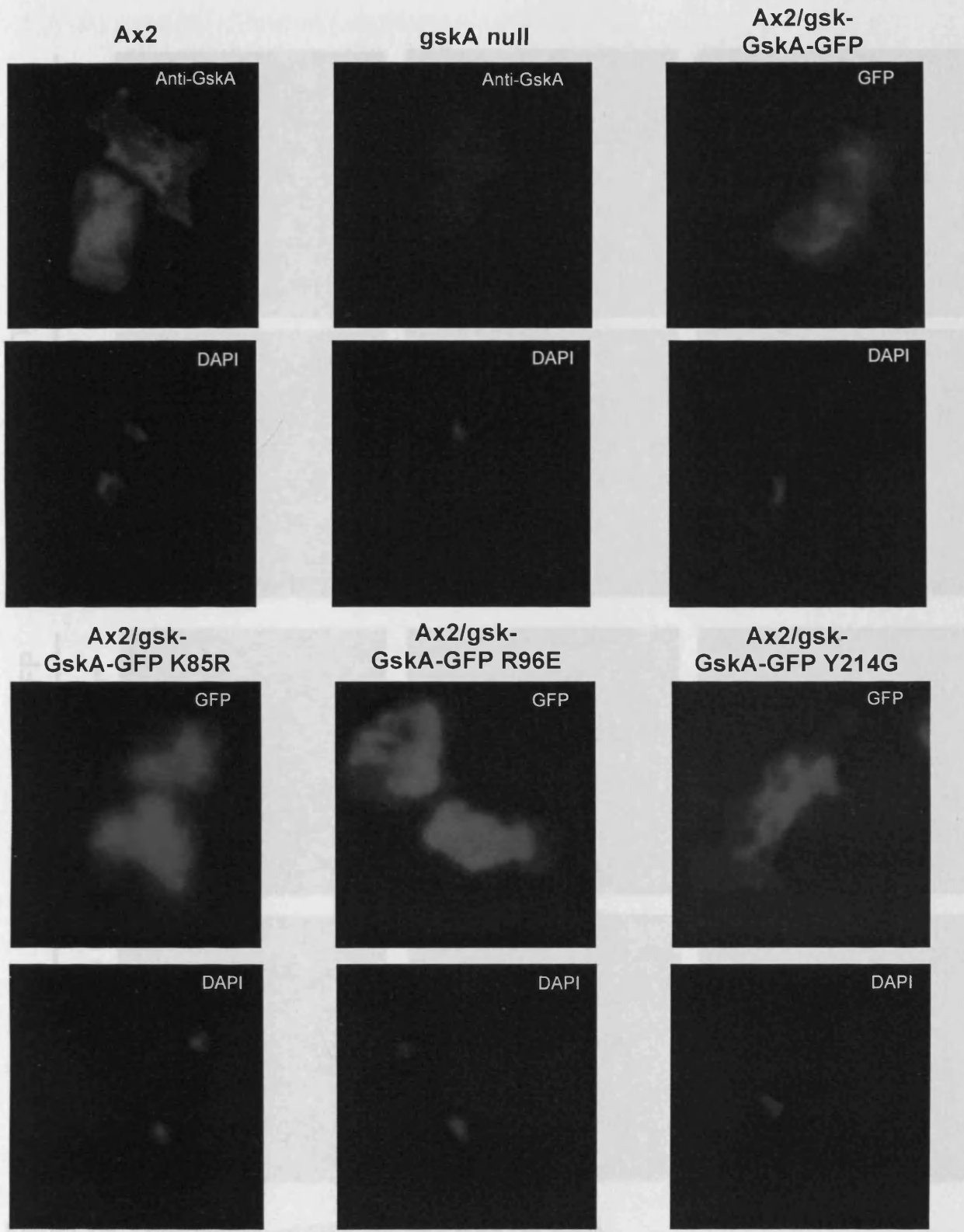


Figure 3.7. Localisation of GskA and GskA-GFP

Ax2 and *gskA* null cells were fixed with methanol and stained with both DAPI and an anti-sgg antibody. Cells expressing GskA-GFP fusion proteins or GFP were fixed and stained with DAPI. These cells were visualized for DAPI and GFP fluorescence. The images presented here are representative of the larger population (n>20)

3.4 Assessment of kinase activity

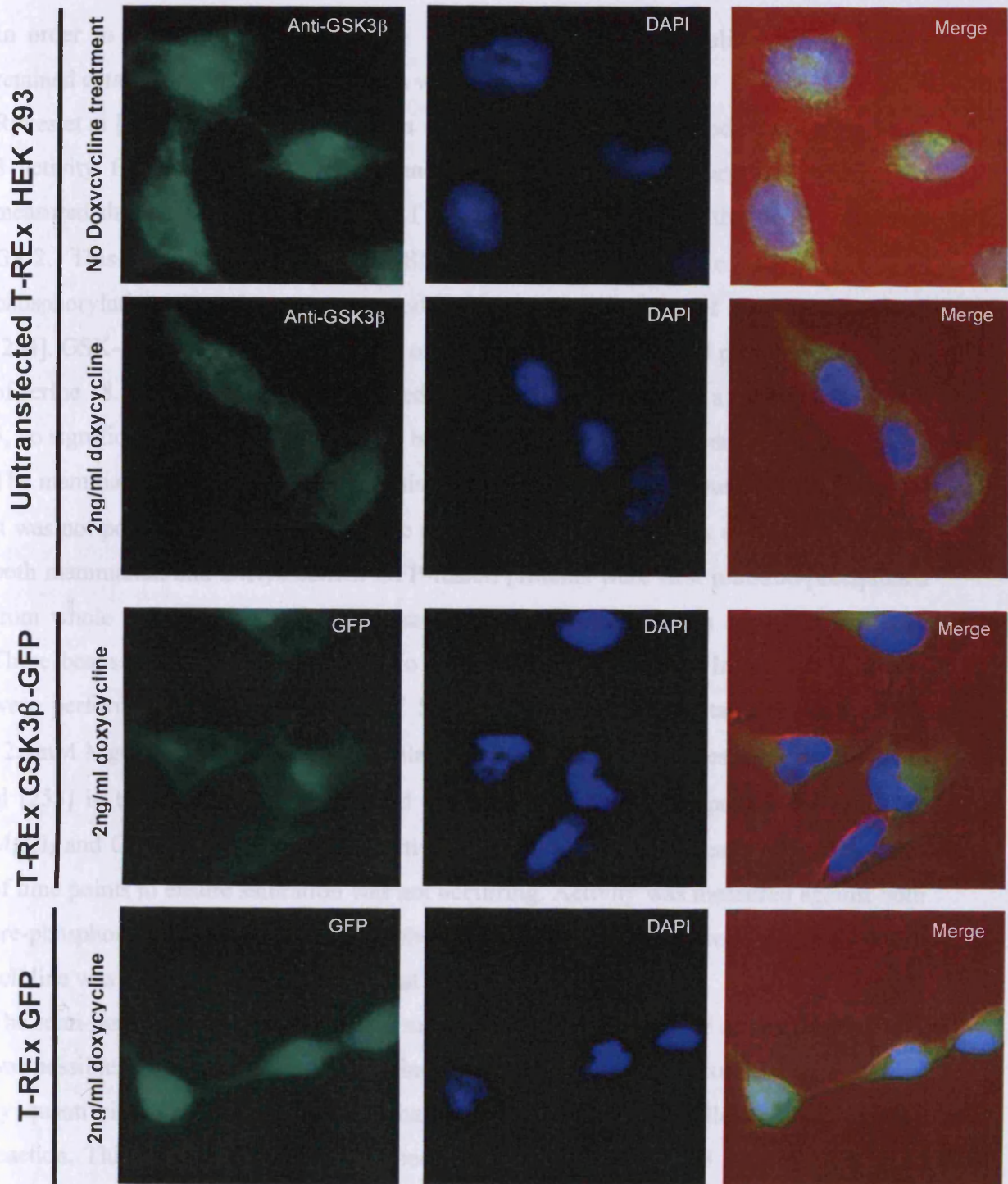


Figure 3.8. Localisation of GSK-3 β and GSK-3 β -GFP

Untransfected T-REx HEK 293 cells +/- 24 hour induction with 2ng/ml Doxycycline were PFA fixed and stained with both DAPI and an anti-GSK-3 β antibody. T-REx cells expressing either GSK-3 β -GFP or GFP were induced with 2ng/ml Doxycycline for 24 hours, PFA fixed and stained with DAPI. Cells were visualized for DAPI and GFP fluorescence. The images presented here are representative of the larger population of cells (n>20)

3.4 Assessment of kinase activity

In order to demonstrate that both the *Dictyostelium* and mammalian fusion proteins retained catalytic activity, kinase assays were performed.

Ryves et al [253] previously described a specific and sensitive method of detecting GSK-3 activity from both *Dictyostelium* and mammalian crude cell extracts where they measured the incorporation of ^{32}P - γ -ATP into a peptide based on the GSK-3 substrate GS-2. This peptide, termed the 'GSM peptide' contained 3 overlapping GSK-3 phosphorylation sites that corresponded to substrate sites 3a-c of glycogen synthase [254]. GSK-3 directed phosphorylation of the GSM peptide required pre-phosphorylation of serine 18. When a non-phosphorylated GSM peptide was used as a substrate for GSK-3, no significant phosphorylation above background levels was detected [253].

The mammalian T-REx cells used in this study expressed endogenous GSK3 β , therefore it was not possible to directly apply the methods outlined by Ryves et al [253]. Instead, both mammalian and *Dictyostelium* GFP-fusion proteins were first immuno-precipitated from whole cell lysates and immobilized on beads coated with an anti-GFP antibody. These beads were then used directly to assess catalytic activity. Initial kinase assays were performed in a total volume of 50 μl of kinase buffer containing 50 μM ATP, 12.5mM MgCl_2 and 425 μM GSM, similar to the assay conditions described by Ryves et al [253] in terms of cell numbers (and inferred GskA / GSK-3 β protein levels) ATP, MgCl_2 and GSM concentration. The activity of each sample was measured over a series of time points to ensure saturation was not occurring. Activity was measured against both pre-phosphorylated GSM and un-phosphorylated GSM and the appropriate GFP control cell line was included to demonstrate that activity was specific.

The semi-purified nature of the protein samples used for these kinase assays meant that it was possible to use the Kinase-Glo luminescent kinase assay to measure catalytic activity by quantifying the amount of ATP that remained in solution following each kinase reaction. This method has previously been used to measure GSK-3 activity [167, 255-258] and represented a non-radioactive, high-through-put approach to quickly assess catalytic activity. This method measured the intensity of the luminescence generated by mono-oxygenation of beetle luciferin by luciferase, in the presence of Mg^{2+} ATP. This

reaction consumed one ATP molecule and produced one photon per turnover, Therefore, the resultant luminescence signal was proportional to the amount of ATP present and inversely correlated to GSK-3 kinase activity.

Kinase assays were terminated by the addition of the kinase-glo reagent and glow-type luminescence measured. Catalytic activity was calculated in reference to samples containing ATP, GSM and beads that were not incubated with cell lysate, and expressed as Δ -relative light units (Δ -RLU) (Figure 3.9). These experiments demonstrated that both the wild-type GskA-GFP and GSK-3 β -GFP fusion proteins were catalytically active and that this activity was specific.

The catalytic activity of each of the *Dictyostelium* GskA-GFP mutant cell lines were also assessed using this technique. In order to directly compare the various GskA-GFP fusion proteins, cell lysates were first normalized based on GFP fluorescence (and inferred GskA-GFP protein content) to ensure an equal amount of protein was available to become immobilized on the anti-GFP beads. Equal levels of protein immobilization were confirmed by western transfer (Figure 3.10).

As expected, the kinase dead GskA-GFP K85R mutant did not exhibit any catalytic activity (Figure 3.10). The GskA-GFP Y214G mutant also failed to exhibit any kinase activity, which is consistent with other studies into the role of Y214 in *Dictyostelium* [81]. The GskA-GFP R96E mutant did exhibit a low level of catalytic activity towards the primed peptide relative to the non-phosphorylated peptide. This finding is consistent with other reports on the effect of mutating Arg96 [259] and is perhaps indicative that the residues R178 and L203 (analogous to R180 and L205 of mammalian GSK3 β respectively) retained the ability to interact with the primed substrate and orientate it appropriately across the catalytic groove.

The experiments described here do not represent a detailed study of the catalytic profiles of the various GSK-3-GFP fusion proteins. Such a study would certainly be informative, however this was not undertaken as part of this current scheme of work as the protein samples used here represented the products of crude affinity purifications and purified proteins would be required to fully assess the function of specific residues. However, the experiments presented here do demonstrate that both the wild-type GskA-GFP and GSK-3 β -GFP fusion proteins exhibited catalytic activity and that this activity was specific.

A

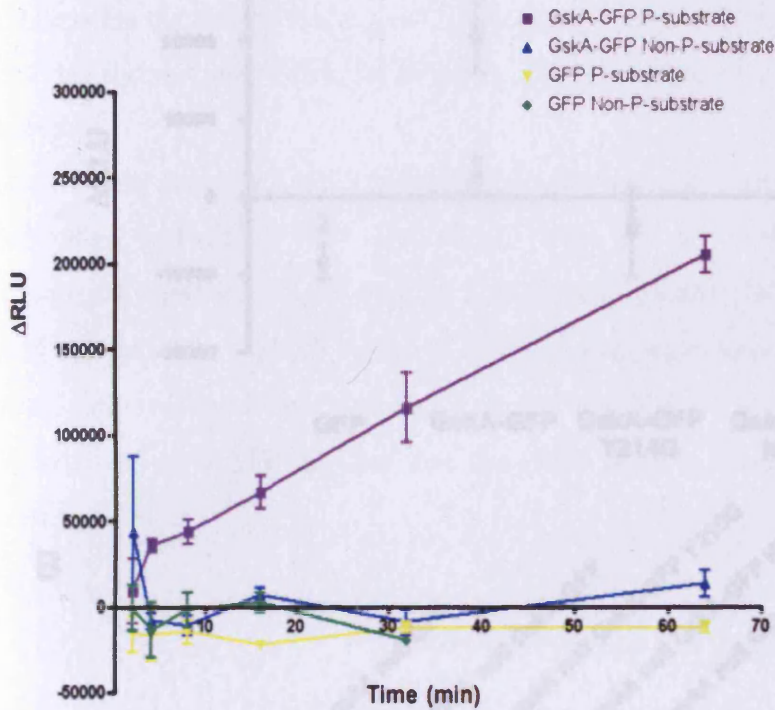
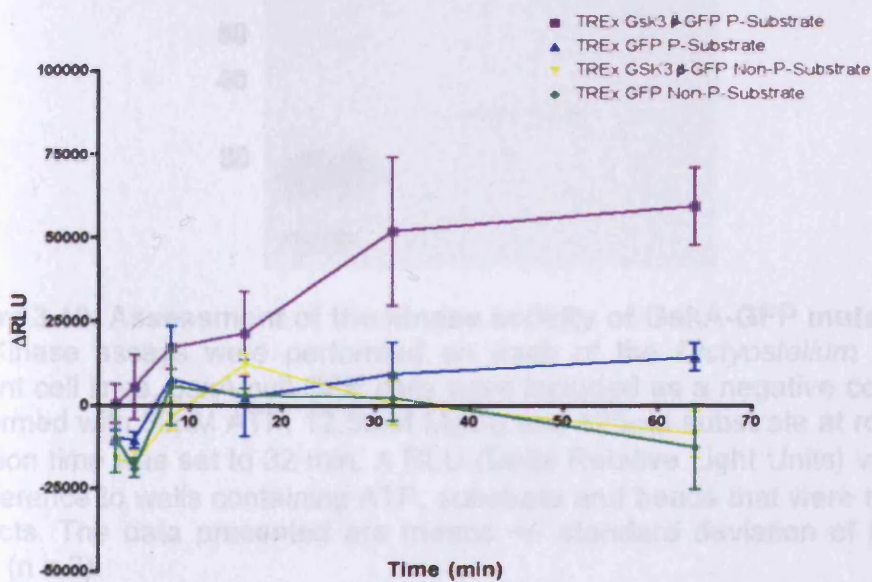


Figure 3.9. Assessment of kinase activity

Kinase assays were performed using cellular extracts from (A) *Dictyostelium* and (B) TREx cells as indicated. Reactions were performed with 50 μ M ATP, 12.5mM MgCl₂ and 425 μ M substrate, at room temperature, over a series of time points. Δ RLU (Delta Relative Light Units) values were calculated in reference to wells containing ATP, substrate and beads that were not incubated with cell extracts. The data presented are means \pm standard deviation of the mean of triplicate wells (n = 3)

B



3.5 Conclusions

In this chapter I have described the generation of a series of *Dictyostelium* null cell lines expressing different GskA-GFP fusion proteins that will be used to further characterize the role of GskA in *Dictyostelium*. I have demonstrated that the addition of a GFP tag did not affect GskA localization and that wild-type GskA-GFP was catalytically active. I have also described the generation of doxycycline inducible HEK293 cell lines expressing GSK-3 β -GFP or GFP alone. These cell lines will be used in chapter 5 to investigate whether GSK-3 β activity is regulated through protein binding partners. I have demonstrated that the levels of GSK-3 β over-expression used in this study did not affect cell viability. I have also demonstrated that the GSK-3 β fusion protein was catalytically active.

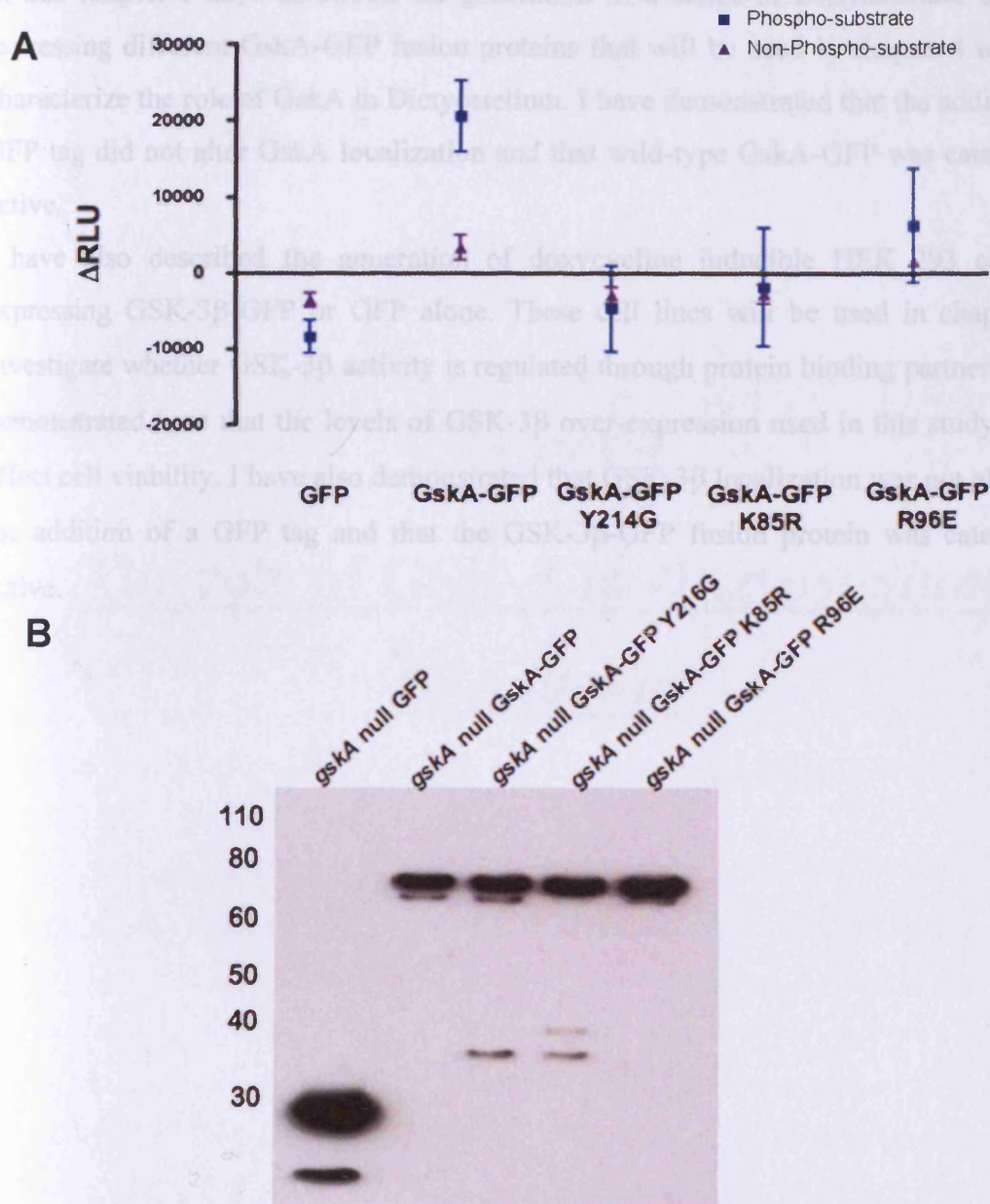


Figure 3.10. Assessment of the kinase activity of GskA-GFP mutants

(A) Kinase assays were performed on each of the *Dictyostelium gskA* null GskA-GFP mutant cell lines, *gskA* null-GFP cells were included as a negative control. Reactions were performed with 50 μ M ATP, 12.5mM MgCl₂ and 425 μ M substrate at room temperature. The reaction time was set to 32 min. Δ RLU (Delta Relative Light Units) values were calculated in reference to wells containing ATP, substrate and beads that were not incubated with cell extracts. The data presented are means \pm standard deviation of the mean of triplicate wells (n = 3).

(B) A Western blot was performed to demonstrate equal loading for the kinase assay, immunoblotted with an anti-GFP antibody.

3.5 Conclusions

In this chapter I have described the generation of a series of *Dictyostelium* cell lines expressing different GskA-GFP fusion proteins that will be used in chapter 4 to further characterize the role of GskA in *Dictyostelium*. I have demonstrated that the addition of a GFP tag did not alter GskA localization and that wild-type GskA-GFP was catalytically active.

I have also described the generation of doxycycline inducible HEK 293 cell lines expressing GSK-3 β -GFP or GFP alone. These cell lines will be used in chapter 5 to investigate whether GSK-3 β activity is regulated through protein binding partners. I have demonstrated here that the levels of GSK-3 β over-expression used in this study did not affect cell viability. I have also demonstrated that GSK-3 β localization was not altered by the addition of a GFP tag and that the GSK-3 β -GFP fusion protein was catalytically active.

Chapter 4

The role of GSK-3 in *Dictyostelium* *discoideum*

In the previous chapter I described the generation of *Dictyostelium* cell lines expressing a series of GskA-GFP tagged proteins. As these cell lines were generated in a *gskA* null background I was able to utilize them to further characterize the role of GskA in *Dictyostelium*, and evaluate the roles of key residues.

Here, I describe the use of dark field microscopy to further characterize the developmental phenotype of the *gskA* null cell line, and describe the ability of each of the GskA-GFP fusion proteins to rescue this phenotype. I will also describe a previously undocumented phenotype exhibited by the *gskA* null cell line that indicates that GskA is important for the regulation of cytokinesis in *Dictyostelium*. Where cell lines expressing GskA-GFP fusion proteins are discussed two independently derived clones were analysed (indicated in Figure 3.1) unless stated otherwise.

4.1 GskA performs a role during early development

The developmental phenotype of the *gskA* null cell line has previously been described; loss of GskA resulted in the formation of small fruiting bodies with a reduced spore head [194, 195]. In order to further characterize the developmental phenotype of the *gskA* null cell line and to establish whether the GskA-GFP construct was capable of rescuing this phenotype, time-lapse movies were taken over a period of 48 hours.

The *gskA* null cell line formed numerous small aggregation territories. However, these cells did not obviously stream, rather the cells appeared to develop small, loose mounds in a random and disordered manner. At the mound stage, cells formed abnormal donut-like structures before continuing on to develop into small fruiting bodies (Figure 4.1 and Figure 4.2). The formation of these donut-like structures has previously been described as a consequence of inhibiting cAMP-dependent activation of an adenylate cyclase (ACA) using caffeine [260, 261], and as a phenotype of cells over-expressing a constitutively active form of the G α 1-subunit of heterotrimeric G-proteins [262].

gskA null cells expressing wild-type GskA-GFP were capable of streaming to a similar degree as Ax2 cells, although they were considerably slower in their initiation. The final fruiting bodies were also comparable in size to Ax2 (Figure 4.1 and Figure 4.2). Cells

expressing kinase dead, GskA-GFP-K85R exhibited a *gskA* null phenotype, indicating that kinase activity was required.

Cells expressing either GskA-GFP-Y216G or GskA-GFP-R96E were able to stream, although aggregation territories were smaller than those of Ax2. The GskA-GFP-R96E cell lines continued to form donut-like structures in a similar manner to the *gskA* null cells (Figure 4.2). Furthermore, this cell line took considerably longer to complete development (nearly 48 hours compared to the normal 24 hours). The finding that both the GskA-GFP R96E and GskA-GFP Y214G cell lines were capable of partially rescuing development was surprising given the results from the kinase assay described in Chapter 3. That both of these cell lines, but not the GskA-GFP K85R mutant were capable of some level of rescue would argue that these fusion proteins did retain some activity. The possible causes of this discrepancy will be discussed at the end of this chapter.

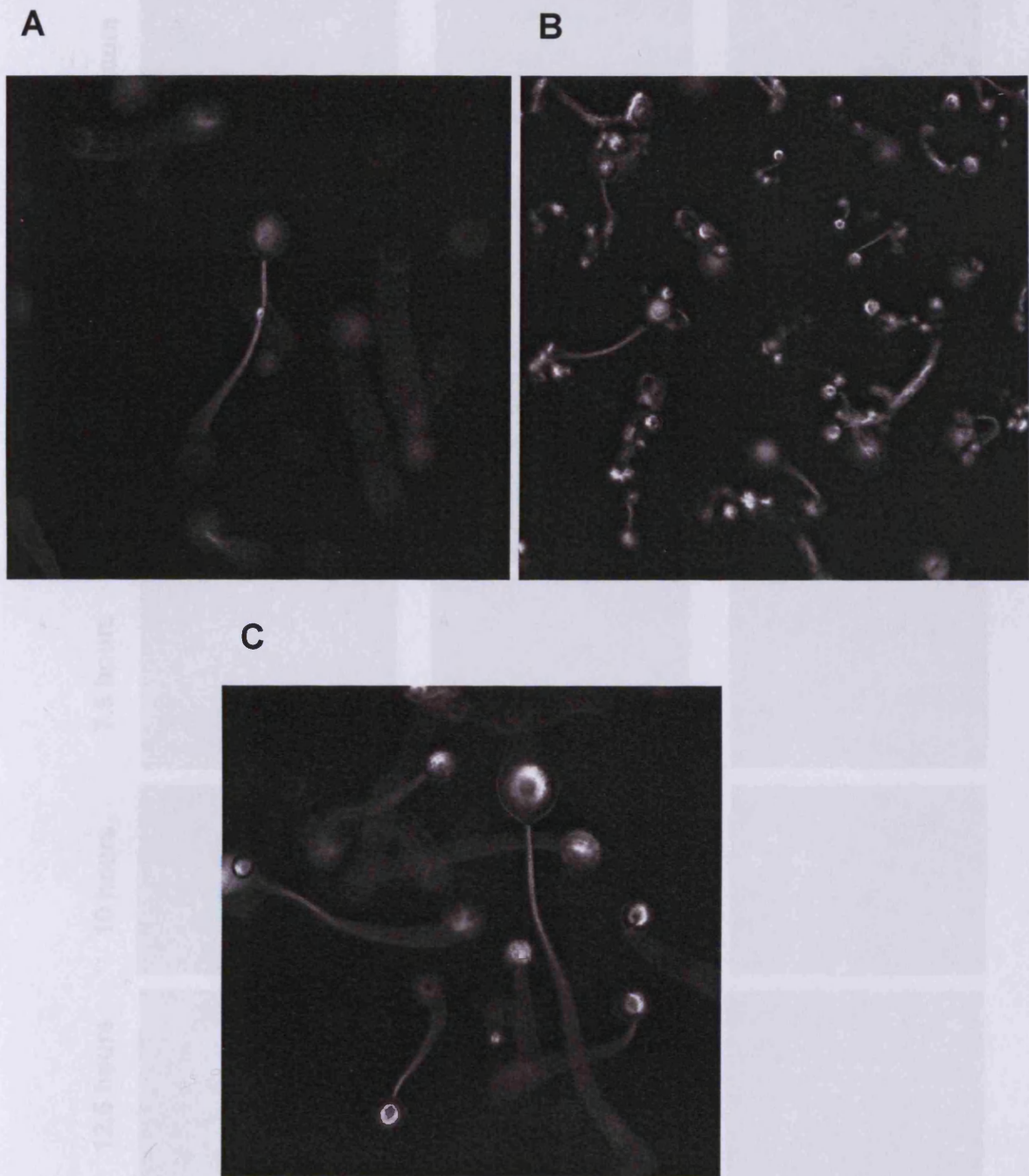


Figure 4.1. Analysis of the terminal morphology of *gskA* null fruiting bodies and the ability of GskA-GFP to rescue
 10^6 cells were allowed to terminally differentiate on agar plates (24 hours) before being imaged under dark field conditions (see later) using a X40 objective. A) Ax2, B) *gskA* null and C) *gskA* null - GskA-GFP

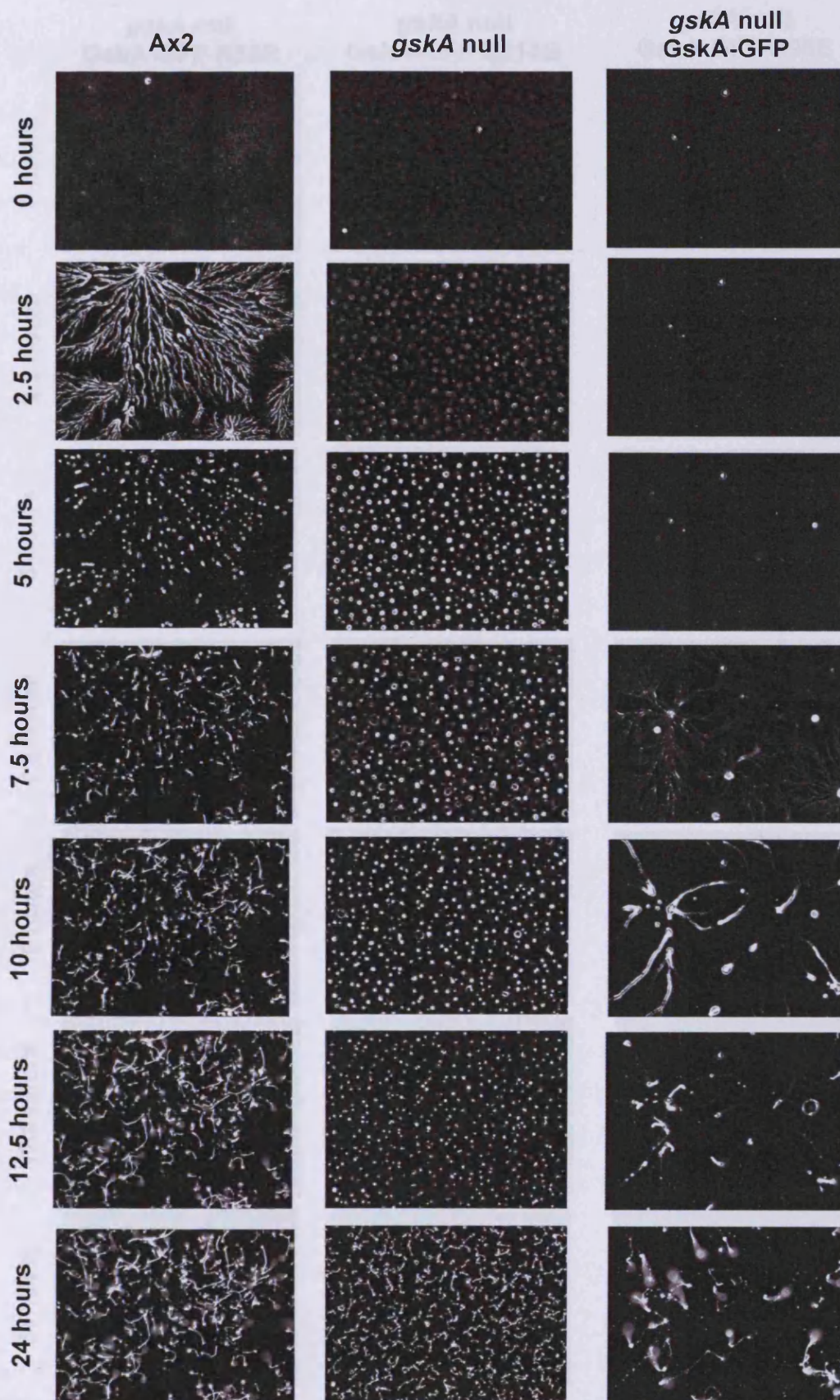


Figure 4.2. Analysis of development

10^6 cells from each cell line were plated onto non-nutrient agar and allowed to develop. Images were taken every 5 minutes over a 48hr period. Experiments were repeated on 3 separate occasions and two independent cell lines expressing each GskA-GFP fusion protein were developed on each occasion.

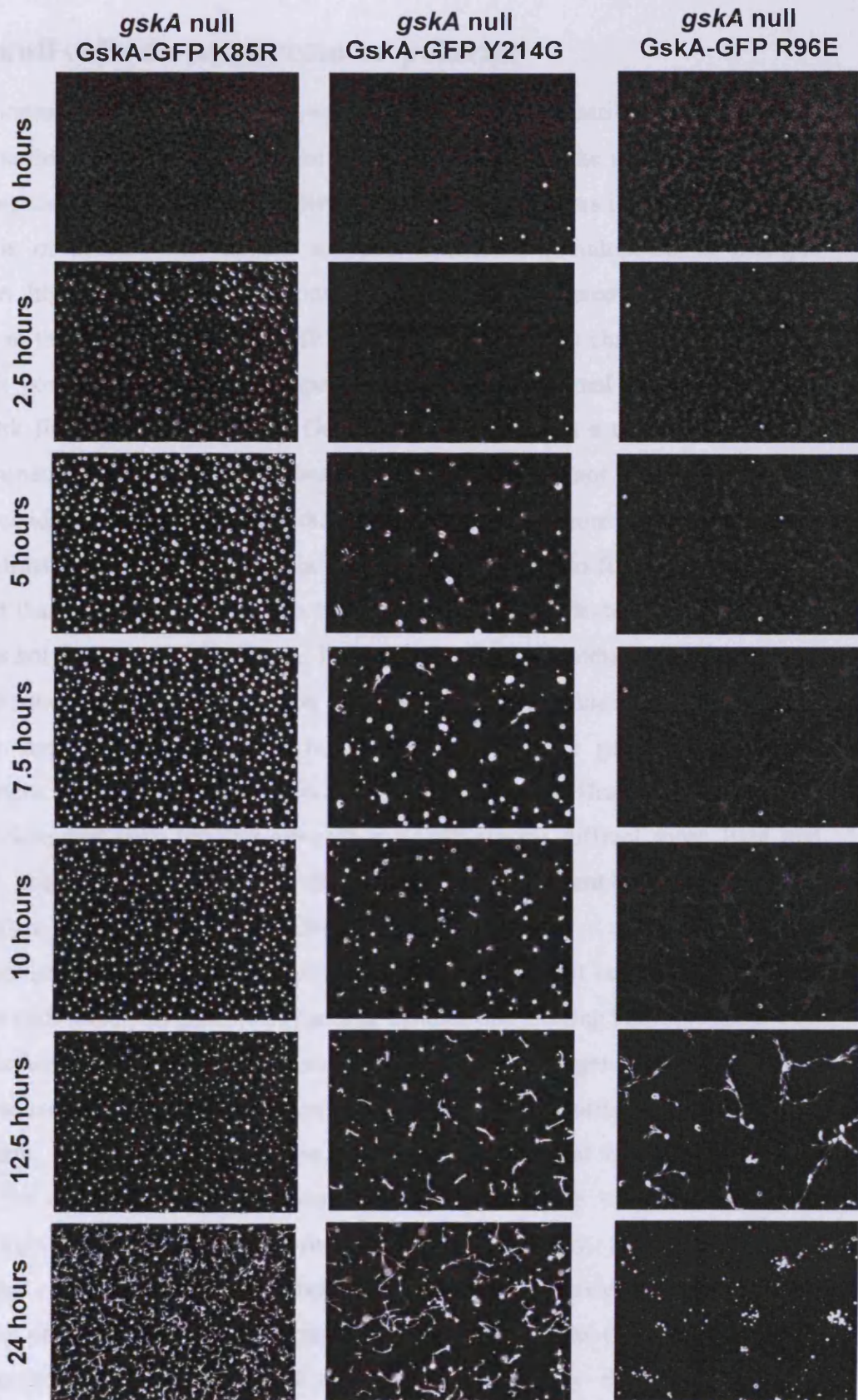


Figure 4.2. Analysis of development

10^6 cells from each cell line were plated onto non-nutrient agar and allowed to develop. Images were taken every 5 minutes over a 48hr period. Experiments were repeated on 3 separate occasions and two independent cell lines expressing each GskA-GFP fusion protein were developed on each occasion.

4.2 *gskA* null cells do not stream or polarize

During development, *Dictyostelium* aggregate in response to pulsatile waves of cAMP that propagate through a population of cells, directing them to the nearest aggregation centre. Throughout aggregation cells undergo characteristic changes in shape; under low concentrations of cAMP cells appear rounded, extending pseudopodia in multiple directions. In high cAMP concentrations cells become elongated and only extend pseudopodia in the direction of the cAMP source. These periodic changes in cell shape have made it possible to study the propagation of a cAMP signal using a technique known as dark field microscopy [263]. Dark field microscopy is a technique that uses oblique illumination to enhance the contrast in samples that are not imaged well under bright-field conditions. Light passing through the specimen from oblique angles is diffracted, refracted, and reflected into the microscope objective to form a bright image. Oblique light that does not pass through the specimen is not collected by the objective lens and does not form part of the image. This has the affect of producing a dark, almost black, background with bright objects on it. Under dark field illumination aggregating *Dictyostelium* appear to form concentric wave patterns. These patterns result from periodic changes in cell shape, round non-moving cells do not diffract light and appear dark, while elongated cells moving towards a cAMP source diffract more light and appear white. These changes in light scattering during cell movement have been shown to directly correlate with waves of cAMP [264].

Timelapse movies revealed that during development the *gskA* null cells failed to stream and yet, these cells were still capable of forming mounds and fruiting bodies (Figure 4.2). In order to further characterize this phenomenon and monitor changes in cell shape, dark-field timelapse microscopy was used to capture cell movements during the first 15 hours of development. The resulting time-lapse movies were processed by subtracting each frame from the one before, so that changes in cell movements were converted into changes in light intensity. By monitoring changes in intensity, it was possible to distinguish the early, uncoordinated random movements of individual cells from the periodic waves of movement as cells aggregate towards a focal point (Figure 4.3).

These movies revealed that *gskA* null cells did not form any discernable patterns associated with changes in cell shape during cell aggregation. This would suggest that

gskA null cells were either not capable of generating cAMP pulses or were unable to respond to them. The *gskA* null-GskA-GFP cell line did form wave patterns during aggregation although they were not as well defined as those of Ax2 cells and, as with development in general, these waves appeared several hours later than in the Ax2 cell line. The *gskA* null-GskA-GFP K85R cell line did not form any discernable patterns during the aggregation process similar to the *gskA* null cell line.

It is unclear whether cells expressing either GskA-GFP-Y214G or GskA-GFP-R96E were capable of forming patterns during aggregation. The formation of wave patterns can be rather subjective and any patterns relating to these cell lines were poorly defined, and were impossible to discern in still images (data not shown).

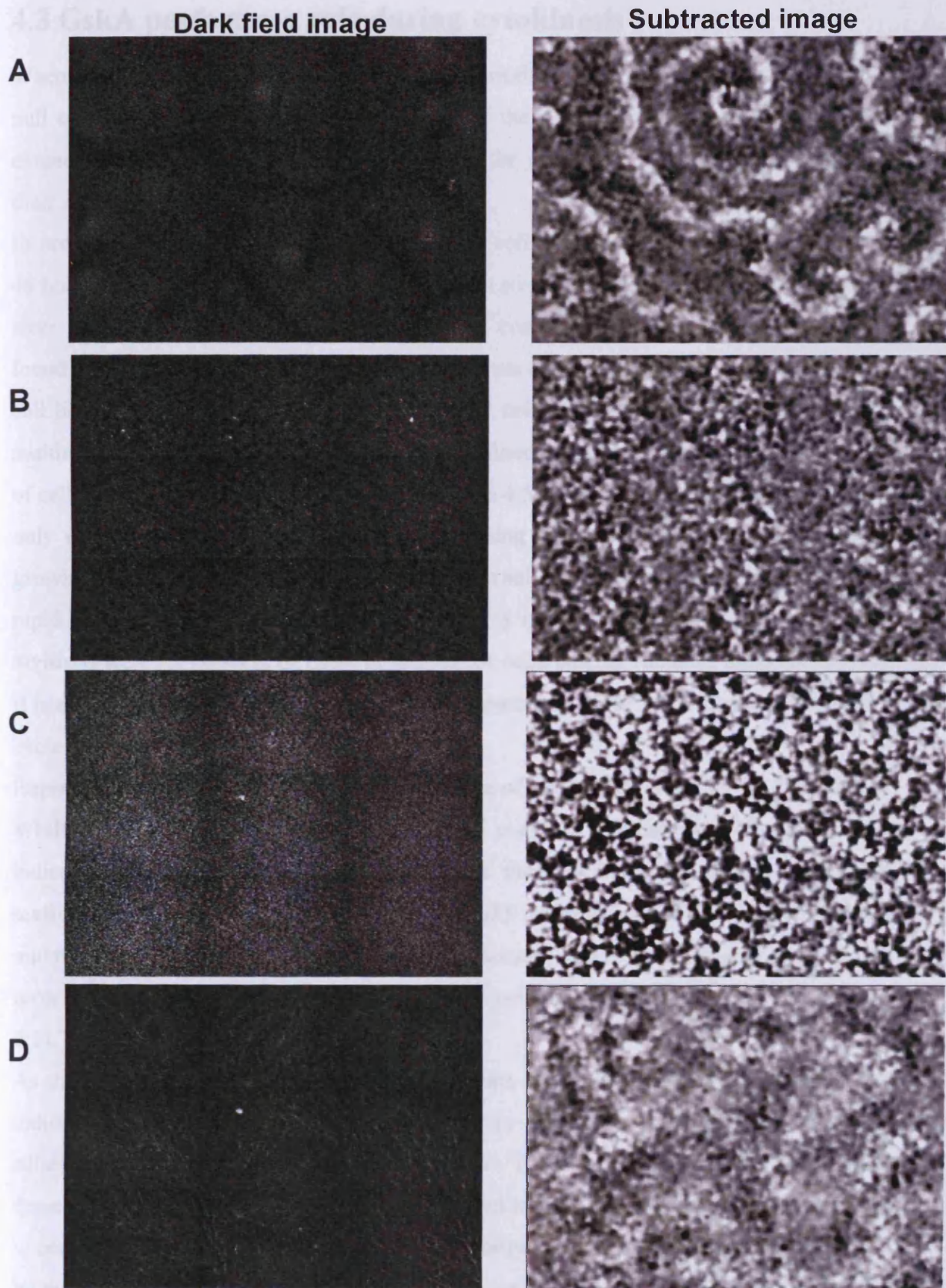


Figure 4.3. Analysis of the cellular morphology of cells during aggregation
 10^5 Ax2(A), *gskA* null (B) and *gskA* null-GskA-GFP (C&D) cells were plated onto non-nutrient agar and allowed to develop. Time-lapse, dark field images were taken every 30 seconds. Images were taken after 4.5 hours (A-C) and 8 hours (D).

4.3 GskA performs a role during cytokinesis

When grown in shaking culture for prolonged periods of time, the growth rate of the *gskA* null cells appeared to slow compared to that of the Ax2 cells. Furthermore, after these extended periods of growth in shaking culture the *gskA* null cells appeared larger than their Ax2 counterparts.

In order to investigate this phenomenon further cells were grown in shaking culture for 48 hours before briefly being allowed to settle on coverslips, fixed and dapi stained. Cells were then scored on the number of nuclei they contained. The *gskA* null cell line was found to have a significant number of multinucleate cells compared to the wild-type Ax2 cell line; the average number of nuclei per Ax2 cell was 1.32 and 24.7% of cells were multinucleate, while the *gskA* null cell line contained on average 2.08 nuclei and 60.13% of cells were multinucleate (Table 4.1 and Figure 4.5). This multinucleate phenotype was only observed when cells were grown in shaking culture. When cells that had been growing in shaking culture were plated out onto a solid surface they underwent a series of rapid divisions to become mononuclear within a matter of hours (Figure 4.6). These divisions were reminiscent of those described for cells lacking the gene encoding myosin II heavy chain (*mhcA*) and appeared to occur independent of the cells' position in the cell-cycle [226].

Expression of wild-type GskA-GFP was capable of rescuing this phenotype (Table 4.1). While expression of GskA-GFP-K85R did not result in any rescue of this phenotype, indicating that kinase activity was required and that GskA was not simply acting as a scaffold in this context. Expression of GskA-GFP carrying either the Y214G or R96E mutations was not sufficient to rescue this phenotype, and cells expressing those fusion proteins continued to form some multi-nucleate cells, albeit at a lower frequency (Table 4.1).

As the *gskA* null cells only became multinucleate when grown in shaking culture, this indicated that they were possibly deficient in Cytokinesis A (myosin-dependent, adhesion-independent) but not Cytokinesis B (myosin-independent, adhesion-dependent)(Figure 1.6). Cytokinesis B is reported to take twice as long as cytokinesis A to complete [224, 225]. In order to investigate further the means of cytokinesis employed by the *gskA* null cells, timelapse movies were generated of cells growing and dividing

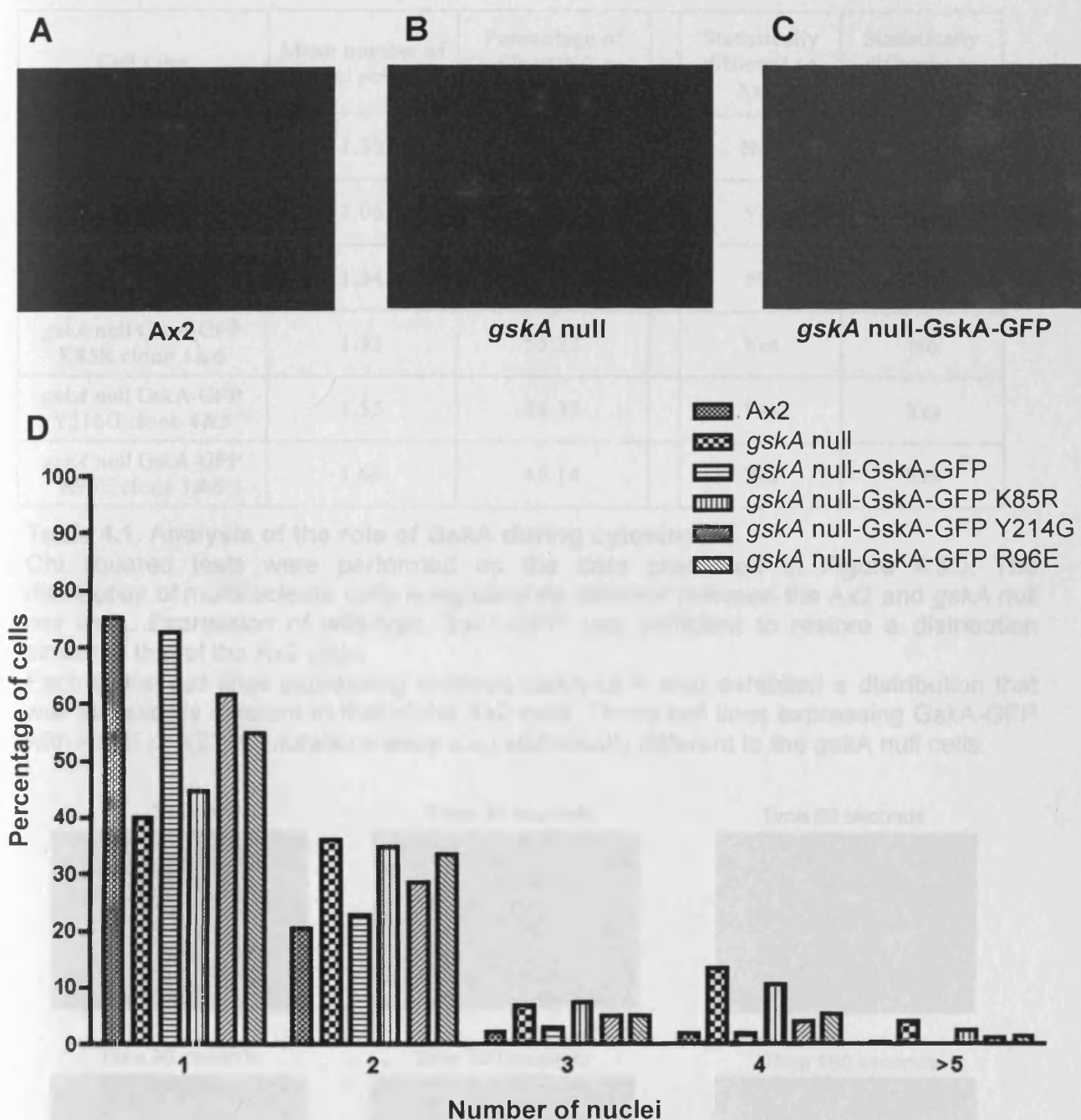


Figure 4.5. Analysis of the role of GskA during cytokinesis

Ax2 (A), *gskA* null (B) and *gskA* null GskA-GFP (C) cells were grown in shaking culture for 48 hours before being allowed to adhere to coverslips, methanol fixed and DAPI stained. DAPI images were taken using a 60x objective.

Slides containing cells expressing GskA-GFP fusion proteins harbouring Y214G, R96E or K85R mutations were prepared in a similar fashion. All cells were scored on the number of nuclei they contained (D). For each cell line expressing a GskA-GFP fusion protein, data from two independent clones was pooled (the same trend was observed for each individual cell line). The data represented here was collected from 3 independent experiments, n>2000 cells.

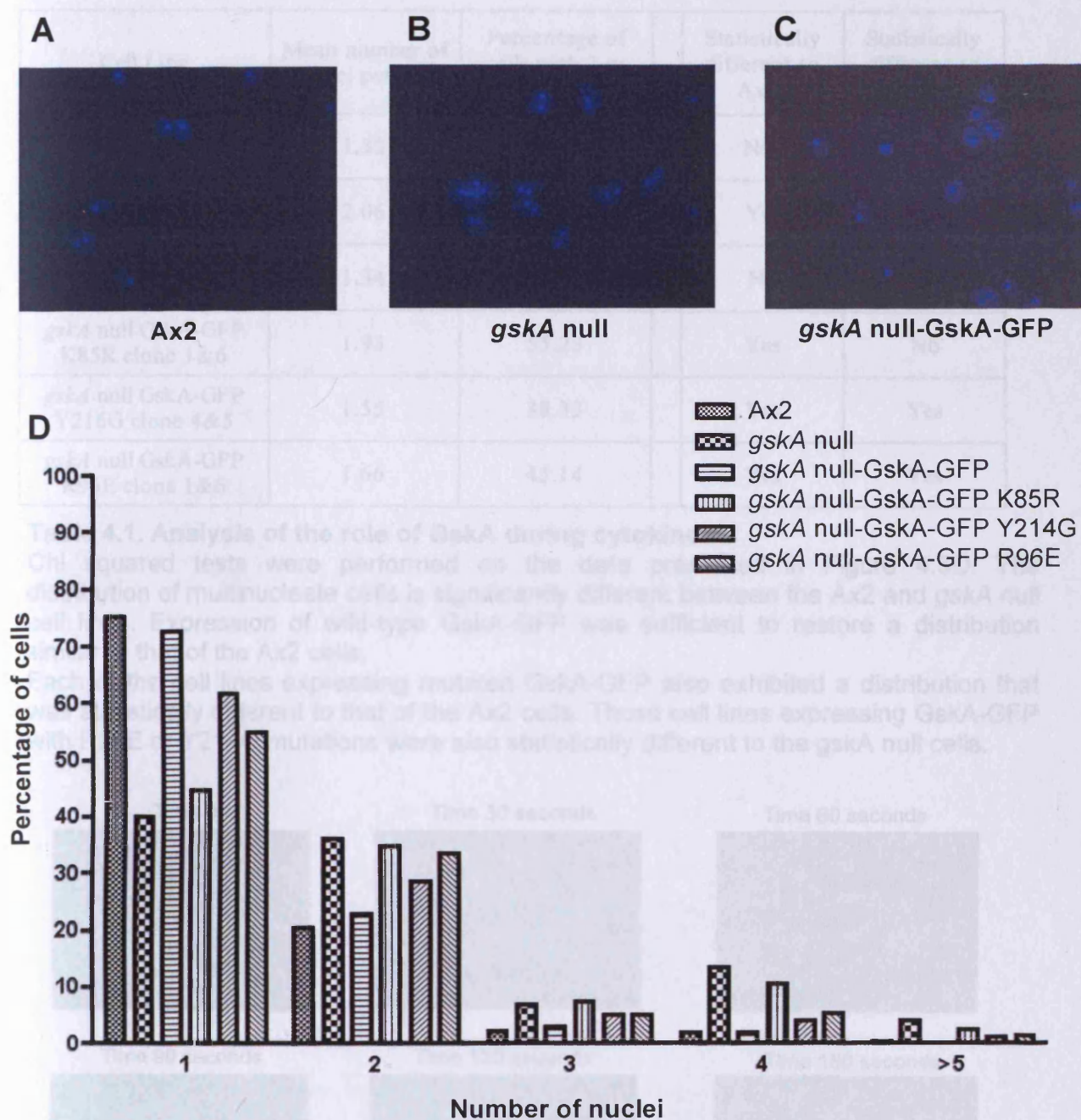


Figure 4.5. Analysis of the role of GskA during cytokinesis

Ax2 (A), *gskA* null (B) and *gskA* null GskA-GFP (C) cells were grown in shaking culture for 48 hours before being allowed to adhere to coverslips, methanol fixed and DAPI stained. DAPI images were taken using a 60x objective.

Slides containing cells expressing GskA-GFP fusion proteins harbouring Y214G, R96E or K85R mutations were prepared in a similar fashion. All cells were scored on the number of nuclei they contained (D). For each cell line expressing a GskA-GFP fusion protein, data from two independent clones was pooled (the same trend was observed for each individual cell line). The data represented here was collected from 3 independent experiments, n>2000 cells.

Cell Line	Mean number of nuclei per cell	Percentage of cells with 2 or more nuclei	Statistically different to Ax2?	Statistically different to <i>gskA</i> null?
Ax2	1.32	24.74	N/A	Yes
<i>gskA</i> null	2.06	60.13	Yes	N/A
<i>gskA</i> null GskA-GFP clone 1&2	1.34	27.47	No	Yes
<i>gskA</i> null GskA-GFP K85R clone 1&6	1.93	55.23	Yes	No
<i>gskA</i> null GskA-GFP Y216G clone 4&5	1.55	38.33	Yes	Yes
<i>gskA</i> null GskA-GFP R96E clone 1&6	1.66	45.14	Yes	Yes

Table 4.1. Analysis of the role of GskA during cytokinesis

Chi squared tests were performed on the data presented in Figure 4.5D. The distribution of multinucleate cells is significantly different between the Ax2 and *gskA* null cell lines. Expression of wild-type GskA-GFP was sufficient to restore a distribution similar to that of the Ax2 cells.

Each of the cell lines expressing mutated GskA-GFP also exhibited a distribution that was statistically different to that of the Ax2 cells. Those cell lines expressing GskA-GFP with R96E or Y214G mutations were also statistically different to the *gskA* null cells.

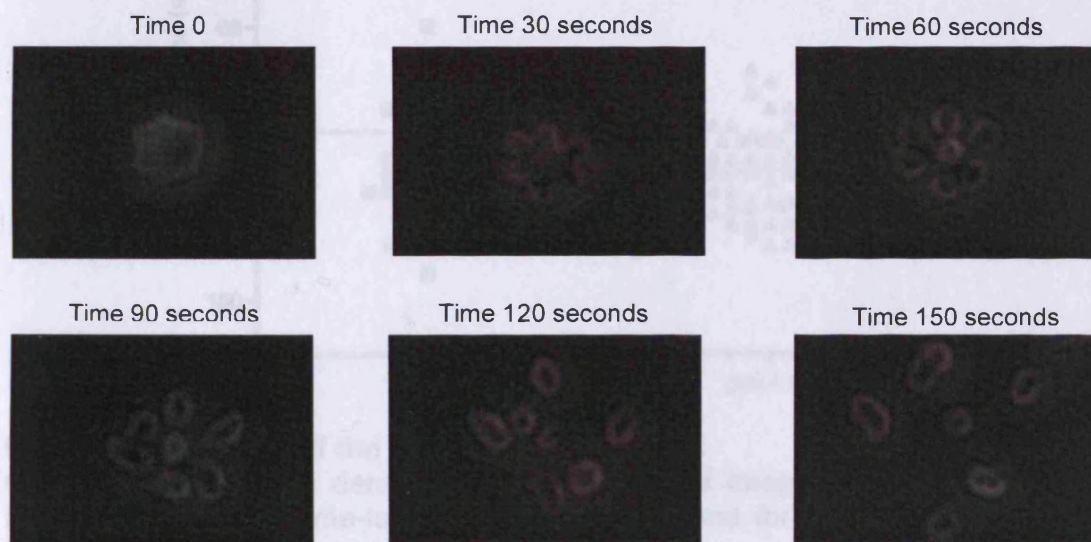


Figure 4.6. *gskA* null cells were deficient in Cytokinesis A

gskA null cells were grown in shaking culture for 48 hours before being returned to a solid surface. Dark-field, time lapse images were taken every 30 seconds using a 20x objective. Here, a single *gskA* null cell is shown undergoing a multi-directional division event to become uni-nuclear.

on a solid surface.

These movies were used to score the time taken for cytokinesis events to occur. The start of cytokinesis was defined as the time at which a cell became rounded and the end of cytokinesis was judged to be the time at which two daughter cells were seen to be clearly separated. The timing of these events could be considered to be largely subjective, so in order to ensure that the data was not biased, these measurements were made without knowing which cell line was being scored.

The timings for the cytokinesis events of the *gskA* null cells were more closely distributed than those of the Ax2 cells, and statistical analysis revealed that the times taken for these cell lines to complete cytokinesis were different (Figure 4.7).

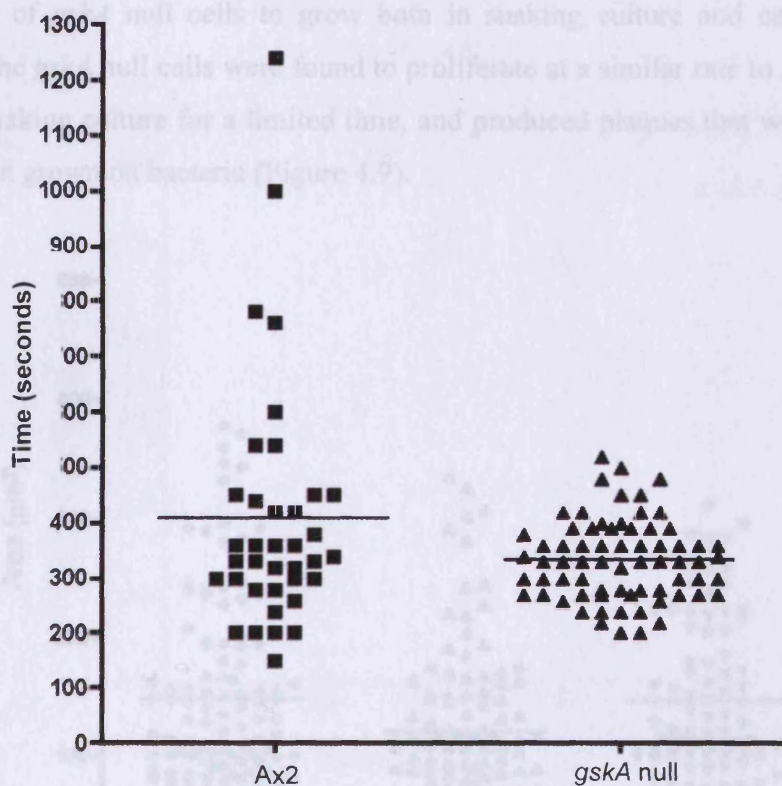


Figure 4.7. Analysis of the timing of cytokinesis

Cells were plated at a density of 10^5 cells/ml and imaged every 30 seconds for 2 hours. The resulting time-lapse movies were scored for the time taken for cells to complete cytokinesis.

This data represents 3 independent experiments, ($n > 37$ cytokinesis events). The time taken for the Ax2 cells to complete cytokinesis was statistically different to that of the *gskA* nulls ($P > 0.05$ un-paired T-test).

4.4 Ax2/*gsk*- cells are smaller than their Ax2 counterparts

Given that the *gskA* null cells appear to have some deficiency during cell division I looked for alterations in cell size or proliferation rates. Indeed, while culturing the *gskA* null cells it was noted that they appeared to be consistently smaller than their Ax2 counterparts; *gskA* null plates consistently yielded more cells than their Ax2 counterparts despite appearing similarly confluent. In order to quantify these differences, time-lapse movies were generated that were then analysed using the 2-dimension dynamic image analysis system (2D-DIAS). This program measured the area occupied by individual cells. *gskA* null cells were found to be smaller than their Ax2 counterparts and expression of GskA-GFP was capable of rescuing this phenotype (Figure 4.8).

The ability of *gskA* null cells to grow both in shaking culture and on bacteria were assessed; The *gskA* null cells were found to proliferate at a similar rate to Ax2 cells when grown in shaking culture for a limited time, and produced plaques that were comparable to Ax2 when grown on bacteria (Figure 4.9).

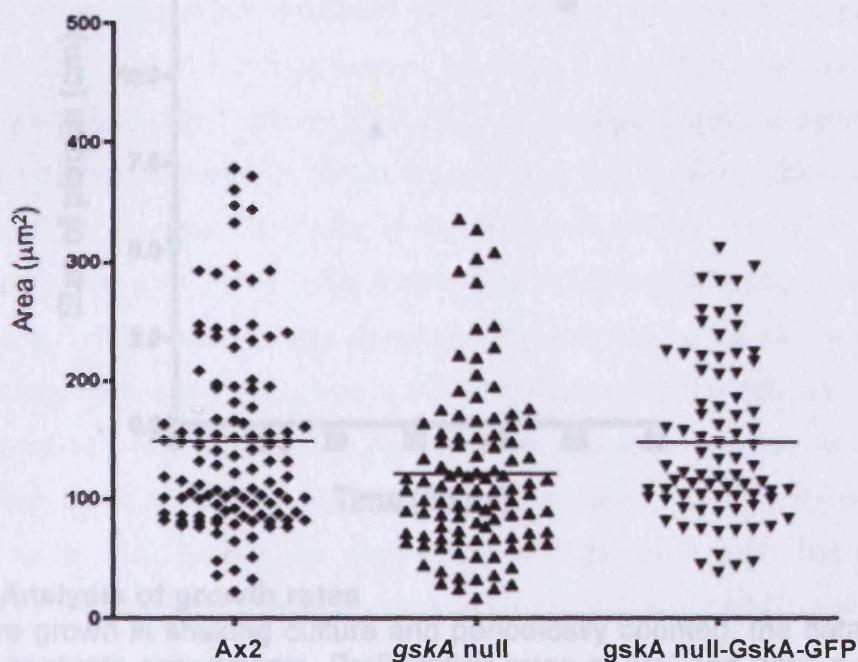


Figure 4.8. Comparison of cell size between cell lines

Timelapse movies of each cell line were analysed using the program 2D-DIAS. Measurements of the area occupied by *gskA* null cells were found to be statistically different to both Ax2 and *gskA* null-GskA-GFP cell lines ($P < 0.05$ One-way Anova, Tukey's multiple comparison test)

4.5 Conclusions

In this chapter I demonstrated that *GskA* functions during the early stages of *Dicryostelium* development and that expression of wild-type *GskA-GFP* is sufficient to rescue the developmental phenotypes of the *gskA* nulls. The delay in covering development of the *gskA* null-*GskA-GFP* cells may result from the control of the *act15* promoter as apposed to the *GskA* promoter. The *act15* promoter is widely used for expression studies in *Dicryostelium* as it is expressed throughout development. However, the expression profile for the *act15* gene (*act15*) differs from that of the gene encoding *GskA*, and may account for the timing differences.

In this chapter I further examined the role of *GskA* during early development using time-lapse microscopy. I demonstrated that the *gskA* null cells did not stream and that these cells formed tiny aggregations to a yeast like structure and small trailing bodies. Furthermore, the dark-field time-lapse movies revealed that the *gskA* nulls did not undergo periodic contractions during aggregation, indicating that these cells were unable to polarize.

The formation of yeast-like structures at the mid and end stage of development has previously been shown as a consequence of inhibiting cAMP-dependent activation of adenylyl cyclase (ACA) using caffeine [26]. Dr Jonathan Beckly, a member of our lab has performed experiments that further support a link between *GskA* and ACA activation. Dr Beckly tested the ability of the *gskA* null cells to respond to a cAMP signal by growing cells with 2-deoxyadenosine 3,5-cyanophosphate (dcAMP), a cAMP derivative. Cells respond to this stimulation by activating ACA and synthesizing cAMP derivatives. However, there was a 5-fold reduction in the amount of cAMP produced by *gskA* null cells. This reduction in cAMP production while *gskA* null cells were able to respond to cAMP, the response was severely attenuated.

This finding would also explain the observation that the *gskA* nulls formed small

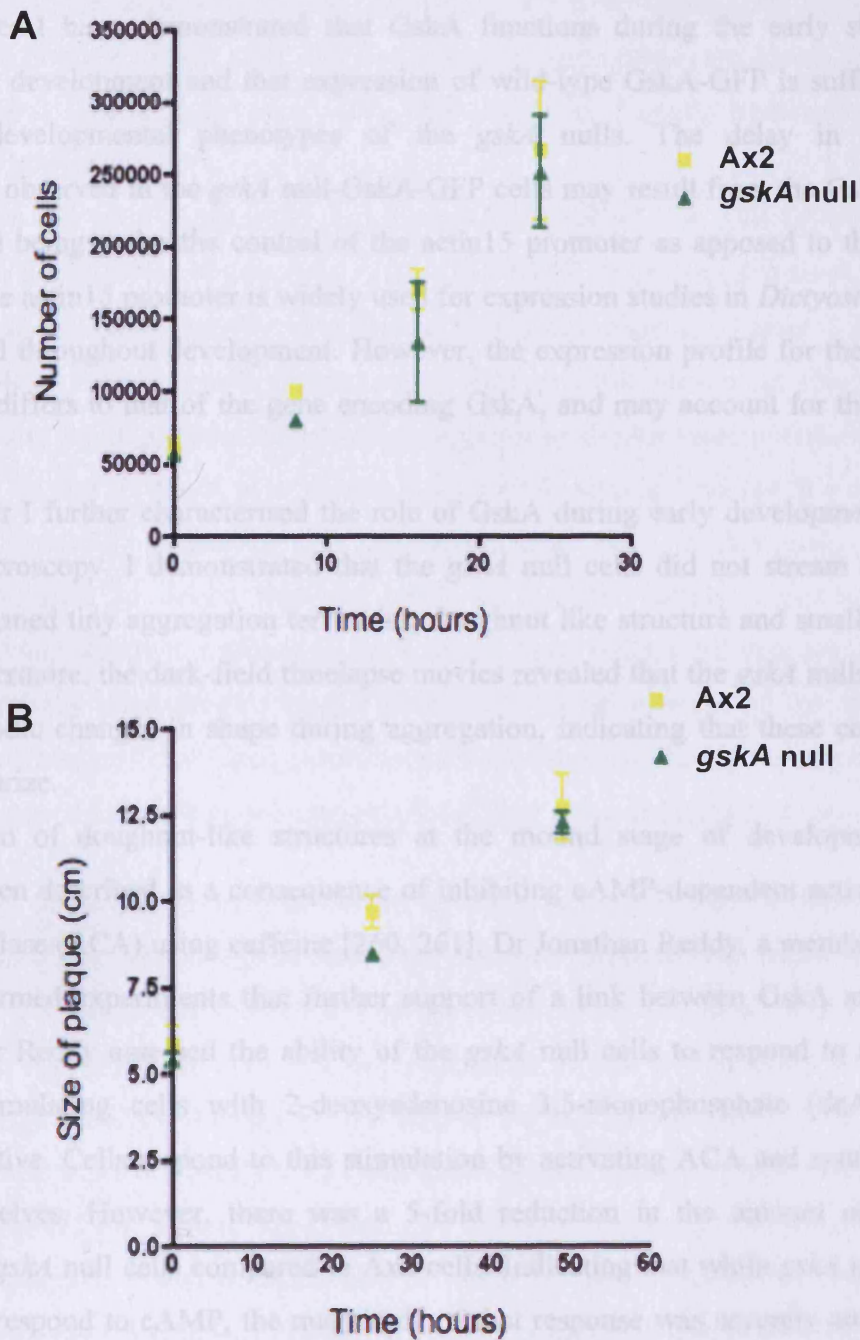


Figure 4.9. Analysis of growth rates

A. Cells were grown in shaking culture and periodically counted, the data presented represent 3 separate experiments. Proliferation rates of Ax2 and *gskA* null cell lines were not statistically different ($P > 0.5$, unpaired t-test)

B. Ax2 and *gskA* null cells were allowed to grow on agar plates with bacteria. For each strain, colonies were grown in triplicate on 6 separate plates. There was no statistical difference between the plaque size attributed to Ax2 and *gskA* null cell lines ($P > 0.5$, un-paired t-test)

4.5 Conclusions

In this chapter I have demonstrated that GskA functions during the early stages of *Dictyostelium* development and that expression of wild-type GskA-GFP is sufficient to rescue the developmental phenotypes of the *gskA* nulls. The delay in entering development, observed in the *gskA* null-GskA-GFP cells may result from the GskA-GFP fusion protein being under the control of the *actin15* promoter as apposed to the GskA promoter. The *actin15* promoter is widely used for expression studies in *Dictyostelium* as it is expressed throughout development. However, the expression profile for the *actin15* gene (*act15*) differs to that of the gene encoding GskA, and may account for the timing differences.

In this chapter I further characterised the role of GskA during early development using timelapse microscopy. I demonstrated that the *gskA* null cells did not stream and that these cells formed tiny aggregation territories, doughnut like structure and small fruiting bodies. Furthermore, the dark-field timelapse movies revealed that the *gskA* nulls did not undergo periodic changes in shape during aggregation, indicating that these cells were unable to polarize.

The formation of doughnut-like structures at the mound stage of development has previously been described as a consequence of inhibiting cAMP-dependent activation of adenylate cyclase (ACA) using caffeine [260, 261]. Dr Jonathan Reddy, a member of our lab has performed experiments that further support of a link between GskA and ACA activation: Dr Reddy assessed the ability of the *gskA* null cells to respond to a cAMP signal by stimulating cells with 2-deoxyadenosine 3,5-monophosphate (dcAMP), a cAMP derivative. Cells respond to this stimulation by activating ACA and synthesizing cAMP themselves. However, there was a 5-fold reduction in the amount of cAMP produced by *gskA* null cells compared to Ax2 cells. Indicating that while *gskA* null cells were able to respond to cAMP, the magnitude of that response was severely attenuated. This finding would also explain the observation that the *gskA* nulls formed small aggregation territories; these cells were unable to produce sufficient cAMP to propagate a signal over a large area.

I have demonstrated that expression of wild-type GskA-GFP was sufficient to rescue the *gskA* null phenotype. Furthermore, I have demonstrated that expression of either GskA-

GFP-R96E or GskA-GFP-Y214G was also sufficient to rescue many aspects of the *gskA* null phenotype. Cells expressing either GskA-GFP-R96E or GskA-GFP-Y214G were able to stream although these cells did form smaller aggregation territories. The cells expressing GskA-GFP-Y214G were also able to form fruiting bodies that were comparable to wild-type.

The phenotype of cells expressing either GskA-GFP-R96E or GskA-GFP-Y214G differed to those expressing kinase dead GskA-GFP K85R indicating that these proteins must retain some catalytic activity. The kinase assays described in chapter 1 indicated that these proteins were not catalytically active. One possible reason for this apparent contradiction may be the method of detection. In previous studies mutation of either R96 or Y214 was shown to result in a reduction in kinase activity but not its complete abolishment [81, 259]. It may be that the kinase assay used in this study was not sufficiently sensitive to detect the low levels of specific activity retained by the constructs. A more sensitive, radioactive method may have yielded different results.

That these proteins were able to rescue some but not all aspects of the *gskA* null phenotype would suggest that GskA performs multiple functions during development and that these compromised proteins are capable of fulfilling some but not all of these roles.

In this chapter I described a novel, previously uncharacterised phenotype of the *gskA* null cells. I demonstrated that the *gskA* null cells became multinucleate when grown in shaking culture. A defect that was rescued by growing cells on a solid surface, indicating that the *gskA* null cells are deficient in cytokinesis A and divide using a surface-dependent mechanism (cytokinesis B). In support of this conclusion, the gene *corA*, encoding coronin, a protein involved in cytokinesis B, was reported to be over-expressed in *gskA* null cells[196]. Again, expression of wild-type GskA-GFP was sufficient to rescue this phenotype, whereas expression of either GskA-GFP-R96E or GskA-GFP-Y214G resulted in an intermediate phenotype, perhaps indicating that these compromised kinases were only capable of a partial rescue and that absolute levels of phosphorylated substrate were an important feature of the affected pathway.

Given that the *gskA* null cells were found to become multi-nucleate when grown in shaking culture it is surprising that they were found to proliferate at a similar rate to Ax2

cells. One might expect the proliferation rate of the *gskA* null cells to lag over time as multi-nucleate cells accumulate within the population. It may be that the *gskA* null cells are only partially defective in Cytokinesis A, and that a difference in proliferation rates is only detectable following prolonged culturing. The observed phenotype is similar to that of *pi3k^{J-2}* null cells [229](see Chapter 1), and could indicate that GskA and PI3K act through a common pathway to regulate cytokinesis.

Chapter 5

Identification of GSK-3 binding partners

Mass spectrometric analysis has furthered our understanding of how proteins interact within signaling pathways through the mapping covalent protein modifications and identification of protein complexes. The generation of GFP-tagged GskA and GSK3 β constructs provided a means of performing large-scale affinity purifications in a cost efficient manner. GFP itself binds very few proteins and is largely free in the cytosol [3] making it ideal as a fusion partner. In this chapter I will demonstrate that the addition of a GFP tag did not prevent GSK-3 β from interacting with known binding partners. I will then describe the approaches used to identify a series of potential GskA and GSK-3 β binding proteins.

5.1 GSK-3 β -GFP still associates with known binding partners

Several mammalian GSK3 β binding partners have previously been identified [19, 41, 43, 96, 98, 265], including the Wnt signalling components Axin and FRAT [41, 96, 98]. In order to demonstrate that the addition of a GFP tag had not compromised the ability of GSK3 β to interact with these binding partners a control pull-down was performed: A FLAG-tagged portion of Axin1 (residues 367-701) or FLAG-tagged FRAT were expressed in both the T-REx GSK3 β -GFP and T-REx GFP cell lines. As a control, FLAG-Axin1 (367-701) containing the point mutation L392P and FLAG-FRAT containing point mutations K208A/E209Q were also expressed. Both of these mutated proteins were shown to exhibit a lowered affinity for GSK3 β [98, 266].

Following induction with doxycycline for 24 hours, cells were lysed in a non-ionic detergent lysis buffer (containing 150mM NaCl). This relatively gentle lysis buffer was used in order to stabilize and preserve protein:protein interactions. After cell lysis, samples were centrifuged to remove the insoluble fraction and the supernatants were subjected to immunoprecipitation using a commercially available antibody raised against GFP, covalently coupled to Protein-G sepharose beads. Angus Lamond and colleagues have achieved good results using this approach [3, 267, 268] and their protocol was utilized for the preparation of these anti-GFP sepharose beads.

Samples were incubated with anti-GFP beads for 1 hour at 4°C. Following incubation the beads were pelleted and washed in buffers containing increasing concentrations of NaCl

to demonstrate that interactions were stable and specific. Subsequent western transfers were probed with an anti-FLAG antibody (Figure 5.1).

Both FLAG-Axin1 (367-701) and FLAG-FRAT co-immunoprecipitated with GSK3 β -GFP (Figure 5.1A and B). Control experiments using cells expressing GFP alone indicated that FLAG Axin1(367-701), FLAG-Axin1 (367-701) L392P and FLAG FRAT all bound to either GFP or the bead matrix (Figure 5.1C and D). Recognition of this 'non-specific' binding was possible as a result of performing washes with increasing concentrations of NaCl and including these fractions on the blot. This highlighted the need for care when validating GSK-3 specific interactions later; proteins identified as GSK-3 binding proteins as the result of mass spectrometry analysis may also bind non-specifically to GFP alone or more likely the bead matrix at levels detectable on a Western blot. Performing increasingly stringent washes on samples to be used for validation experiments would make it possible to distinguish between proteins that a) bound specifically to GSK-3 alone, b) bound specifically to GSK-3, but also to GFP or the bead matrix or c) bound non-specifically to GFP or bead matrix.

To date, no GskA binding partners have been identified so it was not possible to perform a similar experiment using *Dictyostelium* extracts.

5.2 Isolation of potential GSK-3 interaction proteins

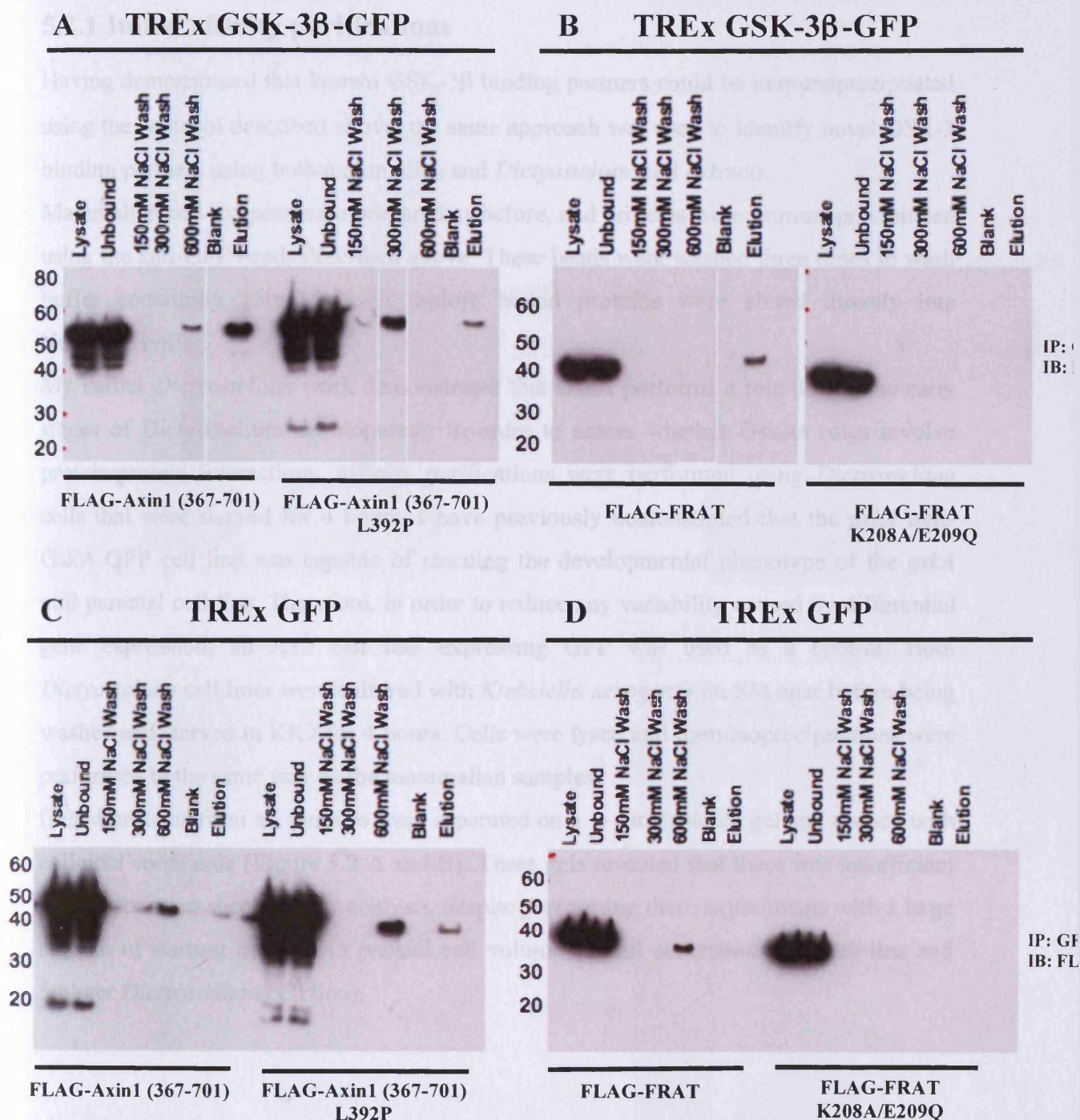


Figure 5.1. GSK3 β -GFP interacts with known binding partners

T-REx GSK3 β -GFP and T-REx GFP cells were transfected separately with plasmids expressing Flag-Axin1, FLAG Axin1 L392P, Flag-FRAT or FLAG-FRAT K208A/E209Q. Cells were allowed to recover for 24 hours before being treated with 2ng/ml of doxycycline for a further 24 hours to induce GSK3 β -GFP/GFP expression. Cells were then harvested, and immuno-precipitations were performed using beads coupled to an anti-GFP antibody. Beads were washed with increasing concentrations of NaCl prior elution. Western blots were probed with an anti-FLAG antibody.

5.2 Isolation of potential GSK-3 interaction proteins

5.2.1 Initial affinity purifications

Having demonstrated that known GSK-3 β binding partners could be immunoprecipitated using the protocol described above, the same approach was used to identify novel GSK-3 binding partners using both mammalian and *Dictyostelium* cell extracts.

Mammalian cell extracts were prepared as before, and proteins were immunoprecipitated using the anti-GFP beads described above. These beads were washed three times in wash buffer containing 150mM NaCl, before bound proteins were eluted directly into NuPAGE buffer.

My earlier *Dictyostelium* work demonstrated that GskA performs a role during the early stages of *Dictyostelium* development. In order to assess whether GskA's roles involve protein:protein interactions, affinity purifications were performed using *Dictyostelium* cells that were starved for 4 hours. I have previously demonstrated that the *gskA* null-GskA-GFP cell line was capable of rescuing the developmental phenotype of the *gskA* null parental cell line. Therefore, in order to reduce any variability caused by differential gene expression, an Ax2 cell line expressing GFP was used as a control. Both *Dictyostelium* cell lines were cultured with *Klebsiella aerogenes* on SM agar before being washed and starved in KK2 for 4 hours. Cells were lysed and immunoprecipitations were performed in the same way as the mammalian samples.

Eluted proteins from all samples were separated on a 1- dimensional gel and stained with colloidal coomassie (Figure 5.2 A and B). These gels revealed that there was insufficient protein for mass spectrometry analysis, despite performing these experiments with a large amount of starting material (a packed cell volume of 2ml per mammalian cell line and 5ml per *Dictyostelium* cell line).

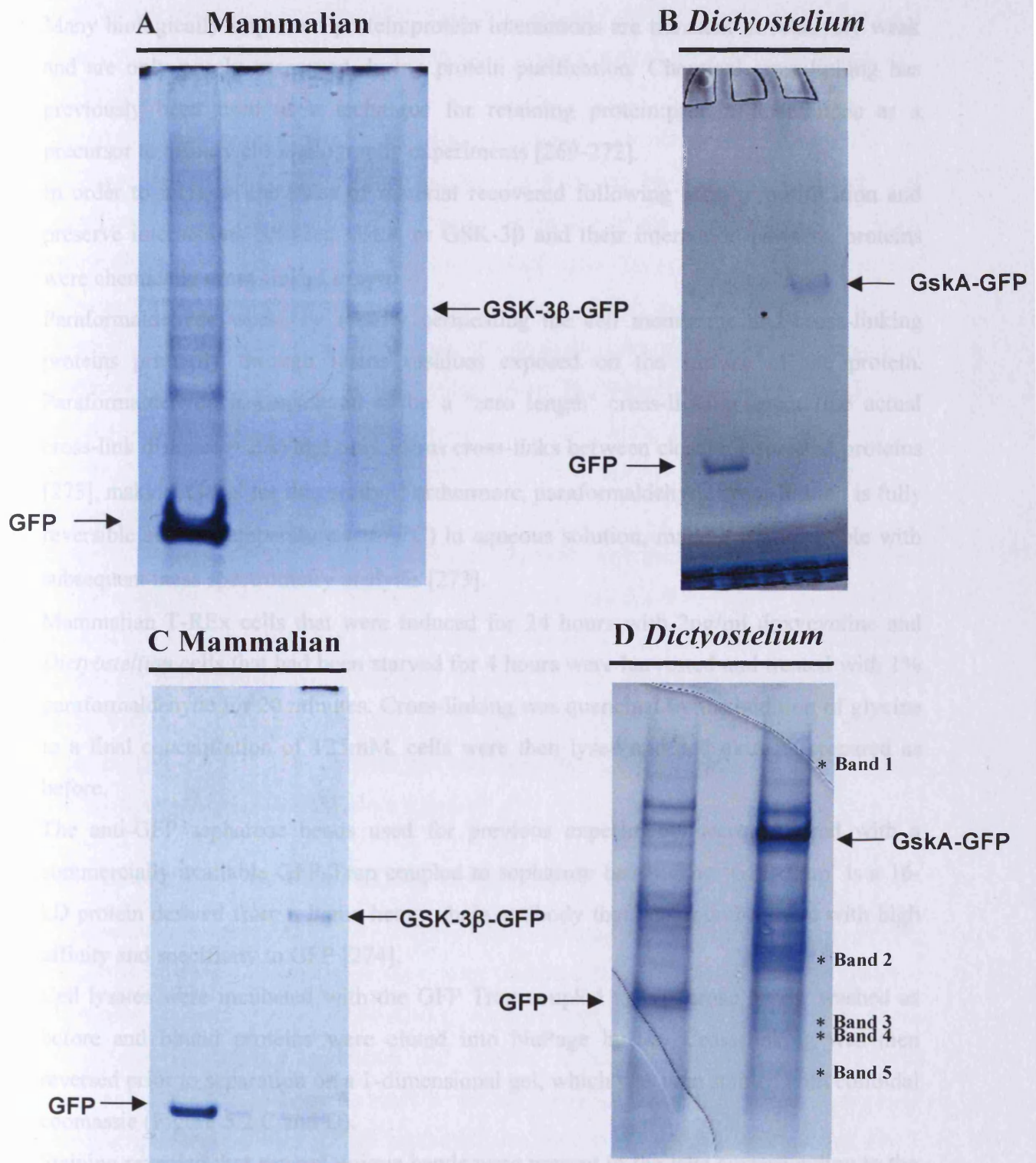


Figure 5.2. Colloidal coomassie stained gels following affinity purification. Affinity purifications were performed using non-fixed samples from (A) T-REx GSK-3 β -GFP and T-REx GFP cell lines and (B) *Dictyostelium gskA* null-GskA-GFP and Ax2-GFP cell lines. Later experiments were performed with PFA fixed samples from (C) T-REx GSK-3 β -GFP and T-REx GFP cell lines and (D) *Dictyostelium gskA* null-GskA-GFP and Ax2-GFP cell lines. Bands selected for further analysis are marked.

5.2.2 Utilization of chemical cross-linking

Many biologically important protein:protein interactions are transient or relatively weak and are only poorly preserved during protein purification. Chemical cross-linking has previously been used as a technique for retaining protein:protein interactions as a precursor to affinity chromatography experiments [269-272].

In order to increase the mass of material recovered following affinity purification and preserve interactions between GskA or GSK-3 β and their interaction partners, proteins were chemically cross-linked *in vivo*.

Paraformaldehyde works by rapidly permeating the cell membrane and cross-linking proteins primarily through lysine residues exposed on the surface of the protein. Paraformaldehyde is considered to be a 'zero length' cross-linking agent (the actual cross-link distance = 2Å) and only forms cross-links between closely associated proteins [273], making it ideal for this study. Furthermore, paraformaldehyde cross-linking is fully reversible at high temperature (>67 °C) in aqueous solution, making it compatible with subsequent mass spectrometry analysis [273].

Mammalian T-REx cells that were induced for 24 hours with 2ng/ml doxycycline and *Dictyostelium* cells that had been starved for 4 hours were harvested and treated with 1% paraformaldehyde for 20 minutes. Cross-linking was quenched by the addition of glycine to a final concentration of 125mM, cells were then lysed and cell extracts prepared as before.

The anti-GFP sepharose beads used for previous experiments were replaced with a commercially available GFP-Trap coupled to sepharose beads; The 'GFP-Trap' is a 16-kD protein derived from a llama heavy chain antibody that was found to bind with high affinity and specificity to GFP [274].

Cell lysates were incubated with the GFP Trap coupled to sepharose beads, washed as before and bound proteins were eluted into NuPage buffer. Cross-linking was then reversed prior to separation on a 1-dimensional gel, which was then stained with colloidal coomassie (Figure 5.2 C and D).

Staining revealed that several unique bands were present in the lane corresponding to the *Dictyostelium* GskA-GFP sample and five bands were isolated and digested with trypsin. Peptides were extracted, separated by nanoflow LC, and introduced into an LTQ Orbitrap

hybrid mass spectrometer. MS/MS analysis and database searching of the sequenced peptides resulted in the identification of 33 proteins, each of which matched to at least 4 unique peptide sequences and had a combined ‘protein score’ deemed to be statistically significant.

For each protein match, Mascot calculates an overall ‘protein score’ that reflects the combined scores of all observed mass spectra that can be matched to amino acid sequences within that protein. The higher score the more confident match. Mass spectrometry experiments do not produce “perfect” data. There is always some level of noise in the data and not every ion that a protein could theoretically generate will be observed in every experiment. Therefore, the analysis software could produce false or random matches; some matches could arise simply by chance. To address this, Mascot calculated a “threshold” score representing a 5% confidence threshold. This score for statistical significance varies from experiment to experiment and was indicated in the Mascot report.

Bands of the equivalent size were not isolated from the control track because at the time as it was felt that it would be impossible to ensure the gel slices of exactly the same size were taken from exactly the same position. However, in hindsight this may have simplified the process of identifying specific GskA interactor proteins as mass spectrometry analysis revealed that each gel slice contained a mixture of multiple proteins. This is likely to be because proteins were only separated on a 1-dimensional gel and multiple proteins migrated close together.

5.3 Analysis of proteins that co-purified with GskA

33 proteins were identified as co-purifying with GskA and each of these proteins roughly correlated in size to the gel band they were extracted from (Table 5.1). These putative interaction partners required validation to confirm their physiological relevance. These downstream validation experiments and detailed molecular characterization are both costly and time consuming and as such it was imperative to focus resources on a subset of potential interactions with a high probability of biological significance. To that end I initially used a bioinformatics approach to narrow the scope of my investigations and eliminate proteins that were unlikely to be biologically relevant.

Protein ID	Protein Name (as it appears in STRING)	Human homolog (where available)	Description	MW of band identified in Figure 5.2 (kDa)	MW of protein (kDa)
DDB0230067	accA	ACACA	acetyl-CoA carboxylase	270 (Band 1)	256.7
DDB0185543	DDBDRAFT_0185543	N/A	unknown	270 (Band 1)	268.7
DDB0201646	pyr1-3	CAD	Dihydroorotase aspartate carbamoyltransferase glutamine-dependent carbamoyl-phosphate synthase	270 (Band 1)	245.9
DDB0191526	talB	TLN2	talInB	270 (Band 1)	277.6
DDB0233340	DDB_0233340	PABPC1	RNA-binding region RNP-1 domain-containing protein RNA recognition motif-containing protein RRM	35 (Band 2)	31.8
DDB0234265	DDBDRAFT_0167100	TGDS	NAD-dependent epimerase/dehydratase family protein	35 (Band 2)	40
DDB0230193	pdhA	PDHE1-A	pyruvate dehydrogenase E1 alpha subunit	35 (Band 2)	42
DDB0185040	pdi1	ERp72	protein disulfide isomerase	35 (Band 2)	39.9
DDB0304584	zpr1	ZPR1	ZPR1-type zinc finger-containing protein	35 (Band 2)	53.5
DDB0201558	ancA	SLC25A4	ADP/ATP translocasetransmembrane protein mitochondrial substrate carrier family protein	27 (band 3)	33.5
DDB0233903	DDBDRAFT_0189501	THUMP	putative SAM dependent methyltransferase	27 (band 3)	22.3
DDB0233914	DDBDRAFT_0202301	COQ3	putative SAM dependent methyltransferase	27 (band 3)	33.8
DDB0231242	rpl5	RPL5	60S ribosomal protein L5	27 (band 3)	32.8
DDB0230021	rps3a	MFTL	40S ribosomal protein S3a	27 (band 3)	30.4
DDB0231470	uox	N/A	urate oxidase, uricase	27 (band 3)	33
DDB0235141	atp6v1d	VMA8	vacuolar ATP synthase subunit D	25 (Band 4)	28.6
DDB0237960	DDBDRAFT_0187734	COQ3	methyltransferase type 11 domain-containing protein	25 (Band 4)	29
DDB0215400	dscA-1	N/A	discoidin I, A chain	25 (Band 4)	28.29
DDB0215401	dscC-1	N/A	discoidin I, C chain and B chain	25 (Band 4)	28.4
DDB0232938	fttb	YWHAE	14-3-3 protein	25 (Band 4)	28.7
DDB0185073	rpl7	RPL7	S60 ribosomal protein L7	25 (Band 4)	27.9
DDB0185202	rpl8	RPL8	60S ribosomal protein L8	25 (Band 4)	27.5
DDB0215391	rps2	RPS2	ribosomal protein S2	25 (Band 4)	28.7
DDB0230023	rps6	RPS6	40S ribosomal protein S6	25 (Band 4)	26.2
DDB0230016	rpsA	RPSA	40S ribosomal protein SA	25 (Band 4)	27.1
DDB0231383	sdhB	SDHB	succinate dehydrogenase	25 (Band 4)	31.6
DDB0185070	vatE	M9.2	vacuolar H ⁺ -ATPase E subunit	25 (Band 4)	26.6
DDB0214935	arcB	p34-ARC	ARP Complex subunit 2	20 (Band 5)	32.9
DDB0214939	limE	MLN50	LIM-type zinc finger-containing protein	20 (Band 5)	22
DDB0233888	mcfN	SLC25A3	mitochondrial substrate carrier family 25 member 3	20 (Band 5)	31.6
DDB0229951	rpl13	RPL13	S60 ribosomal protein L13	20 (Band 5)	23.67
DDB0231338	rpl6	RPL6	60S ribosomal protein L6	20 (Band 5)	25.8
DDB0230170	udpB	UPP1	uridine phosphorylase	20 (Band 5)	32.3

Table 5.1. Proteins identified as co-purifying with *Dictyostelium* GskA

STRING is a database of known and predicted protein associations. These interactions include both direct (physical) and indirect (functional) associations. Information is collated from multiple sources and includes data from direct experiments, co-expression data, previously collated databases and text mining[275-277].

STRING was used to highlight any previously characterized interactions between the putative GskA interaction partners identified from the mass spectrometry analysis. This analysis revealed that a series of interacting ribosomal proteins were included in the dataset (Figure 5.3). STRING also identified 2 previously characterized interactions between VatE and atp6v1d (also known as VatD), between Pyr1-3 and FttB and between sdhB and pdhA. The potential significance of these interactions is discussed briefly below.

STRING did not highlight any previously characterized interactions between GskA, Zak1 or STATA and the dataset. This was not unexpected, as the role of GskA has not been extensively researched in Dictyostelium and several of the proteins identified through these experiments remain to be characterized.

In order to ensure that no previously characterized interactions were overlooked, the mammalian homologues of these Dictyostelium proteins were identified using BLAST searches and these were used for an additional search of the STRING database. However, this search failed to identify any additional links within the dataset.

Despite the bioinformatics approach used to highlight potentially interesting, biologically relevant interactions, validation was largely limited to those proteins that have previously been characterized and details of antibodies had been published. Fresh immunoprecipitations were performed, and probed with antibodies against LimE, FttB and TalB. These westerns revealed that both LimE and FttB bound non-specifically to GFP or the bead matrix. While the antibody raised against TalB failed to detect a band at the appropriate height.

5.4 SILAC-linked Mass Spectrometry

Despite cross-linking attempts to preserve protein-protein interactions I failed to identify any potential Gsk-3 β binding partners from mammalian extracts as there was insufficient material in the resulting coomassie stained gel to identify unique bands of interest. This failure to identify binding partners may be because GSK-3 β does not form any protein-protein complexes in the cell. This is unlikely to be the case as the *W. histolytica* HsK 293 cells (274-282). Furthermore, Fwing et al. (2004) identified several interaction partners using HsK 293 cells, although they did not identify any GSK-3 β interaction partners.

Although the results of using non-optimal purification conditions may be that it is possible to identify interaction partners using HsK 293 cells, it may be that only a small portion of the available GSK-3 β is available for binding to other proteins. Furthermore the bound fraction may be a mixture of different multi-protein complexes. By looking at the co-purified gel prepared from previous experiments, one can conclude that any GSK-3 β interaction partners would be found in the co-purified gel.

It may be that only a small portion of the available GSK-3 β is available for binding to other proteins. Furthermore the bound fraction may be a mixture of different multi-protein complexes. By looking at the co-purified gel prepared from previous experiments, one can conclude that any GSK-3 β interaction partners would be found in the co-purified gel.

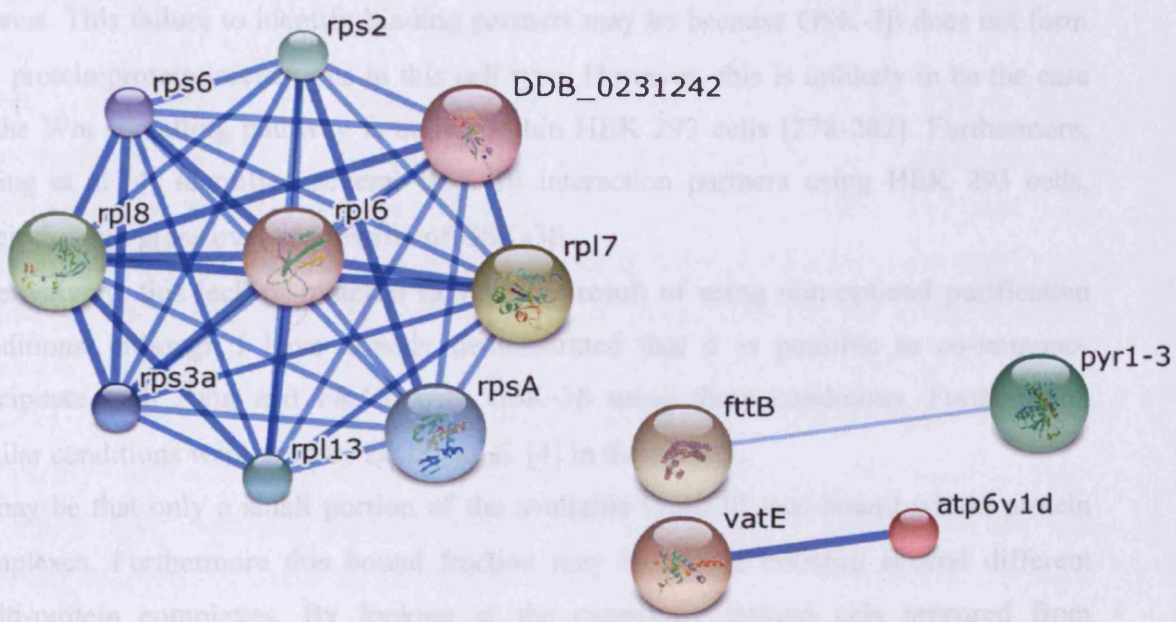


Figure 5.3. STRING analysis of potential GskA interaction partners

33 proteins were identified as co-purifying with GskA and the on-line database STRING was used to identify any previously characterised interactions between these proteins. Lines between proteins indicate a previously characterised interaction, and the thickness of the line indicates the confidence of the interaction; the thicker the line the more well characterised the interaction. STRING revealed that several interacting ribosomal proteins were included within the dataset, and also identified previously characterised interactions between fttB and pyr1-3 and between VatE and atp6v1d. The nature of these interactions is discussed in the text.

insufficient mass to be seen on a coomassie stained gel, then increasing the amount of starting material may alleviate the problem. However, increasing the amount of starting material used for affinity purification is often associated with incomplete cell lysis and increased background. Furthermore, there are technical difficulties associated with this approach: previous experiments used cells harvested from 15 T180 flasks (per cell line), even simply doubling the number of flasks would greatly complicate the process of

5.4 SILAC-linked Mass Spectrometry

Despite cross-linking samples to preserve protein:protein interactions I failed to identify any potential GSK-3 β binding partners from mammalian extracts as there was insufficient material in the resulting coomassie stained gel to identify unique bands of interest. This failure to identify binding partners may be because GSK-3 β does not form any protein:protein interactions in this cell type. However, this is unlikely to be the case as the Wnt signalling pathway is active within HEK 293 cells [278-282]. Furthermore, Ewing et al [4] identified several GSK-3 β interaction partners using HEK 293 cells, albeit through gross over-expression of GSK-3 β .

Alternatively, this lack of material may be the result of using non-optimal purification conditions, although I have already demonstrated that it is possible to co-immunoprecipitate both Axin and FRAT with GSK-3 β using these conditions. Furthermore, similar conditions were used by Ewing et al. [4] in their study.

It may be that only a small portion of the available GSK-3 β was bound within protein complexes. Furthermore this bound fraction may be shared between several different multi-protein complexes. By looking at the coomassie stained gels prepared from previous experiments, one can conclude that any GSK-3 β -interaction partners would need to bind all of the available GSK-3 β in a 1:1 ratio to be clearly identifiable. Binding to only a fraction of the available GSK-3 β , even as much as 50%, may be insufficient to visualize on a coomassie stained gel and render the associated band imperceptible.

If the failure to identify GSK-3 β interaction partners is the result of insufficient material, i.e. a portion of GSK-3 β does form stable interactions in HEK 293 cells and these interactions are maintained during the immunoprecipitation process, but there is insufficient mass to be seen on a coomassie stained gel, then increasing the amount of starting material may alleviate the problem. However, increasing the amount of starting material used for affinity purifications is often associated with incomplete cell lysis and increased background. Furthermore, there are technical difficulties associated with this approach; previous experiments used cells harvested from 15 T180 flasks (per cell line), even simply doubling the number of flasks would greatly complicate the process of

seeding, inducing and harvesting cells, and would ultimately lead to increased variability between samples.

Instead of increasing the amount of starting material, it was decided to adopt an approach that offered increased sensitivity. Accordingly, SILAC-linked mass spectrometry techniques were employed to identify GSK-3 β binding partners from T-REx HEK 293 cells.

Stable isotope labelling by amino acids in cell culture (SILAC) followed by mass spectrometry is a sensitive technique that is used increasingly for the identification of specific but low affinity protein;protein interactions [283-286] (outlined in Figure 5.4). The rationale behind this approach is that two populations of cells are cultivated in cell culture. One is cultured in media containing normal amino acids and the second is grown in media supplemented with amino acids labeled with stable, non-radioactive, heavy isotopes (in this case arginine and lysine containing ^{13}C). Heavy amino acids are completely incorporated into every protein within 5 cell doubling [246]. Equal amounts of protein from both cell populations can then be combined, affinity purified and analyzed together by Mass Spectrometry (Figure 5.4). Pairs of chemically identical peptides of different stable-isotope composition can be differentiated in a mass spectrometer owing to their mass difference. The ratio of peak intensities in the mass spectrum for such peptide pairs accurately reflects the abundance ratio for the two proteins. This approach also reduces experimental variability that inevitably occurs when samples are processed separately.

In this study, TREx GSK3 β -GFP cells were cultured in 'heavy' media while the TREx GFP control cells were cultured in 'light' media. This offered an additional control as any environmental contaminants, which would not be present in equal ratios in both light and heavy cell extracts and therefore might appear to be significant can easily be identified and excluded from analysis.

In previous experiments, both mammalian TREx cell lines were treated with the same concentration of doxycycline. However, this consistently led to higher levels of GFP expression compared to GSK3- β -GFP. This was not unexpected, as one would imagine levels of GSK-3 β expression within a cell would be tightly controlled and over expression of GSK-3 β would be countered by increased degradation while no such

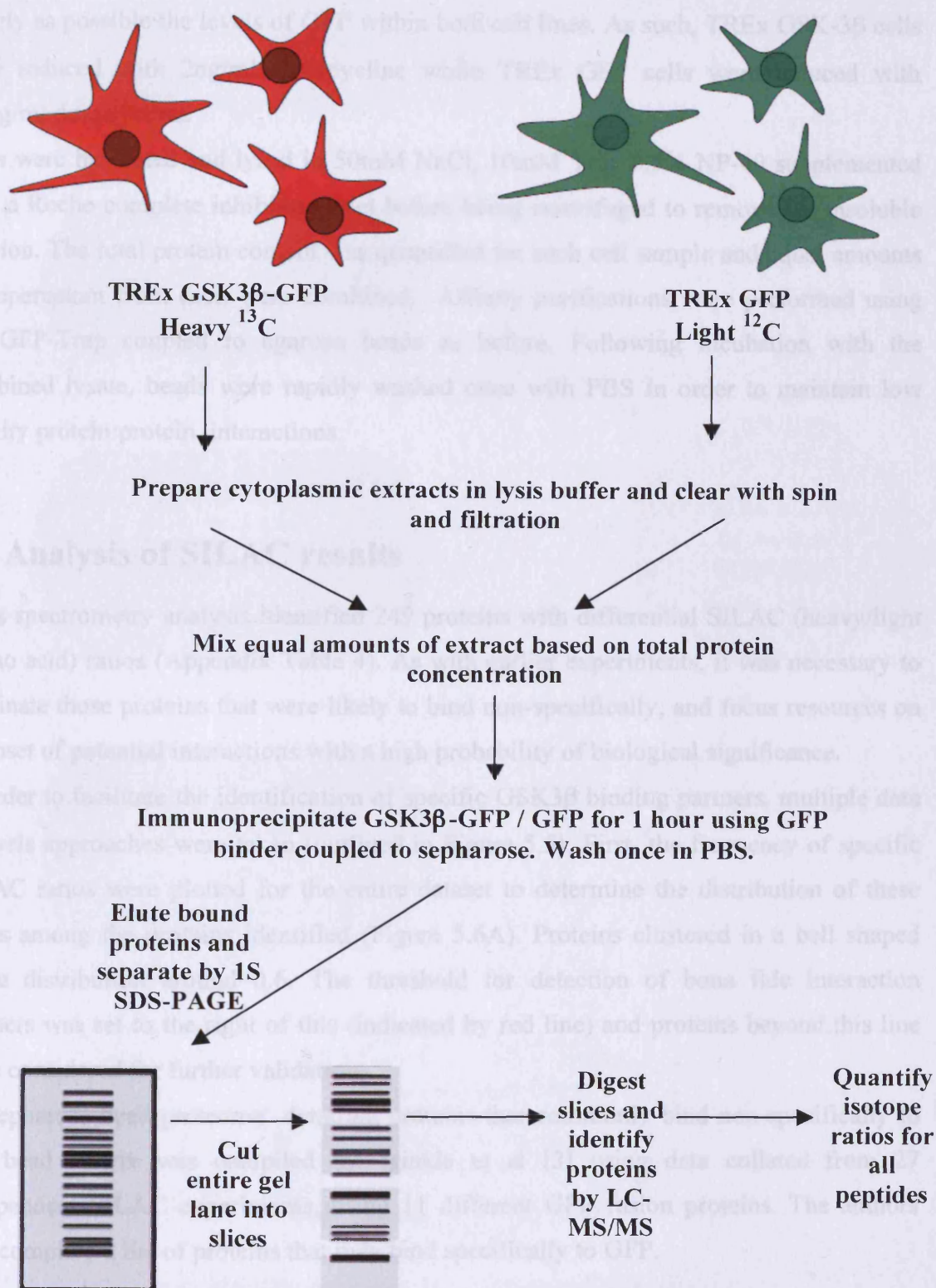


Figure 5.4. Schematic representation SILAC based analysis
Based on diagram in [3]

regulation of protein turnover is likely to exist for GFP. In order to limit any differences between the two protein samples doxycycline titrations were performed to match as closely as possible the levels of GFP within both cell lines. As such, TREx GSK-3 β cells were induced with 2ng/ml doxycycline while TREx GFP cells were induced with 0.4ng/ml doxycycline.

Cells were harvested and lysed in 50mM NaCl, 10mM Tris, 0.5% NP-40 supplemented with a Roche complete inhibitor tablet before being centrifuged to remove the insoluble fraction. The total protein content was quantified for each cell sample and equal amounts of supernatant from each were combined. Affinity purifications were performed using the GFP-Trap coupled to agarose beads as before. Following incubation with the combined lysate, beads were rapidly washed once with PBS in order to maintain low affinity protein:protein interactions.

5.3 Analysis of SILAC results

Mass spectrometry analysis identified 249 proteins with differential SILAC (heavy/light amino acid) ratios (Appendix Table 4). As with earlier experiments, it was necessary to eliminate those proteins that were likely to bind non-specifically, and focus resources on a subset of potential interactions with a high probability of biological significance.

In order to facilitate the identification of specific GSK3 β binding partners, multiple data analysis approaches were taken (outlined in Figure 5.5). First, the frequency of specific SILAC ratios were plotted for the entire dataset to determine the distribution of these ratios among the proteins identified (Figure 5.6A). Proteins clustered in a bell shaped curve distribution around 0.6. The threshold for detection of bona fide interaction partners was set to the right of this (indicated by red line) and proteins beyond this line were considered for further validation.

A 'sepharose bead proteome' detailing proteins that commonly bind non-specifically to this bead matrix was compiled by Trinkle et al [3] using data collated from 27 independent SILAC experiments, using 11 different GFP fusion proteins. The authors also compiled a list of proteins that may bind specifically to GFP.

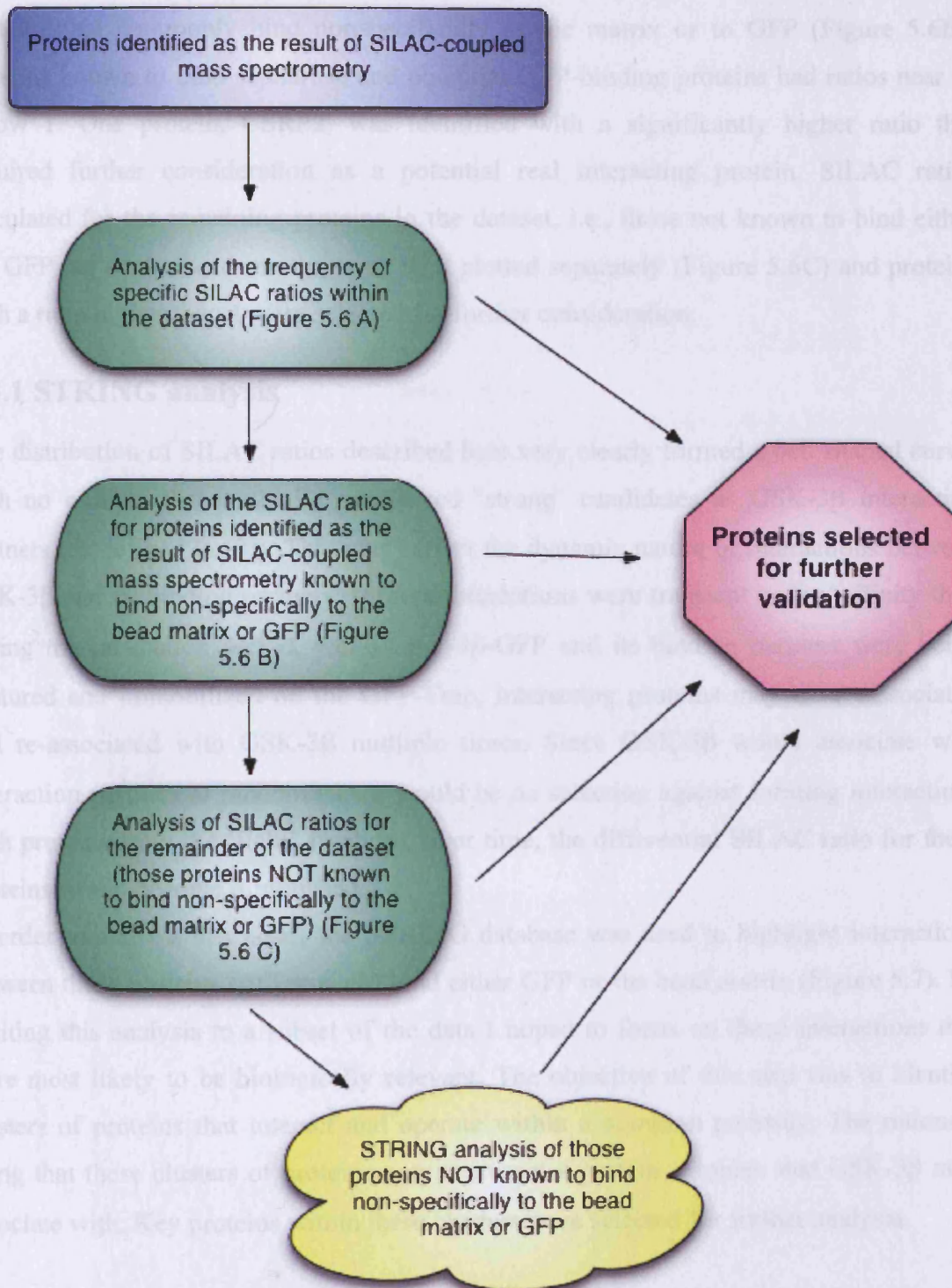


Figure 5.5. Workflow to identify proteins for further validation

249 proteins were identified as the result of SILAC-coupled mass spectrometry analysis. The above work-flow was used to identify proteins likely to represent biologically relevant roles in the regulation of GSK-3 activity for further validation.

Analysis of the current dataset was taken further by applying the ‘sepharose bead proteome’ and list of potential GFP-binders as a filter and grouping the SILAC ratios of proteins that commonly bind nonspecifically to the matrix or to GFP (Figure 5.6B). Proteins known to bind sepharose and potential GFP-binding proteins had ratios near or below 1. One protein, CSRP2, was identified with a significantly higher ratio that required further consideration as a potential real interacting protein. SILAC ratios calculated for the remaining proteins in the dataset, i.e., those not known to bind either the GFP tag or the bead matrix, were then plotted separately (Figure 5.6C) and proteins with a ratio higher than 1 were selected for further consideration.

5.3.1 STRING analysis

The distribution of SILAC ratios described here very clearly formed a bell shaped curve, with no outliers that could be considered ‘strong’ candidates as GSK-3 β interaction partners (as defined in [3]). This may reflect the dynamic nature of interactions between GSK-3 β and its binding partners. If these interactions were transient or low affinity then during the incubation period, while GSK-3 β -GFP and its binding partners were being captured and immobilized on the GFP-Trap, interacting proteins may have dissociated and re-associated with GSK-3 β multiple times. Since GSK-3 β would associate with interaction partners at random (there would be no selection against forming interactions with proteins from the ‘light’ fraction), over time, the differential SILAC ratio for these proteins would become diminished.

In order to address this issue, the STRING database was used to highlight interactions between those proteins not known to bind either GFP or the bead matrix (Figure 5.7). By limiting this analysis to a subset of the data I hoped to focus on those interactions that were most likely to be biologically relevant. The objective of this step was to identify clusters of proteins that interact and operate within a common pathway. The rationale being that these clusters of proteins may represent a protein complex that GSK-3 β may associate with. Key proteins within these clusters were selected for further analysis.

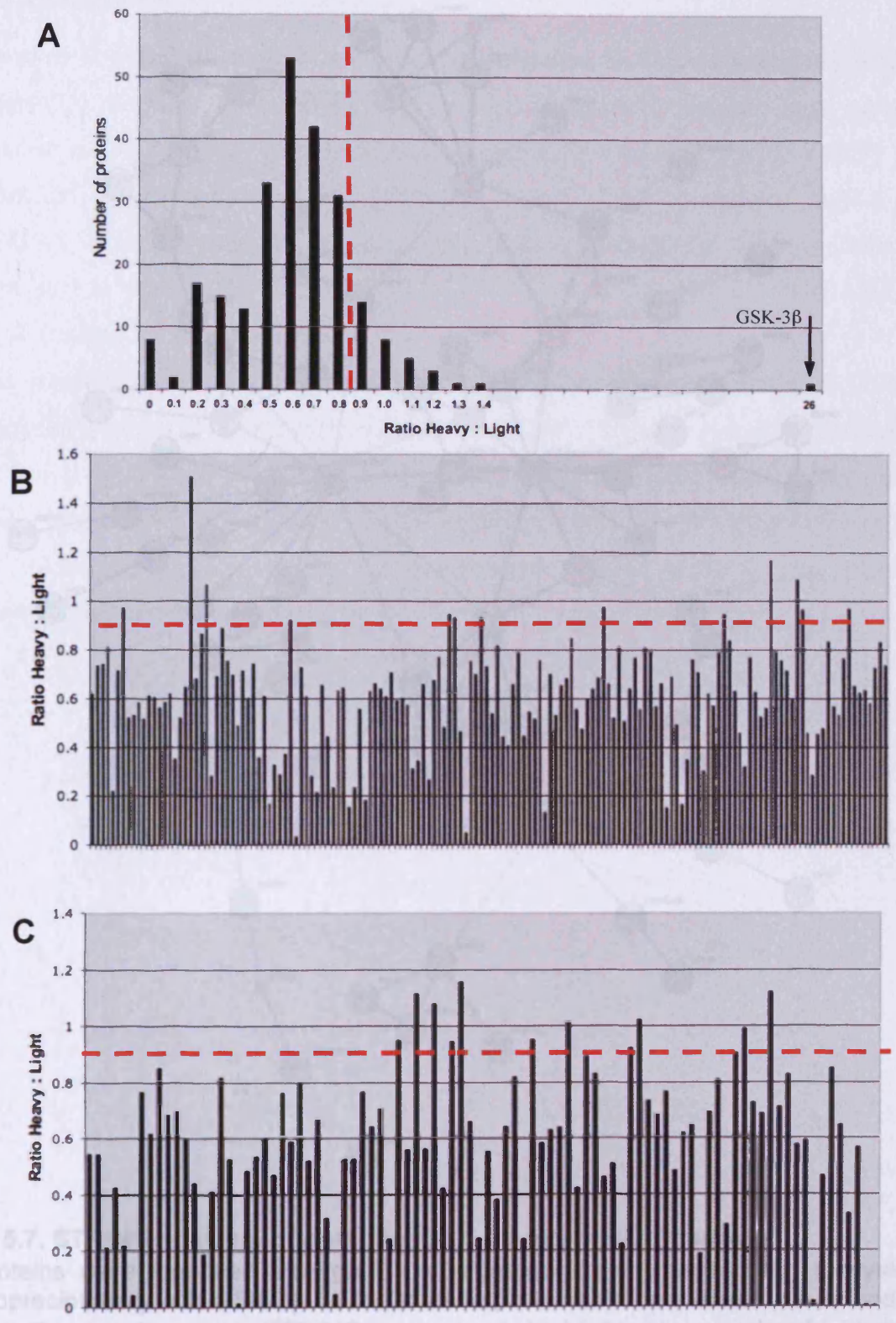


Figure 5.6. Systematic analysis of SILAC results

(A) The frequency of SILAC ratios were plotted for the dataset to determine the distribution of ratios across the dataset. (B) SILAC ratios for proteins known to bind non-specifically to sepharose beads and potential GFP binding partners (as defined by Trinkle et al [1]) were plotted separately to those not known to bind to sepharose beads of GFP (C).

5.4 Validation of interactions

A total of 22 proteins were selected for further validation as GSK-3 β interaction partners (Table 5.2). Requests for antibodies were sent to researchers currently studying these proteins and antibodies were obtained commercially for SUPT16H, CSRP2 and CSNK2A1. Antibodies were also available in-house that recognized SOD-1 and HNRPA1. Fresh immunoprecipitations were performed using the same conditions as those used to demonstrate that GSK-3 β -GFP was able to interact with both Axin and FRAT (section 5.1 of this chapter).

This experiment failed to confirm any of the proteins mentioned above as GSK-3 β interaction partners; The antibody raised against CSRP2 failed to recognize the protein. Antibodies against SUPT16H, CSNK2A1, SOD-1 and HNRPA1 did identify bands at the correct height in the 'lysate' and 'flow-through' fractions for both T-REx GSK-3 β -GFP and T-REx GFP samples, however no bands were observed in the 'elution' fractions corresponding to either cell line.

Proteins selected based on SILAC ratio (these proteins are not known to bind GFP or the bead matrix)

Protein	Description	Ratio
SSRP1	Structure-specific recognition protein 1	0.90595
PSME1	Proteasome activator complex subunit 1	0.92353
LDHB	L-lactate dehydrogenase B chain	0.93528
MTHFD1	Methylenetetrahydrofolate dehydrogenase	0.94856
KPNB1	Karyopherin subunit beta-1	0.94971
PEF1	Peflin	0.95303
TPI1	Triosephosphate isomerase	0.96401
VIM	Vimentin	0.96855
ST13	Suppression of tumorigenicity protein 13	0.99195
PTGES3	Prostaglandin E synthase 3	1.0244
MARS	Methionyl-tRNA synthetase	1.0793
TNPO2	Transportin-1	1.0902
LDHAL6B	L-lactate dehydrogenase A-like 6B	1.1147
SUPT16H	FACT complex subunit SPT16	1.1213
MYH10	Myosin heavy chain 10	1.1585

Proteins selected based on SILAC ratio (these proteins are known to bind GFP or the bead matrix)

Protein	Description	Ratio
CSRP2	Cysteine and glycine-rich protein 2	1.5081

Proteins selected based on STRING analysis

Protein	Description	Ratio
RAN	GTP-binding nuclear protein Ran	0.68553
CSNK2A1	Casein kinase II alpha subunit	0.01516
HNRPC	Heterogeneous nuclear ribonucleoproteins C1/C2	0.55516
HNRPD	Heterogeneous nuclear ribonucleoprotein D0	0.85161
HSP90AA1	Heat shock protein HSP 90-alpha	0.70741
MARS	Methionyl-tRNA synthetase,	1.0793

Table 5.2. Potential GSK-3 β interaction partners selected for further validation

5.5 Conclusions

In this chapter I have outlined the immuno-precipitation approaches that were adapted to identify a number of potential GskA and GSK-3 β interaction partners. I have highlighted the problems associated with these techniques and discussed the logic used to overcome them.

While I have failed to validate any of the interactions identified in this current study, it is worth noting that several of the proteins identified here have previously been reported to interact with GSK-3 either as substrates or as part of a protein complex (Table 5.3). The SILAC coupled mass spectrometry data collected during this study would argue that these interactions are transient or very dynamic.

As part of a much larger study, Ewing et al [4] over-expressed a FLAG-tagged protein library in HEK 293 cells and performed immuno-precipitations to identify binding partners. GSK-3 β was included in this library and a personal communication with Dr Ewing revealed that a number of the GSK-3 β interaction partners identified in this study were also identified as part of his own work (Table 5.4). The overlap identified between this current study and the work of others is certainly encouraging and would suggest that genuine, novel GSK-3 β binding partners remain to be validated from this study, although it remains a case of sorting the wheat from the chaff.

Protein	Description	SILAC Ratio	Nature of interaction with GSK-3β	Known contaminant	Ref
ACLY	ATP-citrate synthase	0.73801	Substrate for GSK3	No	
CSDA	Cold shock domain-containing protein A	0.64898	Substrate for GSK3	Yes	
DDX3X	ATP-dependent RNA helicase DDX3X	0.68483	Associated in protein complex	Yes	
HNRNPD	Heterogeneous nuclear ribonucleoprotein D0	0.85161	Substrate for GSK3	No	
NACAP1	Nascent polypeptide-associated complex subunit alpha	0.75588	Substrate for GSK3	Yes	
PPP1CC	Serine/threonine-protein phosphatase PP1-gamma catalytic subunit	0.46046	Forms a complex with GSK3 and PPP1R3, also component of insulin signalling pathway	No	
PSME1	Proteasome activator complex subunit 1	0.92353	Linked through curated database as component of destruction complex for degradation of β -catenin	No	
PSMD1	26S proteasome non-ATPase regulatory subunit 1	0.22629	Linked through curated database as component of destruction complex for degradation of beta catenin	No	

Table 5.3. Proteins identified as part of this study that have previously been identified as interacting with GSK-3 β

Protein name	Description	SILAC Ratio	Confidence
ACLY	ATP-citrate synthase	0.73801	+
ACTC1	Alpha-cardiac actin	0.54352	+
ALDOA	Fructose-bisphosphate aldolase A	0.21821	+
CAD	Glutamine-dependent carbamoyl-phosphate synthase	0.22187	+
CAND1	Cullin-associated and neddylation-dissociated protein 1	0.71704	+
CCT6A	T-complex protein 1 subunit epsilon	0.6126	+
CCT7	T-complex protein 1 subunit eta	0.56339	+
CCT8	T-complex protein 1 subunit theta	0.58345	+
CSDA	Cold shock domain-containing protein A	0.64898	+
DDX3X	DEAD box protein 3	0.68483	+
DHX9	DEAH box protein 9	0.46934	++
EIF3C	Eukaryotic translation initiation factor 3 subunit C	0.68907	+
EEF2	Elongation factor 2	0.48854	+
GAPDH	Glyceraldehyde-3-phosphate dehydrogenase	0.9251	+
HNRNPA1	Heterogeneous nuclear ribonucleoprotein A1	0.15382	+
HNRNPK	Heterogeneous nuclear ribonucleoprotein K	0.63133	+++
HNRNPU	Heterogeneous nuclear ribonucleoprotein U	0.6413	+
HSP90AB1	Heat shock protein HSP 90-beta	0.59347	+
HSP90B1	Heat shock protein 90 kDa beta member 1	0.60293	+
HSPA1A	Heat shock 70 kDa protein 1	0.57409	+
HSPA5	Heat shock 70 kDa protein 5	0.65864	+
NCL	Nucleolin	0.70134	+
PKM2	Pyruvate kinase isozyme M2	0.4234	+
PPP1CC	Serine/threonine-protein phosphatase PP1-gamma catalytic subunit	0.46046	+
PRKDC	DNA-dependent protein kinase catalytic subunit	0.55606	+
PTBP1	Polypyrimidine tract binding protein 1	0.47554	+
RPLP1	60S acidic ribosomal protein P1	0.5683	+
RPS20	40S ribosomal protein S20	0.6198	++
RPS2	Similar to 40S ribosomal protein S2	0.57133	++
SLC25A5	ADP/ATP translocase 2	1.1693	+
SLC25A6	ADP/ATP translocase 3	0.79247	+++
SNRPD3	Small nuclear ribonucleoprotein Sm D3	0.75624	+
SSBP1	Single-stranded DNA-binding protein	0.29163	++
SYNCRIP	Synaptotagmin-binding, cytoplasmic RNA-interacting protein	0.71368	+
TKT	Transketolase	0.59957	+
TPI1	Triosephosphate isomerase	0.96401	+++
TRAP1	Tumor necrosis factor type 1 receptor-associated protein	0.019344	+
TUBA4A	Tubulin alpha-1B chain	0.45655	+
TUBB	Tubulin beta chain	0.28665	+
TUBB2C	Tubulin beta-2C chain	0.45531	+
UBA1	Ubiquitin-like modifier-activating enzyme 1	0.64777	+
UBA52	Ubiquitin B	0.56589	+
VIM	Vimentin	0.96855	+
XRCC5	ATP-dependent DNA helicase 2 subunit 2	0.56935	+

Table 5.4. Proteins identified as potential GSK-3 β binding partners both as part of this study and by Ewing et al.

Confidence refers to arbitrary scoring by Ewing et al

Chapter 6

Discussion

The primary objectives of this project were to better characterize the role of GSK-3 in *Dictyostelium discoideum*, and to investigate the possibility that protein-binding partners may direct GSK-3 activity in both *Dictyostelium* and mammalian cells.

In Chapter 3, I described the generation of both *Dictyostelium* and mammalian TREx HEK 293 cell lines expressing GskA-GFP and GSK3 β -GFP fusion proteins, respectively. I demonstrated that cellular localization was not altered by the addition of a GFP tag. Furthermore, I established that these GFP fusion proteins retained kinase activity. I also described the generation of a series of *Dictyostelium* cell lines expressing point mutated GskA-GFP fusion proteins that would be used to further investigate the regulation of GskA activity in *Dictyostelium*.

In Chapter 4 I described a role for GskA during the early stages of *Dictyostelium* development and demonstrated that expression of GskA-GFP was sufficient to rescue the developmental phenotypes of the *gskA* null cell line. Furthermore, I reported that fusion proteins harbouring either R96E or Y214G mutations were also capable of partially rescuing this phenotype. I also described a previously unrecorded cytokinesis defect in the *gskA* null cell line and again demonstrated that expression of wild-type GskA-GFP was sufficient to rescue this phenotype.

Finally, in Chapter 5 I demonstrated that GSK-3 β -GFP was still able to bind two known GSK-3 interaction partners: Axin and FRAT, proving in principle that the addition of a GFP tag would not hinder an interaction between GSK-3 β and its binding partners. I also described the difficulties I encountered when trying to identify GskA and GSK-3 β interaction partners and discussed the optimization steps that were implemented in order to identify a series of potential GSK-3 interaction partners.

6.1 The role of GskA in Dictyostelium

During the course of this project, roles for GskA in both early development and cytokinesis were identified. Loss of GskA resulted in a failure of cells to polarize and stream during development. Loss of GskA also resulted in a cytokinesis defect that presented itself when cells were grown in shaking culture.

As part of a separate study, the *gskA* null cells were also found to be deficient in chemotaxis; Dr Regina Teo pulsed cells with cAMP for 5 hours before placing them in a gradient formed from a 1 μ M cAMP source and observing their ability to move toward the source of cAMP. Under these conditions the *gskA* null cells exhibited a complete loss in chemotaxis, a phenotype that was again rescued by expression of wild-type GskA-GFP. Dr Teo also looked at the ability of PI(3,4,5)P₃ to localize to the membrane; the PI(3,4,5)P₃-specific binding protein PH_{CRAC}-GFP was expressed in both Ax2 and *gskA* null cells. When Ax2 cells were globally stimulated with cAMP, PI(3,4,5)P₃ was generated on the entire plasma membrane causing translocation of PH_{CRAC}-GFP from the cytosol to the membrane. No PH_{CRAC}-GFP translocation was seen in the *gskA* null cells, indicating that PI(3,4,5)P₃ accumulation did not occur.

During polarization, chemotaxis and surface independent cytokinesis common signalling pathways operate to coordinate changes in both microtubule dynamics and the actin cytoskeleton. The PI3K / PI(3,4,5)P₃ signalling pathway is one of these pathways and is involved in coordinating cellular polarization and movement during chemotaxis in *Dictyostelium* (discussed in Chapter 1). In response to a cAMP signal, *Dictyostelium* accumulate PI(3,4,5)P₃ at the leading edge of the cell while membrane bound PTEN becomes restricted to the lateral sides and rear [206-208]. Similarly, during myosin-dependent cytokinesis (cytokinesis A) PI(3,4,5)P₃ accumulates at the poles of the dividing cell and PTEN localization becomes restricted to the site of the developing cleavage furrow [229]. In both cases, localization of these factors is required for F-actin polymerization at the leading edge of the cell (PI(3,4,5)P₃) and the formation of an actomyosin network at the rear or furrow region (PTEN).

The finding that the *gskA* null cells fail to polarize, chemotax, localize PI(3,4,5)P₃ to the membrane or complete cytokinesis in shaking culture indicates that GskA may perform some role in co-ordinating one or more aspects of the PI3K / PI(3,4,5)P₃ signalling pathway. However, it remains unclear whether this function involves the direct action of GskA, i.e. GskA phosphorylates a substrate involved in PI3K / PI(3,4,5)P₃ signal transduction, or if GskA acts by regulating transcription of specific genes that are themselves involved PI3K/ PI(3,4,5)P₃ signal transduction.

6.1.1 Potential mechanisms linked to direct action of GskA

1. In mammalian systems, GSK-3 acts to inhibit of glycogen synthase (GS) and regulate the conversion of glucose-6-phosphate (Glc-6-P) to glycogen (discussed in chapter 1). Glc-6-P is also the precursor for myo-inositol production, a reaction catalysed by the enzyme myo-inositol-3 phosphate synthase (*ino1*) [287]. It is possible therefore that GSK-3 activity is required to regulate the availability of Glc-6-P for the synthesis of myo-inositol, which is itself a precursor for PI(3,4)P₂ production. In the absence of GSK-3 there would be no inhibition of GS, this would lead to more Glc-6-P being converted to glycogen and mean that there would be less available Glc-6-P to be converted into myo-inositol. Consequently, this would lead to less PI(3,4)P₂ being available to be converted into PI(3,4,5)P₃ following PI3K activation.

2. A previous member of the lab, Dr Hazel Williams reported that GskA localized to microtubules during mitosis (unpublished). This is consistent with other reports that GSK-3 regulates microtubule dynamics (Discussed in Chapter 1). Previously, it was reported that microtubules did not perform an active role during *Dictyostelium* chemotaxis, but rather they were required for anchoring of the nucleus and other organelles within the cell [200]. However, there is emerging evidence that this may not be their only role; disruption of microtubules through treatment with nocodazole was found to lead to a loss in chemotaxis [288]. Furthermore, two microtubule-associating proteins, CP250 and Tsunami were recently reported to be required for efficient

chemotaxis [289, 290]. Tsunami is the *Dictyostelium* homologue of Fused, a protein shown to interact with GSK-3 in the context of Hedgehog signaling. It remains far from clear whether this kinase interacts with GskA. However, the parallels between the WNT and Hh signaling pathways in terms of signal transduction and the observed role of components of the WNT pathway in regulating microtubule dynamics could lead one to propose that these kinases act through a common pathway to exert an affect on microtubule dynamics resulting in the observed phenotypes.

6.1.2. Potential mechanisms linked to changes in gene expression

The genes encoding *SglA*, *Rac1B* and *GefM* were identified by Stremeki et al [196] as exhibiting altered expression patterns in the *gskA* null cell line. These genes are also associated with GO terms linking them to chemotaxis and/or cytokinesis. Details of the affects of loss- or over-expression of each of these genes have been reported and their phenotypes, and how they might relate to the phenotype of the *gskA* null cell line are discussed below.

1. The gene *sglA* was found to be under-expressed in the *gskA* null cell line [196]. This gene encodes sphingosine-1-phosphate lyase (S1P lyase) a protein involved in the last step in sphingomyelin catabolism where sphingosine-1-phosphate (S1P) is degraded to phosphoethanolamine and hexadecanal [291]. In mammals, ceramide and S1P are both intermediate substrates of the sphingomyelin degradation pathway and both of these molecules perform regulatory roles in controlling cell proliferation and cell death [292]. S1P has also been shown to perform roles in the release of intracellular Ca²⁺ stores, actin polymerization, cell motility, chemotaxis and cell differentiation in mammalian systems[293].

An *sglA* knock-out cell line was generated by Li et al [294] in order to characterize the role of S1P in *Dictyostelium*. *sglA* null cells were found to aggregate faster than their wild-type counterparts and exhibited an inability to form slugs, similar to the phenotype of the *gskA* nulls. These cells also exhibited aberrant F-actin localization and were unable to suppress lateral pseudopodia during chemotaxis [295]. While it remains unclear whether loss of SglA also resulted in an inability complete cytokinesis in shaking culture,

it is reasonable to conclude that the phenotype of the *gskA* nulls may in part be explained by reduced expression of *SglA*.

2. RasGEFM is a multi-domain protein containing six poly-proline stretches, a DEP, RasGEFN and RasGEF catalytic domain. Inactivation of the gene encoding this protein resulted in cells that formed small, flat aggregates and failed to develop further. Chemotaxis towards cAMP was also impaired in this mutant, due to inability to inhibit lateral pseudopods. Adenylyl cyclase activation in response to cAMP pulses was strongly reduced, and the actin polymerization response to cAMP was also altered in the mutant. Expression of the *GefM* gene was found to be under-expressed in the *gskA* null cells, and could explain the inability of the *gskA* cells to activate adenylyl cyclase in response to cAMP stimulation.

3. Rac1B is a small G-protein in the Ras superfamily that has been implicated in the control of cell growth, adhesion, and the actin-based cytoskeleton. Stremeki et al [196] reported that this gene is over-expressed in the *gskA* null cell line. Rac1B was found to co-localize with F-actin in lamellipodia and at sites of cell-to-cell contact. Palmieri et al [296] reported that over expression of this protein led to aberrant F-actin localization. Cells over-expressing Rac1B also became multi-nucleate when grown in shaking culture and divided via cytokinesis C when plated out onto a solid surface [297], similar to the phenotype of the *gskA* null cells.

In reality, it is likely that the phenotype of the *gskA* null cells results from a combination of both an inability to phosphorylate specific substrates and downstream changes in gene expression. In order to dissect the role of GskA further and assess the relative contributions of genes with altered expression patterns in the *gskA* nulls it would be necessary to perform further experiments. These could include re-expression of genes in the *gskA* null cells under an alternative promoter (such as *actin15*) and assessing the ability of these constructs to rescue aspects of the *gskA* null phenotype.

6.2 The role of key residues of GskA

In the course of this project cell lines expressing GskA-GFP constructs carrying K85R, R96E or Y214G point mutations were generated and characterized. The ability of each cell line to rescue aspects of the *gskA* null phenotype differed; kinase dead K85R failed to rescue any aspect of the *gskA* null phenotype, indicating that the role performed by GskA was an active one, GskA does not simply function as a scaffold. Constructs carrying either R96E or Y214G mutations offered partial rescue of the cytokinesis phenotype. These cell lines also rescued some, but not all, aspects of the developmental phenotype of the *gskA* nulls perhaps indicating that GskA performs multiple roles during early development.

6.2.1 Separation of the functions performed by GskA during development

Cell lines expressing either GskA-GFP R96E or GskA-GFP Y214G were able to aggregate and stream during early development, although the aggregation territories observed for these cell lines were smaller than that of Ax2 or *gskA* null-GskA-GFP cell lines. This observation may be evidence of a direct role for GskA in enabling cells to propagate a cAMP signal. In Chapter 4 I described the phenotype of the *gskA* null cells during development and reported that prior to mound formation these cells formed doughnut like structures that were indicative of an inability to activate adenylate cyclase. Experiments performed by Dr Reddy also demonstrated that loss of GskA resulted in an inability of cells to synthesize cAMP. In Chapter 3 I reported that the GskA-GFP R96E and GskA-GFP Y214G fusion proteins were catalytically compromised. The observation that these cell lines formed smaller aggregation territories may be evidence that the GskA-GFP R95E and GskA-GFP Y214G proteins were able to function to activate cAMP synthesis, but not to the same extent as wild-type GskA. Performing a similar experiment to Dr Reddy, and looking at the levels of cAMP production in these cell lines following stimulation with 2-deoxyadenosine 3,5-monophosphate (dcAMP) would shed light on this matter and may help to further characterise the role of GskA.

In chapter 4 I demonstrated using dark field optics that the *gskA* null cells failed to polarize or undergo periodic changes in cell shape during aggregation. Similarly, when viewed under dark field conditions, cell lines expressing either GskA-GFP R96E or GskA-GFP Y214G fusion proteins did not clearly polarize despite an obvious ability to stream. Again, this would indicate that GskA may action multiple effects at this stage of development, and the catalytically compromised GskA-GFP R96E and GskA-GFP Y214G fusion proteins were capable of performing some but not all of these functions. By looking directly at the ability of these cell lines to chemotax in a gradient of cAMP and whether these cell lines were able to localize PI(3,4,5)P₃ to the membrane following stimulation with cAMP, one may be able to separate out further the multiple affects coordinated by GskA during early development.

6.2.2. Regulatory roles of Y214 and R96

While the phenotypes of cells expressing GskA-GFP R96E or GskA-GFP Y214G fusion proteins were very similar, and both were able to rescue aspects of the *gskA* null phenotype there are key differences between these cell lines that require further consideration.

In chapter 4 I reported that cells expressing GskA-GFP R96E continued to form doughnut-like structures at the mound stage, a phenotype of the *gskA* nulls that was rescued by expression of GskA-GFP Y214G. Furthermore, cells expressing GskA-GFP R96E took considerably longer to complete development.

As described in Chapter 3, where possible I tried to ensure that the cell lines used were expressing GskA-GFP at similar levels to that of endogenous GskA. However, in case of GskA-GFP R96E this was not possible as all cell lines exhibited significantly higher levels of expression. This is an important consideration when dissecting the ability of this fusion protein to rescue aspects of the *gskA* null phenotype. Given that GskA-GFP R96E was expressed at higher levels than GskA-GFP Y214G and still failed to rescue some aspects of the *gskA* null phenotype this would indicate that the ability of GskA to recognize primed substrates is central to the regulation of GskA activity.

6.3 Identification of potential GSK-3 interaction partners

In chapter 5, I presented experiments that resulted in the identification of a series of potential GskA or GSK-3 β binding partners. Difficulties were encountered while performing these experiments and insufficient material meant that standard affinity purification and mass spectrometry techniques were not sufficient to identify proteins of interest. In chapter 5 I also described the modifications that were applied to this methodology in order to improve yields and facilitate the identification of potential binding partners.

The underlying reasons for the difficulties encountered may in part be due to the methods used to prepare cellular extracts; cells were lysed and clarified prior to the addition of anti-GFP beads. This clarification step was performed in order to prevent sedimentation of large, insoluble proteins with the bead matrix. Sedimentation would represent a non-specific interaction and could potentially limit the ability of the anti-GFP antibody to recognize and bind GFP. However, it is probably that GSK-3 is contained in this insoluble fraction, bound to nuclei or the cytoskeleton. Therefore, by discarding this fraction I was reducing the amount of GSK-3 available for immunoprecipitation and potentially excluding specific interaction partners.

Difficulties may also have encountered due to the nature of the proteins I was attempting to identify. By definition, scaffolding proteins that direct GSK-3 activity towards specific substrates are likely to be large unstructured proteins. This creates problems when performing immuno-precipitations as these proteins are more likely to undergo proteolysis. Furthermore, samples were separated by 2D-gel electrophoresis prior to mass spectrometry analysis, any particularly large proteins may be too big to pass into the gel.

6.3.1 Identification of ribosomal proteins as GSK-3 binding partners

Several ribosomal proteins were identified as potential GskA or GSK-3 β binding partners. There is some evidence that GSK-3 interacts with, or regulates components of the ribosome. For example, Kim et al [124] reported that lithium inhibition of GSK-3 β activity resulted in proteosomal degradation of 3 ribosomal proteins (rpl14B, rpl18A and rpS15). This treatment also prevented degradation of two other ribosomal proteins (rpL30 and rpS10) indicating perhaps that GSK-3 performs both positive and negative roles in the regulation of ribosomal turnover. Furthermore, GSK-3 β has also previously been shown to phosphorylate and inhibit the translation initiation factor eIF2B [179, 180], indicating that it is possible that GSK-3 may perform some additional role in regulating translation and the ribosomal proteins identified in this study are evidence of this role. However, it is also possible that the ribosomal proteins identified in this study do not represent biologically relevant interactions and only co-purified with either GskA or GSK-3 β during their synthesis. Furthermore, Trinkle et al [3] reported that ribosomal proteins frequently bound non-specifically during their affinity purification experiments. Given the difficulties associated with demonstrating that any interactions between either GskA or GSK-3 β and any ribosomal proteins were specific and biologically important, these proteins were excluded from further analysis.

6.3.2 Potential GskA interaction partners

Expression of wild-type GskA-GFP was found to rescue all aspects of gskA null phenotype investigated in this study, indicating perhaps, that if GskA activity was directed by binding to specific protein partners, that the addition of a GFP tag did not abrogate this interaction.

In chapter 5 I identified a number of potential GskA binding partners although a lack of available antibodies means that these interactions remain to be validated. Interactions between GskA and several of the proteins highlighted in this study are certainly worthy of further investigation. One such protein is AncA. The mammalian homologue of this protein, adenine nucleotide translocase (ANT), is a component of the mitochondrial permeability transition pore (mPTP). These pores are present in mitochondrial

membranes and perform an important role in cell necrosis associated with ischemia and neurodegeneration (reviewed in [298]). The mPTP is a nonselective, high conductance channel that minimally consists of Adenine nucleotide translocase (ANT), Voltage-dependent anion channel (VDAC) and Cyclophilin-D (cyP-D). Opening of this channel is associated with immediate loss of mitochondrial membrane potential and cell death. Mammalian GSK-3 was found to translocate to mitochondria [299, 300] and reportedly binds to ANT [301]. Antibodies that recognise Dictyostelium AncA were not available for the purpose of this current study. However, they have been generated and it would be interesting to investigate whether this interaction is conserved between mammals to Dictyostelium.

The protein ArcB was also identified as a potential GskA binding partner. This protein is a component of the Arp2/3 complex and is recruited to the cell perimeter, and into pseudopodia following stimulation with cAMP [302]. The Arp2/3 complex performs a crucial role mediating the actin polymerization response to chemotactic stimulation and contributes to cell motility, pseudopod extension and adhesion in Dictyostelium [302]. A direct interaction between GskA and components of this complex may represent a mechanism by which GskA acts to directly to regulate both cellular polarization and chemotaxis.

Both the proteins VatD and VatE were identified as potential GskA binding partners in chapter 5. The genes encoding these proteins were also found to be over-expressed in the *gskA* null cell line. VatD and VatE are both subunits of the peripheral V1 complex of vacuolar H⁺-ATPase. V-ATPase is an ATP-driven proton pump that functions to both acidify intracellular compartments and to transport protons across the plasma membrane of eukaryotic cells [303, 304]. Expression of several other V-ATPase subunits, namely VatB, VatH, VatP were also found to be up-regulated in the *gskA* null cell line [196]. However, it remains unclear at this time whether these findings represent a biological role for GskA or are simply co-incidence.

6.3.3 Potential GSK3 β interaction partners

A series of potential GSK-3 β interaction partners were identified in this study. Again, these interactions largely remain to be validated. Of particular interest are those proteins that were highlighted in Table 5.3 of chapter 5 and those proteins that were also identified as part of the study conducted by Ewing et al. [4].

Difficulties were encountered during the course of this project in trying to identify GSK-3 β binding partners. Insufficient material meant that standard affinity purification and mass spectrometry techniques could not be employed and SILAC analysis failed to identify any strong candidates for interaction partners.

In chapter 5 I demonstrated that the addition of a GFP tag did not hinder the ability of GSK-3 β to interact with either Axin or FRAT. Izumi et al [43] similarly demonstrated that the addition of a GFP tag did not prevent GSK-3 β from binding to GCP5. It is unlikely therefore that the failure to identify strong GSK-3 β binding partners was the result of the choice of affinity tag.

A plethora of GSK-3 binding partners have previously been identified (Table 6.1). These interactions were largely identified using yeast-2-hybrid screens and through over-expression studies. These techniques have limitations with the potential to produce false positives in the form of in-direct interactions (yeast-2-hybrid) and the inclusion of GSK-3 in non-physiologically relevant complexes (over-expression). However, it is interesting that very few studies have identified GSK-3 binding partners using endogenous levels of protein expression. Furthermore, only one previously documented GSK-3 binding protein, PPP1CC, was identified as part of this study. It may be that GSK-3 β binding partners are only present in very low abundance in cell or have very high turnover. Axin, a known GSK-3 binding partner was not identified as a binding partner in the SILAC experiment despite demonstrating that this protein does interact with GSK-3 β -GFP when over expressed. Axin is present in the cell at very low levels, and is subject to rapid turnover [305]. Indeed, recent immunoprecipitation experiments conducted with a view to identifying Axin binding partners required the culturing and harvesting of 100 9cm plates of HEK 293 cells to yield enough material for mass spectrometry analysis (personal communication with Prof. Hans Clevers). If GSK-3 β

Species	Interactant	Description	Method of Identification	REF
Homo sapiens	ACLY	ATP citrate lyase	Over-expression of FLAGGSK3 β in HEK 293 cells	[4]
Homo sapiens	AKAP11	A kinase (PKA) anchor protein 11	Yeast-2-hybrid	[5]
Homo sapiens	APC	adenomatous polyposis coli	In vitro Co-IP	[9]
Homo sapiens	AR	Androgen receptor	In vitro Co-IP	[10]
Homo sapiens	AXIN1		In vitro affinity capture	[11]
Homo sapiens	BCL3	B-cell CLL/lymphoma 3	Co-IP with endogenous proteins	[14]
Caenorhabditis elegans	BED finger and Zn-finger	C2H2 type (1J430)	Yeast-2-hybrid	[15]
Homo sapiens	BXDC1	Brix domain containing 1	Over-expression of FLAGGSK3 β in HEK 293 cells	[4]
Caenorhabditis elegans	C01G12.1	Hypothetical protein	Yeast-2-hybrid	[15]
Caenorhabditis elegans	C07G1.6	Hypothetical protein	Yeast-2-hybrid	[18]
Homo sapiens	C14orf129	GSK3-beta interaction protein (GSKIP)	Yeast-2-Hybrid and Over-expression of FLAG-GSK3 β in HEK 293 cells	[4, 19]
Caenorhabditis elegans	CC8.1	Hypothetical protein	Yeast-2-hybrid	[15]
Drosophila melanogaster	CG15185	Hypothetical protein	Yeast-2-hybrid	[20]
Drosophila melanogaster	Cos2	Costal-2	Co-IP with endogenous proteins	[21]
Mus musculus	Csnk2a1	casein kinase 2, alpha 1 polypeptide	In vitro affinity capture	[25]
Homo sapiens	CTNNB1	Beta-catenin	Over-expression of FLAGGSK3 β in HEK 293 cells	[4]
Drosophila melanogaster	Cubitus Interruptus	cubitus interruptus	Over-expression	[21]
Homo sapiens	DDX20	DEAD box protein 20	Over-expression of FLAGGSK3 β in HEK 293 cells	[4]
Homo sapiens	DDX5	DEAD box protein 5	Over-expression of FLAGGSK3 β in HEK 293 cells	[4]
Homo sapiens	DHX36	ATP-dependent RNA helicase / DEAH box protein 36	Over-expression of FLAGGSK3 β in HEK 293 cells	[4]
Homo sapiens	DISC1	Disrupted in schizophrenia 1	Co-IP with endogenous proteins	[34]
Homo sapiens	DNM1L	Dynamin 1-like protein isoform 1	Yeast-2-hybrid	[35]
Homo sapiens	E2F1	E2F transcription factor 1	Co-IP with endogenous proteins	[36]
Homo sapiens	EWSR1	Ewing sarcoma breakpoint region 1 protein	Over-expression of FLAGGSK3 β in HEK 293 cells	[4]
Homo sapiens	FIP1L1	Isoform 1 of Pre-mRNA 3'-endprocessing factor FIP1 (Factor interacting with PAP)	Over-expression of FLAGGSK3 β in HEK 293 cells	[4]
Homo sapiens	FRAT1	Frequently re-arranged in advanced T-cell lymphomas		[40]
Homo sapiens	FRAT2	Frequently re-arranged in advanced T-cell lymphomas		[40, 41]
Homo sapiens	FUS	Isoform Long of RNA-binding protein FUS	Over-expression of FLAGGSK3 β in HEK 293 cells	[4]
	GCP5	tubulin, gamma complex associated protein 5	Over-expression of GSK-3bGFP in HeLa cells	[43]
Homo sapiens	GEMIN4	Gem (nuclear organelle) associated protein 4	Over-expression of FLAGGSK3 β in HEK 293 cells	[4]
Homo sapiens	HIST1H1T	Histone H1t	Over-expression of FLAGGSK3 β in HEK 293 cells	[4]
Homo sapiens	HSD17B4	Peroxisomal multifunctional enzyme type 2 (MFE-2)	Over-expression of FLAGGSK3 β in HEK 293 cells	[4]
Homo sapiens	IGF2BP1	Insulin-like growth factor 2 mRNA-binding protein 1	Over-expression of FLAGGSK3 β in HEK 293 cells	[4]
Homo sapiens	IKBKAP	IkappaB kinase complex-associated protein (p150)	Over-expression of FLAGGSK3 β in HEK 293 cells	[4]
Caenorhabditis elegans	MAC-1	Member of AAA family binding CED-4 family member	Yeast-2-hybrid	[15]
Homo sapiens	MAP2K5	Dual specificity mitogen-activated protein kinase kinase 5	Over-expression of FLAGGSK3 β in HEK 293 cells	[4]

Homo sapiens	MUC1	Mucin-1		[1, 2]
Homo sapiens	MYCN	N-myc proto-oncogene protein	Over-expression of FLAGGSK3 β in HEK 293 cells	[4]
Homo sapiens	NIN	Isoform 1 of Ninein	Yeast-2-hybrid	[8]
Homo sapiens	NIN	Isoform 2 of Ninein	Yeast-2-hybrid	[8]
Homo sapiens	NOTCH		Over-expression of HA-GSK3 β in HEK 293 cells	[17]
Homo sapiens	POLR2B	DNA-directed RNA polymerase II subunit RPB2	Over-expression of FLAGGSK3 β in HEK 293 cells	[4]
Homo sapiens	PPP1CA	protein phosphatase 1, catalytic subunit, alpha	Co-IP with endogenous proteins	[5]
Homo sapiens	PRKAR2A	cAMP-dependent protein kinase type II-alpha regulatory subunit	Co-IP with endogenous proteins	[5]
Drosophila melanogaster	Prune		Yeast-2-Hybrid	
Homo sapiens	PTK2	protein tyrosine kinase 2 isoform b	Co-IP with endogenous proteins	[24]
Homo sapiens	QPCTL	Isoform 1 of Glutaminyl-peptide cyclotransferase-like protein	Over-expression of FLAGGSK3 β in HEK 293 cells	[4]
Homo sapiens	RGS22	Regulator of G-protein signaling 22	Over-expression of FLAGGSK3 β in HEK 293 cells	[4]
Homo sapiens	SF3A1	Splicing factor 3 subunit 1	Over-expression of FLAGGSK3 β in HEK 293 cells	[4]
Homo sapiens	SF3B1	Splicing factor 3B subunit 1	Over-expression of FLAGGSK3 β in HEK 293 cells	[4]
Homo sapiens	SGK3	serum/glucocorticoid regulated kinase 3 isoform 1	Yeast-2-hybrid	[33]
Homo sapiens	SMAD3		Co-IP with endogenous proteins	[38]
Homo sapiens	SMARCA2	SWI/SNF related, matrix associated, actin dependent regulator of chromatin, subfamily a, member 2	Over-expression of FLAGGSK3 β in HEK 293 cells	[4]
Homo sapiens	SMN1	Isoform 1 of Survival motor neuron protein	Over-expression of FLAGGSK3 β in HEK 293 cells	[4]
Homo sapiens	SMN2	Isoform 2 of Survival motor neuron protein	Over-expression of FLAGGSK3 β in HEK 293 cells	[4]
Homo sapiens	SMYD2	SET and MYND domain containing protein 2	Over-expression of FLAGGSK3 β in HEK 293 cells	[4]
Homo sapiens	SNRNP70	Isoform 1 of U1 small nuclear ribonucleoprotein 70 kDa	Over-expression of FLAGGSK3 β in HEK 293 cells	[4]
Homo sapiens	SREBP1	sterol regulatory element binding transcription factor 1 isoform a	In vitro affinity capture	[46]
Homo sapiens	STRAP	Serine-threonine kinase receptor-associated protein	Over-expression of FLAGGSK3 β in HEK 293 cells	[4]
Caenorhabditis elegans	T12G3.1	Hypothetical protein	Yeast-2-hybrid	[15]
Caenorhabditis elegans	T24H7.3	Hypothetical protein	Yeast-2-hybrid	[15]
Rattus norvegicus	Tat	Human immunodeficiency virus 1	Co-IP with over-expressed tat	[47]
Homo sapiens	TP53	Tumor protein p53	Co-IP with endogenous proteins	[52]
Homo sapiens	TPPP	Tubulin polymerization promoting protein	Co-purify in sae fraction following gel-chromatography	[53]
Homo sapiens	TSC1	Isoform 1 of Tuberin (Tuberous sclerosis 2 homolog protein)	Over-expression of FLAGGSK3 β in HEK 293 cells	[4]
Homo sapiens	TSC2	Isoform 2 of Tuberin (Tuberous sclerosis 2 homolog protein)	Over-expression of FLAGGSK3 β in HEK 293 cells	[4]
Homo Sapiens	UPF3A	UPF3 regulator of nonsense transcripts homolog A isoform hUpf3p	Yeast-2-hybrid	[61]
Homo sapiens	XPO6	Exportin-6	Over-expression of FLAGGSK3 β in HEK 293 cells	[4]
Caenorhabditis elegans	Y48E1B.10	Glutathione S-Transferase family member (gst-20)	Yeast-2-hybrid	[15]
Caenorhabditis elegans	ztf-26	Zinc finger transcription factor 26	Yeast-2-hybrid	[15]

Table 6.1 Known GSK-3 interacting proteins

activity towards specific substrates is regulated through interactions with scaffolding proteins, it would make sense for these scaffolding proteins to be present at low levels, thus ensuring they are the rate-limiting factor. It is also possible that GSK-3 β interacts with other proteins only in a transient manner or that the majority of interactions are low affinity. This would mean that during the incubation period with the GFP-binder GSK-3 interaction partners were able to associate and dissociate freely, thus altering the ratio of heavy : light amino acids.

In order to identify GSK-3 β binding partners in future using an affinity purification approach it may be necessary to significantly increase the levels of protein expression, amount of starting material or perform a SILAC experiment were samples are only combined following affinity purification.

It would also be an appreciable goal to extend this research and investigate how GSK-3 binding partners change in response to specific stimuli such as cAMP, WNT or Hh ligands. In the context of the WNT signalling, activation of the pathway has already been shown to alter the binding properties of GSK-3; in chapter 1 I discussed how there is emerging evidence that WNT signal transduction involved the re-localization of GSK-3 and Axin to the plasma membrane and an association between GSK-3 β and LRP6. By looking at how GSK-3 binding partners change in response to specific stimuli we would gain significant insight into the regulatory mechanisms by which GSK-3 activity is directed.

Recently, tissue specific roles for each mammalian GSK-3 isoforms have also been identified; glycogen metabolism was found to be regulated by different GSK-3 isoforms in a tissue specific manner [29, 86]. As such, in order to exhaustively identify all GSK-3 interaction partners and fully understand the regulatory mechanisms of this protein it may be necessary to move over to a mouse model and identify GSK-3 binding partners in a tissue specific manner.

6.4 Conclusions

In summary, I have identified a novel role for GskA in the regulation of myosin-dependent cytokinesis in *Dictyostelium*. I, along with others, have also expanded on our understanding of the role of GskA during the early stages of *Dictyostelium* development. And, I have demonstrated that GskA performs multiple roles during aggregation and is required both for cellular polarization and chemotaxis.

Both cytokinesis and chemotaxis occur as a result of co-ordinated responses involving multiple signalling pathways. The function performed by GskA in co-ordinating these responses can in part be explained through GskA directed regulation of gene expression. However, there is also evidence for a direct role for GskA and as part of this study I have identified a series of potential GskA binding partners that may be involved in directing GskA activity.

The mammalian aspect of this project and the SILAC coupled mass spectrometry experiments did not identify any strong candidates for GSK-3 β binding proteins. However a number of potential binding partners, that were also highlighted as part of a separate study have been identified. Validation of these interactions will continue within the lab.

This study did indicate that any protein:protein interactions involving GSK-3 are likely to be highly dynamic or transient. A finding that reflects the dynamic nature of a protein that functions as a global regulator of cellular processes, acting to co-ordinate multiple changes in the cell.

Appendix

Genes with altered expression in *gskA* null cell line

Gene ID	Gene name	Protein ID	Description	Log2 (ratio <i>gskA</i> null Vs Ax2)
DDB_G0277861	patA	DDB0214945	P-type ATPase, Ca ²⁺ -ATPase	2.0176758
DDB_G0268212	DDB_G0268212	DDB0233906	putative DEAD/DEAH box helicase	1.9205188
DDB_G0269322	DDB_G0269322	DDB0190177		1.8811491
DDB_G0288055	DDB_G0288055	DDB0238154	K ⁺ potassium transporter	1.8808755
DDB_G0277503	amtA	DDB0185017	ammonium transporter	1.7702776
DDB_G0284535	CYP508A4	DDB0232355	cytochrome P450 family protein	1.7295033
DDB_G0285871	DDB_G0285871	DDB0237751	Ran GTPase binding protein, Mog1 family protein, RAN guanine nucleotide release factor	1.6751536
DDB_G0273809	DDB_G0273809	DDB0266641	zinc/iron permease, ZIP family zinc transporter	1.6737599
DDB_G0271672	DDB_G0271672	DDB0232108	ZIP zinc transporter protein, zinc/iron permease	1.672326
DDB_G0277489	DDB_G0277489	DDB0169205		1.6396084
DDB_G0275253	DDB_G0275253	DDB0229926		1.6204642
DDB_G0279713	DDB_G0279713	DDB0230087	putative saposin putative cerebroside sulfate activator	1.5885049
DDB_G0275523	DDB_G0275523	DDB0167196		1.5364555
DDB_G0275475	DDB_G0275475	DDB0167118		1.5274893
DDB_G0293182	expl8	DDB0304867	expansin-like protein	1.4972502
DDB_G0291111	DDB_G0291111	DDB0219645		1.4804599
DDB_G0268208	DDB_G0268208	DDB0189867		1.4209803
DDB_G0279185	cprF	DDB0215002	cysteine proteinase	1.4184733
DDB_G0268208	DDB_G0268208	DDB0189867		1.3275763
DDB_G0290001	DDB_G0290001	DDB0188678		1.3025722
DDB_G0279819	DDB_G0279819	DDB0206309		1.2929857
DDB_G0292736	pipA	DDB0201656	phosphoinositide-specific phospholipase C	1.2869461
DDB_G0289167	DDB_G0289167	DDB0188292	Similar to <i>Rhizobium loti</i> (<i>Mesorhizobium loti</i>). Short-chain oxidoreductase	1.2687382
DDB_G0274181	DDB_G0274181	DDB0252580		1.2280192
DDB_G0292016	-	DDB0184163		1.2202076
DDB_G0291123	glpD	DDB0191397	glycogen phosphorylase 2 glycogen phosphorylase a	1.2096769
DDB_G0277401	vatB	DDB0185207	vacuolar H ⁺ ATPase B subunit	1.2081223
DDB_G0284793	-	DDB0186196		1.1985631
DDB_G0284763	DDB_G0284763	DDB0186177		1.1876217
DDB_G0269892	DDB_G0269892	DDB0190650		1.172243
DDB_G0290431	DDB_G0290431	DDB0188901		1.1307283
DDB_G0285981	DDB_G0285981	DDB0232083	type A von Willebrand factor (VWFA) domain-containing protein	1.125797
DDB_G0277969	DDB_G0277969	DDB0238145	NADH:flavin oxidoreductase/NADH oxidase domain-containing protein	1.1097461
DDB_G0287717	DDB_G0287717	DDB0187589		1.0885663
DDB_G0282209	DDB_G0282209	DDB0238178	type A von Willebrand factor (VWFA) domain-containing protein	1.0842277
DDB_G0281443	DDB_G0281443	DDB0205585		1.0823777
DDB_G0275701	vatE	DDB0185070	vacuolar H ⁺ -ATPase E subunit	1.0592366
DDB_G0276067	ddcB	DDB0237754	group IV decarboxylase, putative diaminopimelate decarboxylase	1.0566069
DDB_G0271988	DDB_G0271988	DDB0168608		1.0524534
DDB_G0275695	ampA	DDB0185088	adhesion modulation protein A prestalk D11 protein precursor	1.0316899
DDB_G0271818	DDB_G0271818	DDB0238818		1.0155513
DDB_G0275469	DNaseV	DDB0233087	putative endonuclease V	1.0148357
DDB_G0268614	msh6	DDB0229918	mutS homolog, DNA mismatch repair protein	1.0068844
DDB_G0275693	DDB_G0275693	DDB0185020	peptidase C53 family protein	0.9956591
DDB_G0288947	DDB_G0288947	DDB0233866		0.9942231
DDB_G0279187	cprG	DDB0215005	cysteine proteinase	0.989646
DDB_G0268622	rac1B	DDB0219941	Rho GTPase	0.9886429
DDB_G0286197	DDB_G0286197	DDB0305103		0.9859124
DDB_G0272434	DDB_G0272434	DDB0217004		0.9807131
DDB_G0285981	DDB_G0285981	DDB0232083	type A von Willebrand factor (VWFA) domain-containing protein	0.9499135
DDB_G0274259	DDB_G0274259	DDB0167806		0.9421814
DDB_G0287671	DDB_G0287671	DDB0219255		0.9368011
DDB_G0281325	DDB_G0281325	DDB0305072	alkaline phosphatase-like protein	0.9327649
DDB_G0278481	DDB_G0278481	DDB0234075	UPF0027 family protein	0.9192288
DDB_G0277429	DDB_G0277429	DDB0237856	regulator of chromosome condensation (RCC1) domain-containing protein BTB/POZ domain-containing protein of chromosome condensation (RCC1) domain-containing protein	0.9161506
DDB_G0274331	DDB_G0274331	DDB0235141	vacuolar ATP synthase subunit D	0.8845514
DDB_G0269454	trpS	DDB0231245	tryptophanyl-tRNA synthetase tryptophan-tRNA ligase	0.8787375
DDB_G0287765	DDB_G0287765	DDB0238148	NADH:flavin oxidoreductase/NADH oxidase domain-containing protein	0.8543896
DDB_G0278649	DDB_G0278649	DDB0218082		0.8463857
DDB_G0285615	DDB_G0285615	DDB0238155		0.8457415
DDB_G0285725	dhps	DDB0266388	deoxyhypusine synthase	0.8218971

DDB_G0289481	glnS	DDB0201644	glutamine-tRNA ligase glutaminyl-tRNA synthetase vegetative specific protein H4	0.8218605
DDB_G0289595	prpf31	DDB0304959	pre-mRNA processing factor 31	0.8169809
DDB_G0292894	DDB_G0292894	DDB0305175	putative ornithine cyclodeaminase	0.8139456
DDB_G0286725	vps13A	DDB0234198	vacuolar protein sorting-associated protein 13 family protein	0.8086366
DDB_G0279443	DDB_G0279443	DDB0205768		0.7907435
DDB_G0271068	DDB_G0271068	DDB0216762		0.7850833
DDB_G0293038	DDB_G0293038	DDB0191738	phosphatidylinositol-4-phosphate 5-kinase (PIP5K) family protein	0.7752078
DDB_G0292978	DDB_G0292978	DDB0219806		0.7711197
DDB_G0275413	DDB_G0275413	DDB0234182	transmembrane protein vacuolar sorting protein 9 domain-containing protein DUF726 family protein	0.7609096
DDB_G0274553	vath	DDB0234266	vacuolar ATP synthase subunit H	0.7527619
DDB_G0277729	DDB_G0277729	DDB0233559		0.7464713
DDB_G0290317	psiJ	DDB0232407	PA14 domain-containing protein	0.7375259
DDB_G0283977	DDB_G0283977	DDB0185789	Probable short-chain dehydrogenase	0.7248511
DDB_G0285975	DDB_G0285975	DDB0218765	Mast cell surface antigen-1.	0.7221299
DDB_G0292214	DDB_G0292214	DDB0267116	protein phosphatase 2C-related protein	0.7171591
DDB_G0286555	racA	DDB0191173	Rho GTPase RhoBTB family protein	0.7137651
DDB_G0293436	abcA3	DDB0201662	ABC transporter A family protein	0.7060042
DDB_G0281815	DDB_G0281815	DDB0266864	DUF410 family protein, UPF0363 family protein	0.6589781
DDB_G0294040	mrp11	DDB0201601	S60 ribosomal protein L11 ribosomal protein L11, mitochondrial	0.6572212
DDB_G0274553	vath	DDB0234266	vacuolar ATP synthase subunit H	0.6279824
DDB_G0274381	vatP	DDB0185071	vacuolar ATPase proteolipid subunit, Vacuolar ATP synthase proteolipid subunit	0.5995834
DDB_G0293438	abcB2	DDB0201670	ABC transporter B family protein	0.5862193
DDB_G0278333	SppA	DDB0205381		0.5656316
DDB_G0280969	prdD	DDB0214953	proteasome subunit alpha type 4, 20S proteasome subunit alpha-4	-0.5220274
DDB_G0278271	DDB_G0278271	DDB0205337		-0.5463779
DDB_G0270358	-	DDB0304448	UAS domain-containing protein, UBX domain-containing protein, ubiquitin interacting motif (UIM) domain-containing protein	-0.5503816
DDB_G0291988	if1	DDB0216175	F1F0-ATPase putative regulatory protein IF1	-0.5635355
DDB_G0271264	usp14	DDB0237695	ubiquitin domain-containing protein, peptidase C19 family protein, putative ubiquitin carboxyl-terminal hydrolase (UCH)	-0.5708384
DDB_G0281865	adh5	DDB0238276	zinc-containing alcohol dehydrogenase (ADH), alcohol dehydrogenase, class 3, formaldehyde dehydrogenase	-0.578092
DDB_G0288933	cda	DDB0230205	cytidine deaminase	-0.5865414
DDB_G0286195	nagB1	DDB0234127	glucosamine-6-phosphate isomerase glucosamine-6-phosphate deaminase PIG-L family protein	-0.5875792
DDB_G0278873	gnpda1	DDB0234126	glucosamine-6-phosphate isomerase glucosamine-6-phosphate deaminase	-0.5922923
DDB_G0280047	yelA	DDB0214918	initiation factor eIF-4 gamma middle domain-containing protein	-0.5996218
DDB_G0268538	psmA5	DDB0232930	proteasome subunit alpha type 5, 20S proteasome subunit alpha-5	-0.6225098
DDB_G0276933	mcfX	DDB0234131	putative transmembrane protein, mitochondrial substrate carrier family protein	-0.6244587
DDB_G0284553	gmd	DDB0231676	GDP-mannose 4,6-dehydratase, GDP-mannose 4,6-hydrolyase, GDP-mannose dehydratase	-0.625974
DDB_G0273865	pakH-2	DDB0266965	STE20 family protein kinase protein kinase, STE group PAKL subfamily protein kinase putative protein serine/threonine phosphatase	-0.6290553
DDB_G0274041	-	DDB0217433		-0.6352066
DDB_G0272684	qdpr	DDB0237752	dihydropteridine reductase quinoid dihydropteridine reductase	-0.6353745
DDB_G0291265	gloA	DDB0230987	lactoylglutathione lyase, glyoxylase I	-0.640263
DDB_G0283679	psmB7	DDB0232933	proteasome subunit beta type 7 20S proteasome subunit beta-7	-0.6458286
DDB_G0274579	pitB	DDB0219979	phosphatidylinositol transfer protein 2	-0.6627077
DDB_G0288495	DDB_G0288495	DDB0187960		-0.6646256
DDB_G0293538	dcd2A	DDB0215370	neutral/alkaline nonlysosomal ceramidase family protein acid ceramidase	-0.6664104
DDB_G0276269	sgcA	DDB0191330	guanylyl cyclase	-0.6708314
DDB_G0272052	DDB_G0272052	DDB0232387	leucine-rich repeat-containing protein (LRR) putative cell surface glycoprotein	-0.6870475
DDB_G0274067	DDB_G0274067	DDB0266924		-0.6917882
DDB_G0271694	DDB_G0271694	DDB0168459		-0.6977485

DDB_G0274409	pakF	DDB0229410	putative protein serine/threonine kinase STE20 family protein kinase protein kinase, STE group PAKL subfamily protein kinase	-0.7038544
DDB_G0274471	tpiA	DDB0231425	triose phosphate isomerase triosephosphate isomerase	-0.7046855
DDB_G0277589	gtaC	DDB0220470	putative GATA-binding transcription factor GATA zinc finger domain-containing protein 3	-0.7196232
DDB_G0279159	aco1	DDB0229908	putative iron regulatory protein, aconitate hydratase, aconitase	-0.7266059
DDB_G0292754	DDB_G0292754	DDB0184545		-0.7304029
DDB_G0292552	dscE	DDB0215382		-0.7405732
DDB_G0276965	glTA	DDB0214944	citrate synthase	-0.7433903
DDB_G0290073	DDB_G0290073	DDB0188711		-0.7449488
DDB_G0270994	psaA	DDB0231238	puromycin-sensitive aminopeptidase-like protein metalloproteinase	-0.7482988
DDB_G0272566	psmD14	DDB0191298	26S proteasome non-ATPase regulatory subunit 14, putative multidrug resistance protein	-0.7503709
DDB_G0285899	DDB_G0285899	DDB0232139	alanine transaminase alanine aminotransferase glutamate pyruvate transaminase	-0.7528904
DDB_G0290405	tpsC	DDB0231988	glycosyltransferase, alpha,alpha-trehalose-phosphate synthase, rehalose 6-phosphate synthase, trehalose-phosphatase	-0.7699584
DDB_G0275441	gtpA	DDB0191350	GTP-binding protein, HSR1-related domain-containing protein	-0.7735737
DDB_G0271086	DDB_G0271086	DDB0216772		-0.7837746
DDB_G0277001	cpIC	DDB0252666	cystatin A3 putative cysteine protease inhibitor	-0.78414
DDB_G0267446	cnbA	DDB0191204, DDB0231422	protein phosphatase 2B, protein serine/threonine phosphatase, CaM-dependent protein phosphatase, regulatory subunit, calcineurin B	-0.7879655
DDB_G0272666	-	DDB0168867	putative ankyrin repeat protein	-0.7933328
DDB_G0282819	sgIA	DDB0214888	sphingosine-1-phosphate lyase S1P lyase	-0.7946592
DDB_G0276205	DDB_G0276205	DDB0203511		-0.7993476
DDB_G0270990	DDB_G0270990	DDB0234155	putative acyl-CoA oxidase	-0.7998533
DDB_G0277675	DDB_G0277675	DDB0233770	RasGTPase-activating protein	-0.8073312
DDB_G0284353	osbl	DDB0237802	oxysterol binding family protein, member 9	-0.8166823
DDB_G0280135	DDB_G0280135	DDB0231749	methionine adenosyltransferase regulatory beta subunit	-0.818261
DDB_G0283483	srfD	DDB0220493	putative MADS-box transcription factor	-0.8231618
DDB_G0273979	psmD8-2	DDB0266350	26S proteasome regulatory subunit S14, 26S proteasome non-ATPase regulatory subunit 8	-0.8251649
DDB_G0285989	DDB_G0285989	DDB0218772		-0.8285445
DDB_G0289145	pde7	DDB0238626	cAMP phosphodiesterase cGMP phosphodiesterase	-0.8341998
DDB_G0290883	DDB_G0290883	DDB0238325	RING zinc finger-containing protein TRAF-type zinc finger-containing protein meprin and TRAF homology (MATH) domain-containing protein	-0.8386995
DDB_G0274273	DDB_G0274273	DDB0167842		-0.8563842
DDB_G0283261	acoA	DDB0191408	acyl-CoA oxidase	-0.8571647
DDB_G0292668	DDB_G0292668	DDB0184513		-0.8617781
DDB_G0277083	DDB_G0277083	DDB0302576	N-terminal delta endotoxin domain-containing protein	-0.8621387
DDB_G0286353	erka	DDB0201635	extracellular signal-regulated protein kinase protein serine/threonine kinase MAP kinase MAPK family protein kinase ERK subfamily protein kinase mitogen-activated protein kinase	-0.864247
DDB_G0272969	psmB1	DDB0232957	proteasome subunit beta type 1, 20S proteasome subunit beta-1	-0.8751341
DDB_G0292136	hatC	DDB0232313	actin binding protein hisactophilin III	-0.8753327
DDB_G0270836	fbp	DDB0216231	D-fructose-1,6-bisphosphate 1-phosphohydrolase fructose-1,6-bisphosphatase	-0.895145
DDB_G0293166	DDB_G0293166	DDB0219817		-0.9054417
DDB_G0274607	gefM	DDB0191326	Ras guanine nucleotide exchange factor	-0.906573
DDB_G0272208	idhC	DDB0231401	isocitrate dehydrogenase (NADP+) isocitrate dehydrogenase (NADP+), cytosolic	-0.9084229
DDB_G0278581	psiF	DDB0215398	PA14 domain-containing protein, discoidin-inducing complex (DIC) protein	-0.9156646
DDB_G0272210	idhM	DDB0231402	isocitrate dehydrogenase (NADP+) isocitrate dehydrogenase (NADP+), mitochondrial	-0.9380368
DDB_G0274025	DDB_G0274025	DDB0238175		-0.9560863
DDB_G0291081	pefA	DDB0191092	penta EF hand calcium binding protein	-0.9680113
DDB_G0284357	DDB_G0284357	DDB0238182		-0.9979598
DDB_G0295801		DDB0252620	B lectin domain-containing protein	-1.004698
DDB_G0280171	psiP	DDB0232405	PA14 domain-containing protein	-1.0205791
DDB_G0289145	pde7	DDB0238626	cAMP phosphodiesterase, cGMP phosphodiesterase	-1.030317
DDB_G0292790	CYP508D1	DDB0232976	cytochrome P450 family protein	-1.0349713

DDB_G0274085	DDB_G0272628	DDB0238196	zinc-containing alcohol dehydrogenase (ADH)	-1.0363343
DDB_G0278787	DDB_G0278787	DDB0206191		-1.0365695
DDB_G0293066	DDB_G0293066	DDB0191758		-1.0396728
DDB_G0280575	DDB_G0280575	DDB0206051		-1.0511661
DDB_G0283847	DDB_G0283847	DDB0238256	cyclopropane fatty acid synthase cyclopropane-fatty-acyl-phospholipid synthase	-1.0600885
DDB_G0267930	DDB_G0267930	DDB0238238		-1.0747543
DDB_G0277569		DDB0252835	GNS1/SUR4 family protein	-1.0803989
DDB_G0289551	DDB_G0289551	DDB0219450		-1.0926258
DDB_G0272738	iunH	DDB0231227	N-D-ribosylpurine ribohydrolase, inosine-uridine nucleoside N-ribohydrolase	-1.0938916
DDB_G0274369	DDB_G0274369	DDB0167931		-1.1013836
DDB_G0290177	DDB_G0290177	DDB0238177	putative transmembrane protein	-1.1173406
DDB_G0269160	nxA	DDB0191502, DDB0232009	annexin VII	-1.1187316
DDB_G0272831	psmA7	DDB0185059	proteasome subunit alpha type 7 20S proteasome subunit alpha-7	-1.1452071
DDB_G0286963	DDB_G0286963	DDB0215712		-1.1467406
DDB_G0273641	fnkD-2	DDB0304863	FNIP repeat-containing protein protein kinase, STE group FNIPK subfamily protein kinase	-1.1472071
DDB_G0275559	DDB_G0275559	DDB0238156	short-chain dehydrogenase/reductase (SDR) family protein, glucose/ribitol dehydrogenase family protein	-1.1878153
DDB_G0274051	cpnB-2	DDB0238176	phospholipid-binding protein copine B	-1.1910011
DDB_G0282993	sodC	DDB0232186	superoxide dismutase	-1.1975426
DDB_G0291029	DDB_G0291029	DDB0230064	sulfate adenylyltransferase adenylylsulfate kinase	-1.2631565
DDB_G0277863	pdiA	DDB0214948	cAMP phosphodiesterase inhibitor, phosphodiesterase inhibitor	-1.272552
DDB_G0270826	abcG22	DDB0214899	ABC transporter G family protein	-1.3340623
DDB_G0277697	DDB_G0277697	DDB0304392		-1.3876734
DDB_G0272396	DDB_G0272396	DDB0235352	putative transmembrane protein	-1.4668139
DDB_G0285995	pdsA	DDB0219974	cAMP phosphodiesterase cGMP phosphodiesterase	-1.4736577
DDB_G0291710	roco10	DDB0201665	Kelch repeat-containing protein, RGS domain-containing protein, eucine-rich repeat-containing protein (LRR) RhoGAP domain-containing protein protein kinase, TKL group tyrosine kinase-like protein ROCO family protein kinase	-1.4767169
DDB_G0275551	DDB_G0275551	DDB0167353		-1.5359432
DDB_G0268090	DDB_G0268090	DDB0238183	glycoside hydrolase family 18 protein	-1.5658384
DDB_G0273919	dscA-2	DDB0266623	discoidin I, A chain discoidin I, alpha chain	-1.6539738
DDB_G0281113	DDB_G0281113	DDB0238194		-1.6824252
DDB_G0273887	dscD-2	DDB0266625	discoidin I, D chain	-1.6941822
DDB_G0278577	DDB_G0278577	DDB0205548		-1.7087304
DDB_G0282121	DDB_G0282121	DDB0238184		-1.7366221
DDB_G0278313	DDB_G0278313	DDB0238239	pectin lyase-like family protein polymorphic membrane protein repeat-containing protein	-1.7382121
DDB_G0273887	dscD-2	DDB0266625	discoidin I, D chain	-1.7956611
DDB_G0274045	3B-2	DDB0238744	prespore-specific protein	-1.8794726
DDB_G0270726	DDB_G0270726	DDB0238162	pyridoxal phosphate-dependent decarboxylase family protein	-2.0785263
DDB_G0279815	DDB_G0279815	DDB0238808	putative transmembrane protein	-2.0835617
DDB_G0283885	DDB_G0283885	DDB0231670		-2.1064092
DDB_G0268600	DDB_G0268600	DDB0233913		-2.1146566
DDB_G0290885	DDB_G0290885	DDB0238168		-3.6581148
DDB_G0282749	bzpG	DDB0216335	putative basic-leucine zipper (bZIP) transcription factor	-3.8507577

Table A.1. Genes with altered expression in gskA null cell line

This list of genes was provided in a personal communication with Gareth Bloomfield and was described by Stremecki et al [169]

GO term analysis

The Gene Ontology project provides a categorization system that separates genes into three categories based on molecular functions, biological processes and cellular localization, each with several subcategories. By collating the available gene ontology (GO) terms for genes whose expression is altered by loss of GskA it was possible to assess whether these genes shared a common function. Of the original 193 genes, GO terms relating to biological processes were available for 129 genes. These GO terms were used to cluster genes together under higher-level GO parents terms (often referred to as GOslim terms). This clustering revealed that the genes affected by loss of GskA were associated with a wide range of biological processes, with the largest proportion of these involved in metabolic processes.

In order to determine if specific GO terms were enriched within the dataset the program 'Generic Gene Ontology (GO) Term Finder' was used to compare the number of genes in a given category with the number of genes that might appear in the same category if genes were selected at random from the genome. This analysis was performed separately on those genes that are over- or under-expressed and revealed that several GO terms were over-represented in each group. A higher than average number of genes that are under-expressed in *gskA* null cells were associated with catabolic and proteolytic processes (Table 4.1). While a significant number of genes that were over-expressed are associated with processing of ATP, and biosynthetic and metabolic pathways linked to ribonucleotides

Over represented GO terms among those genes that were over-expressed in the *gskA* null cell line

Gene ontology term	Cluster frequency	Genome frequency	Corrected P-value	Genes annotated to the term
cation transport	9 of 81 genes, 11.1%	106 of 12098 genes, 0.9%	7.93E-06	DDB0185207, DDB0234266, DDB0185017, DDB0185071, DDB0235141, DDB0238154, DDB0185070, DDB0232108, DDB0214945
energy coupled proton transport, down electrochemical gradient	5 of 81 genes, 6.2%	18 of 12098 genes, 0.1%	2.26E-05	DDB0185207, DDB0185070, DDB0234266, DDB0185071, DDB0235141
ATP synthesis coupled proton transport	5 of 81 genes, 6.2%	18 of 12098 genes, 0.1%	2.26E-05	DDB0185207, DDB0185070, DDB0234266, DDB0185071, DDB0235141
ion transmembrane transport	5 of 81 genes, 6.2%	18 of 12098 genes, 0.1%	2.26E-05	DDB0185207, DDB0185070, DDB0234266, DDB0185071, DDB0235141
ATP biosynthetic process	5 of 81 genes, 6.2%	19 of 12098 genes, 0.2%	3.05E-05	DDB0185207, DDB0185070, DDB0234266, DDB0185071, DDB0235141
ATP metabolic process	5 of 81 genes, 6.2%	20 of 12098 genes, 0.2%	4.04E-05	DDB0185207, DDB0185070, DDB0234266, DDB0185071, DDB0235141
ion transport	9 of 81 genes, 11.1%	138 of 12098 genes, 1.1%	7.79E-05	DDB0185207, DDB0234266, DDB0185017, DDB0185071, DDB0235141, DDB0238154, DDB0185070, DDB0232108, DDB0214945
purine ribonucleoside triphosphate biosynthetic process	5 of 81 genes, 6.2%	24 of 12098 genes, 0.2%	0.0001	DDB0185207, DDB0185070, DDB0234266, DDB0185071, DDB0235141
monovalent inorganic cation transport	6 of 81 genes, 7.4%	46 of 12098 genes, 0.4%	0.00013	DDB0185207, DDB0238154, DDB0185070, DDB0234266, DDB0185071, DDB0235141
purine nucleoside triphosphate biosynthetic process	5 of 81 genes, 6.2%	25 of 12098 genes, 0.2%	0.00013	DDB0185207, DDB0185070, DDB0234266, DDB0185071, DDB0235141
ribonucleoside triphosphate biosynthetic process	5 of 81 genes, 6.2%	25 of 12098 genes, 0.2%	0.00013	DDB0185207, DDB0185070, DDB0234266, DDB0185071, DDB0235141
purine ribonucleoside triphosphate metabolic process	5 of 81 genes, 6.2%	25 of 12098 genes, 0.2%	0.00013	DDB0185207, DDB0185070, DDB0234266, DDB0185071, DDB0235141
hydrogen transport	5 of 81 genes, 6.2%	26 of 12098 genes, 0.2%	0.00016	DDB0185207, DDB0185070, DDB0234266, DDB0185071, DDB0235141
purine nucleoside triphosphate metabolic process	5 of 81 genes, 6.2%	26 of 12098 genes, 0.2%	0.00016	DDB0185207, DDB0185070, DDB0234266, DDB0185071, DDB0235141
ribonucleoside triphosphate metabolic process	5 of 81 genes, 6.2%	26 of 12098 genes, 0.2%	0.00016	DDB0185207, DDB0185070, DDB0234266, DDB0185071, DDB0235141
proton transport	5 of 81 genes, 6.2%	26 of 12098 genes, 0.2%	0.00016	DDB0185207, DDB0185070, DDB0234266, DDB0185071, DDB0235141
nucleoside triphosphate biosynthetic process	5 of 81 genes, 6.2%	29 of 12098 genes, 0.2%	0.00029	DDB0185207, DDB0185070, DDB0234266, DDB0185071, DDB0235141
purine nucleoside biosynthetic process	5 of 81 genes, 6.2%	31 of 12098 genes, 0.3%	0.00041	DDB0185207, DDB0185070, DDB0234266, DDB0185071, DDB0235141
purine ribonucleoside biosynthetic process	5 of 81 genes, 6.2%	31 of 12098 genes, 0.3%	0.00041	DDB0185207, DDB0185070, DDB0234266, DDB0185071, DDB0235141
nucleoside triphosphate metabolic process	5 of 81 genes, 6.2%	32 of 12098 genes, 0.2%	0.00049	DDB0185207, DDB0185070, DDB0234266, DDB0185071, DDB0235141
oxidative phosphorylation	5 of 81 genes, 6.2%	33 of 12098 genes, 0.3%	0.00057	DDB0185207, DDB0185070, DDB0234266, DDB0185071, DDB0235141
nucleoside biosynthetic process	5 of 81 genes, 6.2%	33 of 12098 genes, 0.3%	0.00057	DDB0185207, DDB0185070, DDB0234266, DDB0185071, DDB0235141
ribonucleoside biosynthetic process	5 of 81 genes, 6.2%	33 of 12098 genes, 0.3%	0.00057	DDB0185207, DDB0185070, DDB0234266, DDB0185071, DDB0235141
purine ribonucleotide biosynthetic process	5 of 81 genes, 6.2%	38 of 12098 genes, 0.3%	0.00119	DDB0185207, DDB0185070, DDB0234266, DDB0185071, DDB0235141
purine ribonucleotide metabolic process	5 of 81 genes, 6.2%	40 of 12098 genes, 0.3%	0.00154	DDB0185207, DDB0185070, DDB0234266, DDB0185071, DDB0235141
ribonucleotide biosynthetic process	5 of 81 genes, 6.2%	40 of 12098 genes, 0.3%	0.00154	DDB0185207, DDB0185070, DDB0234266, DDB0185071, DDB0235141

Gene ontology term	Cluster frequency	Genome frequency	Corrected P-value	Genes annotated to the term
ribonucleotide metabolic process	5 of 81 genes, 6.2%	42 of 12098 genes, 0.3%	0.00197	DDB0185207, DDB0185070, DDB0234266, DDB0185071, DDB0235141
transmembrane transport	5 of 81 genes,	42 of 12098 genes 0.3%	0.00197	DDB0185207, DDB0185070, DDB0234266, DDB0185071, DDB0235141
nucleobase, nucleoside and nucleotide biosynthetic process	5 of 81 genes, 6.2%	43 of 12098 genes, 0.4%	0.00222	DDB0185207, DDB0185070, DDB0234266, DDB0185071, DDB0235141
nucleobase, nucleoside, nucleotide and nucleic acid biosynthetic process	5 of 81 genes, 6.2%	43 of 12098 genes, 0.4%	0.00222	DDB0185207, DDB0185070, DDB0234266, DDB0185071, DDB0235141
purine ribonucleoside metabolic process	5 of 81 genes,	44 of 12098 genes, .4%	0.0025	DDB0185207, DDB0185070, DDB0234266, DDB0185071, DDB0235141
localization	17 of 81 genes, 21.0%	774 of 12098 genes, 6.4%	0.00268	DDB0201662, DDB0185088, DDB0185017, DDB0235141, DDB0219941, DDB0205768, DDB0230087, DDB0234198, DDB0191173, DDB0238154, DDB0232108, DDB0201670, DDB0214945, DDB0185207, DDB0234266, DDB0185071, DDB0185070
purine nucleoside metabolic process	5 of 81 genes, 6.2%	45 of 12098 genes, 0.4%	0.00279	DDB0185207, DDB0185070, DDB0234266, DDB0185071, DDB0235141
ribonucleoside metabolic process	5 of 81 genes,	48 of 12098 genes, 0.4%	0.00386	DDB0185207, DDB0185070, DDB0234266, DDB0185071, DDB0235141
generation of precursor metabolites and energy	6 of 81 genes,	82 of 12098 genes, 0.7%	0.00414	DDB0185207, DDB0185070, DDB0234266, DDB0185071, DDB0235141, DDB0191397
nitrogen compound biosynthetic process	6 of 81 genes, 7.4%	91 of 12098 genes, 0.8%	0.00753	DDB0237754, DDB0185207, DDB0185070, DDB0234266, DDB0185071, DDB0235141
nucleoside metabolic process	5 of 81 genes, 6.2%	58 of 12098 genes, 0.5%	0.0098	DDB0185207, DDB0185070, DDB0234266, DDB0185071, DDB0235141

Table A.2. GO term enrichment within genes that are over-expressed in *gskA* null cell line

Data correct - Wed Sep 2 05:21:06 EDT 2009, P-value cutoff = 0.01, Annotation file = gene_association.ddb, Evidence codes used - IEA (14589), IEP (80), IGI (103), NAS (16), IPI (201) ND (4191), IC (212), ISS (8901), IDA (1435), IMP (978), TAS (485)

Over represented GO terms among those genes that were under-expressed in the *gskA* null cell line

Gene ontology term	Cluster frequency	Genome frequency	Corrected P-value	Genes annotated to the term
cellular catabolic process	14 of 113 genes, 12.4%	218 of 12098 genes, 1.8%	2.92E-06	DDB0185059, DDB0230205, DDB0219974, DDB0232933, DDB0232957, DDB0191408, DDB0238626, DDB0231227, DDB0191298, DDB0214953, DDB0214888, DDB0214944, DDB0232930, DDB0237695
catabolic process	16 of 113 genes, 14.2%	424 of 12098 genes, 3.5%	0.00039	DDB0185059, DDB0230205, DDB0219974, DDB0232933, DDB0232957, DDB0231425, DDB0191408, DDB0238626, DDB0231227, DDB0191298, DDB0214953, DDB0214888, DDB0231238, DDB0214944, DDB0232930, DDB0237695
ubiquitin-dependent protein catabolic process	7 of 113 genes, 6.2%	72 of 12098 genes, 0.6%	0.00094	DDB0185059, DDB0232933, DDB0232930, DDB0232957, DDB0237695, DDB0191298, DDB0214953
modification-dependent protein catabolic process	7 of 113 genes, 6.2%	72 of 12098 genes, 0.6%	0.00094	DDB0185059, DDB0232933, DDB0232930, DDB0232957, DDB0237695, DDB0191298, DDB0214953
modification-dependent macromolecule catabolic process	7 of 113 genes, 6.2%	72 of 12098 genes, 0.6%	0.00094	DDB0185059, DDB0232933, DDB0232930, DDB0232957, DDB0237695, DDB0191298, DDB0214953
cellular protein catabolic process	7 of 113 genes, 6.2%	72 of 12098 genes, 0.6%	0.00094	DDB0185059, DDB0232933, DDB0232930, DDB0232957, DDB0237695, DDB0191298, DDB0214953
proteolysis involved in cellular protein catabolic process	7 of 113 genes, 6.2%	72 of 12098 genes, 0.6%	0.00094	DDB0185059, DDB0232933, DDB0232930, DDB0232957, DDB0237695, DDB0191298, DDB0214953
carbohydrate biosynthetic process	5 of 113 genes, 4.4%	31 of 12098 genes, 0.3%	0.00186	DDB0231676, DDB0231425, DDB0216231, DDB0231749, DDB0231988
cellular biopolymer catabolic process	7 of 113 genes, 6.2%	98 of 12098 genes, 0.8%	0.00724	DDB0185059, DDB0232933, DDB0232930, DDB0232957, DDB0237695, DDB0191298, DDB0214953
cellular macromolecule catabolic process	7 of 113 genes, 6.2%	98 of 12098 genes, 0.8%	0.00724	DDB0185059, DDB0232933, DDB0232930, DDB0232957, DDB0237695, DDB0191298, DDB0214953

Table A.3. GO term enrichment within genes that are under-expressed in *gskA* null cell line

Data correct - Wed Sep 2 05:21:06 EDT 2009, P-value cutoff = 0.01, Annotation file = gene_association.ddb, Evidence codes used - IEA (14589), IEP (80), IGI (103), NAS (16), IPI (201) ND (4191), IC (212), ISS (8901), IDA (1435), IMP (978), TAS (485)

Proteins identified through SILAC analysis

Protein name (as it appears in STRING)	Protein Description	Ratio H/L
ACLY	ATP-citrate synthase	0.73801
ACP1	Adipocyte acid phosphatase	0.54539
ACTC1	Actin, alpha cardiac muscle 1	0.54352
ACTG1	Actin, cytoplasmic 2;Gamma-actin	0.21454
ACTN4	Alpha-actinin-4	0.6217
AHCY	Adenosylhomocysteinase	0.42499
ALDOA	Fructose-bisphosphate aldolase A	0.21821
AMFR	Autocrine motility factor receptor	0.043116
ANXA2	Annexin A2	0.73658
ARF3	ADP-ribosylation factor 3	0.76676
AS160	Akt substrate of 160 kDa	0.61729
ATP5A	ATP synthase subunit alpha, mitochondrial	0.74519
ATP5B	ATP synthase subunit beta, mitochondrial	0.81403
AUF1	AU-rich element RNA-binding protein 1	0.85161
BAT1	DEAD box protein UAP56;ATP-dependent RNA helicase DDX39	0.68774
C1QBP	Complement component 1 Q subcomponent-binding protein, mitochondrial	0.69795
CAD	Glutamine-dependent carbamoyl-phosphate synthase	0.22187
CALM3	calmodulin 3	0.59895
CAND1	Cullin-associated and neddylation-dissociated protein 1	0.71704
CANX	Calnexin	0.44125
CAPRIN1	Cytoplasmic activation- and proliferation-associated protein 1	0.97348
CAPZA1	F-actin-capping protein subunit alpha-1	0.19074
CCT1	T-complex protein 1 subunit alpha;CCT-alpha	0.52134
CCT2	T-complex protein 1 subunit beta;CCT-beta	0.53048
CCT3	T-complex protein 1 subunit gamma;CCT-gamma	0.58434
CCT4	T-complex protein 1, delta subunit;CCT-delta	0.51643
CCT6A	T-complex protein 1 subunit epsilon;CCT-epsilon	0.6126
CCT6A	T-complex protein 1 subunit zeta;CCT-zeta;CCT-zeta-1	0.60714
CCT7	T-complex protein 1 subunit eta;CCT-eta	0.56339
CCT8	T-complex protein 1 subunit theta;CCT-theta	0.58345
CFL1	Cofilin-1	0.61873
CIP29	Cytokine induced protein 29 kDa	0.0088642
CKB	Creatine kinase B-type	0.41252
CLTC	Clathrin heavy chain 1	0.35168
COPG	Coatomer subunit gamma;Gamma-coat protein;Coatomer subunit gamma-2;Gamma-2-coat protein	0.81723
CRKL	Crk-like protein	0.52143
CSDA	Cold shock domain-containing protein A	0.64898
CSE1L	Chromosome segregation 1-like protein	0.52743
CSNK2A1	casein kinase 2, alpha 1 polypeptide	0.01516
CSRP2	Cysteine and glycine-rich protein 2	1.5081
CSTB	Cystatin-B;Stefin-B	0.48429
CTPS	CTP synthase 1	0.53662
DDX21	Nucleolar RNA helicase 2;DEAD box protein 21	0.60226
DDX3X	ATP-dependent RNA helicase DDX3X	0.68483
DHX15	Putative pre-mRNA-splicing factor ATP-dependent RNA helicase DHX15	0.86643
DHX35	DEAH (Asp-Glu-Ala-His) box polypeptide 35	1.0682
DHX9	ATP-dependent RNA helicase A;DEAH box protein 9	0.46934
DUT	Deoxyuridine 5'-triphosphate nucleotidohydrolase, mitochondrial	0.28338
EIF3C	Eukaryotic translation initiation factor 3 subunit C	0.68907
EEF1D	Eukaryotic translation elongation factor 1 delta	0.88675

Protein name (as it appears in STRING)	Protein Description	Ratio H/L
EEF1E1	Eukaryotic translation elongation factor 1 epsilon-1	0.75524
EEF1E1	Elongation factor 1-alpha 1	0.69808
EEF2	Elongation factor 2	0.48854
EEF1B2	Elongation factor 1-beta	0.71659
EIF3B	Eukaryotic translation initiation factor 3 subunit B	0.60356
EIF4A2	Eukaryotic initiation factor 4A-I	0.74322
EIF5A	Eukaryotic translation initiation factor 5A-1	0.35785
ENO-1	Alpha-enolase	0.61107
EPB4IL3	Band 4.1-like protein 3;4.1B;Differentially expressed in adenocarcinoma of the lung protein 1	0.76346
ERCC2	Telophase disk protein of 60 kDa	0.5877
FARSA	Phenylalanyl-tRNA synthetase alpha chain	0.17023
FARSB	Phenylalanyl-tRNA synthetase beta chain	0.3288
FASN	Fatty acid synthase	0.28853
FILIP1L	Filamin-A	0.79965
FKBP4	FK506-binding protein 4	0.52078
G3BP1	Ras GTPase-activating protein-binding protein 1	0.37438
GANAB	Neutral alpha-glucosidase AB;Glucosidase II subunit alpha;Alpha-glucosidase 2	0.67015
GAPDH	Glyceraldehyde-3-phosphate dehydrogenase	0.9251
GART	Trifunctional purine biosynthetic protein adenosine-3	0.31783
GDI2	Rab GDP dissociation inhibitor beta	0.047982
GLO1	Lactoylglutathione lyase	0.52807
GNB2L1	Guanine nucleotide binding protein (G protein), beta polypeptide 2-like 1 variant	0.033608
GPI	Glucose-6-phosphate isomerase	0.52603
GSK3	Glycogen synthase kinase-3 beta	25.995
GSR	Glutathione reductase, mitochondrial	0.72979
H2AFX	H2A histone family, member V, isoform CRA_b	0.61038
H3F3A	Histone H3.3	0.51374
HAGH	Hydroxyacylglutathione hydrolase	0.28117
HDAC6	Histone deacetylase 6	0.21416
HIST1H1T	Histone H1t	0.65397
HIST1H2AD	Histone H2A type 2-B	0.44339
HIST1H2BN	Histone H2B type 1-N	0.23473
HIST1H4A	Histone H4	0.63483
HIST2H2BE	Histone H2B type 2-E	0.64501
HNRNPA1	Heterogeneous nuclear ribonucleoprotein A1	0.15382
HNRNPA2B1	Heterogeneous nuclear ribonucleoproteins A2/B1	0.23682
HNRNPC	Heterogeneous nuclear ribonucleoproteins C1/C2	0.55516
HNRNPF	Heterogeneous nuclear ribonucleoprotein F	0.18409
HNRNPK	Heterogeneous nuclear ribonucleoprotein K	0.63133
HNRNPM	Heterogeneous nuclear ribonucleoprotein M	0.66256
HNRNPU	Heterogeneous nuclear ribonucleoprotein U (Scaffold attachment factor A)	0.6413
HPRT1	Hypoxanthine-guanine phosphoribosyltransferase	0.7668
HSC70	Heat shock 70 kDa protein 8	0.61144
HSP90AA1	Heat shock protein HSP 90-alpha	0.70741
HSP90AB1	Heat shock protein HSP 90-beta	0.59347
HSP90B1	Heat shock protein 90 kDa beta member 1	0.60293
HSPA1A	Heat shock 70 kDa protein 1	0.57409
HSPA1A	cDNA FLJ54303, highly similar to Heat shock 70 kDa protein 1	0.31541
HSPA4	Heat shock 70 kDa protein 4	0.34611

Protein name (as it appears in STRING)	Protein Description	Ratio H/L
HSPA5	Heat shock 70 kDa protein 5	0.65864
HSPA9	Heat shock 70 kDa protein 9	0.26788
HSPD1	Heat shock protein 60;60 kDa chaperonin	0.676
HSPH1	Heat shock protein 105 kDa	0.77219
ILF2	Interleukin enhancer-binding factor 2	0.48291
IPO5	Importin-5	0.70671
ISYNA1	Inositol-3-phosphate synthase	0.64132
Kappa-actin	Beta-actin-like protein 2;Kappa-actin	0.24193
KIF14	Kinesin-like protein KIF14	0.27686
KPNB1	Importin subunit beta-1	0.94971
KT3K	Ketosamine-3-kinase	0.55895
LDHA	L-lactate dehydrogenase A chain	0.9493
LDHAL6B	L-lactate dehydrogenase A-like 6B	1.1147
LDHB	L-lactate dehydrogenase B chain	0.93528
LRPPRC	Leucine-rich PPR motif-containing protein, mitochondrial	0.56144
MARS	Methionyl-tRNA synthetase	1.0793
MATR3	Uncharacterized protein MATR3;Matrin-3	0.46621
MCM6	DNA replication licensing factor MCM6	0.42334
MIF	Macrophage migration inhibitory factor;Phenylpyruvate tautomerase;Glycosylation-inhibiting factor	0.048729
MTHFD1	Methylenetetrahydrofolate dehydrogenase	0.94856
MYH10	Myosin heavy chain 10	1.1585
MYH9	Myosin heavy chain 9	0.83271
NACAP1	Nascent polypeptide-associated complex subunit alpha	0.75588
NAP1L1	Nucleosome assembly protein 1-like 1	0.65963
NCL	Nucleolin	0.70134
NME1	Nucleoside diphosphate kinase 1	0.93289
NME2	Nucleoside diphosphate kinase 2	0.73345
NPM1	Nucleophosmin	0.53953
NSUN2	tRNA (cytosine-5-)-methyltransferase NSUN2	0.24496
NUP155	Nuclear pore complex protein Nup155	0.81936
NVL	Transitional endoplasmic reticulum ATPase	0.55248
OK/SW-cl.83	40S ribosomal protein S8;Ribosomal protein S8	0.4429
OPA1	Optic atrophy protein 1;Dynamin-like 120 kDa protein	0.38274
P4HB	Prolyl 4-hydroxylase subunit beta	0.64163
PABPC3	Polyadenylate-binding protein 3	0.40946
PAICS	Phosphoribosylaminoimidazole-succinocarboxamide synthase	0.81882
PARK7	Protein DJ-1;Oncogene DJ1;Parkinson disease protein 7	0.65927
PARP1	Poly [ADP-ribose] polymerase 1	0.78862
PCBP1	Poly(rC)-binding protein 1	0.44872
PCBP2	Poly(RC)-binding protein 2 isoform b variant	0.54493
PDCD6	Programmed cell death protein 6	0.24363
PDIA3	Protein disulfide-isomerase A3	0.51916
PEF1	Peflin	0.95303
PFN1	Profilin-1	0.75672
PGAM1	Phosphoglycerate mutase 1	0.58304
PGD	6-phosphogluconate dehydrogenase	0.63076
PGK1	Phosphoglycerate kinase 1	0.63919
PHB2	Prohibitin-2	0.13511
PHGDH	D-3-phosphoglycerate dehydrogenase	1.015
PKM2	Pyruvate kinase isozymes M1/M2	0.4234
PPA1	Pyrophosphate phospho-hydrolase	0.89308

Protein name (as it appears in STRING)	Protein Description	Ratio H/L
PPIA	Peptidyl-prolyl cis-trans isomerase A	0.70144
PPMIG	Protein phosphatase 1G	0.83175
PPP1CC	Serine/threonine-protein phosphatase PP1-gamma catalytic subunit	0.46046
PPP2R1B	Serine/threonine-protein phosphatase 2A 65 kDa regulatory subunit R1-alpha isoform	0.5077
PRDX1	Peroxiredoxin-1	0.5317
PRDX2	Peroxiredoxin-2	0.65441
PRDX3	Thioredoxin-dependent peroxide reductase, mitochondrial	0.68279
PRDX6	Peroxiredoxin-6	0.8494
PRKDC	DNA-dependent protein kinase catalytic subunit	0.55606
PSMD1	26S proteasome non-ATPase regulatory subunit 1;	0.22629
PSME1	Proteasome activator complex subunit 1	0.92353
PTBP1	Polypyrimidine tract binding protein 1	0.47554
PTGES3	Prostaglandin E synthase 3	1.0244
PTMA	Prothymosin alpha;Thymosin alpha-1	0.73361
RAN	GTP-binding nuclear protein Ran	0.68553
RANBP1	Ran-specific GTPase-activating protein	0.76612
RARS	Arginyl-tRNA synthetase, cytoplasmic;Arginine--tRNA ligase	0.486
RPL11	60S ribosomal protein L11	0.60004
RPL12	60S ribosomal protein L12	0.64147
RPL17	60S ribosomal protein L23	0.68597
RPL18A	60S ribosomal protein L18a	1.1532
RPL22	60S ribosomal protein L22	0.97536
RPL23	60S ribosomal protein L23	0.66184
RPL23A	60S ribosomal protein L23a	0.5221
RPL24	60S ribosomal protein L24	0.81511
RPL27	60S ribosomal protein L27	0.50588
RPL3	60S ribosomal protein L3	0.64188
RPL31	60S ribosomal protein L31	0.66162
RPL35A	60S ribosomal protein L35a	0.76785
RPL7	60S ribosomal protein L7	0.55557
RPL9	60S ribosomal protein L9	0.81153
RPLP0	60S acidic ribosomal protein P0	0.79259
RPLP1	60S acidic ribosomal protein P1	0.5683
RPLP2	60S acidic ribosomal protein P2	0.66183
RPS10	40S ribosomal protein S10	0.15308
RPS12	40S ribosomal protein S12	0.69208
RPS13	40S ribosomal protein S13	0.49199
RPS15A	40S ribosomal protein S15a	0.16665
RPS16	40S ribosomal protein S16	0.34846
RPS17	40S ribosomal protein S17	0.76157
RPS18	40S ribosomal protein S18	0.70896
RPS19	40S ribosomal protein S19	0.30303
RPS20	40S ribosomal protein S20	0.6198
RPS2	40S ribosomal protein S2	0.57133
RPS23	40S ribosomal protein S23	0.78789
RPS24	40S ribosomal protein S24	0.94976
RPS25	40S ribosomal protein S25	0.84012
RPS26	40S ribosomal protein S26	0.63172
RPS3	40S ribosomal protein S3	0.45991
RPS3A	40S ribosomal protein S3a	0.31959
RPS4X	40S ribosomal protein S4, X isoform	0.76665

Protein name (as it appears in STRING)	Protein Description	Ratio H/L
RPS5	40S ribosomal protein S5	0.62628
RPS7	40S ribosomal protein S7	0.52349
RPSA	40S ribosomal protein SA	0.56191
SERBP1	SERPINE1 mRNA-binding protein 1	0.62175
SET	Protein SET;Phosphatase 2A inhibitor I2PP2A	0.64799
SFRS3	Splicing factor, arginine/serine-rich 3	0.18829
SLC25A5	ADP/ATP translocase 2;Solute carrier family 25 member 5	1.1693
SLC25A6	ADP/ATP translocase 3;Solute carrier family 25 member 4	0.79247
SNRPD3	Small nuclear ribonucleoprotein Sm D3;snRNP core protein D3	0.75624
SOD1	Superoxide dismutase [Cu-Zn]	0.69676
SSB	Sjogren syndrome type B antigen	0.80989
SSBP1	Single-stranded DNA-binding protein, mitochondrial	0.29163
SSRP1	FACT complex subunit SSRP1;Structure-specific recognition protein 1	0.90595
ST13	Suppression of tumorigenicity protein 13	0.99195
STIP1	Stress-induced-phosphoprotein 1	0.72812
SUB1	Activated RNA polymerase II transcriptional coactivator p15	0.71629
SUMO3	Small ubiquitin-related modifier 3	0.68981
SUPT16	FACT complex subunit SPT16	1.1213
SYNCRIP	Synaptotagmin-binding, cytoplasmic RNA-interacting protein	0.71368
SYT7	cDNA FLJ53554	0.0062105
TAGLN2	Transgelin-2;SM22-alpha homolog	0.82943
TARS	Threonyl-tRNA synthetase	0.57749
TBA4B	Putative tubulin-like protein alpha-4B;Alpha-tubulin 4B	0.59098
TKT	Transketolase	0.59957
TKTL1	Transketolase-like protein 1	0.061555
TNPO2	Transportin-2	1.0902
TPI1	Triosephosphate isomerase	0.96401
TRAP1	Heat shock protein 75 kDa, mitochondrial	0.019344
TRIM28	Transcription intermediary factor 1-beta	0.46712
TUBA4A	Tubulin alpha-1B chain	0.45655
TUBB	Tubulin beta chain	0.28665
TUBB2A	Tubulin beta-2A chain;Tubulin beta-2B chain	0.85237
TUBB2C	Tubulin beta-2C chain	0.45531
TUBB4Q	Tubulin beta-4 chain	0.47874
TXN	Thioredoxin	0.83698
UBA1	Ubiquitin-like modifier-activating enzyme 1	0.64777
UBA52	Ubiquitin B	0.56589
UBE2E2	Ubiquitin-conjugating enzyme E2 N	0.53301
UBE2L3	Ubiquitin-conjugating enzyme E2 L3	0.3325
VDAC3	Voltage-dependent anion-selective channel protein 3	0.76323
VIM	Vimentin	0.96855
XPO1	Exportin-1	0.65204
XRCC5	ATP-dependent DNA helicase 2 subunit 2	0.56935
XRCC6	ATP-dependent DNA helicase 2 subunit 1	0.62447
YWHAE	14-3-3 protein epsilon	0.63467
YWHAQ	14-3-3 protein theta	0.58257
YWHAZ	14-3-3 protein zeta	0.72575

Bibliography

1. Li, Y., et al., *Interaction of glycogen synthase kinase 3beta with the DF3/MUC1 carcinoma-associated antigen and beta-catenin*. *Mol Cell Biol*, 1998. **18**(12): p. 7216-24.
2. Li, Y., et al., *The c-Src tyrosine kinase regulates signaling of the human DF3/MUC1 carcinoma-associated antigen with GSK3 beta and beta-catenin*. *J Biol Chem*, 2001. **276**(9): p. 6061-4.
3. Trinkle-Mulcahy, L., et al., *Identifying specific protein interaction partners using quantitative mass spectrometry and bead proteomes*. *J Cell Biol*, 2008. **183**(2): p. 223-39.
4. Ewing, R.M., et al., *Large-scale mapping of human protein-protein interactions by mass spectrometry*. *Mol Syst Biol*, 2007. **3**: p. 89.
5. Tanji, C., et al., *A-kinase anchoring protein AKAP220 binds to glycogen synthase kinase-3beta (GSK-3beta) and mediates protein kinase A-dependent inhibition of GSK-3beta*. *J Biol Chem*, 2002. **277**(40): p. 36955-61.
6. Embi, N., D.B. Rylatt, and P. Cohen, *Glycogen synthase kinase-3 from rabbit skeletal muscle. Separation from cyclic-AMP-dependent protein kinase and phosphorylase kinase*. *Eur J Biochem*, 1980. **107**(2): p. 519-27.
7. Rylatt, D.B., et al., *Glycogen synthase from rabbit skeletal muscle. Amino acid sequence at the sites phosphorylated by glycogen synthase kinase-3, and extension of the N-terminal sequence containing the site phosphorylated by phosphorylase kinase*. *Eur J Biochem*, 1980. **107**(2): p. 529-37.
8. Hong, Y.R., et al., *Cloning and characterization of a novel human ninein protein that interacts with the glycogen synthase kinase 3beta*. *Biochim Biophys Acta*, 2000. **1492**(2-3): p. 513-6.
9. Davies, G., W.G. Jiang, and M.D. Mason, *The interaction between beta-catenin, GSK3beta and APC after motogen induced cell-cell dissociation, and their involvement in signal transduction pathways in prostate cancer*. *Int J Oncol*, 2001. **18**(4): p. 843-7.
10. Wang, L., et al., *Suppression of androgen receptor-mediated transactivation and cell growth by the glycogen synthase kinase 3 beta in prostate cells*. *J Biol Chem*, 2004. **279**(31): p. 32444-52.
11. Nakamura, T., et al., *Axin, an inhibitor of the Wnt signalling pathway, interacts with beta-catenin, GSK-3beta and APC and reduces the beta-catenin level*. *Genes Cells*, 1998. **3**(6): p. 395-403.
12. Ali, A., K.P. Hoefflich, and J.R. Woodgett, *Glycogen synthase kinase-3: properties, functions, and regulation*. *Chem Rev*, 2001. **101**(8): p. 2527-40.
13. Andoh, T., Y. Hirata, and A. Kikuchi, *Yeast glycogen synthase kinase 3 is involved in protein degradation in cooperation with Bul1, Bul2, and Rsp5*. *Mol Cell Biol*, 2000. **20**(18): p. 6712-20.
14. Viatour, P., et al., *GSK3-mediated BCL-3 phosphorylation modulates its degradation and its oncogenicity*. *Mol Cell*, 2004. **16**(1): p. 35-45.
15. Li, S., et al., *A map of the interactome network of the metazoan C. elegans*. *Science*, 2004. **303**(5657): p. 540-3.
16. Yao, H.B., et al., *Expression of glycogen synthase kinase-3 isoforms in mouse tissues and their transcription in the brain*. *J Chem Neuroanat*, 2002. **23**(4): p. 291-7.

17. Espinosa, L., et al., *Phosphorylation by glycogen synthase kinase-3 beta down-regulates Notch activity, a link for Notch and Wnt pathways*. J Biol Chem, 2003. **278**(34): p. 32227-35.
18. Simonis, N., et al., *Empirically controlled mapping of the Caenorhabditis elegans protein-protein interactome network*. Nat Methods, 2009. **6**(1): p. 47-54.
19. Chou, H.Y., et al., *GSKIP Is Homologous to the Axin GSK3beta Interaction Domain and Functions as a Negative Regulator of GSK3beta*. Biochemistry, 2006. **45**(38): p. 11379-11389.
20. Giot, L., et al., *A protein interaction map of Drosophila melanogaster*. Science, 2003. **302**(5651): p. 1727-36.
21. Zhang, W., et al., *Hedgehog-regulated Costal2-kinase complexes control phosphorylation and proteolytic processing of Cubitus interruptus*. Dev Cell, 2005. **8**(2): p. 267-78.
22. Woodgett, J.R., *Molecular cloning and expression of glycogen synthase kinase-3/factor A*. Embo J, 1990. **9**(8): p. 2431-8.
23. Hoefflich, K.P., et al., *Requirement for glycogen synthase kinase-3[beta] in cell survival and*. 2000.
24. Huang, D., et al., *Focal adhesion kinase (FAK) regulates insulin-stimulated glycogen synthesis in hepatocytes*. J Biol Chem, 2002. **277**(20): p. 18151-60.
25. Bek, S. and R. Kemler, *Protein kinase CKII regulates the interaction of beta-catenin with alpha-catenin and its protein stability*. J Cell Sci, 2002. **115**(Pt 24): p. 4743-53.
26. Beg, A.A., et al., *Embryonic lethality and liver degeneration in mice lacking the RelA component of NF-kappa B*. Nature, 1995. **376**(6536): p. 167-70.
27. Li, Q., et al., *Severe liver degeneration in mice lacking the IkappaB kinase 2 gene*. Science, 1999. **284**(5412): p. 321-5.
28. Liu, K.J., et al., *Chemical rescue of cleft palate and midline defects in conditional GSK-3beta mice*. Nature, 2007.
29. MacAulay, K., et al., *Glycogen synthase kinase 3alpha-specific regulation of murine hepatic glycogen metabolism*. Cell Metab, 2007. **6**(4): p. 329-37.
30. Mukai, F., et al., *Alternative splicing isoform of tau protein kinase I/glycogen synthase kinase 3beta*. J Neurochem, 2002. **81**(5): p. 1073-83.
31. Wood-Kaczmar, A., et al., *An alternatively spliced form of glycogen synthase kinase-3beta is targeted to growing neurites and growth cones*. Mol Cell Neurosci, 2009.
32. Gupta, S., et al., *Selective interaction of JNK protein kinase isoforms with transcription factors*. Embo J, 1996. **15**(11): p. 2760-70.
33. Dai, F., et al., *Human serum and glucocorticoid-inducible kinase-like kinase (SGKL) phosphorylates glycogen synthase kinase 3 beta (GSK-3beta) at serine-9 through direct interaction*. Biochem Biophys Res Commun, 2002. **293**(4): p. 1191-6.
34. Mao, Y., et al., *Disrupted in schizophrenia 1 regulates neuronal progenitor proliferation via modulation of GSK3beta/beta-catenin signaling*. Cell, 2009. **136**(6): p. 1017-31.
35. Hong, Y.R., et al., *Human dynamin-like protein interacts with the glycogen synthase kinase 3beta*. Biochem Biophys Res Commun, 1998. **249**(3): p. 697-703.

36. Zhou, F., et al., *The association of GSK3 beta with E2F1 facilitates nerve growth factor-induced neural cell differentiation*. J Biol Chem, 2008. **283**(21): p. 14506-15.
37. English, J.M., et al., *Isolation of MEK5 and differential expression of alternatively spliced forms*. J Biol Chem, 1995. **270**(48): p. 28897-902.
38. Guo, X., et al., *Axin and GSK3- control Smad3 protein stability and modulate TGF- signaling*. Genes Dev, 2008. **22**(1): p. 106-20.
39. Hanks, S.K. and T. Hunter, *Protein kinases 6. The eukaryotic protein kinase superfamily: kinase (catalytic) domain structure and classification*. Faseb J, 1995. **9**(8): p. 576-96.
40. Freemantle, S.J., et al., *Characterization and tissue-specific expression of human GSK-3-binding proteins FRAT1 and FRAT2*. Gene, 2002. **291**(1-2): p. 17-27.
41. Bax, B., et al., *The structure of phosphorylated GSK-3beta complexed with a peptide, FRATtide, that inhibits beta-catenin phosphorylation*. Structure, 2001. **9**(12): p. 1143-52.
42. Schaffer, B., M. Wiedau-Pazos, and D.H. Geschwind, *Gene structure and alternative splicing of glycogen synthase kinase 3 beta (GSK-3beta) in neural and non-neural tissues*. Gene, 2003. **302**(1-2): p. 73-81.
43. Izumi, N., et al., *GSK-3beta regulates proper mitotic spindle formation in cooperation with a component of the gamma-tubulin ring complex, GCP5*. J Biol Chem, 2008. **283**(19): p. 12981-91.
44. Kwok, J.B., et al., *GSK3B polymorphisms alter transcription and splicing in Parkinson's disease*. Ann Neurol, 2005. **58**(6): p. 829-39.
45. Abrahamsson, A.E., et al., *Glycogen synthase kinase 3beta missplicing contributes to leukemia stem cell generation*. Proc Natl Acad Sci U S A, 2009. **106**(10): p. 3925-9.
46. Punga, T., M.T. Bengoechea-Alonso, and J. Ericsson, *Phosphorylation and ubiquitination of the transcription factor sterol regulatory element-binding protein-1 in response to DNA binding*. J Biol Chem, 2006. **281**(35): p. 25278-86.
47. Maggirwar, S.B., et al., *HIV-1 Tat-mediated activation of glycogen synthase kinase-3beta contributes to Tat-mediated neurotoxicity*. J Neurochem, 1999. **73**(2): p. 578-86.
48. Fiol, C.J., et al., *Formation of protein kinase recognition sites by covalent modification of the substrate. Molecular mechanism for the synergistic action of casein kinase II and glycogen synthase kinase 3*. J Biol Chem, 1987. **262**(29): p. 14042-8.
49. Dajani, R., et al., *Structural basis for recruitment of glycogen synthase kinase 3beta to the axin-APC scaffold complex*. Embo J, 2003. **22**(3): p. 494-501.
50. Dajani, R., et al., *Crystal structure of glycogen synthase kinase 3 beta: structural basis for phosphate-primed substrate specificity and autoinhibition*. Cell, 2001. **105**(6): p. 721-32.
51. ter Haar, E., et al., *Structure of GSK3beta reveals a primed phosphorylation mechanism*. Nat Struct Biol, 2001. **8**(7): p. 593-6.
52. Watcharasit, P., et al., *Direct, activating interaction between glycogen synthase kinase-3beta and p53 after DNA damage*. Proc Natl Acad Sci U S A, 2002. **99**(12): p. 7951-5.

53. Martin, C.P., et al., *P24, a glycogen synthase kinase 3 (GSK 3) inhibitor*. Biochim Biophys Acta, 2002. **1586**(1): p. 113-22.
54. Fiol, C.J., et al., *Ordered multisite protein phosphorylation. Analysis of glycogen synthase kinase 3 action using model peptide substrates*. J Biol Chem, 1990. **265**(11): p. 6061-5.
55. Hagen, T., et al., *Expression and characterization of GSK-3 mutants and their effect on beta-catenin phosphorylation in intact cells*. J Biol Chem, 2002. **277**(26): p. 23330-5.
56. Frame, S., P. Cohen, and R.M. Biondi, *A common phosphate binding site explains the unique substrate specificity of GSK3 and its inactivation by phosphorylation*. Mol Cell, 2001. **7**(6): p. 1321-7.
57. Cole, A.R., et al., *Distinct priming kinases contribute to differential regulation of collapsin response mediator proteins by glycogen synthase kinase-3 in vivo*. J Biol Chem, 2006.
58. Diehl, J.A., et al., *Glycogen synthase kinase-3beta regulates cyclin D1 proteolysis and subcellular localization*. Genes Dev, 1998. **12**(22): p. 3499-511.
59. Twomey, C. and J.V. McCarthy, *Presenilin-1 is an unprimed glycogen synthase kinase-3beta substrate*. FEBS Lett, 2006. **580**(17): p. 4015-20.
60. Zeng, X., et al., *A dual-kinase mechanism for Wnt co-receptor phosphorylation and activation*. Nature, 2005. **438**(7069): p. 873-7.
61. Lehner, B. and C.M. Sanderson, *A protein interaction framework for human mRNA degradation*. Genome Res, 2004. **14**(7): p. 1315-23.
62. Godemann, R., et al., *Phosphorylation of tau protein by recombinant GSK-3beta: pronounced phosphorylation at select Ser/Thr-Pro motifs but no phosphorylation at Ser262 in the repeat domain*. FEBS Lett, 1999. **454**(1-2): p. 157-64.
63. Sutherland, C. and P. Cohen, *The alpha-isoform of glycogen synthase kinase-3 from rabbit skeletal muscle is inactivated by p70 S6 kinase or MAP kinase-activated protein kinase-1 in vitro*. FEBS Lett, 1994. **338**(1): p. 37-42.
64. Sutherland, C., I.A. Leighton, and P. Cohen, *Inactivation of glycogen synthase kinase-3 beta by phosphorylation: new kinase connections in insulin and growth-factor signalling*. Biochem J, 1993. **296** (Pt 1): p. 15-9.
65. Cross, D.A., et al., *Inhibition of glycogen synthase kinase-3 by insulin mediated by protein kinase B*. Nature, 1995. **378**(6559): p. 785-9.
66. Fang, X., et al., *Phosphorylation and inactivation of glycogen synthase kinase 3 by protein kinase A*. Proc Natl Acad Sci U S A, 2000. **97**(22): p. 11960-5.
67. Saito, Y., J.R. Vandenheede, and P. Cohen, *The mechanism by which epidermal growth factor inhibits glycogen synthase kinase 3 in A431 cells*. Biochem J, 1994. **303** (Pt 1): p. 27-31.
68. Fukumoto, S., et al., *Akt participation in the Wnt signaling pathway through Dishevelled*. J Biol Chem, 2001. **276**(20): p. 17479-83.
69. Yuan, H., et al., *Suppression of glycogen synthase kinase activity is not sufficient for leukemia enhancer factor-1 activation*. J Biol Chem, 1999. **274**(43): p. 30419-23.
70. Wakefield, J.G., D.J. Stephens, and J.M. Tavaré, *A role for glycogen synthase kinase-3 in mitotic spindle dynamics and chromosome alignment*. J Cell Sci, 2003. **116**(Pt 4): p. 637-46.

71. Oinuma, I., H. Katoh, and M. Negishi, *R-Ras controls axon specification upstream of GSK-3beta through integrin-linked kinase*. J Biol Chem, 2006.
72. McManus, E.J., et al., *Role that phosphorylation of GSK3 plays in insulin and Wnt signalling defined by knockin analysis*. Embo J, 2005. **24**(8): p. 1571-83.
73. Papadopoulou, D., M.W. Bianchi, and M. Bourouis, *Functional studies of shaggy/glycogen synthase kinase 3 phosphorylation sites in Drosophila melanogaster*. Mol Cell Biol, 2004. **24**(11): p. 4909-19.
74. Kannan, N. and A.F. Neuwald, *Evolutionary constraints associated with functional specificity of the CMGC protein kinases MAPK, CDK, GSK, SRPK, DYRK, and CK2alpha*. Protein Sci, 2004. **13**(8): p. 2059-77.
75. Robbins, D.J., et al., *Regulation and properties of extracellular signal-regulated protein kinases 1 and 2 in vitro*. J Biol Chem, 1993. **268**(7): p. 5097-106.
76. Hughes, K., et al., *Modulation of the glycogen synthase kinase-3 family by tyrosine phosphorylation*. Embo J, 1993. **12**(2): p. 803-8.
77. Cole, A., S. Frame, and P. Cohen, *Further evidence that the tyrosine phosphorylation of glycogen synthase kinase-3 (GSK3) in mammalian cells is an autophosphorylation event*. Biochem J, 2004. **377**(Pt 1): p. 249-55.
78. Lochhead, P.A., et al., *A chaperone-dependent GSK3beta transitional intermediate mediates activation-loop autophosphorylation*. Mol Cell, 2006. **24**(4): p. 627-33.
79. Sayas, C.L., et al., *GSK-3 Is Activated by the Tyrosine Kinase Pyk2 during LPA1-mediated Neurite Retraction*. Mol Biol Cell, 2006.
80. Plyte, S.E., et al., *Glycogen synthase kinase-3 (GSK-3) is regulated during Dictyostelium development via the serpentine receptor cAR3*. Development, 1999. **126**(2): p. 325-33.
81. Kim, L., A. Harwood, and A.R. Kimmel, *Receptor-dependent and tyrosine phosphatase-mediated inhibition of GSK3 regulates cell fate choice*. Dev Cell, 2002. **3**(4): p. 523-32.
82. Kim, L., J. Liu, and A.R. Kimmel, *The novel tyrosine kinase ZAK1 activates GSK3 to direct cell fate specification*. Cell, 1999. **99**(4): p. 399-408.
83. Rayasam, G.V., et al., *Glycogen synthase kinase 3: more than a namesake*. Br J Pharmacol, 2009. **156**(6): p. 885-98.
84. Roach, P.J., *Glycogen and its metabolism*. Curr Mol Med, 2002. **2**(2): p. 101-20.
85. Cohen, P., *The Croonian Lecture 1998. Identification of a protein kinase cascade of major importance in insulin signal transduction*. Philos Trans R Soc Lond B Biol Sci, 1999. **354**(1382): p. 485-95.
86. Patel, S., et al., *Tissue-specific role of glycogen synthase kinase 3beta in glucose homeostasis and insulin action*. Mol Cell Biol, 2008. **28**(20): p. 6314-28.
87. Seidensticker, M.J. and J. Behrens, *Biochemical interactions in the wnt pathway*. Biochim Biophys Acta, 2000. **1495**(2): p. 168-82.
88. MacDonald, B.T., K. Tamai, and X. He, *Wnt/beta-catenin signaling: components, mechanisms, and diseases*. Dev Cell, 2009. **17**(1): p. 9-26.
89. Angers, S. and R.T. Moon, *Proximal events in Wnt signal transduction*. Nat Rev Mol Cell Biol, 2009. **10**(7): p. 468-77.

90. Hagen, T. and A. Vidal-Puig, *Characterisation of the phosphorylation of beta-catenin at the GSK-3 priming site Ser45*. *Biochem Biophys Res Commun*, 2002. **294**(2): p. 324-8.
91. Peifer, M., L.M. Pai, and M. Casey, *Phosphorylation of the Drosophila adherens junction protein Armadillo: roles for wingless signal and zeste-white 3 kinase*. *Dev Biol*, 1994. **166**(2): p. 543-56.
92. Yost, C., et al., *The axis-inducing activity, stability, and subcellular distribution of beta-catenin is regulated in Xenopus embryos by glycogen synthase kinase 3*. *Genes Dev*, 1996. **10**(12): p. 1443-54.
93. Wu, G. and X. He, *Threonine 41 in beta-catenin serves as a key phosphorylation relay residue in beta-catenin degradation*. *Biochemistry*, 2006. **45**(16): p. 5319-23.
94. Amit, S., et al., *Axin-mediated CKI phosphorylation of beta-catenin at Ser 45: a molecular switch for the Wnt pathway*. *Genes Dev*, 2002. **16**(9): p. 1066-76.
95. Hart, M.J., et al., *Downregulation of beta-catenin by human Axin and its association with the APC tumor suppressor, beta-catenin and GSK3 beta*. *Curr Biol*, 1998. **8**(10): p. 573-81.
96. Ikeda, S., et al., *Axin, a negative regulator of the Wnt signaling pathway, forms a complex with GSK-3beta and beta-catenin and promotes GSK-3beta-dependent phosphorylation of beta-catenin*. *Embo J*, 1998. **17**(5): p. 1371-84.
97. Itoh, K., V.E. Krupnik, and S.Y. Sokol, *Axis determination in Xenopus involves biochemical interactions of axin, glycogen synthase kinase 3 and beta-catenin*. *Curr Biol*, 1998. **8**(10): p. 591-4.
98. Fraser, E., et al., *Identification of the Axin and Frat binding region of glycogen synthase kinase-3*. *J Biol Chem*, 2002. **277**(3): p. 2176-85.
99. Yamamoto, H., et al., *Phosphorylation of axin, a Wnt signal negative regulator, by glycogen synthase kinase-3beta regulates its stability*. *J Biol Chem*, 1999. **274**(16): p. 10681-4.
100. Rubinfeld, B., et al., *Binding of GSK3beta to the APC-beta-catenin complex and regulation of complex assembly*. *Science*, 1996. **272**(5264): p. 1023-6.
101. Rubinfeld, B., D.A. Tice, and P. Polakis, *Axin-dependent phosphorylation of the adenomatous polyposis coli protein mediated by casein kinase Iepsilon*. *J Biol Chem*, 2001. **276**(42): p. 39037-45.
102. Ferrarese, A., et al., *Chemical dissection of the APC Repeat 3 multistep phosphorylation by the concerted action of protein kinases CK1 and GSK3*. *Biochemistry*, 2007. **46**(42): p. 11902-10.
103. Xing, Y., et al., *Crystal structure of a beta-catenin/APC complex reveals a critical role for APC phosphorylation in APC function*. *Mol Cell*, 2004. **15**(4): p. 523-33.
104. Xing, Y., et al., *Crystal structure of a beta-catenin/axin complex suggests a mechanism for the beta-catenin destruction complex*. *Genes Dev*, 2003. **17**(22): p. 2753-64.
105. Ha, N.C., et al., *Mechanism of phosphorylation-dependent binding of APC to beta-catenin and its role in beta-catenin degradation*. *Mol Cell*, 2004. **15**(4): p. 511-21.

106. Tamai, K., et al., *LDL-receptor-related proteins in Wnt signal transduction*. Nature, 2000. **407**(6803): p. 530-5.
107. Cong, F., L. Schweizer, and H. Varmus, *Wnt signals across the plasma membrane to activate the beta-catenin pathway by forming oligomers containing its receptors, Frizzled and LRP*. Development, 2004. **131**(20): p. 5103-15.
108. Itasaki, N., et al., *Wise, a context-dependent activator and inhibitor of Wnt signalling*. Development, 2003. **130**(18): p. 4295-305.
109. Kato, M., et al., *Cbfa1-independent decrease in osteoblast proliferation, osteopenia, and persistent embryonic eye vascularization in mice deficient in Lrp5, a Wnt coreceptor*. J Cell Biol, 2002. **157**(2): p. 303-14.
110. Axelrod, J.D., et al., *Differential recruitment of Dishevelled provides signaling specificity in the planar cell polarity and Wingless signaling pathways*. Genes Dev, 1998. **12**(16): p. 2610-22.
111. Boutros, M., et al., *Signaling specificity by Frizzled receptors in Drosophila*. Science, 2000. **288**(5472): p. 1825-8.
112. Rothbacher, U., et al., *Dishevelled phosphorylation, subcellular localization and multimerization regulate its role in early embryogenesis*. Embo J, 2000. **19**(5): p. 1010-22.
113. Umbhauer, M., et al., *The C-terminal cytoplasmic Lys-thr-X-X-X-Trp motif in frizzled receptors mediates Wnt/beta-catenin signalling*. Embo J, 2000. **19**(18): p. 4944-54.
114. Smalley, M.J., et al., *Interaction of axin and Dvl-2 proteins regulates Dvl-2-stimulated TCF-dependent transcription*. Embo J, 1999. **18**(10): p. 2823-35.
115. Zeng, X., et al., *Initiation of Wnt signaling: control of Wnt coreceptor Lrp6 phosphorylation/activation via frizzled, dishevelled and axin functions*. Development, 2008. **135**(2): p. 367-75.
116. Mao, B., et al., *LDL-receptor-related protein 6 is a receptor for Dickkopf proteins*. Nature, 2001. **411**(6835): p. 321-5.
117. Tamai, K., et al., *A mechanism for Wnt coreceptor activation*. Mol Cell, 2004. **13**(1): p. 149-56.
118. Piao, S., et al., *Direct inhibition of GSK3beta by the phosphorylated cytoplasmic domain of LRP6 in Wnt/beta-catenin signaling*. PLoS One, 2008. **3**(12): p. e4046.
119. Mi, K., P.J. Dolan, and G.V. Johnson, *The low density lipoprotein receptor-related protein 6 interacts with glycogen synthase kinase 3 and attenuates activity*. J Biol Chem, 2006. **281**(8): p. 4787-94.
120. Wu, G., et al., *Inhibition of GSK3 phosphorylation of beta-catenin via phosphorylated PPPSPXS motifs of Wnt coreceptor LRP6*. PLoS One, 2009. **4**(3): p. e4926.
121. Thomas, G.M., et al., *A GSK3-binding peptide from FRAT1 selectively inhibits the GSK3-catalysed phosphorylation of axin and beta-catenin*. FEBS Lett, 1999. **458**(2): p. 247-51.
122. Yost, C., et al., *GBP, an inhibitor of GSK-3, is implicated in Xenopus development and oncogenesis*. Cell, 1998. **93**(6): p. 1031-41.
123. van Amerongen, R., et al., *Frat is dispensable for canonical Wnt signaling in mammals*. Genes Dev, 2005. **19**(4): p. 425-30.

124. Kim, N.G., C. Xu, and B.M. Gumbiner, *Identification of targets of the Wnt pathway destruction complex in addition to beta-catenin*. Proc Natl Acad Sci U S A, 2009. **106**(13): p. 5165-70.
125. Nusse, R., *Wnts and Hedgehogs: lipid-modified proteins and similarities in signaling mechanisms at the cell surface*. Development, 2003. **130**(22): p. 5297-305.
126. Kalderon, D., *Similarities between the Hedgehog and Wnt signaling pathways*. Trends Cell Biol, 2002. **12**(11): p. 523-31.
127. Ingham, P.W. and A.P. McMahon, *Hedgehog signaling in animal development: paradigms and principles*. Genes Dev, 2001. **15**(23): p. 3059-87.
128. Chen, C.H., et al., *Nuclear trafficking of Cubitus interruptus in the transcriptional regulation of Hedgehog target gene expression*. Cell, 1999. **98**(3): p. 305-16.
129. Aza-Blanc, P., et al., *Proteolysis that is inhibited by hedgehog targets Cubitus interruptus protein to the nucleus and converts it to a repressor*. Cell, 1997. **89**(7): p. 1043-53.
130. Jia, J., et al., *Shaggy/GSK3 antagonizes Hedgehog signalling by regulating Cubitus interruptus*. Nature, 2002. **416**(6880): p. 548-52.
131. Price, M.A. and D. Kalderon, *Proteolysis of the Hedgehog signaling effector Cubitus interruptus requires phosphorylation by Glycogen Synthase Kinase 3 and Casein Kinase 1*. Cell, 2002. **108**(6): p. 823-35.
132. Jia, J., et al., *Phosphorylation by double-time/CKIepsilon and CKIalpha targets cubitus interruptus for Slimb/beta-TRCP-mediated proteolytic processing*. Dev Cell, 2005. **9**(6): p. 819-30.
133. Robbins, D.J., et al., *Hedgehog elicits signal transduction by means of a large complex containing the kinesin-related protein costal2*. Cell, 1997. **90**(2): p. 225-34.
134. Sisson, J.C., et al., *Costal2, a novel kinesin-related protein in the Hedgehog signaling pathway*. Cell, 1997. **90**(2): p. 235-45.
135. Stegman, M.A., et al., *Identification of a tetrameric hedgehog signaling complex*. J Biol Chem, 2000. **275**(29): p. 21809-12.
136. McMahon, A.P., P.W. Ingham, and C.J. Tabin, *Developmental roles and clinical significance of hedgehog signaling*. Curr Top Dev Biol, 2003. **53**: p. 1-114.
137. Alcedo, J., et al., *The Drosophila smoothed gene encodes a seven-pass membrane protein, a putative receptor for the hedgehog signal*. Cell, 1996. **86**(2): p. 221-32.
138. Alcedo, J. and M. Noll, *Hedgehog and its patched-smoothened receptor complex: a novel signalling mechanism at the cell surface*. Biol Chem, 1997. **378**(7): p. 583-90.
139. Deneff, N., et al., *Hedgehog induces opposite changes in turnover and subcellular localization of patched and smoothed*. Cell, 2000. **102**(4): p. 521-31.
140. Chen, Y. and G. Struhl, *In vivo evidence that Patched and Smoothed constitute distinct binding and transducing components of a Hedgehog receptor complex*. Development, 1998. **125**(24): p. 4943-8.
141. Stone, D.M., et al., *The tumour-suppressor gene patched encodes a candidate receptor for Sonic hedgehog*. Nature, 1996. **384**(6605): p. 129-34.

142. Marigo, V., et al., *Biochemical evidence that patched is the Hedgehog receptor*. Nature, 1996. **384**(6605): p. 176-9.
143. Lum, L., et al., *Hedgehog signal transduction via Smoothened association with a cytoplasmic complex scaffolded by the atypical kinesin, Costal-2*. Mol Cell, 2003. **12**(5): p. 1261-74.
144. Ogden, S.K., et al., *Identification of a functional interaction between the transmembrane protein Smoothened and the kinesin-related protein Costal2*. Curr Biol, 2003. **13**(22): p. 1998-2003.
145. Ruel, L., et al., *Stability and association of Smoothened, Costal2 and Fused with Cubitus interruptus are regulated by Hedgehog*. Nat Cell Biol, 2003. **5**(10): p. 907-13.
146. Echelard, Y., et al., *Sonic hedgehog, a member of a family of putative signaling molecules, is implicated in the regulation of CNS polarity*. Cell, 1993. **75**(7): p. 1417-30.
147. Wang, B., J.F. Fallon, and P.A. Beachy, *Hedgehog-regulated processing of Gli3 produces an anterior/posterior repressor gradient in the developing vertebrate limb*. Cell, 2000. **100**(4): p. 423-34.
148. Cheung, H.O., et al., *The kinesin protein Kif7 is a critical regulator of Gli transcription factors in mammalian hedgehog signaling*. Sci Signal, 2009. **2**(76): p. ra29.
149. Endoh-Yamagami, S., et al., *The mammalian Cos2 homolog Kif7 plays an essential role in modulating Hh signal transduction during development*. Curr Biol, 2009. **19**(15): p. 1320-6.
150. Preat, T., et al., *A putative serine/threonine protein kinase encoded by the segment-polarity fused gene of Drosophila*. Nature, 1990. **347**(6288): p. 87-9.
151. Chen, M.H., et al., *Mice deficient in the fused homolog do not exhibit phenotypes indicative of perturbed hedgehog signaling during embryonic development*. Mol Cell Biol, 2005. **25**(16): p. 7042-53.
152. Kise, Y., et al., *Sufu recruits GSK3beta for efficient processing of Gli3*. Biochem Biophys Res Commun, 2009. **387**(3): p. 569-74.
153. Craig, A.M. and G. Banker, *Neuronal polarity*. Annu Rev Neurosci, 1994. **17**: p. 267-310.
154. Dotti, C.G., C.A. Sullivan, and G.A. Banker, *The establishment of polarity by hippocampal neurons in culture*. J Neurosci, 1988. **8**(4): p. 1454-68.
155. Desai, A. and T.J. Mitchison, *Microtubule polymerization dynamics*. Annu Rev Cell Dev Biol, 1997. **13**: p. 83-117.
156. Watanabe, T., et al., *Phosphorylation of CLASP2 by GSK-3beta regulates its interaction with IQGAP1, EB1 and microtubules*. J Cell Sci, 2009. **122**(Pt 16): p. 2969-79.
157. Zumbunn, J., et al., *Binding of the adenomatous polyposis coli protein to microtubules increases microtubule stability and is regulated by GSK3 beta phosphorylation*. Curr Biol, 2001. **11**(1): p. 44-9.
158. Lovestone, S., et al., *Phosphorylation of tau by glycogen synthase kinase-3 beta in intact mammalian cells: the effects on the organization and stability of microtubules*. Neuroscience, 1996. **73**(4): p. 1145-57.

159. Sanchez, C., M. Perez, and J. Avila, *GSK3beta-mediated phosphorylation of the microtubule-associated protein 2C (MAP2C) prevents microtubule bundling*. Eur J Cell Biol, 2000. **79**(4): p. 252-60.
160. Ciani, L., et al., *A divergent canonical WNT-signaling pathway regulates microtubule dynamics: dishevelled signals locally to stabilize microtubules*. J Cell Biol, 2004. **164**(2): p. 243-53.
161. Jiang, H., et al., *Both the establishment and the maintenance of neuronal polarity require active mechanisms: critical roles of GSK-3beta and its upstream regulators*. Cell, 2005. **120**(1): p. 123-35.
162. Gartner, A., X. Huang, and A. Hall, *Neuronal polarity is regulated by glycogen synthase kinase-3 (GSK-3{beta}) independently of Akt/PKB serine phosphorylation*. J Cell Sci, 2006. **119**(Pt 19): p. 3927-34.
163. Eickholt, B.J., F.S. Walsh, and P. Doherty, *An inactive pool of GSK-3 at the leading edge of growth cones is implicated in Semaphorin 3A signaling*. J Cell Biol, 2002. **157**(2): p. 211-7.
164. Rosslenbroich, V., et al., *Collapsin response mediator protein-4 regulates F-actin bundling*. Exp Cell Res, 2005. **310**(2): p. 434-44.
165. Uchida, Y., et al., *Semaphorin3A signalling is mediated via sequential Cdk5 and GSK3beta phosphorylation of CRMP2: implication of common phosphorylating mechanism underlying axon guidance and Alzheimer's disease*. Genes Cells, 2005. **10**(2): p. 165-79.
166. Tighe, A., et al., *GSK-3 inhibitors induce chromosome instability*. BMC Cell Biol, 2007. **8**(1): p. 34.
167. Mishima, M., et al., *Two structurally distinct inhibitors of glycogen synthase kinase 3 induced centromere positive micronuclei in human lymphoblastoid TK6 cells*. Mutat Res, 2008. **643**(1-2): p. 29-35.
168. Shero, J.H. and P. Hieter, *A suppressor of a centromere DNA mutation encodes a putative protein kinase (MCK1)*. Genes Dev, 1991. **5**(4): p. 549-60.
169. Schlesinger, A., et al., *Wnt pathway components orient a mitotic spindle in the early Caenorhabditis elegans embryo without requiring gene transcription in the responding cell*. Genes Dev, 1999. **13**(15): p. 2028-38.
170. McCartney, B.M., et al., *Drosophila APC2 and Armadillo participate in tethering mitotic spindles to cortical actin*. Nat Cell Biol, 2001. **3**(10): p. 933-8.
171. Dikovskaya, D., I.P. Newton, and I.S. Nathke, *The adenomatous polyposis coli protein is required for the formation of robust spindles formed in CSF Xenopus extracts*. Mol Biol Cell, 2004. **15**(6): p. 2978-91.
172. Green, R.A. and K.B. Kaplan, *Chromosome instability in colorectal tumor cells is associated with defects in microtubule plus-end attachments caused by a dominant mutation in APC*. J Cell Biol, 2003. **163**(5): p. 949-61.
173. Hadjihannas, M.V., et al., *Aberrant Wnt/beta-catenin signaling can induce chromosomal instability in colon cancer*. Proc Natl Acad Sci U S A, 2006. **103**(28): p. 10747-52.
174. Loberg, R.D., E. Vesely, and F.C. Brosius, 3rd, *Enhanced glycogen synthase kinase-3beta activity mediates hypoxia-induced apoptosis of vascular smooth muscle cells and is prevented by glucose transport and metabolism*. J Biol Chem, 2002. **277**(44): p. 41667-73.

175. Pap, M. and G.M. Cooper, *Role of glycogen synthase kinase-3 in the phosphatidylinositol 3-Kinase/Akt cell survival pathway*. J Biol Chem, 1998. **273**(32): p. 19929-32.
176. Johnson-Farley, N.N., T. Travkina, and D.S. Cowen, *Cumulative activation of akt and consequent inhibition of glycogen synthase kinase-3 by brain-derived neurotrophic factor and insulin-like growth factor-1 in cultured hippocampal neurons*. J Pharmacol Exp Ther, 2006. **316**(3): p. 1062-9.
177. Bijur, G.N., P. De Sarno, and R.S. Jope, *Glycogen synthase kinase-3beta facilitates staurosporine- and heat shock-induced apoptosis. Protection by lithium*. J Biol Chem, 2000. **275**(11): p. 7583-90.
178. Chu, B., et al., *Transcriptional activity of heat shock factor 1 at 37 degrees C is repressed through phosphorylation on two distinct serine residues by glycogen synthase kinase 3 and protein kinases Calpha and Czeta*. J Biol Chem, 1998. **273**(29): p. 18640-6.
179. Pap, M. and G.M. Cooper, *Role of translation initiation factor 2B in control of cell survival by the phosphatidylinositol 3-kinase/Akt/glycogen synthase kinase 3beta signaling pathway*. Mol Cell Biol, 2002. **22**(2): p. 578-86.
180. Welsh, G.I. and C.G. Proud, *Glycogen synthase kinase-3 is rapidly inactivated in response to insulin and phosphorylates eukaryotic initiation factor eIF-2B*. Biochem J, 1993. **294** (Pt 3): p. 625-9.
181. de Groot, R.P., et al., *Negative regulation of Jun/AP-1: conserved function of glycogen synthase kinase 3 and the Drosophila kinase shaggy*. Oncogene, 1993. **8**(4): p. 841-7.
182. Nikolakaki, E., et al., *Glycogen synthase kinase 3 phosphorylates Jun family members in vitro and negatively regulates their transactivating potential in intact cells*. Oncogene, 1993. **8**(4): p. 833-40.
183. Sears, R., et al., *Multiple Ras-dependent phosphorylation pathways regulate Myc protein stability*. Genes Dev, 2000. **14**(19): p. 2501-14.
184. Tullai, J.W., et al., *GSK-3 represses CREB-targeted immediate early genes in quiescent cells*. J Biol Chem, 2007.
185. Beals, C.R., et al., *Nuclear export of NF-ATc enhanced by glycogen synthase kinase-3*. Science, 1997. **275**(5308): p. 1930-4.
186. Neal, J.W. and N.A. Clipstone, *Glycogen synthase kinase-3 inhibits the DNA binding activity of NFATc*. J Biol Chem, 2001. **276**(5): p. 3666-73.
187. Xavier, I.J., et al., *Glycogen synthase kinase 3beta negatively regulates both DNA-binding and transcriptional activities of heat shock factor 1*. J Biol Chem, 2000. **275**(37): p. 29147-52.
188. Ginger, R.S., et al., *Glycogen synthase kinase-3 enhances nuclear export of a Dictyostelium STAT protein*. Embo J, 2000. **19**(20): p. 5483-91.
189. Boyle, W.J., et al., *Activation of protein kinase C decreases phosphorylation of c-Jun at sites that negatively regulate its DNA-binding activity*. Cell, 1991. **64**(3): p. 573-84.
190. Grimes, C.A. and R.S. Jope, *CREB DNA binding activity is inhibited by glycogen synthase kinase-3 beta and facilitated by lithium*. J Neurochem, 2001. **78**(6): p. 1219-32.

191. Cong, F. and H. Varmus, *Nuclear-cytoplasmic shuttling of Axin regulates subcellular localization of beta-catenin*. Proc Natl Acad Sci U S A, 2004. **101**(9): p. 2882-7.
192. Franca-Koh, J., et al., *The regulation of glycogen synthase kinase-3 nuclear export by Frat/GBP*. J Biol Chem, 2002. **277**(46): p. 43844-8.
193. Strmecki, L., D.M. Greene, and C.J. Pears, *Developmental decisions in Dictyostelium discoideum*. Dev Biol, 2005. **284**(1): p. 25-36.
194. Schilde, C., et al., *GSK3 is a multifunctional regulator of Dictyostelium development*. Development, 2004. **131**(18): p. 4555-65.
195. Harwood, A.J., et al., *Glycogen synthase kinase 3 regulates cell fate in Dictyostelium*. Cell, 1995. **80**(1): p. 139-48.
196. Strmecki, L., et al., *Proteomic and microarray analyses of the Dictyostelium Zak1-GSK-3 signaling pathway reveal a role in early development*. Eukaryot Cell, 2007. **6**(2): p. 245-52.
197. Janetopoulos, C. and R.A. Firtel, *Directional sensing during chemotaxis*. FEBS Lett, 2008. **582**(14): p. 2075-85.
198. Stephens, L., L. Milne, and P. Hawkins, *Moving towards a better understanding of chemotaxis*. Curr Biol, 2008. **18**(11): p. R485-94.
199. Franca-Koh, J., Y. Kamimura, and P. Devreotes, *Navigating signaling networks: chemotaxis in Dictyostelium discoideum*. Curr Opin Genet Dev, 2006. **16**(4): p. 333-8.
200. Rubino, S., et al., *Location of actin, myosin, and microtubular structures during directed locomotion of Dictyostelium amebae*. J Cell Biol, 1984. **98**(2): p. 382-90.
201. Egelhoff, T.T., T.V. Naismith, and F.V. Brozovich, *Myosin-based cortical tension in Dictyostelium resolved into heavy and light chain-regulated components*. J Muscle Res Cell Motil, 1996. **17**(2): p. 269-74.
202. Jay, P.Y., C. Pasternak, and E.L. Elson, *Studies of mechanical aspects of amoeboid locomotion*. Blood Cells, 1993. **19**(2): p. 375-86; discussion 386-8.
203. Jin, T., et al., *Localization of the G protein betagamma complex in living cells during chemotaxis*. Science, 2000. **287**(5455): p. 1034-6.
204. Xiao, Z., et al., *Dynamic distribution of chemoattractant receptors in living cells during chemotaxis and persistent stimulation*. J Cell Biol, 1997. **139**(2): p. 365-74.
205. Sasaki, A.T., et al., *Localized Ras signaling at the leading edge regulates PI3K, cell polarity, and directional cell movement*. J Cell Biol, 2004. **167**(3): p. 505-18.
206. Huang, Y.E., et al., *Receptor-mediated regulation of PI3Ks confines PI(3,4,5)P3 to the leading edge of chemotaxing cells*. Mol Biol Cell, 2003. **14**(5): p. 1913-22.
207. Iijima, M., Y.E. Huang, and P. Devreotes, *Temporal and spatial regulation of chemotaxis*. Dev Cell, 2002. **3**(4): p. 469-78.
208. Funamoto, S., et al., *Spatial and temporal regulation of 3-phosphoinositides by PI 3-kinase and PTEN mediates chemotaxis*. Cell, 2002. **109**(5): p. 611-23.
209. Kortholt, A., et al., *Phospholipase C regulation of phosphatidylinositol 3,4,5-trisphosphate-mediated chemotaxis*. Mol Biol Cell, 2007. **18**(12): p. 4772-9.
210. Loovers, H.M., et al., *Distinct roles of PI(3,4,5)P3 during chemoattractant signaling in Dictyostelium: a quantitative in vivo analysis by inhibition of PI3-kinase*. Mol Biol Cell, 2006. **17**(4): p. 1503-13.

211. Matsuoka, S., et al., *Single-molecule analysis of chemoattractant-stimulated membrane recruitment of a PH-domain-containing protein*. J Cell Sci, 2006. **119**(Pt 6): p. 1071-9.
212. Dormann, D., et al., *Visualizing PI3 kinase-mediated cell-cell signaling during Dictyostelium development*. Curr Biol, 2002. **12**(14): p. 1178-88.
213. Postma, M., et al., *Uniform cAMP stimulation of Dictyostelium cells induces localized patches of signal transduction and pseudopodia*. Mol Biol Cell, 2003. **14**(12): p. 5019-27.
214. Ruchira, et al., *Pleckstrin homology domain diffusion in Dictyostelium cytoplasm studied using fluorescence correlation spectroscopy*. J Biol Chem, 2004. **279**(11): p. 10013-9.
215. Meili, R., et al., *Chemoattractant-mediated transient activation and membrane localization of Akt/PKB is required for efficient chemotaxis to cAMP in Dictyostelium*. Embo J, 1999. **18**(8): p. 2092-105.
216. Funamoto, S., et al., *Role of phosphatidylinositol 3' kinase and a downstream pleckstrin homology domain-containing protein in controlling chemotaxis in dictyostelium*. J Cell Biol, 2001. **153**(4): p. 795-810.
217. Klein, P.S. and D.A. Melton, *A molecular mechanism for the effect of lithium on development*. Proc Natl Acad Sci U S A, 1996. **93**(16): p. 8455-9.
218. Robinson, D.N., et al., *Dictyostelium cytokinesis: from molecules to mechanics*. J Muscle Res Cell Motil, 2002. **23**(7-8): p. 719-27.
219. Uyeda, T.Q. and A. Nagasaki, *Variations on a theme: the many modes of cytokinesis*. Curr Opin Cell Biol, 2004. **16**(1): p. 55-60.
220. Barr, F.A. and U. Gruneberg, *Cytokinesis: placing and making the final cut*. Cell, 2007. **131**(5): p. 847-60.
221. Knecht, D.A. and W.F. Loomis, *Antisense RNA inactivation of myosin heavy chain gene expression in Dictyostelium discoideum*. Science, 1987. **236**(4805): p. 1081-6.
222. De Lozanne, A. and J.A. Spudich, *Disruption of the Dictyostelium myosin heavy chain gene by homologous recombination*. Science, 1987. **236**(4805): p. 1086-91.
223. Neujahr, R., et al., *Microtubule-mediated centrosome motility and the positioning of cleavage furrows in multinucleate myosin II-null cells*. J Cell Sci, 1998. **111** (Pt 9): p. 1227-40.
224. Neujahr, R., C. Heizer, and G. Gerisch, *Myosin II-independent processes in mitotic cells of Dictyostelium discoideum: redistribution of the nuclei, re-arrangement of the actin system and formation of the cleavage furrow*. J Cell Sci, 1997. **110** (Pt 2): p. 123-37.
225. Uyeda, T.Q., C. Kitayama, and S. Yumura, *Myosin II-independent cytokinesis in Dictyostelium: its mechanism and implications*. Cell Struct Funct, 2000. **25**(1): p. 1-10.
226. Nagasaki, A., E.L. de Hostos, and T.Q. Uyeda, *Genetic and morphological evidence for two parallel pathways of cell-cycle-coupled cytokinesis in Dictyostelium*. J Cell Sci, 2002. **115**(Pt 10): p. 2241-51.
227. Spudich, J.A., *In pursuit of myosin function*. Cell Regul, 1989. **1**(1): p. 1-11.

228. Nagasaki, A. and T.Q. Uyeda, *Chemotaxis-mediated scission contributes to efficient cytokinesis in Dictyostelium*. *Cell Motil Cytoskeleton*, 2008. **65**(11): p. 896-903.
229. Janetopoulos, C., et al., *Temporal and spatial regulation of phosphoinositide signaling mediates cytokinesis*. *Dev Cell*, 2005. **8**(4): p. 467-77.
230. Sasaki, A.T., et al., *G protein-independent Ras/PI3K/F-actin circuit regulates basic cell motility*. *J Cell Biol*, 2007. **178**(2): p. 185-91.
231. Nagasaki, A., et al., *Genetic approaches to dissect the mechanisms of two distinct pathways of cell cycle-coupled cytokinesis in Dictyostelium*. *Cell Struct Funct*, 2001. **26**(6): p. 585-91.
232. Hibi, M., et al., *Dictyostelium discoideum talin A is crucial for myosin II-independent and adhesion-dependent cytokinesis*. *J Muscle Res Cell Motil*, 2004. **25**(2): p. 127-40.
233. Manstein, D.J., et al., *Cloning vectors for the production of proteins in Dictyostelium discoideum*. *Gene*, 1995. **162**: p. 129-134.
234. Levi, S., M. Polyakov, and T.T. Egelhoff, *Green fluorescent protein and epitope tag fusion vectors for Dictyostelium discoideum*. *Plasmid*, 2000. **44**(3): p. 231-8.
235. Haas, J., E.C. Park, and B. Seed, *Codon usage limitation in the expression of HIV-1 envelope glycoprotein*. *Curr Biol*, 1996. **6**(3): p. 315-24.
236. Cormack, B.P., R.H. Valdivia, and S. Falkow, *FACS-optimized mutants of the green fluorescent protein (GFP)*. *Gene*, 1996. **173**(1 Spec No): p. 33-8.
237. Andersson, S., et al., *Cloning, structure, and expression of the mitochondrial cytochrome P-450 sterol 26-hydroxylase, a bile acid biosynthetic enzyme*. *J Biol Chem*, 1989. **264**(14): p. 8222-9.
238. Boshart, M., et al., *A very strong enhancer is located upstream of an immediate early gene of human cytomegalovirus*. *Cell*, 1985. **41**(2): p. 521-30.
239. Hillen, W. and C. Berens, *Mechanisms underlying expression of Tn10 encoded tetracycline resistance*. *Annu Rev Microbiol*, 1994. **48**: p. 345-69.
240. Hillen, W., et al., *Control of expression of the Tn10-encoded tetracycline resistance genes. Equilibrium and kinetic investigation of the regulatory reactions*. *J Mol Biol*, 1983. **169**(3): p. 707-21.
241. Nelson, J.A., C. Reynolds-Kohler, and B.A. Smith, *Negative and positive regulation by a short segment in the 5'-flanking region of the human cytomegalovirus major immediate-early gene*. *Mol Cell Biol*, 1987. **7**(11): p. 4125-9.
242. Graham, F.L., et al., *Characteristics of a human cell line transformed by DNA from human adenovirus type 5*. *J Gen Virol*, 1977. **36**(1): p. 59-74.
243. Pang, K.M., M.A. Lynes, and D.A. Knecht, *Variables controlling the expression level of exogenous genes in Dictyostelium*. *Plasmid*, 1999. **41**(3): p. 187-97.
244. Schlatterer, C., G. Knoll, and D. Malchow, *Intracellular calcium during chemotaxis of Dictyostelium discoideum: a new fura-2 derivative avoids sequestration of the indicator and allows long-term calcium measurements*. *Eur J Cell Biol*, 1992. **58**(1): p. 172-81.
245. Knecht, D. and K.M. Pang, *Electroporation of Dictyostelium discoideum*. *Methods Mol Biol*, 1995. **47**: p. 321-30.

246. Ong, S.E. and M. Mann, *Stable isotope labeling by amino acids in cell culture for quantitative proteomics*. *Methods Mol Biol*, 2007. **359**: p. 37-52.
247. Harsha, H.C., H. Molina, and A. Pandey, *Quantitative proteomics using stable isotope labeling with amino acids in cell culture*. *Nat Protoc*, 2008. **3**(3): p. 505-16.
248. Olsen, J.V., et al., *Parts per million mass accuracy on an Orbitrap mass spectrometer via lock mass injection into a C-trap*. *Mol Cell Proteomics*, 2005. **4**(12): p. 2010-21.
249. Shevchenko, A., et al., *Mass spectrometric sequencing of proteins silver-stained polyacrylamide gels*. *Anal Chem*, 1996. **68**(5): p. 850-8.
250. Cox, J. and M. Mann, *MaxQuant enables high peptide identification rates, individualized p.p.b.-range mass accuracies and proteome-wide protein quantification*. *Nat Biotechnol*, 2008. **26**(12): p. 1367-72.
251. He, X., et al., *Glycogen synthase kinase-3 and dorsoventral patterning in Xenopus embryos*. *Nature*, 1995. **374**(6523): p. 617-22.
252. Berridge, M.V.e.a., *The Biochemical and Cellular Basis of Cell Proliferation Assays That Use Tetrazolium Salts*. *Biochemica*, 1996. **4**: p. 15-19.
253. Ryves, W.J., et al., *An assay for glycogen synthase kinase 3 (GSK-3) for use in crude cell extracts*. *Anal Biochem*, 1998. **264**(1): p. 124-7.
254. Woodgett, J.R., *Use of peptide substrates for affinity purification of protein-serine kinases*. *Anal Biochem*, 1989. **180**(2): p. 237-41.
255. Baki, A., et al., *A high throughput luminescent assay for glycogen synthase kinase-3beta inhibitors*. *Assay Drug Dev Technol*, 2007. **5**(1): p. 75-83.
256. Rinnab, L., et al., *Inhibition of glycogen synthase kinase-3 in androgen-responsive prostate cancer cell lines: are GSK inhibitors therapeutically useful?* *Neoplasia*, 2008. **10**(6): p. 624-34.
257. Uno, Y., et al., *Efficacy of a novel, orally active GSK-3 inhibitor 6-Methyl-N-[3-[[3-(1-methylethoxy)propyl]carbamoyl]-1H-pyrazol-4-yl]pyridine-3-carboxamide in tau transgenic mice*. *Brain Res*, 2009. **1296**: p. 148-63.
258. Polgar, T., et al., *Comparative virtual and experimental high-throughput screening for glycogen synthase kinase-3beta inhibitors*. *J Med Chem*, 2005. **48**(25): p. 7946-59.
259. Meares, G.P. and R.S. Jope, *Resolution of the nuclear localization mechanism of glycogen synthase kinase-3: functional effects in apoptosis*. *J Biol Chem*, 2007. **282**(23): p. 16989-7001.
260. Siegert, F. and C. Weijer, *Digital image processing of optical density wave propagation in Dictyostelium discoideum and analysis of the effects of caffeine and ammonia*. *J Cell Sci*, 1989. **93**(2): p. 325-335.
261. Brenner, M. and S.D. Thoms, *Caffeine blocks activation of cyclic AMP synthesis in Dictyostelium discoideum*. *Dev Biol*, 1984. **101**(1): p. 136-46.
262. Dharmawardhane, S., et al., *Regulatory role of the G alpha 1 subunit in controlling cellular morphogenesis in Dictyostelium*. *Development*, 1994. **120**(12): p. 3549-61.
263. Alcantara, F. and M. Monk, *Signal propagation during aggregation in the slime mould Dictyostelium discoideum*. *J Gen Microbiol*, 1974. **85**(2): p. 321-34.

264. Tomchik, K.J. and P.N. Devreotes, *Adenosine 3',5'-monophosphate waves in Dictyostelium discoideum: a demonstration by isotope dilution--fluorography*. Science, 1981. **212**(4493): p. 443-6.
265. Kobayashi, T., et al., *Glycogen synthase kinase 3 and h-prune regulate cell migration by modulating focal adhesions*. Mol Cell Biol, 2006. **26**(3): p. 898-911.
266. Zhang, N., et al., *Insights into unbinding mechanisms upon two mutations investigated by molecular dynamics study of GSK3beta-axin complex: role of packing hydrophobic residues*. Proteins, 2007. **67**(4): p. 941-9.
267. Vagnarelli, P., et al., *Condensin and Repo-Man-PP1 co-operate in the regulation of chromosome architecture during mitosis*. Nat Cell Biol, 2006. **8**(10): p. 1133-42.
268. Trinkle-Mulcahy, L., et al., *Repo-Man recruits PP1 gamma to chromatin and is essential for cell viability*. J Cell Biol, 2006. **172**(5): p. 679-92.
269. Tagwerker, C., et al., *A tandem affinity tag for two-step purification under fully denaturing conditions: application in ubiquitin profiling and protein complex identification combined with in vivocross-linking*. Mol Cell Proteomics, 2006. **5**(4): p. 737-48.
270. Guerrero, C., et al., *An integrated mass spectrometry-based proteomic approach: quantitative analysis of tandem affinity-purified in vivo cross-linked protein complexes (QTAX) to decipher the 26 S proteasome-interacting network*. Mol Cell Proteomics, 2006. **5**(2): p. 366-78.
271. Sutherland, B.W., J. Toews, and J. Kast, *Utility of formaldehyde cross-linking and mass spectrometry in the study of protein-protein interactions*. J Mass Spectrom, 2008. **43**(6): p. 699-715.
272. Vasilescu, J., X. Guo, and J. Kast, *Identification of protein-protein interactions using in vivo cross-linking and mass spectrometry*. Proteomics, 2004. **4**(12): p. 3845-54.
273. Miernyk, J.A. and J.J. Thelen, *Biochemical approaches for discovering protein-protein interactions*. Plant J, 2008. **53**(4): p. 597-609.
274. Rothbauer, U., et al., *A versatile nanotrapp for biochemical and functional studies with fluorescent fusion proteins*. Mol Cell Proteomics, 2008. **7**(2): p. 282-9.
275. von Mering, C., et al., *STRING: a database of predicted functional associations between proteins*. Nucleic Acids Res, 2003. **31**(1): p. 258-61.
276. von Mering, C., et al., *STRING: known and predicted protein-protein associations. integrated and transferred across organisms*. Nucleic Acids Res, 2005. **33**(Database issue): p. D433-7.
277. Jensen, L.J., et al., *STRING 8--a global view on proteins and their functional interactions in 630 organisms*. Nucleic Acids Res, 2009. **37**(Database issue): p. D412-6.
278. Zhu, H., et al., *Analysis of Wnt gene expression in prostate cancer: mutual inhibition by WNT11 and the androgen receptor*. Cancer Res, 2004. **64**(21): p. 7918-26.
279. Brookes, M.J., et al., *A role for iron in Wnt signalling*. Oncogene, 2008. **27**(7): p. 966-75.

280. Lee, Y.N., Y. Gao, and H.Y. Wang, *Differential mediation of the Wnt canonical pathway by mammalian Dishevelleds-1, -2, and -3*. Cell Signal, 2008. **20**(2): p. 443-52.
281. de la Roche, M., J. Worm, and M. Bienz, *The function of BCL9 in Wnt/beta-catenin signaling and colorectal cancer cells*. BMC Cancer, 2008. **8**: p. 199.
282. Cho, G.W., et al., *TCF/beta-catenin plays an important role in HCCR-1 oncogene expression*. BMC Mol Biol, 2009. **10**: p. 42.
283. Ong, S.E., L.J. Foster, and M. Mann, *Mass spectrometric-based approaches in quantitative proteomics*. Methods, 2003. **29**(2): p. 124-30.
284. Gafken, P.R. and P.D. Lampe, *Methodologies for characterizing phosphoproteins by mass spectrometry*. Cell Commun Adhes, 2006. **13**(5-6): p. 249-62.
285. Zhang, G. and T.A. Neubert, *Use of stable isotope labeling by amino acids in cell culture (SILAC) for phosphotyrosine protein identification and quantitation*. Methods Mol Biol, 2009. **527**: p. 79-92, xi.
286. Pimienta, G., R. Chaerkady, and A. Pandey, *SILAC for global phosphoproteomic analysis*. Methods Mol Biol, 2009. **527**: p. 107-16, x.
287. Azab, A.N., et al., *Glycogen synthase kinase-3 is required for optimal de novo synthesis of inositol*. Mol Microbiol, 2007. **63**(4): p. 1248-1258.
288. Ueda, M. and S. Ogihara, *Microtubules are required in amoeba chemotaxis for preferential stabilization of appropriate pseudopods*. J Cell Sci, 1994. **107** (Pt 8): p. 2071-9.
289. Blau-Wasser, R., et al., *CP250, a novel acidic coiled coil protein of the Dictyostelium centrosome, affects growth, chemotaxis, and the nuclear envelope*. Mol Biol Cell, 2009. **20**(20): p. 4348-61.
290. Tang, L., et al., *tsunami, the Dictyostelium homolog of the Fused kinase, is required for polarization and chemotaxis*. Genes Dev, 2008. **22**(16): p. 2278-90.
291. van Veldhoven, P.P. and G.P. Mannaerts, *Sphingosine-phosphate lyase*. Adv Lipid Res, 1993. **26**: p. 69-98.
292. Spiegel, S., *Sphingosine 1-phosphate: a prototype of a new class of second messengers*. J Leukoc Biol, 1999. **65**(3): p. 341-4.
293. Pyne, S. and N.J. Pyne, *Sphingosine 1-phosphate signalling and termination at lipid phosphate receptors*. Biochim Biophys Acta, 2002. **1582**(1-3): p. 121-31.
294. Li, G., et al., *Sphingosine-1-phosphate lyase has a central role in the development of Dictyostelium discoideum*. Development, 2001. **128**(18): p. 3473-83.
295. Kumar, A., et al., *Sphingosine-1-phosphate plays a role in the suppression of lateral pseudopod formation during Dictyostelium discoideum cell migration and chemotaxis*. Cell Motil Cytoskeleton, 2004. **59**(4): p. 227-41.
296. Palmieri, S.J., et al., *Mutant Rac1B expression in Dictyostelium: effects on morphology, growth, endocytosis, development, and the actin cytoskeleton*. Cell Motil Cytoskeleton, 2000. **46**(4): p. 285-304.
297. Duleh, S.N., J.T. Collins, and R.K. Pope, *Morphological and functional analysis of Rac1B in Dictyostelium discoideum*. J Electron Microsc (Tokyo), 2005. **54**(6): p. 519-28.
298. Crompton, M., *The mitochondrial permeability transition pore and its role in cell death*. Biochem J, 1999. **341** (Pt 2): p. 233-49.

299. Petit-Paitel, A., et al., *Involvement of cytosolic and mitochondrial GSK-3beta in mitochondrial dysfunction and neuronal cell death of MPTP/MPP-treated neurons*. PLoS One, 2009. **4**(5): p. e5491.
300. Xi, J., et al., *Mechanism for resveratrol-induced cardioprotection against reperfusion injury involves glycogen synthase kinase 3beta and mitochondrial permeability transition pore*. Eur J Pharmacol, 2009. **604**(1-3): p. 111-6.
301. Nishihara, M., et al., *Modulation of the mitochondrial permeability transition pore complex in GSK-3beta-mediated myocardial protection*. J Mol Cell Cardiol, 2007. **43**(5): p. 564-70.
302. Langridge, P.D. and R.R. Kay, *Mutants in the Dictyostelium Arp2/3 complex and chemoattractant-induced actin polymerization*. Exp Cell Res, 2007. **313**(12): p. 2563-74.
303. Jefferies, K.C., D.J. Cipriano, and M. Forgac, *Function, structure and regulation of the vacuolar (H⁺)-ATPases*. Arch Biochem Biophys, 2008. **476**(1): p. 33-42.
304. Saroussi, S. and N. Nelson, *The little we know on the structure and machinery of V-ATPase*. J Exp Biol, 2009. **212**(Pt 11): p. 1604-10.
305. Lee, E., et al., *The roles of APC and Axin derived from experimental and theoretical analysis of the Wnt pathway*. PLoS Biol, 2003. **1**(1): p. E10.

Protein for

Format: [GenPept](#) [FASTA](#) [Graphics](#) [More Formats](#)

CBI Reference Sequence: NP_056986.2

E3 ubiquitin-protein ligase UBR5 [Homo sapiens]

[Comment](#) [Features](#) [Sequence](#)

LOCUS NP_056986 2799 aa linear PRI 25-APR-010

DEFINITION E3 ubiquitin-protein ligase UBR5 [Homo sapiens].

ACCESSION NP_056986

VERSION NP_056986.2 GI:15147337

RESOURCE REFSEQ: accession [NM_015902.4](#)

KEYWORDS .

SOURCE Homo sapiens (human)

ORGANISM [Homo sapiens](#)
Eukaryota; Metazoa; Chordata; Craniata; Vertebrata; Euteleostomi; Mammalia; Eutheria; Euarchontoglires; Primates; Haplorrhini; Catarrhini; Hominidae; Homo.

REFERENCE 1 (residues 1 to 2799)
AUTHORS Kim,M.S., Oh,J.E., Eom,H.S., Yoo,N.J. and Lee,S.H.
TITLE Mutational analysis of UBR5 gene encoding an E3 ubiquitin ligase in common human cancers
JOURNAL Pathology 42 (1), 93-94 (2010)
PUBMED [20025491](#)
REMARK GeneRIF: study confirmed the presence of UBR5 mutation in exon 45 in high microsatellite instability cacarcinomas; could not identify exon 42 mutations in colorectal cancers and exon 51 mutations in breast cancers

REFERENCE 2 (residues 1 to 2799)
AUTHORS O'Brien,P.M., Davies,M.J., Scurry,J.P., Smith,A.N., Barton,C.A., Henderson,M.J., Saunders,D.N., Gloss,B.S., Patterson,K.I., Clancy,J.L., Heinzelmann-Schwarz,V.A., Murali,R., Scolyer,R.A., Zeng,Y., Williams,E.D., Scurr,L., Defazio,A., Quinn,D.I., Watts,C.K., Hacker,N.F., Henshall,S.M. and Sutherland,R.L.
TITLE The E3 ubiquitin ligase EDD is an adverse prognostic factor for serous epithelial ovarian cancer and modulates cisplatin resistance in vitro
JOURNAL Br. J. Cancer 98 (6), 1085-1093 (2008)
PUBMED [18349819](#)
REMARK GeneRIF: These results identify EDD as a new independent prognostic marker for outcome in serous ovarian cancer
Erratum:[Br J Cancer. 2008 Jun 3;98(11):1880. Murali, Rajmohan [added]]

REFERENCE 3 (residues 1 to 2799)
AUTHORS Munoz,M.A., Saunders,D.N., Henderson,M.J., Clancy,J.L., Russell,A.J., Lehrbach,G., Musgrove,E.A., Watts,C.K. and Sutherland,R.L.
TITLE The E3 ubiquitin ligase EDD regulates S-phase and G(2)/M DNA damage checkpoints
JOURNAL Cell Cycle 6 (24), 3070-3077 (2007)
PUBMED [18073532](#)
REMARK GeneRIF: EDD plays the role in the maintenance of genomic stability, emphasising the potential importance of dysregulated EDD expression and/or function in the evolution of cancer.

REFERENCE 4 (sites)
AUTHORS Matsuoka,S., Ballif,B.A., Smogorzewska,A., McDonald,E.R. III, Hurov,K.E., Luo,J., Bakalarski,C.E., Zhao,Z., Solimini,N., Lerenthal,Y., Shiloh,Y., Gygi,S.P. and Elledge,S.J.
TITLE ATM and ATR substrate analysis reveals extensive protein networks responsive to DNA damage
JOURNAL Science 316 (5828), 1160-1166 (2007)
PUBMED [17525332](#)

REFERENCE 5 (residues 1 to 2799)
AUTHORS Ewing,R.M., Chu,P., Elisma,F., Li,H., Taylor,P., Climie,S., McBroom-Cerajewski,L., Robinson,M.D., O'Connor,L., Li,M., Taylor,R., Dharsee,M., Ho,Y., Heilbut,A., Moore,L., Zhang,S., Ornatsky,O., Bukhman,Y.V., Ethier,M., Sheng,Y., Vasilescu,J., Abu-Farha,M., Lambert,J.P., Duwel,H.S., Stewart,I.I., Kuehl,B., Hogue,K., Colwill,K., Gladwish,K., Muskat,B., Kinach,R., Adams,S.L., Moran,M.F., Morin,G.B., Topaloglou,T. and Figeys,D.
TITLE Large-scale mapping of human protein-protein interactions by mass spectrometry
JOURNAL Mol. Syst. Biol. 3, 89 (2007)
PUBMED [17353931](#)

REFERENCE 6 (residues 1 to 2799)
AUTHORS Olsen,J.V., Blagoev,B., Gnand,F., Macek,B., Kumar,C., Mortensen,P. and Mann,M.
TITLE Global, in vivo, and site-specific phosphorylation dynamics in signaling networks
JOURNAL Cell 127 (3), 635-648 (2006)
PUBMED [17081963](#)

REFERENCE 7 (sites)
AUTHORS Olsen,J.V., Blagoev,B., Gnand,F., Macek,B., Kumar,C., Mortensen,P.

[Change Region Shown](#)
[Customize View](#)

Analyze This Sequence

- [Run BLAST](#)
- [Identify Conserved Domains](#)

Articles about the UBR5 gene

- [Mutational analysis of UBR5 gene encoding an E3 ubiq\[Pathology. 2010\]](#)
 - [The E3 ubiquitin ligase EDD is an adverse prognostic\[Br J Cancer. 2008\]](#)
 - [The E3 ubiquitin ligase EDD regulates S-phase and G\(2\)/M\[Cell Cycle. 2007\]](#)
- [» See all...](#)

Identical Proteins for NP_056986.2

- [Ubiquitin protein ligase E3 c\[AAI37235\]](#)
 - [RecName: Full=E3 ubiquitin-\[O95071\]](#)
 - [progesterin induced protein \[\[AAD01259\]](#)
- [» See all...](#)

Pathways for the UBR5 gene what's this?

- [Ubiquitin mediated proteolysis - Protein ubiquitination plays an important role in eukaryotic cellular](#)

RefSeq mRNA

See reference mRNA sequence for the UBR5 gene (NM_015902.4).

More about the UBR5 gene


This gene encodes a progesterin-induced protein, which belongs to the HECT (homology to E6-AP carboxyl terminus) family. The HECT family prote...
Also Known As: DD5, EDD, EDD1, FLJ1131...

Homologs of the UBR5 gene

The UBR5 gene is conserved in dog, cow, mouse, rat, chicken, zebrafish, fruit fly, mosquito, and C.elegans.

Recent activity

[Turn Off](#) [Clear](#)

 E3 ubiquitin-protein ligase UBR5 [Homo sapiens]

Protein

[» See more...](#)

All links from this record

- [BLINK](#)
- [Related sequences](#)
- [Identical proteins](#)
- [BioSystems](#)
- [Conserved domains](#)
- [Domain relatives](#)
- [Full text in PMC](#)
- [Gene](#)
- [Gene genotype](#)
- [GeneView in dbSNP](#)
- [Genome](#)
- [Genome project](#)

and Mann, M.

TITLE Global, in vivo, and site-specific phosphorylation dynamics in signaling networks

JOURNAL Cell 127 (3), 635-648 (2006)

PUBMED [17001983](#)

REFERENCE 8 (sites)

AUTHORS Nousiainen, M., Sillje, H.H., Sauer, G., Nigg, E.A. and Korner, R.

TITLE Phosphoproteome analysis of the human mitotic spindle

JOURNAL Proc. Natl. Acad. Sci. U.S.A. 103 (14), 5391-5396 (2006)

PUBMED [16565220](#)

REFERENCE 9 (sites)

AUTHORS Kim, J.E., Tannenbaum, S.R. and White, F.M.

TITLE Global phosphoproteome of HT-29 human colon adenocarcinoma cells

JOURNAL J. Proteome Res. 4 (4), 1339-1346 (2005)

PUBMED [16083285](#)

REFERENCE 10 (sites)

AUTHORS Rush, J., Moritz, A., Lee, K.A., Guo, A., Goss, V.L., Spek, E.J., Zhang, H., Zha, X.M., Polakiewicz, R.D. and Comb, M.J.

TITLE Immunofluorescence profiling of tyrosine phosphorylation in cancer cells

JOURNAL Nat. Biotechnol. 23 (1), 94-101 (2005)

PUBMED [15592455](#)

REFERENCE 11 (residues 1 to 2799)

AUTHORS Eblen, S.T., Kumar, N.V., Shah, K., Henderson, M.J., Watts, C.K., Shokat, K.M. and Weber, M.J.

TITLE Identification of novel ERK2 substrates through use of an engineered kinase and ATP analogs

JOURNAL J. Biol. Chem. 278 (17), 14926-14935 (2003)

PUBMED [12594221](#)

REFERENCE 12 (residues 1 to 2799)

AUTHORS Henderson, M.J., Russell, A.J., Hird, S., Munoz, M., Clancy, J.L., Lehrbach, G.M., Calanni, S.T., Jans, D.A., Sutherland, R.L. and Watts, C.K.

TITLE EDD, the human hyperplastic discs protein, has a role in progesterone receptor coactivation and potential involvement in DNA damage response

JOURNAL J. Biol. Chem. 277 (29), 26468-26478 (2002)

PUBMED [12011095](#)

REMARK GeneRIF: ubiquitin-protein ligase EDD interacts with importin alpha 5 through consensus basic nuclear localization signals and is localized in cell nuclei. EDD also binds progesterone receptor (PR) and potentiates progesterin-mediated gene transactivation.

REFERENCE 13 (residues 1 to 2799)

AUTHORS Honda, Y., Tojo, M., Matsuzaki, K., Anan, T., Matsumoto, M., Ando, M., Saya, H. and Nakao, M.

TITLE Cooperation of HECT-domain ubiquitin ligase hHYD and DNA topoisomerase II-binding protein for DNA damage response

JOURNAL J. Biol. Chem. 277 (5), 3599-3605 (2002)

PUBMED [11714696](#)

REFERENCE 14 (residues 1 to 2799)

AUTHORS Deo, R.C., Sonenberg, N. and Burley, S.K.

TITLE X-ray structure of the human hyperplastic discs protein: an ortholog of the C-terminal domain of poly(A)-binding protein

JOURNAL Proc. Natl. Acad. Sci. U.S.A. 98 (8), 4414-4419 (2001)

PUBMED [11287654](#)

REFERENCE 15 (residues 1 to 2799)

AUTHORS Callaghan, M.J., Russell, A.J., Woollatt, E., Sutherland, G.R., Sutherland, R.L. and Watts, C.K.

TITLE Identification of a human HECT family protein with homology to the Drosophila tumor suppressor gene hyperplastic discs

JOURNAL Oncogene 17 (26), 3479-3491 (1998)

PUBMED [10020672](#)

COMMENT REVIEWED REFSEQ: This record has been curated by NCBI staff. The reference sequence was derived from [AF006010.2](#), [AB020703.2](#), [AL833555.1](#) and [BC037843.1](#).
On Aug 10, 2001 this sequence version replaced [gi:7705340](#).

Summary: This gene encodes a progesterin-induced protein, which belongs to the HECT (homology to E6-AP carboxyl terminus) family. The HECT family proteins function as E3 ubiquitin-protein ligases, targeting specific proteins for ubiquitin-mediated proteolysis. This gene is localized to chromosome 8q22 which is disrupted in a variety of cancers. This gene potentially has a role in regulation of cell proliferation or differentiation. [provided by RefSeq].

Publication Note: This RefSeq record includes a subset of the publications that are available for this gene. Please see the Entrez Gene record to access additional publications.

FEATURES

source 1..2799
/organism="Homo sapiens"
/db_xref="taxon:9606"
/chromosome="8"
/map="8q22"

Protein 1..2799
/product="E3 ubiquitin-protein ligase UBR5"
/note="ubiquitin-protein ligase; progesterin induced protein; hyperplastic discs protein homolog; E3 identified by differential display; E3 ubiquitin protein ligase, HECT domain containing, 1; hHYD; progesterin-induced protein; E3 ubiquitin-protein ligase, HECT domain-containing 1"
/calculated_mol_wt=309223

Region 180..>212
/region_name="E3_UbLigase_EDD"
/note="E3 ubiquitin ligase EDD; pfam11547"
/db_xref="CDD:151983"

Site 287
/site_type="phosphorylation"
/experiment="experimental evidence, no additional details recorded"
/citation=[2]

Site 327
 /site_type="phosphorylation"
 /experiment="experimental evidence, no additional details recorded"
 /citation=[8]
Region 1177..1244
 /region_name="zf-UBR"
 /note="Putative zinc finger in N-recognin (UBR box); c102595"
 /db_xref="CDD:155001"
Site 1549
 /site_type="phosphorylation"
 /experiment="experimental evidence, no additional details recorded"
 /citation=[6]
Site 1746
 /site_type="phosphorylation"
 /experiment="experimental evidence, no additional details recorded"
 /citation=[10]
Site 2026
 /site_type="phosphorylation"
 /experiment="experimental evidence, no additional details recorded"
 /citation=[9]
Site 2028
 /site_type="phosphorylation"
 /experiment="experimental evidence, no additional details recorded"
 /citation=[6]
Site 2071
 /site_type="phosphorylation"
 /experiment="experimental evidence, no additional details recorded"
 /citation=[4]
Region 2389..2452
 /region_name="PABP"
 /note="Poly-adenylate binding protein, unique domain; c102642"
 /db_xref="CDD:155033"
Site 2424
 /site_type="phosphorylation"
 /experiment="experimental evidence, no additional details recorded"
 /citation=[6]
Site 2434
 /site_type="phosphorylation"
 /experiment="experimental evidence, no additional details recorded"
 /citation=[6]
Site 2437
 /site_type="phosphorylation"
 /experiment="experimental evidence, no additional details recorded"
 /citation=[6]
Region 2503..2775
 /region_name="HECTc"
 /note="HECT domain; C-terminal catalytic domain of a subclass of Ubiquitin-protein ligase (E3). It binds specific ubiquitin-conjugating enzymes (E2), accepts ubiquitin from E2, transfers ubiquitin to substrate lysine side chains, and transfers additional...; c100077"
 /db_xref="CDD:153492"
Site order(2547,2732,2762..2763,2766..2770)
 /site_type="other"
 /note="catalytic cleft"
 /db_xref="CDD:28959"
Site order(2575,2578..2579,2581..2582,2591,2598,2600,2604..2605,2612,2617,2634,2638)
 /site_type="other"
 /note="E2 interaction site"
 /db_xref="CDD:28959"
CDS 1..2799
 /gene="UBR5"
 /gene_synonym="DD5; EDD; EDD1; FLJ11310; HYD; KIAA0896; MGC57263"
 /coded_by="NM_015902.4:34..8433"
 /db_xref="CCDS:CCDS34933.1"
 /db_xref="GeneID:51366"
 /db_xref="HGNC:16806"
 /db_xref="HPRD:06436"
 /db_xref="MIM:608413"

IGIN
 1 mtsihfvvhp lpgtedqlnd rlvsekl n kynlnshppl nvleqatikq cvvgpnhaaf
 61 lledgrvcrl gfsvqpdrlr lqkpdnndgs klnsnsgagr tsrpgrtsds pfwlsgsetl
 121 grlagntlgs rwssgvvgsg ggssgrssag ardsrrqtrv irtgrdrqsg llsgqppvi
 181 pasvipeeli sqagvvlqgk srsviirelq rtnldvnlav nllsrded gddgddtase
 241 sylpgeelms lldadihsah psviidadam feedisyfyg psfrrsslsr lgsrvlllp
 301 lerdsellre resvrlrler rwdgasfdn ergstskege pnlldkntpv qspvslgedl
 361 qwpdkdgtk ficigalyse llavsskgel yqwkwsesep yrnaqnpsh hpratflgl
 421 nekivilsan siratvaten nkvatvvdet lssvaskleh taqtyselgg erivslhcca
 481 lytcaqlens lywgvvpfs qrkkmlekar aknkkpkssa gissmpnitv gtqvcrlrnp
 541 lyhagavafs isagipkvsv lmesvwnmd scrflrspe slknmekask tteakpeskq
 601 epvktemgpp spastcsda ssiassamp ykrrrstpap keeekvneq wslrevvfe
 661 dvknvpvgkv lkvdgayvav kfpgtssntn cqnsqpdad pssllqdcrl lridelgvvk
 721 tggtpkvpdc fqrtpkklci pekteilavn vdskgvhavl ktgnwvryci fdlatgkaeq
 781 ennftssia figqnerova iftaggespi ilrdngntiy pmakdcmggi rdpdwdlpp
 841 isslmgvhs linlpansti kkaaviima vekqtlmqhi lrcdyeacrq ylmnlqavv
 911 lerdqllmgt fishrcdgnr nilhacvsvc fptsnketke eeeaeern tfaerlsav
 961 aianaisvsv snpggnrags sssrslrre mmrrslraag lgrheagass shdqdpvssp
 1021 iappsvvpdp pamdpdgid filapavgs1 ttaatgtgqg pststippps tepsvveskd

1081 rkanahfilk llcdsvvlqp ylrellsacd argmtpfmsa vsgraypaai tiletaqkia
1141 kaeissseke edvfmqmvcp sgtnpddspl yvlccndtcs fwtgahin qdifeqrtcg
1201 lleslcccte carvchkghd cklkrtspta ycdcwekckc ktliagqksa rldillyrllt
1261 atnlvtlpls rgehllllflv qtvarqtveh cqyrpprire drnrktaspe dsdmpdhle
1321 pprfaqlale rvlqdwalk smimfsgen kdplsassri ghllpeeovy lnqsgtirl
1381 dcftthclivk ctadillldt llgtlvkelq nkytpgrree aiavtmrflr svarvfvlis
1441 vemasskkkn nfipppigkc krvfqallpy aveelcnvae slivpvrngi arptapftla
1501 stsidamqgs eelfsvpepl prpssdqsss ssqsgssyii rnpqqrrisq sqpvgrdee
1561 qddivsvadve evevvegag eedhhdeqee hgeenaeaeq qhdehdedgs dmeildllaaa
1621 etesdesesh sqdnasgrr svvtaatags eagassvpaf feeddsqsnd ssdsdsssq
1681 sddiegetfm ldeplerttn sshangaaga prsmqwavrn tqhqrasta psststpaas
1741 sagliyidps nlrsgtist saaaaaaale asnassylts asslaraysi virqisdimg
1801 lipkynhlvy sqipaavklt ygdavnlqny veekliptwn wmvsimdste aqlrygsala
1861 sagdpghpnh plhasqnsar rermtareea sirtlegrrr atllsarqgm msargdflny
1921 alslnrshnd ehsvlplvd vcsikhvayv fqaliywika mnqgttldtp qlerkrrel
1981 lelqidneds ehendddtng satlndkddd slpaetgqnh pffrrsdsmf flgcipnnpf
2041 evplaeaipl adqphllqpn arkedlfgrp sqglyssas sgkclmevtv drnclevipt
2101 kmsyaanlkn vmnmqnrqkk egeeqpvipe etesskpgps ahdlaaqkks sllaeiglte
2161 segppltsfr pqcsfmgmvi shdmligrwr lslelfgrvf medvgaepgs iltelggfev
2221 keskfreme klrnqqsrdl slevdrdrdl liqgtmrqln nhfgrrcatt pmavhrvkt
2281 fkdepegsgq varsfytaia qaflsnekpl nlecignank gthtslmqrl rnrgerdrer
2341 ereremrers glragrrdr drdfrqrli dtrpfrpase gnpsddpepl pahrqalger
2401 lyprvqamqp afaskitgml lelsqaqlll llasedsira rvdeamelii ahgengads
2461 iildglvdes ekvqenrkr hgssrsvdm dlddtdgdd naplfyqpgk rgfytprpgk
2521 ntearlncfr nigrilglcl lqnelcpitl nrhvikvllg rkvnwhdfaf fdpvmyeslr
2581 qiliasqssd adavfsamd afaidlcke gggqvelipn gvnipvtqn vyeyvrkyae
2641 hrmlvvaepq lhamrkgllid vipknsledl taedfrllvn gcgevnvqml isftsfnades
2701 genaekllqf krwfwivek msmtqrqdlv yfwtspslp aseegfqmp sitirppddg
2761 hiptantcis rlyvplyssk qilkkllla iktknfgfv

[Write to the Help Desk](#)

[NCBI](#) | [NLM](#) | [NIH](#)

[Department of Health & Human Services](#)

[Privacy Statement](#) | [Freedom of Information Act](#) | [Disclaimer](#)

